Supramolecular chemistry of cyclic imides tethered carboxylic acids and related compounds

A Dissertation submitted to the
Indian Institute of Technology Guwahati as
partial fulfillment for the Degree of
Doctor of Philosophy in Chemistry

Submitted by

Devendra Singh

Department of Chemistry

Indian Institute of Technology Guwahati

October 2011

Dedicated to My Parents…

…who taught me the value of education.

Statement

I hereby declare that this thesis entitled "**Supramolecular chemistry of cyclic imides tethered carboxylic acids and related compounds**" is the outcome of research work carried out by me under the supervision of Prof. Jubaraj B. Baruah, at the Department of Chemistry, Indian Institute of Technology Guwahati, India.

In keeping with the general practice of reporting scientific observations, due acknowledgement has been made whenever work described here has been based on the findings of other investigators.

IIT Guwahati
October, 2011

Devendra Singh

Certificate

This is to certify that Devendra Singh has been working under my supervision since August, 2007 as a regular registered Ph. D. student. I am forwarding his thesis entitled "**Supramolecular chemistry of cyclic imides tethered carboxylic acids and related compounds**" being submitted for the Ph. D. (Science) Degree of this Institute.

I certify that he has fulfilled all the requirements according to the rules of this institute regarding the investigations embodied in his thesis and this work has not been submitted elsewhere for a degree.

IIT Guwahati
October, 2010

Prof. Jubaraj B. Baruah

Acknowledgements

This thesis might not have seen through its completion unless I had the support and encouragement of numerous people around me. Today, when I bring it to an end, I would like to express few words of appreciation to the people who actually made this thesis a reality and an unforgettable experience for me.

To begin with, I would like to thank my supervisor, Prof. Jubaraj B. Baruah. The enlightening experience of doing science under his guidance can hardly be described in words. The numerous discussions and interactions I had with him expanded my horizons to hitherto unknown frontiers of science and knowledge. I am indebt to this wonderful person for all that he has given me and above all for motivating me towards scientific research.

I would like to acknowledge my sincere gratitude to all my doctoral committee members for their insightful advices and valuable suggestions. I am also grateful to the entire faculty and staff in the Department of Chemistry, Indian Institute of Technology Guwahati for providing a wonderful work atmosphere throughout this period.

I would like to thank my lab mates Dr. Anirban Karmakar, Dr. W. Marjit Singh, Dr. Rupam sarma, dipjyoti, Babulal, Bigyan, Bhaskar, Jayant, Prithviraj whom I had an opportunity to work with and other group members Somashekhar, Chipem and Himanshu for their timely help, support and for the wonderful time we shared during this period. No words can express my thankfulness for giving me their time and companionship, which made the time spent in the laboratory and outside pleasant and memorable. I would like to give my special thanks to my lab senior Dr. Marjit Singh for his valuable support and suggestions throughout my research career.

This thesis wouldn't have seen the light of this day without the care and encouragement of my chemistry teachers Dr. Rajendra K. Sharma and Dr. Simpal Sharma. I would like to furnish my sincere gratitude to these two wonderful person of my life for their excellent teaching and constant motivation which made me reach this point.

The financial support from Council of Scientific and Industrial Research (CSIR), New Delhi for the research fellowship is duly acknowledged.

Finally, I would like to thank my family for their understanding, encouragement, patience, unending support and blessings in my every endeavor without which my Ph.D. could not be completed. They are the main soul and inspiration for each and every step that I achieve in my life.

Preview

Host-guest crystalline materials are of special interest in solid state because of their possible applications in the areas of catalysis, size selective separation, gas absorption, pharmaceuticals, biomimetics, etc. Cyclic imide derivatives have been proved as versatile scaffolds in host-guest chemistry to design the crystals of specific molecular arrangements. Cyclic imides attached to aromatic rings possess dipolar nature and this effect provide extra stability to the packing arrangement. This thesis deals with the studies on synthesis, characterization and supramolecular aspects of a number of inclusion compounds of cyclic imide tethered carboxylic acids with aromatic nitrogen containing heterocycles. The structural aspects along with optical properties are investigated with an objective to understand their self-assembly processes. Studies on the gel formation in cyclic imide carboxylic acids as a low molecular weight organic gelators and solvent dependent fluorescence emissions of some cyclic imide heterocycles are also studied. Synthesis, characterization and structural elucidation along with understanding physical properties such as solid state fluorescence emission of transition metal complexes of phthalimide and naphthalimide derivatives is also presented in thesis. A fair amount of work is devoted to understand the role of non-covalent interactions and properties of host-guest self assembled networks derived from cyclic imides.

The thesis contains six chapters based on the results of experimental works performed during the research period.

Chapter 1: Introduction

A general introduction to the cyclic imides is brought forward with their synthesis, structural features, and spectroscopic properties in this chapter. The role of weak intermolecular interactions in the construction of supramolecular architecture of various cyclic imides is presented. Importance of various cyclic imide derivatives in the field of photochemistry, anion and cation sensing, molecular recognition, supramolecular chemistry, coordination chemistry, biochemicals and medicinal chemistry is also described. Various applications related to optical properties of cyclic imides are elaborated. Important structural characteristics needed to modulate the optoelectronic and material aspects of imide containing systems are presented to extend the scope of study.

Chapter 2: Host-guest complexes of cyclic imides containing hydroxy benzoic acids with aromatic N-heterocycles

In this chapter, we have studied the structures of host-guest complexes of pyridine/bipyridine and quinoline with some of the aromatic hydroxy carboxylic acids that are tethered by naphthalimide or naphthalene diimide. The cyclic imide compounds used in this study are prepared by cyclocondensation reactions of 1,8-naphthalic anhydride and 1,4,5,8-naphthalenetetracarboxylic dianhydride with respective amino hydroxy benzoic acids and shown below in Chart 1.

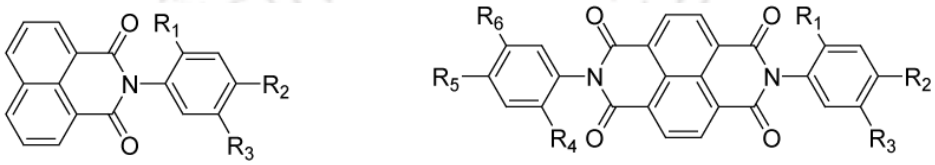

Where R_1-R_6 = H, OH, COOH

Chart 1.

Various host-guest complexes of these compounds with pyridine/bipyridine and quinoline are prepared. Single crystal X-ray structure of all these complexes are determined which exhibit O-H···N interactions. Various types of intermolecular hydrogen bonding interactions are found to responsible for the formation of channels filled by guest molecules in all these host-guest 3D supramolecular architectures. Two types of hydrogen bond motifs, namely, discrete O-H···N interactions and a combination of O-H···N and C-H···O interactions making cyclic $R_2^2(7)$ hydrogen bond motif, are observed in the structures of these host-guest complexes. DFT calculations on analogous motifs derived from formic acid/pyridine and formic acid/quinoline are also carried out to establish these motifs in the solid state. It is observed that the energy differences between these motifs are very small and within the limit of very weak hydrogen bonds. Such small energy differences account for the formation of both types of structural patterns in these host-guest complexes depending on the steric requirements. The Salt formation is not observed in these complexes, however, DFT calculations show that the salt formation between pyridine and formic acid is not a favorable process but it may occur in case of quinoline and formic acid.

Chapter 3: Polymorphism and pseudopolymorphism in pyridine and quinoline solvates of cyclic imide carboxylic acids

This part of study reports the different ways of inclusion of guest aromatic N-heterocycles, namely, pyridine and quinoline, in the assemblies of host aromatic dicarboxylic acids tethered by naphthalene diimide and pyromellitic diimide units. The crystallization of a naphthalene diimide host at two different conditions led to the formation of two polymorphic solvates with pyridine in a ratio 1:4 (Scheme 1).

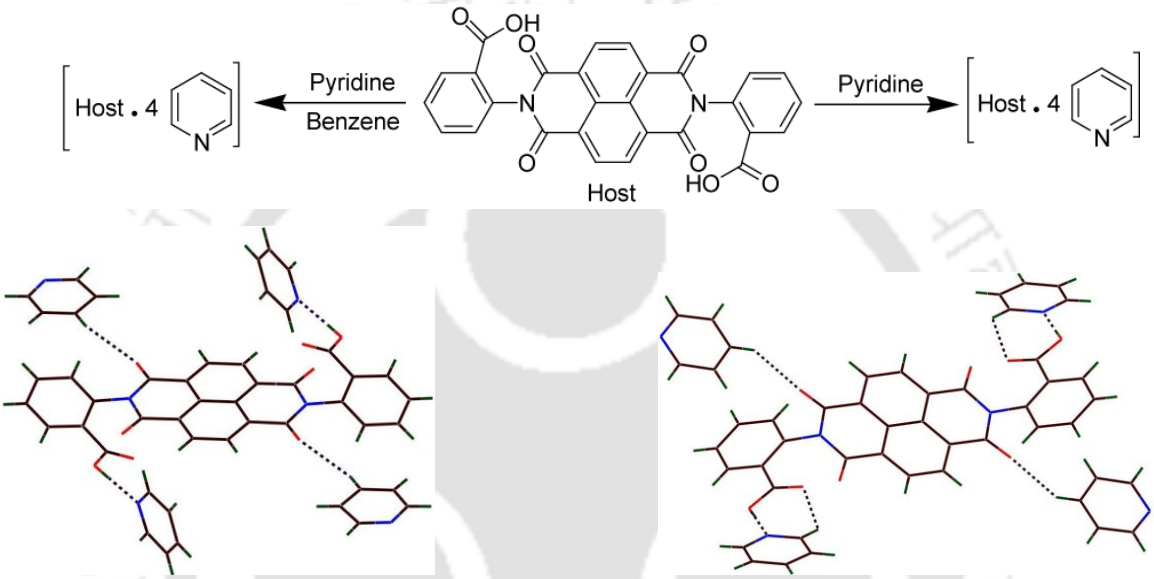

Scheme 1.

When quinoline was used as a solvent of crystallization for similar host, two different solvates are obtained which are also the pseudopolymorphs to each other, in which the ratio of host to quinoline is 1: 5 and 1:3, respectively. The former solvate (1:5) is obtained by crystallization of host from quinoline, whereas latter (1:3) is formed by crystallization of host from mixed solvent of quinoline and pyridine. The crystallization conditions show that quinoline solvate of that host is formed preferentially in the presence of both pyridine and quinoline solvents. This selective binding of quinoline over pyridine by the host in the formation of solvates is also demonstrated by fluorescence titration experiments. Two different solvates (pseudopolymorphs) of a pyromellitic diimide host with guest pyridine molecules are also obtained by varying crystallization conditions (Scheme 2). Both the solvates are crystallized in same space group containing two halves of symmetry independent molecules of host with three and two guest pyridine molecules in their crystallographic asymmetric units, respectively.

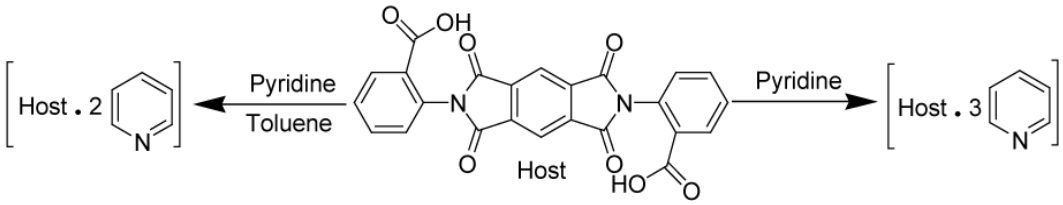

Scheme 2.

Chapter 4: Gel formation in cyclic imide carboxylic acids and solvent dependent fluorescence emission in cyclic imide heterocycles

In this chapter, synthesis and characterization of a number of cyclic imide carboxylic acids (Chart 2) and their gel formation properties are discussed. When these imides are dissolved in DMSO followed by addition of water; they form gels. A series of gels are prepared and the conditions for their formation are described. SEM analyses show that the morphologies of the gels varies from each other and they are found to have short thick fibre-like structure or interconnected fiber network or plate-like structures of micron size.

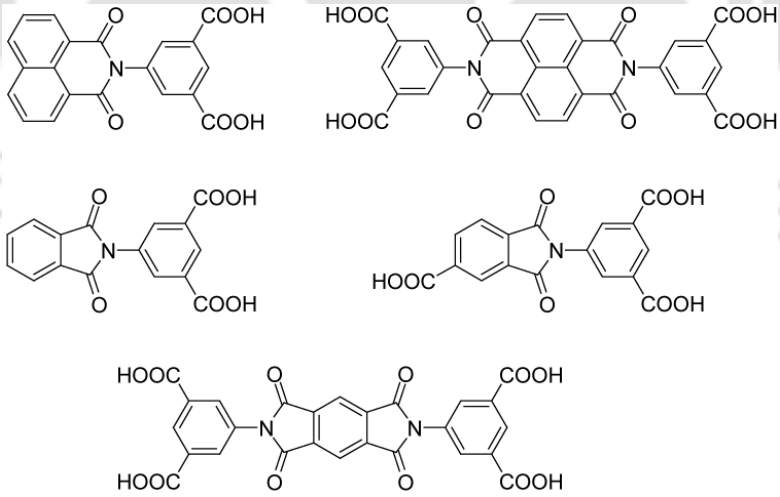

Chart 2.

A number of cyclic imide compounds having isoquinoline backbone are also synthesized (Chart 3) and their solvent dependent fluorescence emission properties are studied as a part of this chapter. The nitro groups of these compounds are reduced to obtain amino derivatives and their solvent dependent emissions and changes in emission properties on protonation of

amine group are studied. The amino groups on these compounds are further functionalized to obtain various derivatives and the electronic effects caused to the presence of various substituents are studied by the changes in fluorescence emissions.

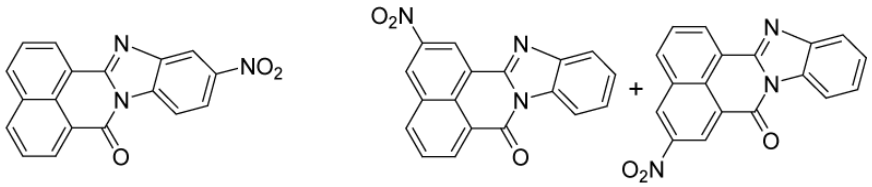

Chart 3.

Chapter 5: Supramolecular aspects of transition metal complexes of cyclic imides tethered carboxylic acids

In this chapter, we present the syntheses, characterization and supramolecular structural features of transition metal complexes of conformational flexible methyl cyclohexane carboxylic acids that are tethered by phthalimide (**L1H**) and naphthalimide (**L2H**) units (Chart 4).

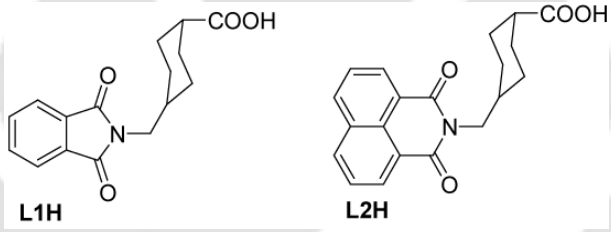

Chart 4.

A series of mononuclear complexes of L1 with Mn(II), Cu(II), Zn(II) and Cd(II) is synthesized and their single crystal X-ray structures are determined. All these complexes adopt octahedral geometries around the M(II) centers except the Cu(II) complex which possess square pyramidal geometry. The structural features of supramolecular architectures of these complexes are described. Coordination environments around the metal centers affect the dimensionality and features of supramolecular architectures. In the case of M(II) complexes of L1; Mn(II) complex shows a zigzag 3D architecture whereas other complexes exhibit supramolecular 3D channels like structures containing the coordinated pyridine rings inside these channels.

Mononuclear Co(II), Cu(II) and Cd(II) complexes of L2 are also synthesized and their supramolecular structural features are studied. The carboxylate groups of L2 are found to coordinate with M(II) centers in monodentate coordination modes in the case of Co(II) and Cd(II) complexes whereas Cu(II) complex shows chelating coordination modes. Intermolecular hydrogen bond interactions result in the formation of 3D helical supramolecular network containing channels in the crystal lattice of Cu(II) complex. The channels created in the lattice are filled by guest pyridine molecules which also interact to each other via C-H…π (dc_{27}…π 3.64) interactions in the lattice (Figure 1). The solid state fluorescence properties of free organic ligand **L1H** and **L2H** as well as their M(II) complexes are also investigated at room temperature.

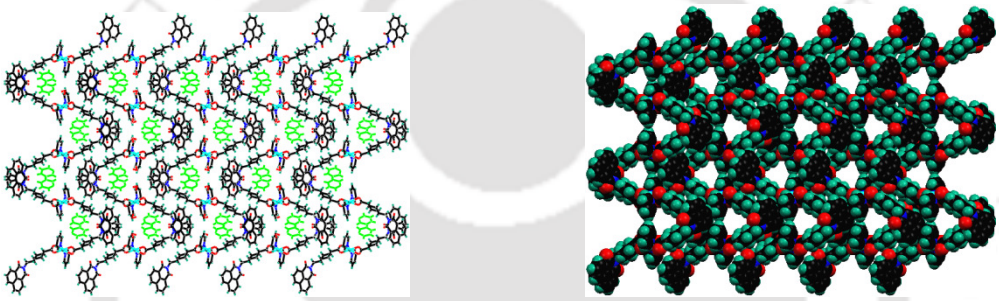

Figure 1.

Chapter 6: Cyclic imides containing hydroxy carboxylic acids in the syntheses of manganese(II), zinc(II) and cadmium(II) complexes

This chapter deals with the study on the supramolecular structural features of Mn(II), Zn(II) and Cd(II) complexes of flexible aliphatic and rigid aromatic hydroxy carboxylic acids tethered by cyclic imide units. The reaction of organic ligand **$L3H_2$** with Mn(II) acetate, followed by crystallization from water yields the Mn(II) complex. A similar reaction of organic ligand **$L3H_2$** with Zn(II) acetate, followed by crystallization from pyridine, gives a 1D Zn(II) coordination polymer (Scheme 3). Single crystal X-ray structure analysis reveals the formation of one dimensional (1D) coordination polymer, $[\{Mn(L3H)_2(H_2O)\}.8H_2O]_n$ along with a mononuclear complex, $[Mn(L3H)_2(H_2O)_2]$, in a single crystal. Both these complexes adopt distorted octahedral geometries showing different coordination modes of the carboxylate groups of L3 (Figure 2). The distorted octahedral geometry of Zn(II) coordination polymer shows similar coordination environment as observed for 1D polymer of

Mn(II) complex, only showing difference of a coordinated pyridine ligand than water (Figure 3).

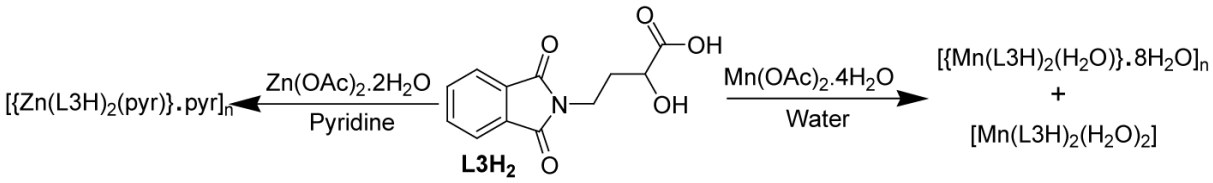

Scheme 3.

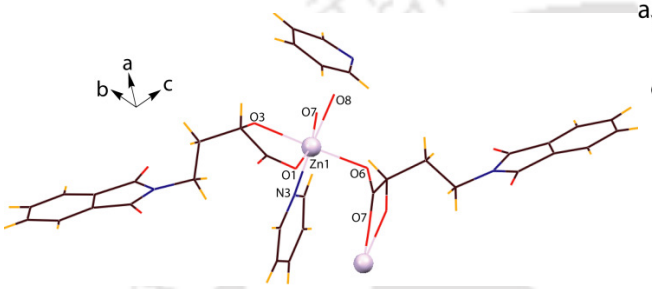

Figure 2.

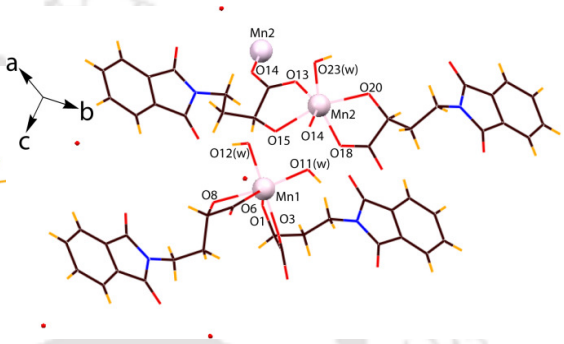

Figure 3.

A seven coordinated Cd(II) complex of **L4H$_2$** is also synthesized and characterized (Scheme 4) which crystallized in monoclinic $P2_1/c$ space group and possess two symmetry non-equivalent Cd(II) complex molecules in its crystallographic asymmetric unit. Two carboxylates groups of L4H are in trans chelating coordination mode; remaining three positions are occupied by pyridine ligand molecules in a distorted pentagonal bipyramidal geometry of Cd(II) complex.

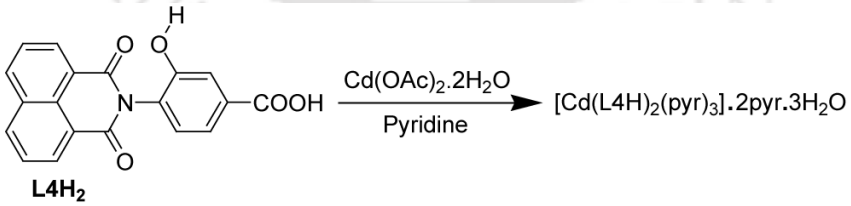

Scheme 4.

The role of weak intermolecular interactions in the formation of various types of supramolecular architecture of these complexes are described in details. The peaks obtained in the solid state photoluminescence spectra of Mn(II) and Zn(II) complexes are different from those observed for free organic ligand **L3H$_2$**; suggesting the ligand to metal charge

transfer transitions (LMCT) in these complexes. The solid state fluorescence emissions of **L4H$_2$** and its complex Cd(II) complex are similar to each other.

The synthetic procedures and experimental details, for each of the compounds and complexes synthesized, are included with the corresponding chapter. The cumulative references are also listed at the end of the corresponding chapter. The instrumental details, hydrogen bond parameters, selected bond length and angles of the metal complexes and crystallographic data of single crystal X-ray structures are tabulated in the appendix section towards the end of the thesis.

Contents

Chapter 1

Introduction

1.1 General features and occurrence of cyclic imides

Imide refers to a functional group consisting of two carbonyl groups bound to a nitrogen atom, or in other words, imides are special kind of substituted amides in which NH is functionalized by two acyl or aroyl groups.[1] These compounds are structurally related to acid anhydrides. The relationship between esters and amides is analogous to that of imides and anhydrides. Imide functional groups can be associated with acyclic or a cyclic ring structure, shown as **1.1** and **1.2**.

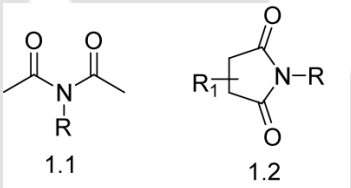

Most cyclic imides are derived from dicarboxylic acids and their names reflect the parent acid. Examples are succinimide derived from succinic acid, phthalimide derived from phthalic acid and 1,8-naphthalimide derived from naphthalene-1,8-dicarboxylic acid. For imides derived from amines, the N-substituent is indicated by a prefix, e.g. N-ethylsuccinimide is derived from succinic acid and ethylamine.

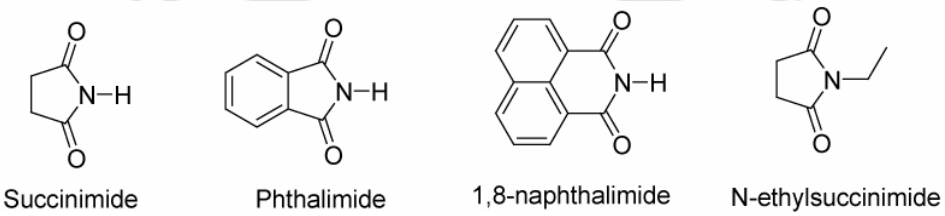

Most common imides are prepared by heating dicarboxylic acids or their anhydrides and ammonia or primary amines. The result is a condensation reaction:

$$(RCO)_2O + R'NH_2 \rightarrow (RCO)_2NR' + H_2O$$

These reactions proceed via the intermediacy of amides. To form cyclic imide, the intramolecular reaction of a carboxylic acid with an amide is far faster than the intermolecular reaction, which is rarely observed. Being highly polar, imides exhibit good solubility in polar media. The N-H center for imides derived from ammonia is acidic and can participate in hydrogen bonding. Unlike the structurally related acid anhydrides, they are stable towards hydrolysis and some can even be recrystallized from boiling water. Since the imides contain amide bonds, it is essential to understand the special features of an amide bond contributing to their structure and reactivity. The partial double bond character of carbon-nitrogen bond is rationalized by taking into account of the conjugation of the lone pair of electrons on the nitrogen atom with the π-orbital of carbonyl group as shown in Scheme 1.1.[2] Spectroscopic studies of different amides have shown that the rotation about amide carbon-nitrogen bond is restricted at room temperature. The amide carbon-nitrogen bond is also found to be shorter than the C-N bonds present in primary or N-substituted amines; this suggests that the amide carbon-nitrogen bond may have partial double bond character.[3,4]

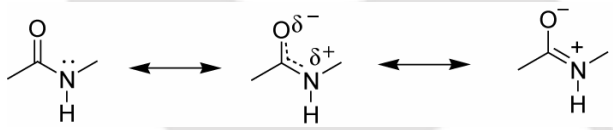

Scheme 1.1.

The electronic effects that contribute to structure and reactivity of an amide are comparable to an acyclic imide; however, in the case of cyclic imides, a slightly modified resonance scheme is to be adopted to understand their reactivity. For example in phthalimide, two structural models **1.3** and **1.4** are frequently used to describe the structural features.[5] The features of the phthalimides can be explained by using either of the models that deemed fit to explain the property under consideration.[6-10]

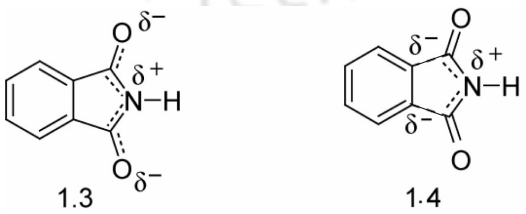

1.3 1.4

Cyclic imides in monomeric or polymeric forms have industrial as well as biological applications. A simplest example is N-ethylmaleimide which have been used frequently as

biochemical reagent. Many high strength or electrically conductive polymers contain imide subunits, i.e. the polyimides. One example is Kapton, a high strength polymer used to make space suits, where the repeated unit consists of two imide groups derived from aromatic tetracarboxylic acids.[11] Interest in the bioactivity of imide-containing compounds was sparked by the early discovery of the high bioactivity of the cycloheximide as an inhibitor of protein biosynthesis in certain organisms.[11] Thalidomide was used as medicine which was later found to cause many birth defects. A number of fungicides and herbicides contain the imide functionality.[11] Examples include Captan, a controversial herbicide, which has been phased out because of its carcinogenic properties.[12]

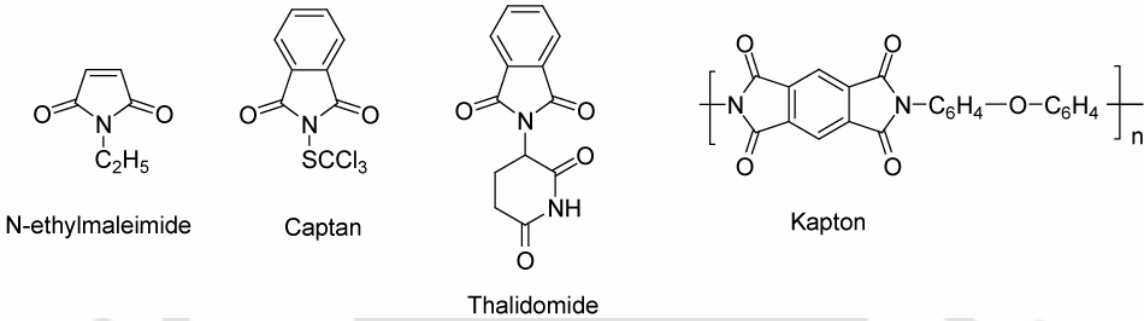

1.2 Synthesis of cyclic imides and their derivatives

The most important synthesis of cyclic imides, for example phthalimide; a simplest cyclic imide having an aromatic ring, is the dehydrative condensation of phthalic anhydride at high temperatures with primary amines, when the amine is available (Scheme 1.2). In the case of more sterically hindered amine, this condensation reaction is not very effective. Thus in such cases, the reaction of amine with phthaloyl chloride in presence of a base such as pyridine is used to prepare N-substituted phthalimides.[13]

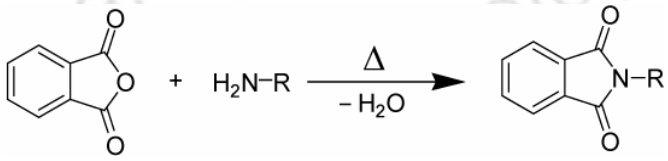

Scheme 1.2.

When the amine is not readily accessible, the direct N-alkylation of phthalimides with alcohols under Mitsunobu condition and of potassium phthalimide with alkyl halides (Gabriel synthesis) are popular alternative approaches to synthesize N-substiuted phthalimides (Scheme 1.3).[14-16]

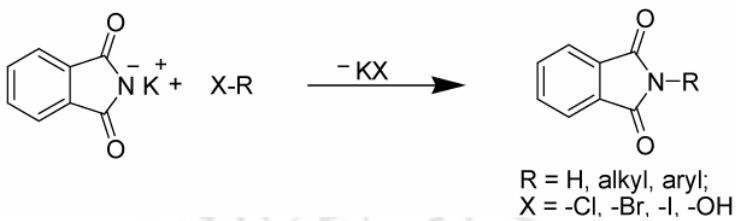

Scheme 1.3.

Reddy et al reported an economical and practical method for the synthesis of a wide range of imide derivatives under mild conditions. In this method, cyclic imides and analogous compounds were synthesized in the presence of zinc bromide and hexamethyldisilazane (HMDS; also known as bis(trimethylsilyl)amine) under refluxing conditions (Scheme 1.4).[17]

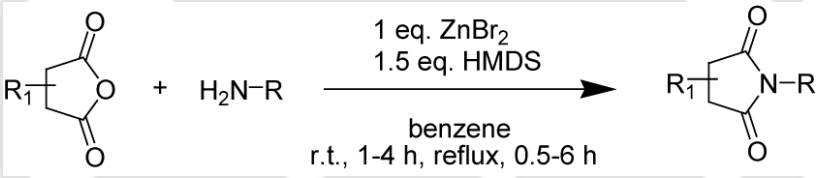

Scheme 1.4.

Synthesis of various cyclic imides from the corresponding anhydrides is reported by using $TaCl_5$-silica gel as Lewis acid under microwave irradiation (Scheme 1.5).[18]

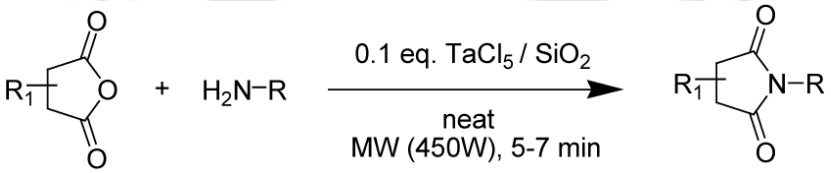

Scheme 1.5.

A convenient, efficient, and selective N-alkylation of N-acidic heterocyclic compounds with alkyl halides is accomplished in ionic liquids [Bmim]BF_4 or [Bmim]PF_6 in the presence of

potassium hydroxide as a base (Scheme 1.6). By this procedure, imides such as succinimide, phthalimide as well as indole, benzimidazole can be successfully alkylated.[19]

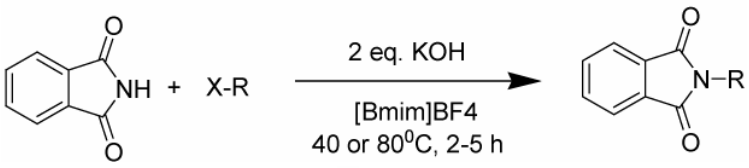

Scheme 1.6.

Phthalimide and analogous compounds can be N-functionalized by treating the parent imide with an allylic alcohol in the presence of triphenylphosphine (PPh_3) and diethylazodicarboxylate (DEAD) at room temperature (Scheme 1.7).[20,21]

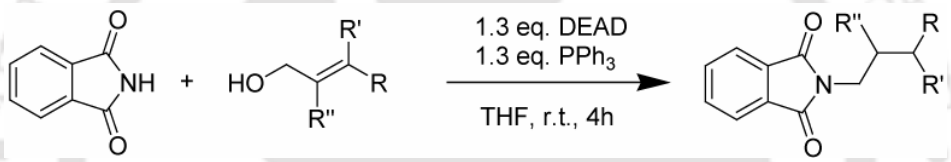

Scheme 1.7.

An efficient method to synthesize cyclic imides in high yields via cocrystal-controlled solid state synthesis between aromatic amines and anhydrides is also reported.[22] In this method, the cocrystals of the aromatic amines and anhydrides were prepared first by solvent drop grinding which were further converted to get desired imides by simply heating in the absence of solvent (Scheme 1.8).

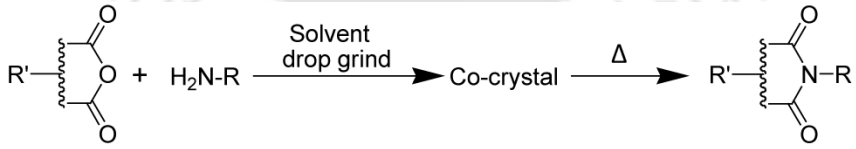

Scheme 1.8.

An environmentally benign synthesis of naphthalene tetracarboxylic acid bisbenzimidazole (NTCBI), perylene tetracarboxylicacid bisbenzimidazole (PTCBI) and similar benzimidazoles focused on limiting byproducts and waste, and minimal organic solvent use is reported

recently.[23] Various benzimidazoles were prepared using a solvent free green process based on heating carboxylic acid anhydrides and arylene diamines in the presence of zinc acetate in the solid state (Scheme 1.9).

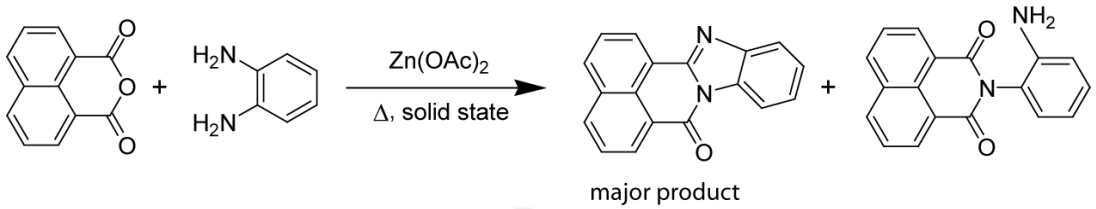

Scheme 1.9.

1.3 Deprotection of amine groups from N-protected cyclic imides

As mentioned in the foregoing discussion that cyclic imides can easily be synthesized by condensation reactions of primary amines with corresponding anhydrides and this process has significance in the protection of amine functionality. In peptide synthesis, the exhaustive substitution of primary amines is desirable to block both hydrogens and avoid racemization of the substrates. Imides are suitable protective groups for this purpose, such as tetrachloro-phthalimide, 4-nitro-N-phthalimides have been used as protecting groups to achieve the subtrates like aminoglycosides.[24] The imide derivatives can also be easily hydrolyzed to get back original amines, but beyond the most frequently used methods of hydrazinolysis and basic hydrolysis, there are only a few deprotection methods that are gentle and near-neutral, which is a drawback. The hydrolytic deprotection of N-substituted phthamides is usually very slow and is conveniently done by treating with hydrazine (Scheme 1.10). The reaction leads to the formation of parent amine and phthalylhydrazide.[25-27]

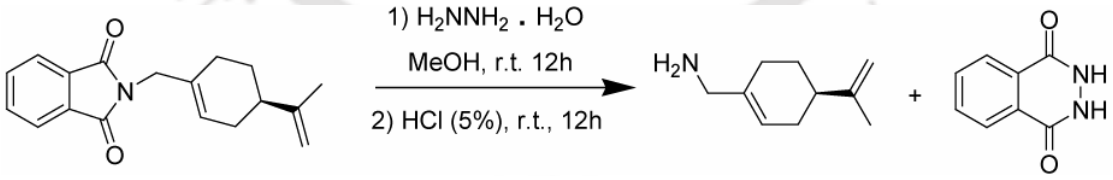

Scheme 1.10.

The synthesis of isomerically pure allylic amines, including farnesyl amine, is achieved in excellent yields using a modified Gabriel synthesis (Scheme 1.11).[28]

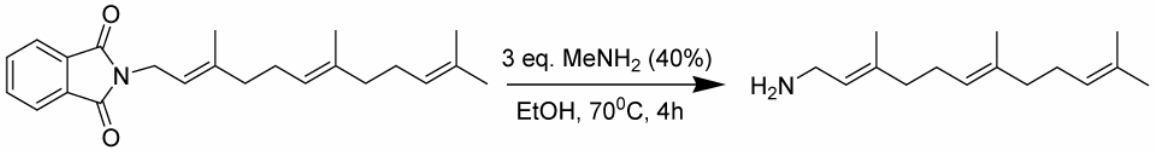

Scheme 1.11.

An efficient, two-stage, one-flask operation using $NaBH_4$/2-propanol followed by addition of acetic acid is reported to convert the phthalimides into primary amines (Scheme 1.12). Phthalimides of α-amino acids are smoothly deprotected with no measurable loss of optical activity in this method.[29]

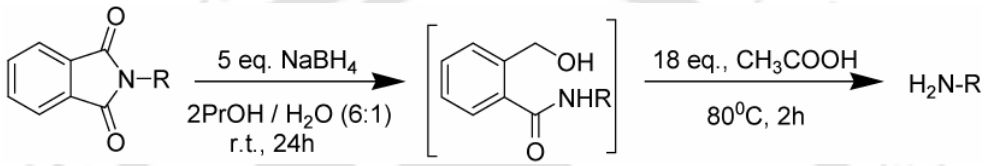

Scheme 1.12.

The nickel-mediated cross-coupling of phthalimides with diorganozinc reagents is reported recently which proceeds via a decarbonylative process to produce ortho-substituted benzamides in high yields.[30] In addition to tolerating diverse phthalimide functionality, including alkyl, aryl, and heteroatom containing substituents, the coupling of phthalimide with Et_2Zn was achieved in 96% yield with the use of stoichiometric $Ni(OAc)_2$ and bipy in dioxane at 95^0C (Scheme 1.13).

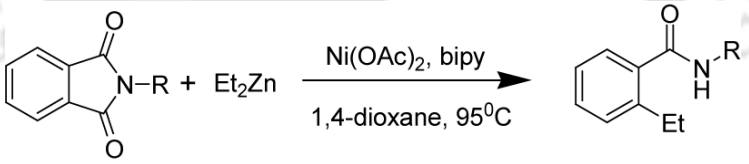

Scheme 1.13.

1.4 Photochemical and photophysical properties of cyclic imides

Phthalimide derivatives having electron-donating groups such as ethers, thioethers, amines, alkenes, arenes, and carboxylates as well as α-trialkylsilyl activated heteroatom-substituents show interesting photophysical properties.[31-33] Intra and intermolecular photoinduced electron

transfer (PET) reactions based on the phthalimide chromophores as the oxidizing species have been intensively studied during the last two decades.[34-45] These reactions can be efficiently applied for the synthesis of five- and six-membered ring heterocycles, medium-sized and macrocyclic products such as macrolides, cyclopeptides, crown ethers or thioethers as well as Grignard-alike products. Extensive studies begun in the 1970s by Kanaoka and coworkers, showing that phthalimides excited states participate in hydrogen atom abstraction.[46] In addition, irradiation of N-alkylphthalimides leads to preferential γ-hydrogen atom abstraction as part of N-heterocyclic ring-forming reactions.[47,48] As illustrated by photochemical transformations of the phthalimido-amines (**1.5**)[49] and phthalimido-thioethers (**1.6**)[50] (Scheme 1.14), the normal preference for γ-hydrogen atom abstraction is not adhered to in excited states of phthalimides which contain good electron donors in their N-tethers. In substrates that contain N-linked thioether and amine electron donors, photo induced single electron transfer (SET) dominates other pathways for excited-state decay, and it generates intermediate zwitterionic biradicals that serve as precursors of the heterocyclic products (Scheme 1.14).

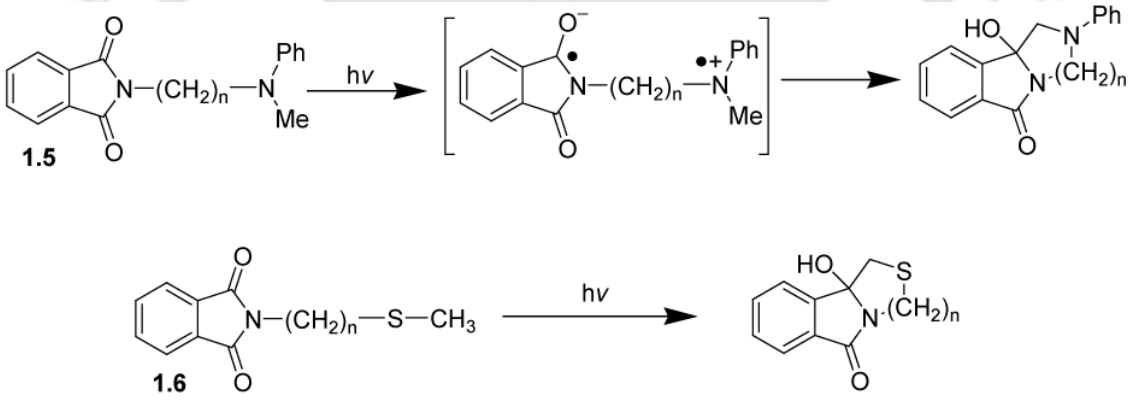

Scheme 1.14.

Another unique excited-state reaction, discovered by Kanaoka and his co-workers, is photodecarboxylation of N-phthalimido-α-amino acids (**1.7**; Scheme 1.15).[51] Upon irradiation in acetone, extrusion of carbon dioxide solely occurred from the α-position. The mechanism of α-decarboxylation has been intensively studied by Yoon et al.,[43] who proved that this process is initiated by hydrogen atom abstraction and further proceeds via azomethine ylide intermediates. These intermediates could be trapped by cycloaddition with carbonyl or alkene dipolarophiles and were additionally observed by laser flash photolysis studies.[35]

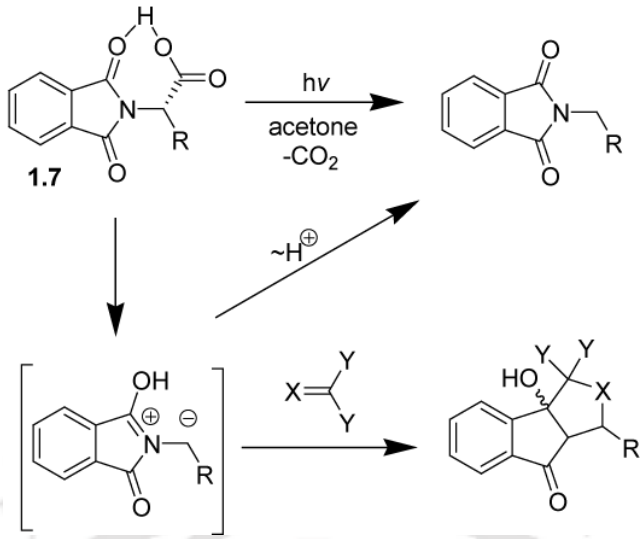

Scheme 1.15.

PET reactions of α-trialkylsilyl (TMS) methoxy substituted phthalimides (**1.8**) have also been intensively studied by Yoon and Mariano.[32] The presence of the silyl group additionally enhances the efficiency and regioselectivity of the subsequent photocyclization, and the yields and conversion rates were much higher if compared to the N-alkoxyalkylphthalimides.[45,47] The general mechanistic scenario is outlined in (Scheme 1.16). PET from the oxygen donor to the excited phthalimide leads to the formation of the corresponding radical ion pair. Solvent promoted silyl transfer, radical combination and hydrolysis yields the oxygen-containing macrocycle. This synthetic concept was expanded to a variety of novel and structurally complex heterocycles.

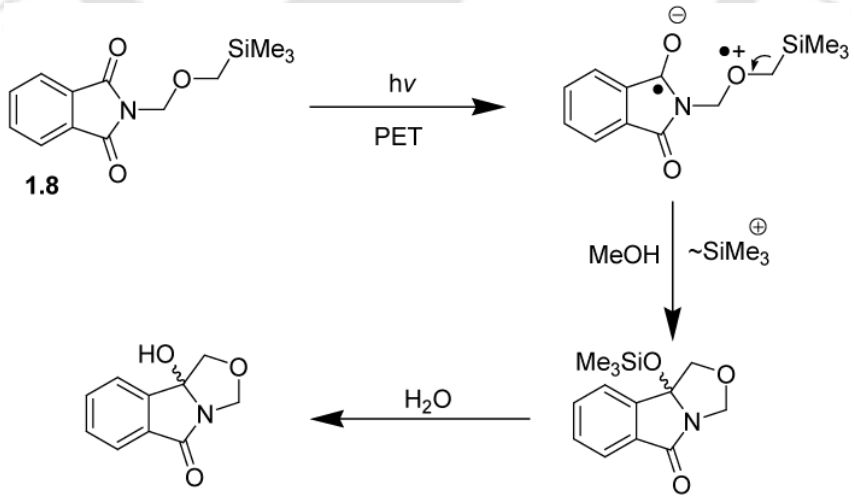

Scheme 1.16.

Efficient and regioselective photocyclizations were observed from α-trialkylsilyl methylthio-substituted N-alkylphthalimides (**1.9**).[52,53] The yields were moderate to high even for large ring targets (Scheme 1.17). Another powerful directing and activating group for PET reactions was the carboxylate group located in α-position to an electron-donating heteroatom.[54] Phthalimidoalkylsulfanyl acetates (**1.10**) were cleanly transformed into the corresponding tricyclic ring systems with high regioselectivities and in good to excellent yields of 60–98% (Scheme 1.18).

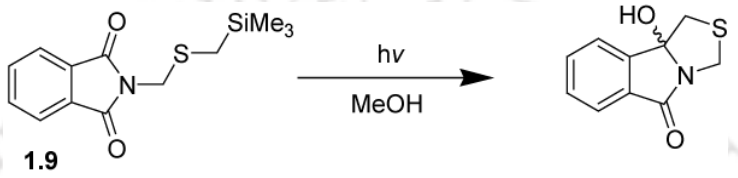

Scheme 1.17.

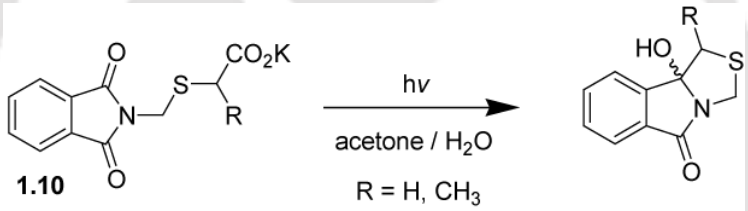

Scheme 1.18.

An interesting application of the intramolecular photocyclization of aminoalkyl-substituted phthalimides (**1.11**) was reported by Coyle et al. They used this method for the synthesis of tetracyclic protoberine[55] and yohimbane alkaloid skeletons,[56] respectively. Key-step in both cases was a PET cyclization followed by Brönsted-acid catalyzed retro-Mannich reaction[57] to give the corresponding isoquinoline derivatives (**1.12**; Scheme 1.19).

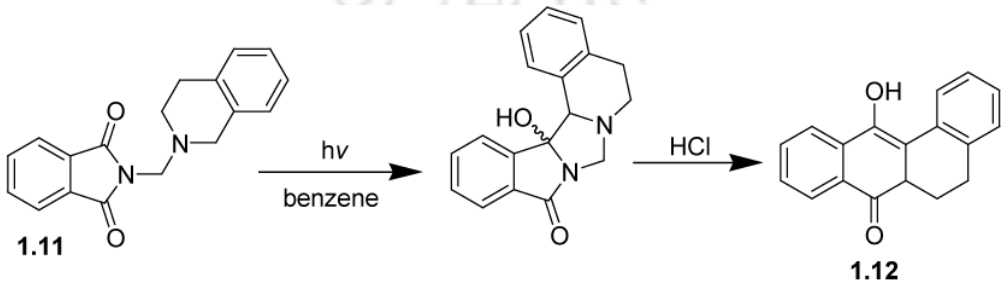

Scheme 1.19.

Compared to phthalimides, the photochemistry of their higher analogues (containing more than one aromatic ring), i.e. naphthalimides or naphthaldiimides has not received the same attention and consequently, the number of conducted photoreactions is rather small. Among these, photoinduced transformations with alkenes have been most researched. Their general reactivity is thus exemplarily shown in Scheme 1.20. Electron-deficient alkenes undergo insertion into the C(=O)–N bond via a formal $[\pi^2+\sigma^2]$ cycloaddition (path A), whereas electron rich alkenes may favor photoinduced electron transfer (PET) reactions (path B).

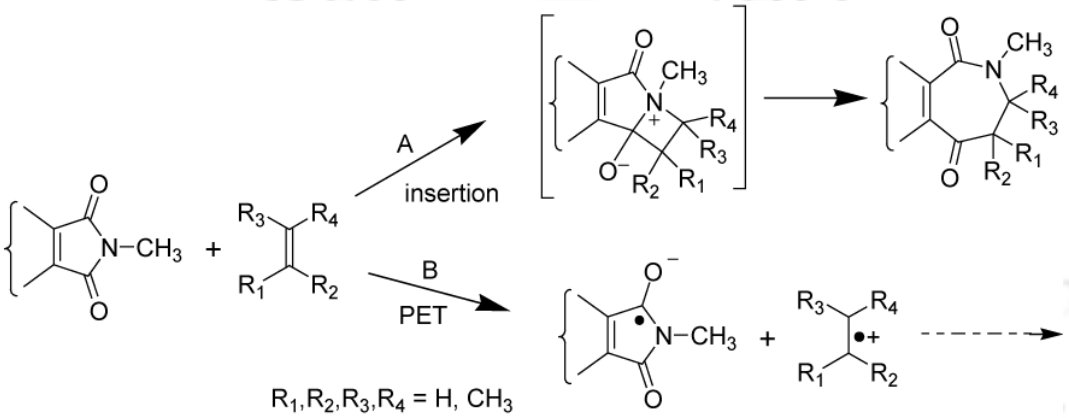

Scheme 1.20.

Photoreactions of N-methyl-1,8-naphthalimide (**1.13**) with substituted alkenes in benzene predominantly gave cyclobutane **1.14** through cycloaddition at the 1,2-position of the naphthalene ring (Scheme 1.21).[58,59] The cyclobutanes formed from the aliphatic olefins 2,3-dimethyl-2-butene and 2-methyl-2-butene and ethyl vinyl ether were unstable to heat or prolonged irradiation and decomposed (even at room temperature) back into the starting materials.

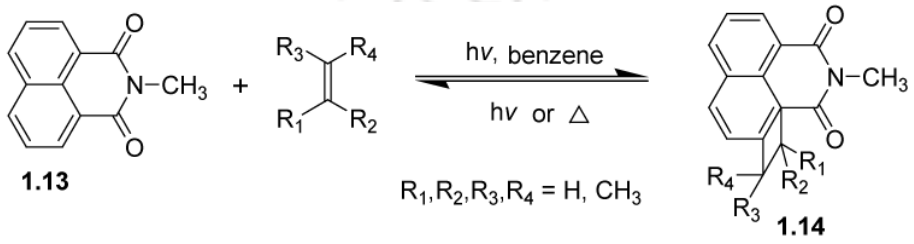

Scheme 1.21.

Yoon and coworkers demonstrated that N-trimethylsilylmethyl-1,8-naphthalimide (**1.17**) was converted into the simple desilylation product **1.13** when irradiated in either acetonitrile or methanol.[35,36,41] The presence of an azomethine ylide was proven via trapping experiments with acrylnitrile or methylacrylate. Subsequent γ-elimination yielded the corresponding naphthoindolizidines **1.18** (Scheme 1.22). Upon irradiation in acetone, however, no solvent trapping was observed and compound **1.13** was obtained instead.

Increasing the chain length led to the generation of a dimeric product (**1.20**), which was isolated in a yield of 17% (Scheme 1.23).[40] Its formation was explained through dehydration of the initially generated cyclic amidol, enamide-acyliminium ion coupling and subsequent addition of water. The transformation also operated in neat acetonitrile but was found to be much less efficient.

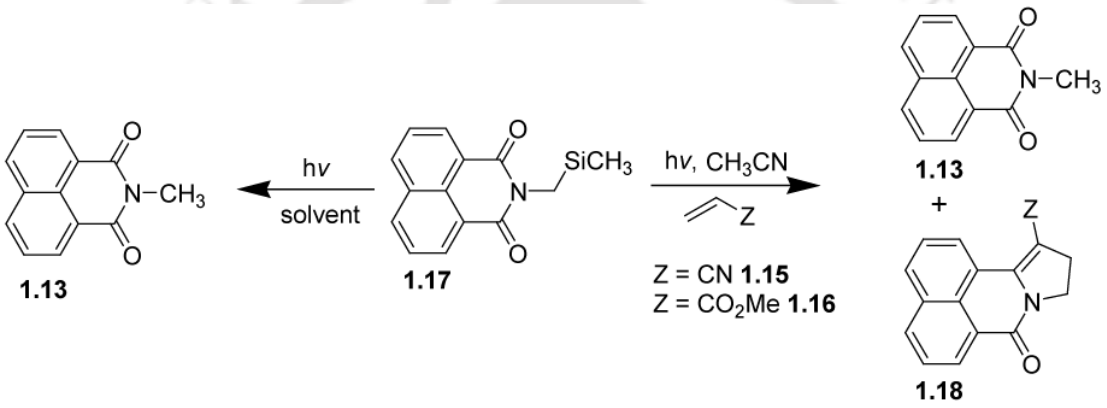

Scheme 1.22.

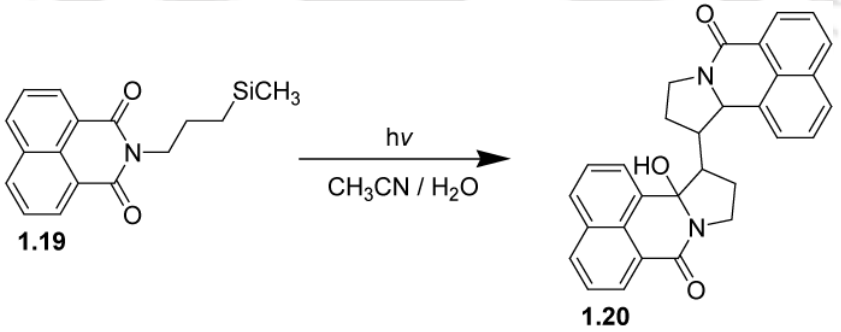

Scheme 1.23.

N-sulfonyloxy-1,8-naphthalimides (**1.21**) have been successfully applied as photoacid generators.[60-63] Homolytic cleavage of the N–O bond and acid release has been proposed to occur via the singlet excited state. In acetonitrile, decarboxylation and formation of

benzindolone (**1.22**) operated. In contrast, irradiation in ethanol furnished carbamate **1.23** instead (Scheme 1.24).[60] Likewise, N-carbamoyloxy-1,8-naphthalimides have been investigated as photobase generators, i.e. for the release of amines.[64]

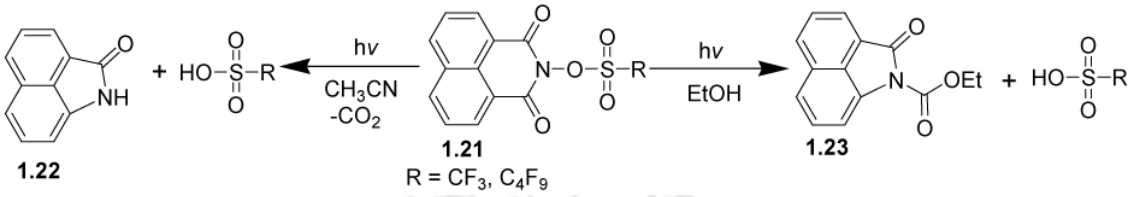

Scheme 1.24.

An intramolecular photocyclization reaction has been developed for the naphthalimides **1.24**.[65] Upon irradiation in dichloromethane, cycloaromatization followed by rapid radical induced 1,3-hydrogen transfer furnished dye compounds **1.25** in 30% yield (Scheme 1.25). The dimethylamino-derivative (**1.25**; R=Me_2N) is a potential NIR fluorescence imaging agent.

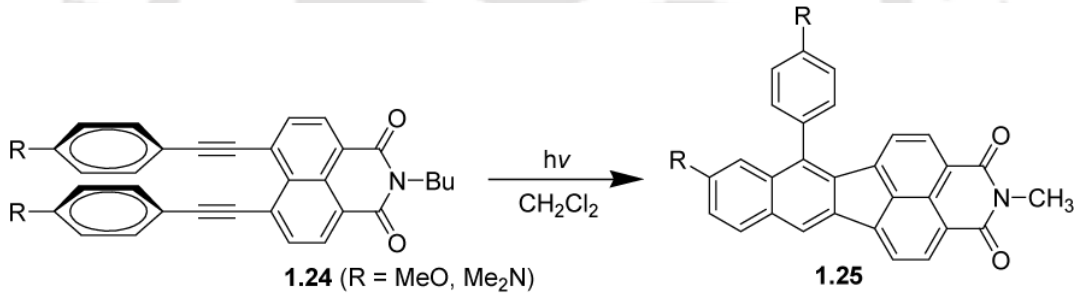

Scheme 1.25.

Photochemical transformations involving 1,4,5,8-naphthaldiimides are rare, which may be associated to their challenging synthesis and low solubility in most organic solvents. Within the context of photocleavage of DNA, Saito and coworkers have developed hydroperoxide **1.26** as an efficient photo-Fenton reagent. Upon irradiation in acetonitrile, hydroxylradicals were released via γ-hydrogen abstraction and the ester **1.27** was obtained quantitatively (Scheme 1.26).[66] In the presence of oxygen, the superoxide anion radical was furthermore detected and may consequently contribute to oxidative DNA damage.[67]

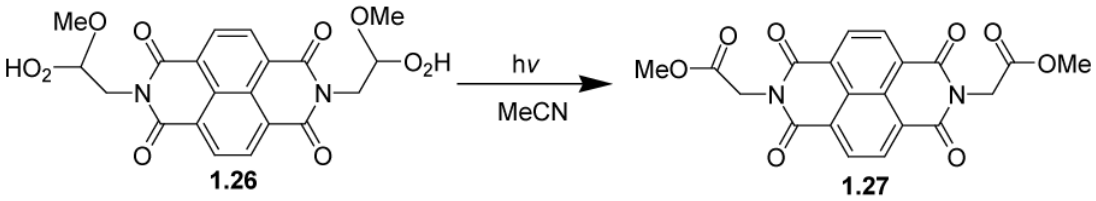

Scheme 1.26.

Photocleavage has been reported for naphthalene diimides **1.28** possessing carboxylate groups in their N-side chains.[68] Independent from the structure of the amino acid involved, the parent 1,4,5,8-naphthaldiimide (**1.29**) was obtained (Scheme 1.27).

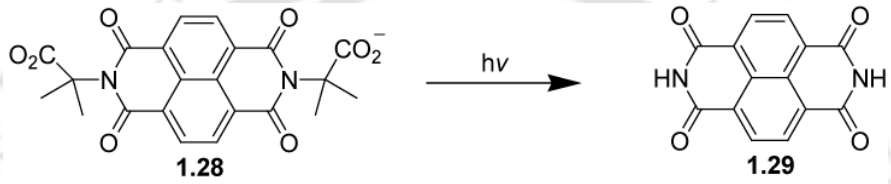

Scheme 1.27.

1.5 Cyclic imides as sensors for anions and cations

Due to its unique photophysical properties, the naphthalimide structure has found application in both cation and anion sensing to date. Its absorption and fluorescence emission spectra lie within the UV and visible regions, and the various photophysical properties can be easily fine tuned through judicious structural design. Synthetic modifications are readily accommodated on either the aromatic 'naphthalene' moiety itself, or at the 'N-imide site', allowing for varieties of functional groups and structural motifs to be incorporated.

1.5.1 Cyclic imide probes in anion sensing

The 1,8-naphthalimide-based structure where systems using ureas, thioureas and amides as hydrogen-bonding receptors, as well as charged receptors have been extensively used in the field of anion recognition and sensing in both organic and aqueous solutions, or within various polymeric networks, such as hydrogels. In the last decade, many excellent examples of naphthalimide-based anion sensors have been published, clearly demonstrating the versatility of this structure within this fast growing field of research.

In this context, Liu and Tian reported 4-benzoylamido-N-butyl-1,8-naphthalimide (**1.30**) as both colorimetric and fluorescent selective chemosensor which shows great promise for the

selective detection of fluoride ions in the presence of other halides even at low fluoride concentrations in a range of 20–100 μM in CH_3CN.[69] The striking colorless to yellow color change and blue to orange emission color change are thought to be due to the deprotonation of the 4-amino moiety of the naphthalimide fluorophore (Scheme 1.28). The obvious absorption and fluorescence variation upon the addition of fluoride ion can be observed both by the naked eye and by optical responses. Other halide anions such as Cl^- , Br^- , and I^- were found to hardly induce any variation in either the absorption or fluorescence spectra.

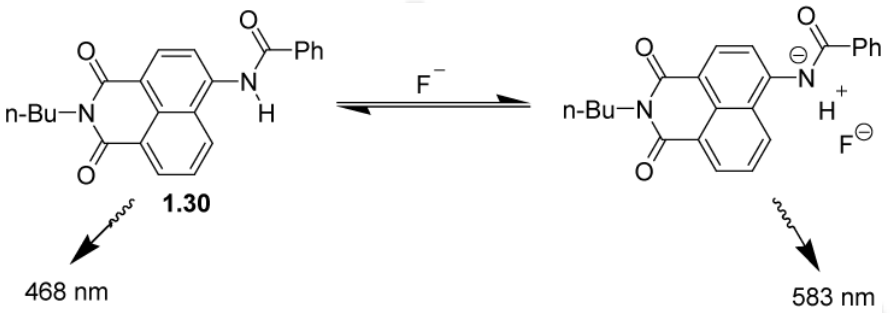

Scheme 1.28.

Gunnlaugsson et al reported design and synthesis of two fluorescent PET anion sensors (**1.31** and **1.32**) using simple diaromatic thioureas with a fluorophore naphthalimide moiety, based on the principle of 'fluorophore-spacer-(anion) receptor'.[70] Upon recognition of anions such as F^- and AcO^- in DMSO, the fluorescence emission of **1.31** and **1.32** was 'switched off', with no significant changes in the UV–vis spectra. This recognition shows a 1:1 binding between the receptor and the anions.

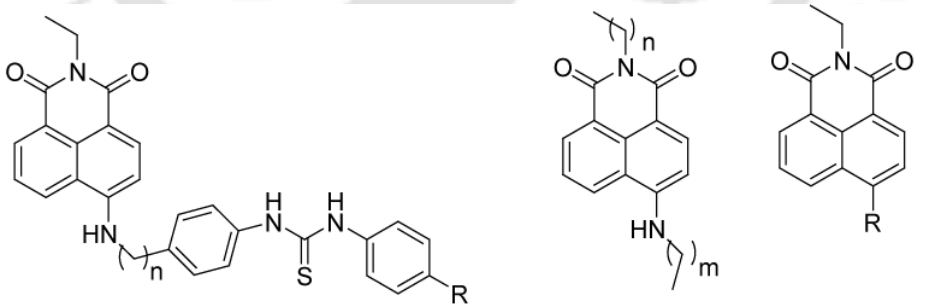

Further to this, Gunnlaugsson et al also reported some simple 4-amino-1,8-naphthalimide based chemosensors **1.33**, **1.34** and **1.36** which show striking green to purple colour changes due to the deprotonation of the 4-amino moiety on interaction with strongly basic anions such as F^-.[71]

These colour changes reverse gradually with time due to the fixation of atmospheric CO_2 (as HCO_3^-) yielding 1:1 adducts as demonstrated by X-ray crystallography.

The 4-amino-1,8-naphthalimide-based anion receptor **1.37** binds $H_2PO_4^-$ with 1:1 stoichiometry through cooperative hydrogen bonding to a naphthalimide N–H and thiourea N-H groups. [72] This was clearly established from ^{1}HNMR titration experiments in DMSO-d_6 where a substantial shift in the resonance for the naphthalimide N–H was observed concomitant with the change in chemical shift of N–H of thiourea upon successive additions of $H_2PO_4^-$. However, whilst ^{1}HNMR titration experiments indicate that **1.37** was capable of binding other anions such as acetate, the naphthalimide N–H does not participate and the N–H resonance was essentially invariant during the titration.

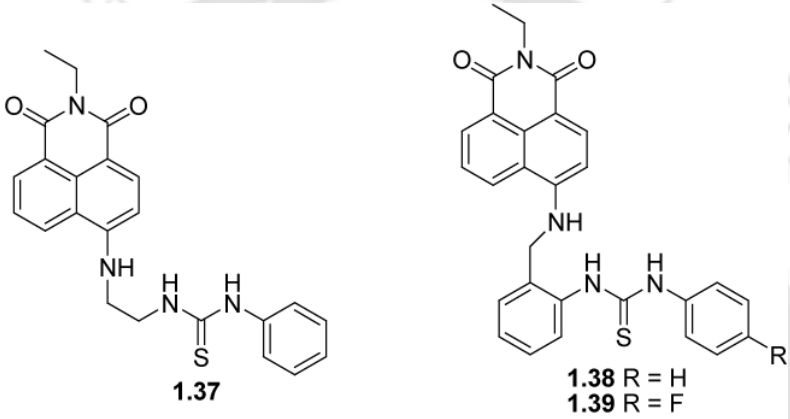

The receptor **1.37** was further modified to **1.38** and **1.39** by Pfeffer et al.,[75] and evaluated for the anion binding capabilities with $H_2PO_4^-$. The electron rich o-substituted amino benzyl amine spacer was introduced to facilitate pre-organisation and a phenyl receptor was also employed to increase the acidity of the thiourea N–H protons. Indeed, this design proved somewhat successful with cooperative binding of $H_2PO_4^-$ being observed for both **1.38** and **1.39**, as determined by ^{1}H-NMR titrations in DMSO-d_6. As anticipated, the binding constant for **1.38** was larger than that reported for the precursor **1.37**. However, only minor quenching of the fluorescence of **1.38** was observed (6.5% and 31% with $H_2PO_4^-$ and AcO^-, respectively). In contrast, the fluorescence emission of the fluoro-based receptor, **1.39**, was quenched by 36% and 59% after the addition of only five equivalents of $H_2PO_4^-$ and AcO^-, respectively.

Naphthalimide-based calixarene for anion sensing, **1.40**, was reported by Qian and Yoon et al[76] in which four hydrogen atoms are available in a hydrogen-bonding pocket to interact with anions. Upon titration with anions such as $H_2PO_4^-$, HSO_4^-, AcO^-, I^-, Br^-, and Cl^- in CH_3CN,

only quenching of the emission (490 nm) was observed for F^- . These changes were attributed to hydrogen bonding and consequent deprotonation, in which the latter was supported by the appearance of the HF_2^- triplet at 16 ppm in the ^{1}H-NMR spectrum of **1.40** in DMSO-d_6 upon titration with F^-.

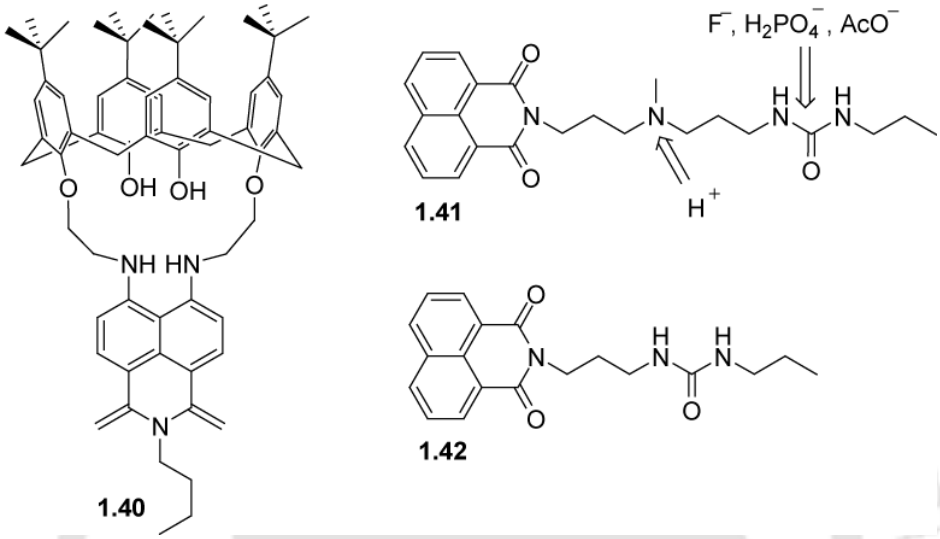

Pischel et al.[77,78] described the synthesis and photophysical characterisation of the fluorophore-spacer-receptor-spacer-receptor system, **1.41**, in which PET also occurs through the imide of the naphthalimide moiety in CH_3CN, upon interaction with cations and anions. Protonation of the amino group of **1.41**, with one equivalent of trifluoroacetic acid leads to a 20 times enhancement in the fluorescence of **1.41**, due to blocking of the PET pathway. In contrast to this, anion binding to the urea lead to the quenching of fluorescence emission by PET. Additionally, titration of mono protonated **1.41** with F^- lead to quenching of the emission and the simultaneous binding of cations and anions also resulted in quenching of the emission, most likely through electrostatic interactions between the protonated ammonium amine and the anions. Due to the observed fluorescence quenching of **1.41** by the amino function, binding constants were obtained by titrating **1.42** with various anions. Significant fluorescent quenching of **1.42** was observed and, hence, values for the 1:1 complexation of **1.42** with F^-, AcO^- and $H_2PO_4^-$, were determined by binding constants.

Naphthalene diimide (NDI) based probes have also been employed as fluorescent and colorimetric sensor for selective anion recognition. Recently, Guha and Saha reported the discovery of supramolecular interaction (anion-π and charge/electron transfer,CT/ET)

involving F^- ion and π-electron deficient colorless NDI receptor bearing bis-pyridyl group (**1.43**).[79] Strong electronic interactions between lone-pair electrons of F^- ion and π^*-orbitals of the NDI unit lead to an unprecedented $F^- \rightarrow$NDI ET event, which produces an orange colored $NDI^{\bullet-}$ radical anion. Further reduction of $NDI^{\bullet-}$ by another F^- ion produces a pink colored NDI^{2-} dianion, rendering NDI a selective colorimetric sensor for F^- ions over the various other anions (Scheme 1.29).

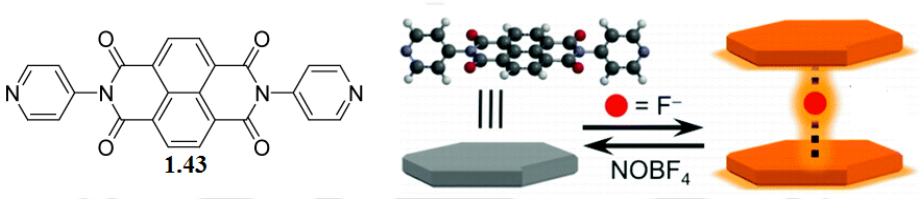

Scheme 1.29.

A highly fluorescent core-substituted naphthalene diimide sensor bearing a bis-sulfonamide group (**1.44**) is reported recently for selective anion sensing.[80] The compound shows a unique selectivity and reactivity for the F^- ions over other anions such as $H_2PO_4^-$, HSO_4^-, AcO^-, I^-, Br^-, and Cl^- in $CHCl_3$ by a two-stage deprotonation process leading to a colorimetric response. In DMSO solution, the sensor is shown to be highly selective for fluoride ($Ka \sim 10^6$ M^{-1}) over other anions with more pronounced changes in absorption characteristics (Scheme 1.30).

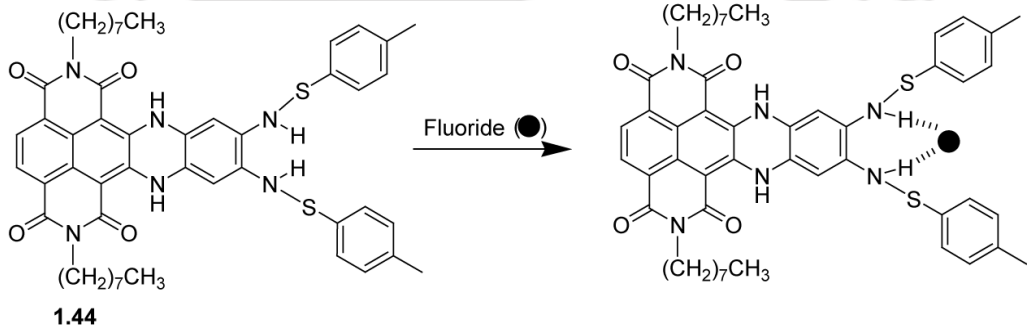

Scheme 1.30.

1.5.2 Cyclic imide probes in cation sensing

The 4-amino-1,8-naphthalimide derivatives are usually found to be highly emissive in organic solvents such as dichloromethane and chloroform, with quantum yield often being reported to be close to unity; while in water, significant quenching is observed. Nevertheless, the use of 4-aminonaphthalimide for sensing of cations in water is well established. Sensors **1.45-1.50** are just a few recent examples where the receptors are connected to the fluorophore via the amino functionality of the aryl ring. In these, depending on the design principles employed, the naphthalimide absorption and emission spectra were highly modulated upon binding of cations at the respective binding sites. Of these, **1.45** was developed for the sensing of H^+, where through an electron-transfer mechanism, the excited state of the naphthalimide is quenched

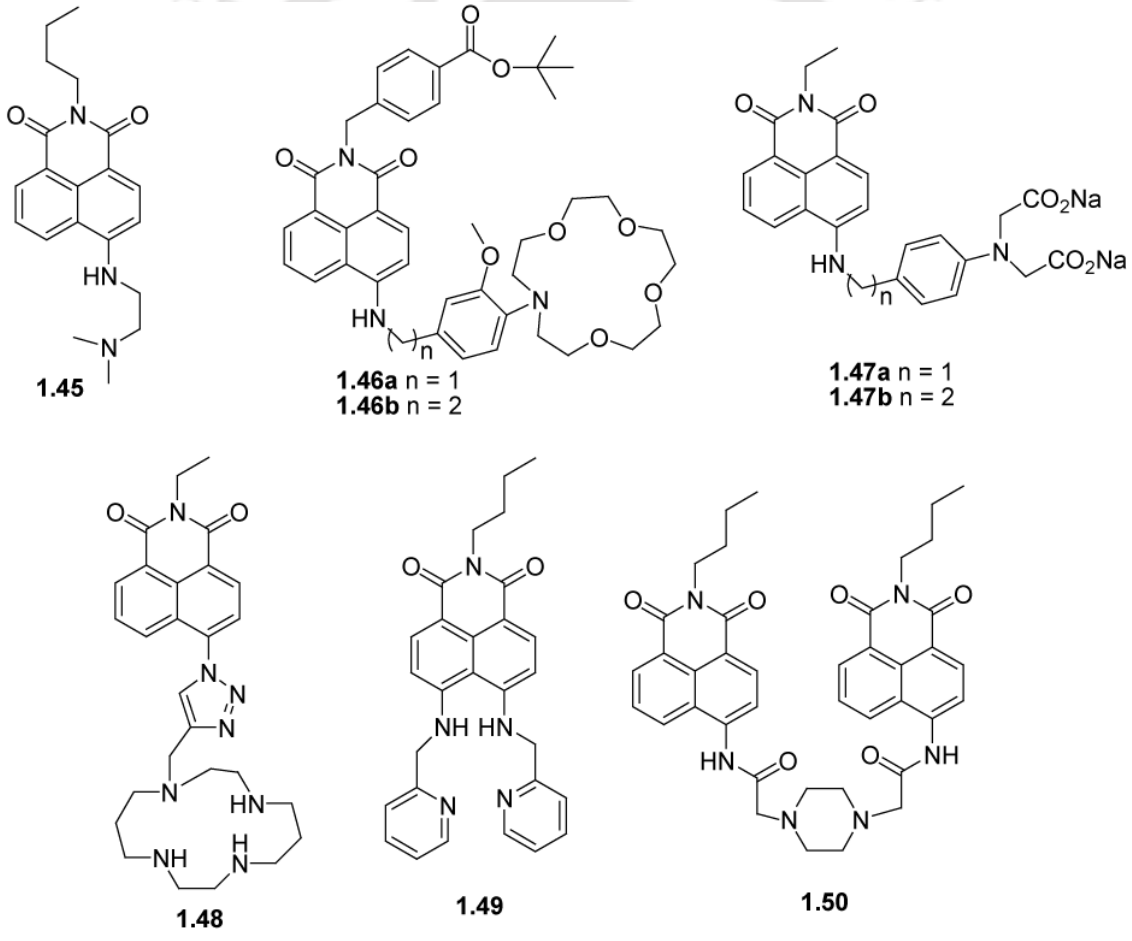

upon protonation of the tertiary aliphatic amine.[81] Many other examples of such pH dependent PET naphthalimide sensors have been developed to date, for use in solution or on solid supports.[82] In contrast, compound **1.46**, possessing a crown ether receptor was developed for

analysis of Na^+ in blood samples,[83] while **1.47**[84] and **1.48**[85] have been developed for detecting Zn(II). Compound **1.47** has also recently been used for imaging of bone structures using epifluorescence microscopy.[86] The Zn(II) sensors **1.47a** and **1.47b** are based on the fluorophore–spacer–receptor principle, and were shown to bind the Zn(II) ion in a highly selective manner at the iminodiacetate moiety in competitive media at pH 7.4; this increases the oxidation potential of the receptor, preventing photoinduced electron transfer quenching taking place from the receptor to the excited state of the fluorophore, and hence, this caused the naphthalimide fluorescence to be 'switched on'. Here, the 4-amino moiety does not participate directly in ion binding and hence, the absorption spectrum was not significantly affected. Similarly, large enhancements were seen in the emission spectra of **1.48**, developed by Watkinson et al,[85] upon binding to Zn(II). Recently, Watkinson et al, have extended their design to form naphthalimide dimers, using Cu(II) catalysed click chemistry.[87] In contrast, compound **1.49**, developed as sensors for Cu(II), where binding of Cu(II) engages the two aryl amines in the binding.[88] Hence, the absorption spectrum is significantly affected, and indeed so much so that the binding is visible to the naked eye; hence **1.49** is a colorimetric as well as a fluorescent sensor for Cu(II). Similarly, **1.50** showed large changes in the absorption and the emission spectra of the naphthalimide moiety upon sensing of Cu(II).[89]

Recently, Xu et al reported an amide-containing receptor for Zn^{2+}, combined with a naphthalimide fluorophore (**1.51**). The fluorescence, absorption detection, NMR, and IR studies indicated that **1.51** bound Zn^{2+} in an imidic acid tautomeric form of the amide/di-2-picolylamine receptor in aqueous solution, while most other transition metal ions were bound to the sensor in an amide tautomeric form (Scheme 1.31). Due to this differential binding mode, **1.51** showed excellent selectivity for Zn^{2+} over most competitive transition metal ions with an enhanced fluorescence (22-fold) as well as a red-shift in emission from 483 to 514 nm.[90]

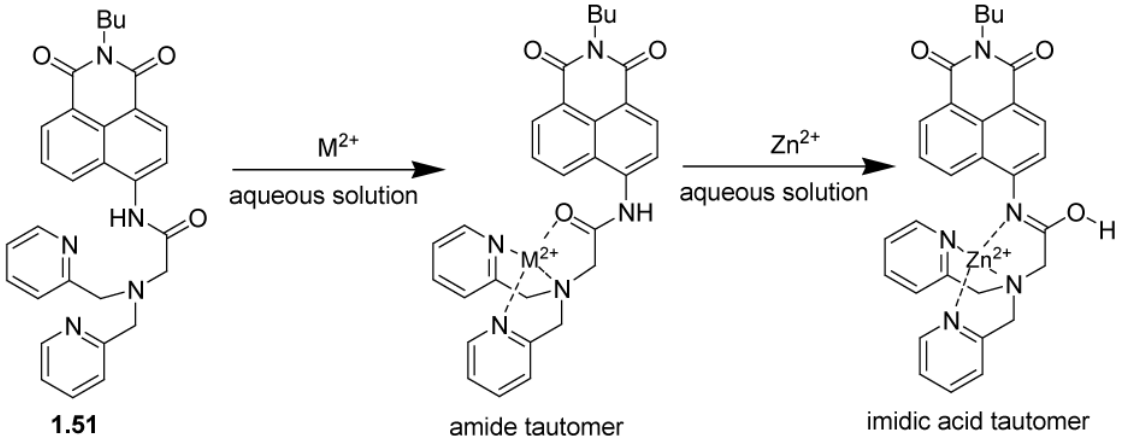

Scheme 1.31.

In chemosensor **1.52**, reported by the Qian group,[91] the receptor N,N-di-(2-picolyl)ethylenediamine (DPEN) was attached to the fluorophore through a benzene ring on the naphthalimide moiety using the virtually decoupled fluorophore–receptor linking strategy. The lone pair electron of the aniline nitrogen quenches the fluorescence of the excited fluorophore 4-aminonaphthalimide by the PET mechanism. When the electron-donating aniline nitrogen is complexed with Zn^{2+}, the PET process is blocked to get a 6-fold increase in emission. Xu et al. incorporated N,N,N′-tris(pyridin-2-ylmethyl)ethylenediamine (TRPEN) with N-substituted-4-bromo- 5-nitro-1,8-naphthalimide to develop a ratiometric chemosensor **1.53** for Zn^{2+}.[92] The capture of Zn^{2+} by the receptor resulted in the deprotonation of the secondary amine conjugated to 1,8-naphthalimide so that the electron-donating ability of the N atom would be greatly enhanced; thus **1.53** showed a 56 nm red-shift in absorption (507 nm) and fluorescence spectra (593 nm), respectively, from which one could sense Zn^{2+} ratiometrically and colorimetrically. Xu et al then extended the Zn^{2+} deprotonation mechanism to construct chemosensor **1.54** which can discriminate Zn^{2+} and Cd^{2+} by undergoing different intermolecular charge transfer (ICT) processes.[93] Cd^{2+} binding induces a blue shift in emission from 531 nm to 487 nm based on a general ICT mechanism, while Zn^{2+} binding produces a red shift in emission from 531 nm to 558 nm through the deprotonation-ICT mechanism.

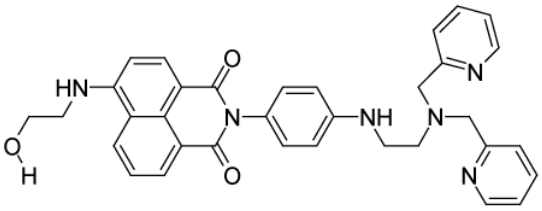

1.52

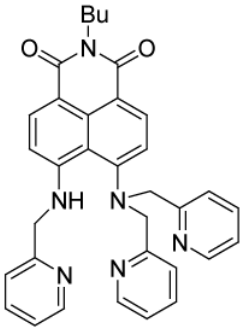

1.53

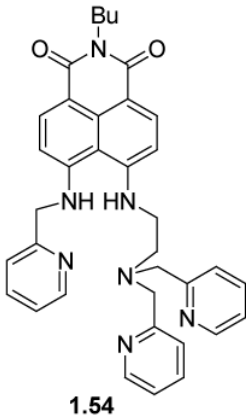

1.54

The development of naphthalimide based optical probes as fluorescent and colorimetric chemosensors for the detection of precious metal ions such as silver, gold and platinum ions has also been reported recently. Zhu and Qian et al described a fluorescent sensor **1.55**, based on the naphthalimide chromophore, exhibiting dual signalling behaviors for Hg^{2+} and Ag^{+} in ethanol–water solution at pH 7.14.[94] Upon the addition of Hg^{2+}, a 5-fold fluorescence enhancement and a slight blue shift in the emission maximum from 547 to 532 nm were observed while upon the addition of Ag^{+} ions, **1.55** exhibited a quenched fluorescence due to the intramolecular d–π interaction between the fluorophore and Ag^{+}. Two naphthalimide derivatives **1.56** and **1.57** were reported by Yoon and Spring et al. in 2010.[95] Compound **1.56** can detect Ag^{+} with a selective fluorescence enhancement (14 fold) in $CH_3CN–H_2O$ solution at pH 7.4. Furthermore, Ag^{+} could be detected at least down to 1.0×10^{-8} M, which suggested that **1.56** is a highly selective chemosensor for Ag^{+} with turn-on fluorescence in aqueous solution. On the other hand, the reference compound **1.57** without the carbonyl group does not show a strong binding with Ag^{+}, therefore proving that the carbonyl group positioned between the 1,8-naphthalimide and [15]aneNO_2S_2 plays a key role in displaying the selective fluorescence enhancement.

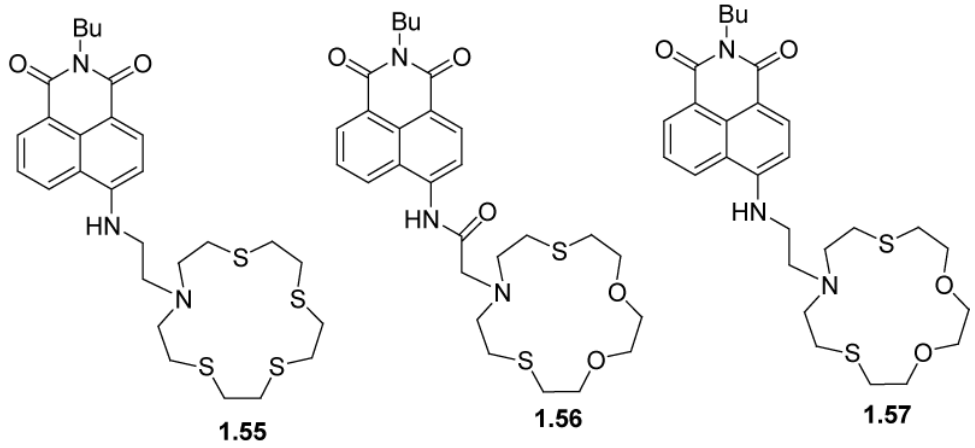

These examples are all based on the use of 4-amino-1,8- naphthalimide structures, where the focus has been on the detection of cations, but the 3-amino-1,8-naphthalimide structures have also been employed in such sensing, as demonstrated elegantly by de Silva et al.[96]

1.6 Supramolecular and host-guest chemistry of cyclic imides

One of the key goals of supramolecular chemistry is to assemble structural building blocks into regular arrays with new properties and emergent phenomena. Host–guest chemistry has tremendous potential to provide us with strategies with which to design and build these structures. Non-covalent interactions between π-donor and π-acceptor ring systems govern the self assembly of a variety of complexes and interlocked compounds in both the solid and solution state.[97] These interactions define and rule the self-assembly process that lead to the formation of molecular and supramolecular architecture and dynamic processes that occur within the self-assembled structures and superstructures. These new properties may improve our understanding of non-covalent interactions, or they may endow useful functionality. The structural and chemical properties make aromatic cyclic imides as ideal candidates for host-guest interactions in particular donor–acceptor charge transfer type complexes. It has been shown earlier from our group that 2-hydroxyethylphthalimide forms 1:1 adducts with 1,3-dihydroxybenzene and 1,3,5-trihydroxybenzene when co-crystallized from CH_2Cl_2-Et_2O using a stoichiometric amount of the 2-hydroxyethylphthalimide and the two phenols. Formation of supramolecular layered architecture in these adducts is described by charge transfer donor-acceptor interactions (Scheme 1.32).[98]

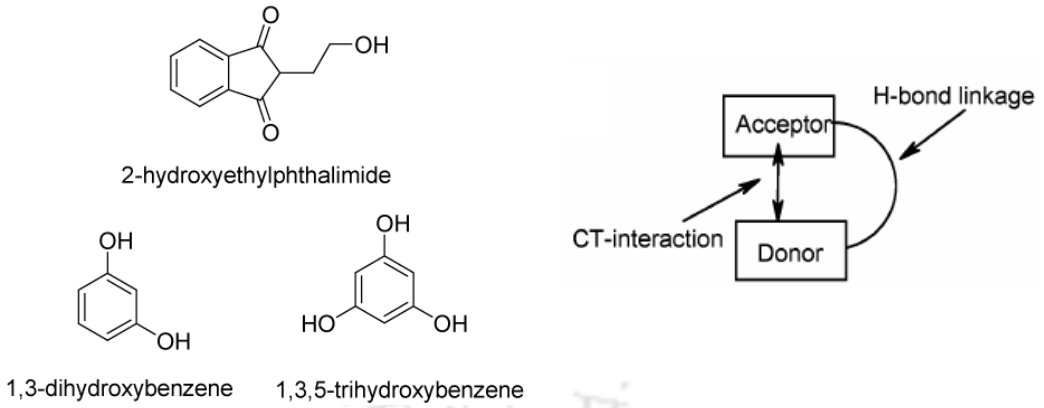

Scheme 1.32.

The electron deficient and aromatic nature of such imides is important for face-to-face aromatic interactions and their rigid, planar structure along with the ability to be functionalized with a wide variety of side groups to tune their properties; means that their assemblies have strong, well defined directionality in space. Cyclic imides have been widely studied with respect to host–guest systems such as intercalation,[99,100] foldamers,[101,102] ion channels,[103,104] catenanes[105,106] and rotaxanes.[107,108] Hydrogen bonding is the most predominant organizational tool in the construction of these supramolecular host-guest solids. Another interaction that is a recurrent motif in crystalline solids is π…π stacking between aromatic rings. It has long been established that the order of stability in the interaction of two π- systems is π-deficient ‒ π-deficient > π-deficient ‒ π-rich > π-rich ‒ π-rich.[109] In the past few years, Reger et al. have focused on exploiting the π…π stacking capabilities of the strongly π-deficient 1,8-naphthalimide group.[110-114] They have recently reported the formation of different types of supramolecular architectures (from 1D to 3D) in a series of molecules containing a carboxylic acid and a 1,8-naphthalimide group joined by different linkers (**1.58-1.63**).[115] Alternating hydrogen bonding of the carboxylic acids and π…π stacking interactions of the naphthalimide groups assembling the molecules into parallel chains that are linked into sheets by a second set of π…π stacking interactions (Figure 1.1).

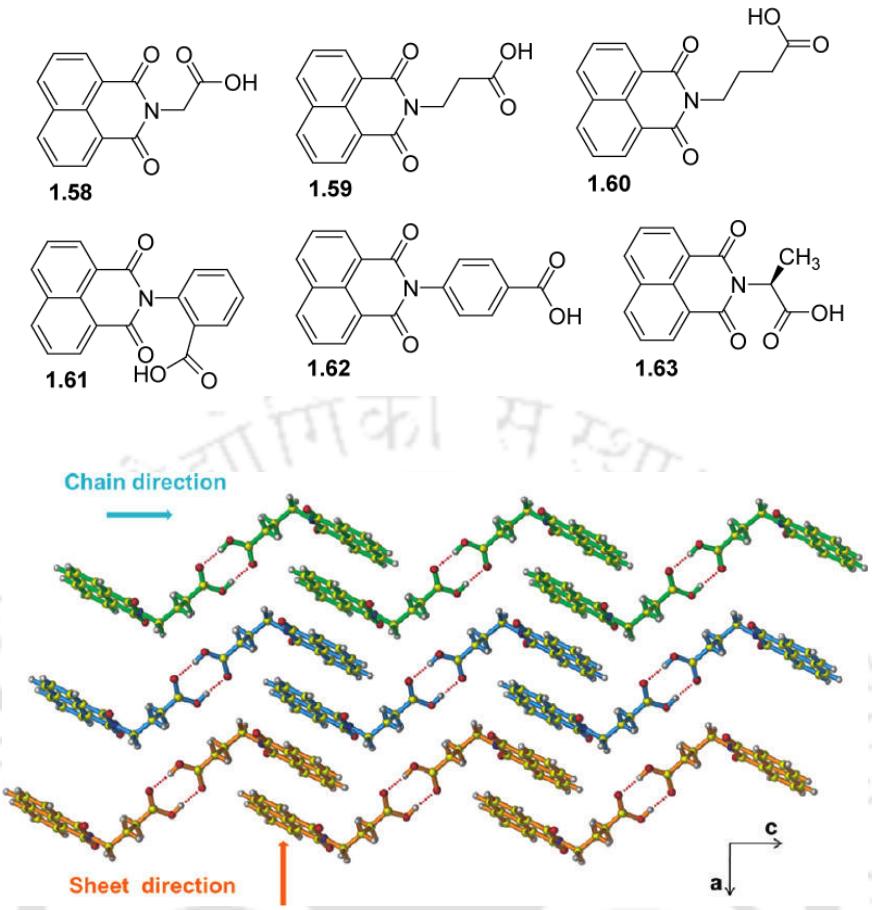

Figure 1.1: Structure of molecules **1.58-1.63** and formation of 2D sheets in the structure of **1.59**.

The role of less directional π-deficient ‗ π-rich stacking interactions in the formation of extended molecular assemblies has also been shown earlier by our group. It is reported that compound N,N´-bis(glycinyl)pyromellitic diimide (**1.64**) forms molecular complexes (**1.65-1.68**) with aromatic hydrocarbons such as anthracene, phenanthrene and perylene as well as tetrathiafulvalene.[116] In these complexes, a primary self-assembly is governed by the hydrogen bonding of the carboxylic acid groups assembling the host molecules into 1D zig-zag chains that are further linked into sheets by second set of π…π stacking interactions between the aromatic π-donor guest molecules and electron deficient π-acceptor units of host molecules (Figure 1.2).

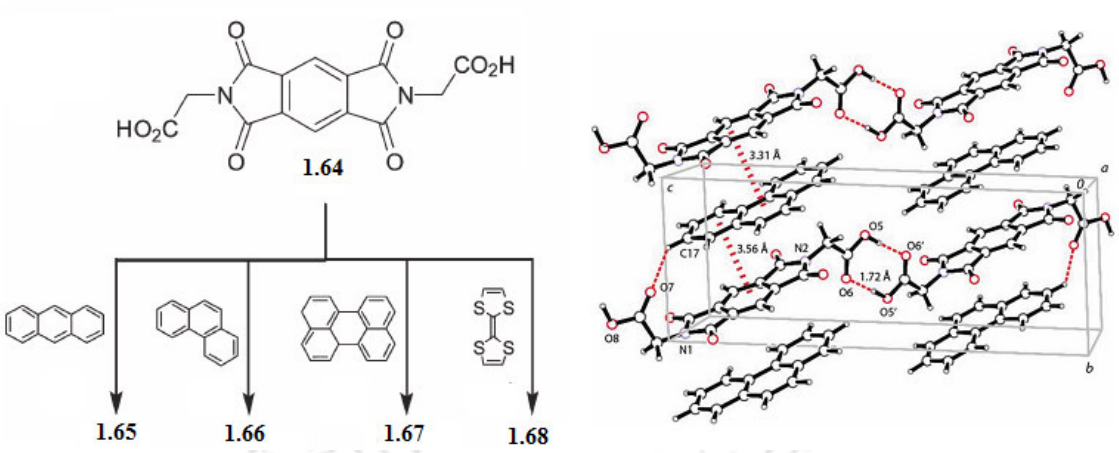

Figure 1.2: Formation of molecular complexes and weak interactions in the structure of **1.66**.

Further to this, Degenhardt et al reported a pyromellitic diimide tethered aromatic carboxylic acids atropisomer (**1.69**) as a conformationally imprinted receptor for molecular recognition.[117] When atropisomeric diacid **1.69** is heated in the presence of a ethyl adenine-9-acetate guest molecule, it rotates and coordinates with the guest molecule via hydrogen bonding. This results

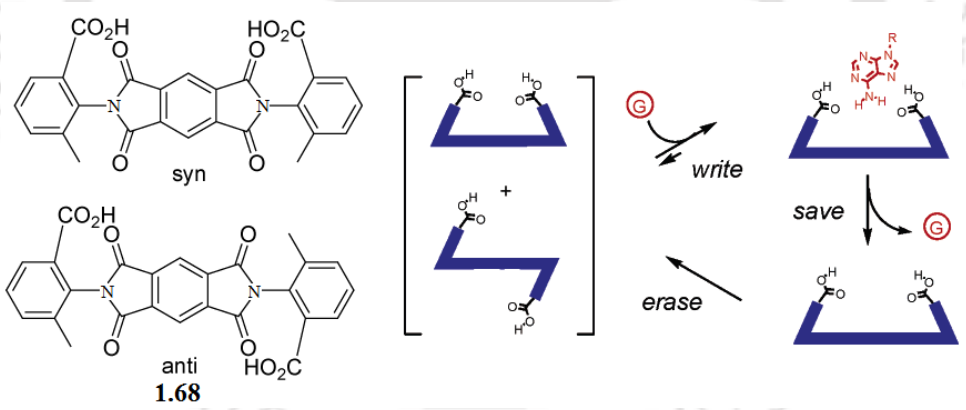

Scheme 1.33.

in an isomeric shift to the guest accommodating syn conformer. This complementary conformation is stable even upon removal of guest and lowering of temperature. The imprinted host can be returned back to its original state by heating in the absence of a guest (Scheme 1.33).

Rasberry et al developed a bispyridyl based pyromellitic diimide hydrogen bonding charge transfer (CT) receptor **1.69**, to demonstrate and study the origins of the excellent selectivity of the sensor against various aromatic diols.[118] Despite its low association constants of

(~10^1 M^{-1}), receptor **1.69** was highly selective forming CT complexes of varying color and intensity with different phenol and naphthol guests. The CT band can simultaneously report multiple characteristics about a guest such as size, recognition ability, and electronic structure.[119] The differences in the colorimetric responses are due to a combination of the abilities of the guests to form stable hydrogen-bonded complexes and the electronic structure of the guest (Scheme 1.34).

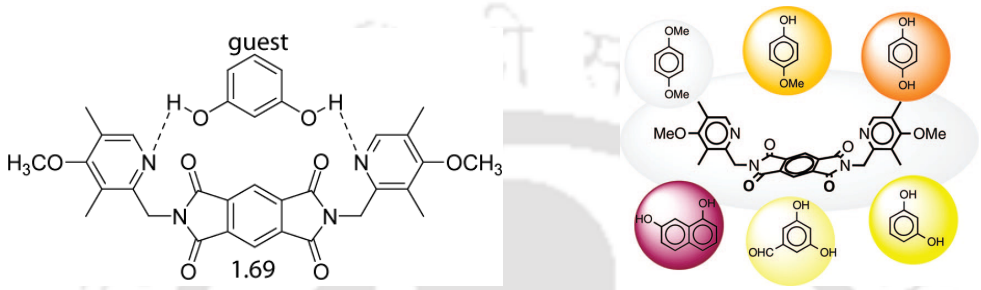

Scheme 1.34.

Shinkai and co-workers have described the features of a naphthalene diimide low molecular weight gelator **1.70** with utility in sensing the seven different positional isomers of dihydroxynaphthalene at millimolar concentrations by visible colour changes (Scheme 1.35).[120] Temperature-dependent spectral changes upon the addition of the dihydroxynaphthalenes indicate a mixture of π…π stacking and partial charge transfer interactions stabilizing the complexes. The NDI gelator **1.70** forms stable gels in some common organic solvents and shows a reversible sol–gel transition. It is important to note that solvophobic effects alone cannot explain the binding of the dihydroxynaphthalenes in the organogel matrix and hence this reorganisation process takes place.

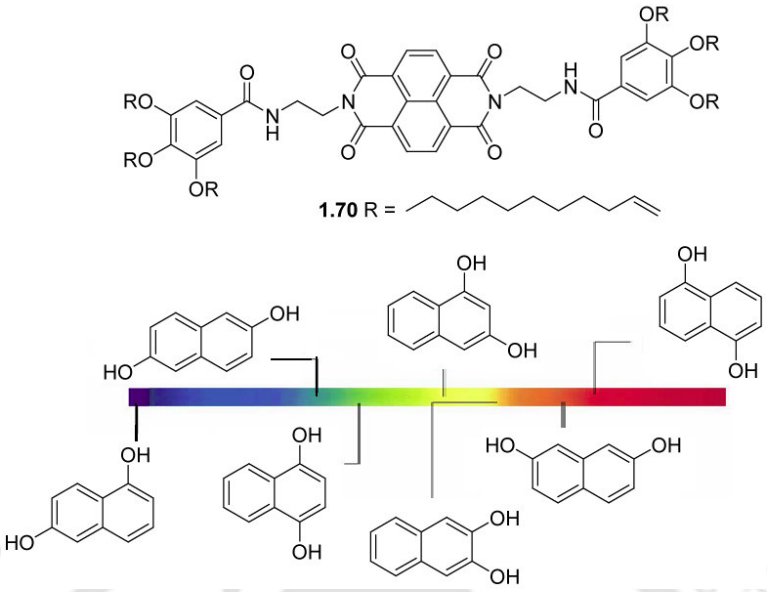

Scheme 1.35.

Colquhoun et al reported macrocyclic receptors which are accessible by cycloimidization of an amine-functionalized aryl ether-sulfone with pyromellitic dianhydride or 1,4,5,8-naphthalenetetracarboxylic dianhydride, **1.71** and **1.72**, respectively.[121] These receptors bind a wide range of electron-donor substrates via π-stacking donor-acceptor interactions. Addition of the π-electron donor molecules such as pyrene, perylene, 2,6-dimethoxynaphthalene, tetrathiafulvalene, and pyren-1-ol to solutions of the almost colorless **1.71** and **1.72** produced intense colors assigned to intermolecular charge-transfer absorptions, and ^{1}H-NMR spectra for equimolar ratios of receptor to substrate showed large ring-current-induced complexation shifts (Figure 1.3).

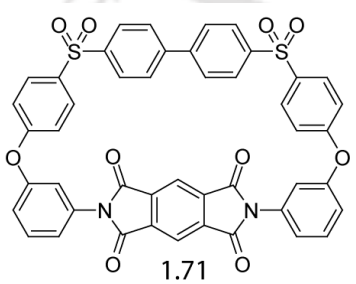

1.71

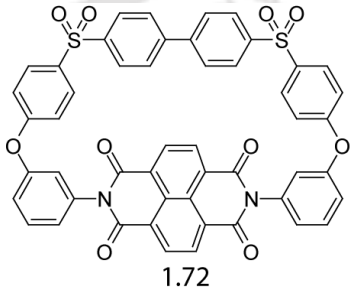

1.72

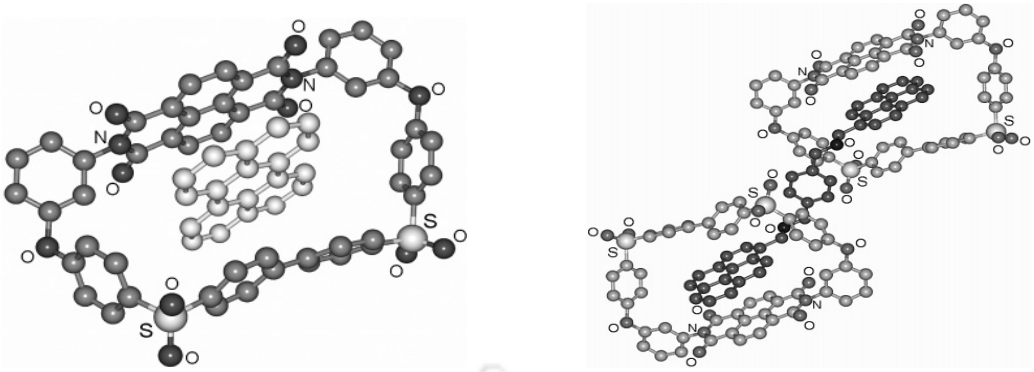

Figure 1.3: Structures of **1.71** and **1.72** and the complexes of **1.72** with perylene and pyrene guests.

Iwanaga et al reported a pyromellitic diimide based cyclophane-type macrocycles (**1.73**) as building blocks for the formation of tubular structures which encapsulate electron rich guest molecules like p-xylene and toluene.[122] The complex **1.74** (1:2 *p*-xylene) is reported as "cyclophane within cyclophane" that has been confirmed by X-ray crystallography whose driving force is a CT interaction (Scheme 1.36). In this structure, *p*-xylene guest molecule is arranged in a parallel fashion with the benzene ring of the facing pyromellitic diimide moiety which suggests the importance of a CT-type π…π interaction for the inclusion of guest molecule.

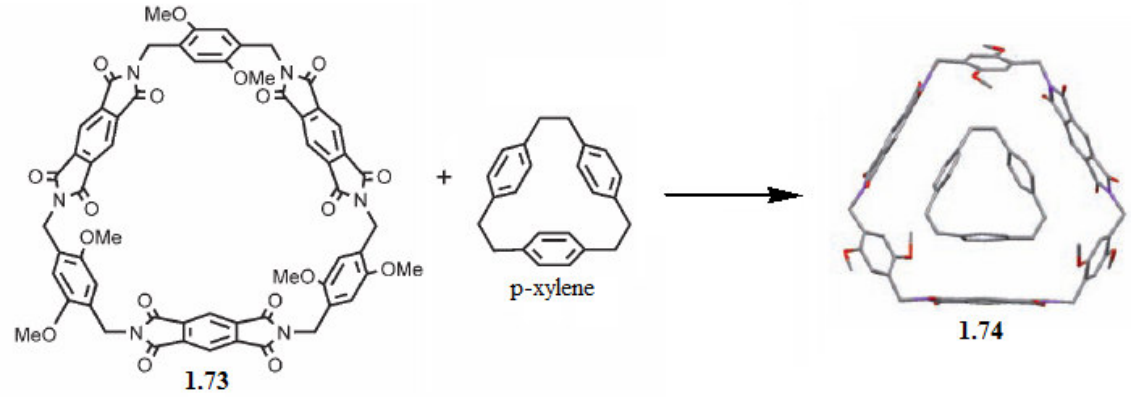

Scheme 1.36.

Self-assembly of naphthalene diimides (NDI) bearing carboxylic acid groups have also been shown to form cylindrical microstructures on the surface of solid substrates.[123] The hydrogen bonding between carboxylic acid termini combined with the hydrophobic contacts between the

NDI cores is mainly responsible for the formation of these supramolecular arrays. This approach has been evolved at a molecular level into hydrogen-bonded helical organic nanotubes by utilising the chirality in a series of NDIs containing chiral α-amino acid derivatives.[124] The chirality of such nanotubes is determined by the constituent amino acid but is independent of the nature of the side chains. Crystal structure of amino acid derivative of NDI (**1.75**) reveals that amino acid side chains adopt a syn geometry with respect to the NDI plane which allows carboxylic acid groups of three different molecules to interdigitate through two strong intermolecular hydrogen bonds assembling in a hydrogen bonded nanotubular supramolecular structure, in which NDI cores are coplanar with each other, forming the walls of the nanotube (Figure 1.4).

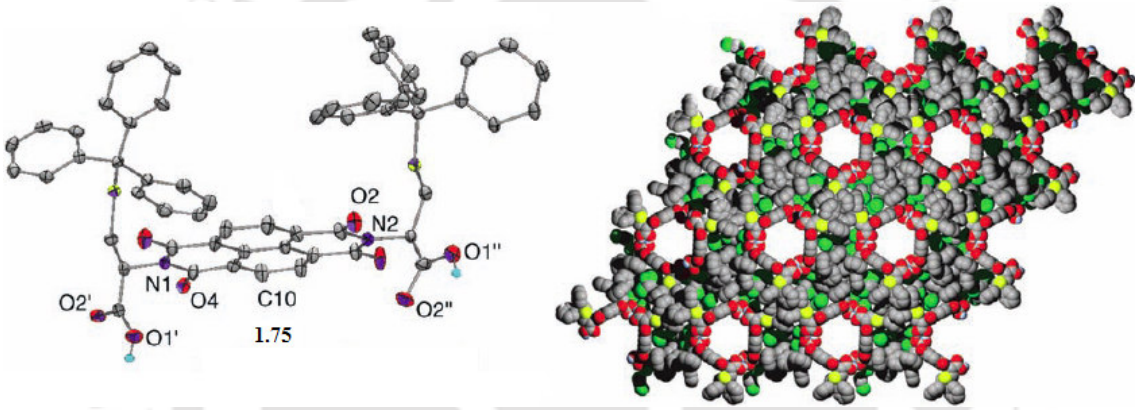

Figure 1.4: Formation of nanotubes in the structures of **1.75**.

1.7 Coordination chemistry of cyclic imides

Highly organized structures both with and without metal ions can be built partially or completely with supramolecular interactions, where "supramolecular" refers to the chemistry beyond the covalent bond.[125] A variety of supramolecular architectures have been synthesized with a large range of bonding forces; depending on the systems, the interactions can range from classic M-donor atom bonds, to strong halogen or hydrogen bonds to much weaker forces such as weak hydrogen bonds and π…π stacking of small aromatics. A fair amount of work has been devoted by Reger group in the construction of metal-organic frameworks (MOFs) using the strong π…π stacking interaction of the 1,8-naphthalimide group which leads to association into dimers of metal complexes in both solution and the solid state. They have demonstrated

synthesis of metal complexes built around the copper carboxylate dimer core by preparing ligands that contain both the carboxylate and the 1,8-naphthalimide group.[113] The substituted carboxylate compounds N-(3-propanoic acid)-1,8-naphthalimide (**1.59**) and N-(4-butanoic acid)-1,8-naphthalimide (**1.60**; also shown in previous subsection) produce the dimeric Cu (II) complexes in the presence of either pyridine (py) or 4,4´-bipyridine (bipy) containing the square $Cu_2(O_2CR)_4$ paddlewheel secondary building unit (SBU) structural motif. Strong π-π stacking interactions of the 1,8-naphthalimide groups organize these structures into sheets and into a 3D structure for $Cu_2(1.59)_4$(bipy), **1.76** (Figure 1.5).

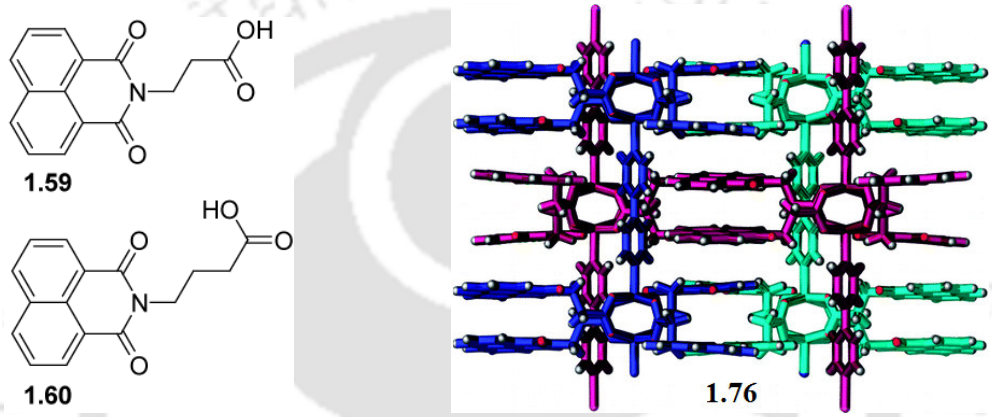

Figure 1.5: Two ligands **1.59**, **1.60** and a π…π stacked 3D structure of complex **1.76**.

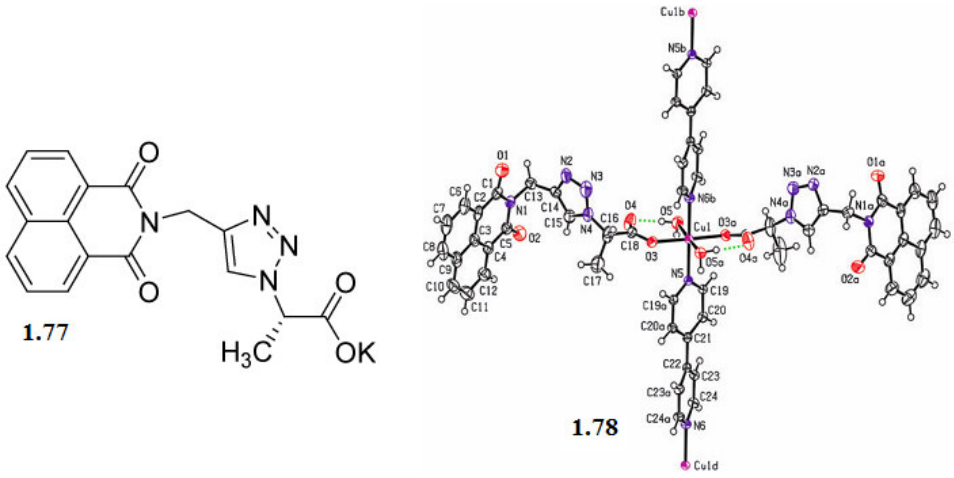

Figure 1.6: Structure of ligand **1.77** and its homochiral Cu (II) complex **1.78**.

Reger et al have also been reported a new trifunctional ligand, **1.77**, containing a carboxylate donor group, a homochiral center derived from L-alanine and a strong π…π stacking, 1,8-naphthalimide synthon, which has been used to prepare the copper(II) complex $[Cu(1.77)_2(bipy)(H_2O)_2].4.25H_2O$, **1.78**, that has a homochiral, helical, supramolecular metal–organic framework 3D structure, organized in one dimension solely by strong non-covalent forces (Figure 1.6).[126]

Recently, an enantiopure ligand built from connecting the π…π stacking 1,8-naphthalimide supramolecular synthon with L-asparagine, **1.79**, is reported to form tetrameric $[Cu_4(1.79)_8(py)(MeOH)]$, **1.80** (Figure 1.7). The methanol ligand, located in a chiral pocket, is replaced enantioselectively when exposed to racemic ethyl lactate vapor to yield $[Cu_4(1.79)_8(py)((S)$-ethyl lactate)], in a single-crystal to single crystal gas/solid transformation.[127]

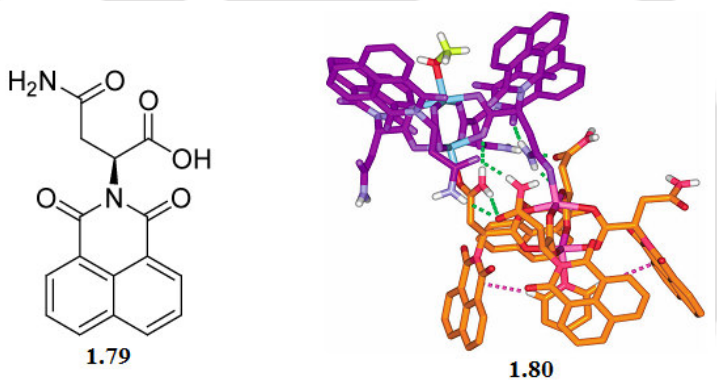

Figure 1.7: Structure of ligand **1.79** and its π…π stacked tetrameric Cu (II) complex **1.80**.

Trimellitic imide based transition metal complexes have potential application in the field of gas absorption. For example, Zaworotko et al reported a trimellitic imide analogue of nicotinic acid, **1.81**, which can be prepared in high yield using cocrystal controlled solid-state synthesis and sustains porous bcu nets when coordinated to Co(II), Ni(II), Cu(II), and Cd(II).[128] These isostructural porous metal-organic materials were studied in context of their hydrogen sorption properties. Crystal structure analysis of $\{Cd(1.81)_2(guest)_x\}_n$, **1.82**, revealed the formation of approximately 9.4 Å by 9.4 Å (van der Waals considered) square channels lined by the **1.81**'s two aromatic moieties in a centrosymmetric manner containing DMF and disordered nitrobenzene molecules (Figure 1.8).

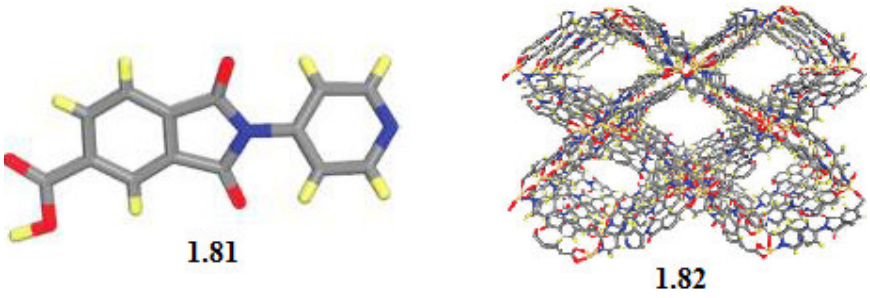

Figure 1.8: Structure of ligand **1.81** and 3D channel architecture of its Cd(II) complex **1.82**.

A phthalimide derivative of benzene-1,3- dicarboxylic acid, 5-(N-phthalimide)isophthalic acid (**1.83**), is reported to form two supramolecular isomers with [M_2(carboxylate)$_4$] paddlewheels to afford either a Kagomé lattice or NbO net, depending upon which solvent is used for the reaction (Figure 1.9).[129] Two isomers of formula $Cu_2(1.83)_2$.Solvent$_2$, one of which exists as a Kagomé lattice when diethylformamide (DEF) was used as solvent whereas another as an NbO net when dimethylacetamide, DMA was used, are reported.

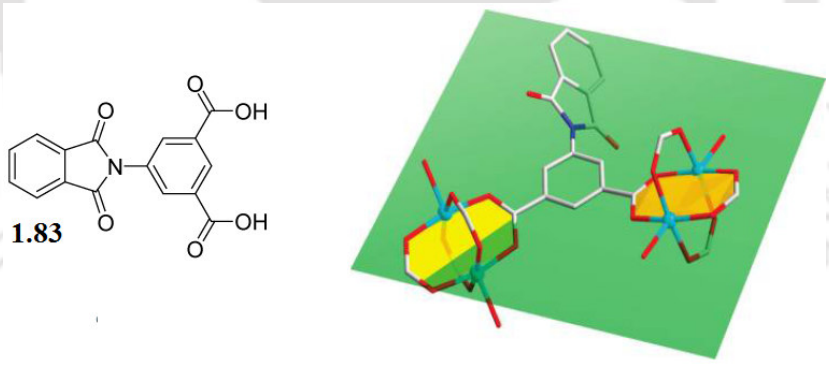

Figure 1.9: Ligand **1.83** and a paddlewheel unit in the formation of its two Cu(II) isomers.

Photoluminescence properties of coordination polymers of d^{10} metals have been studied widely which make them useful in view of potential applications as photoactive materials.[130] The metal complexation behaviour of various N-donor bispyridyl diimide ligands with spacers of varying flexibility and angularity is reported with d^{10} metals. In this respect, Kang et al reported Cd(II) metal complexes of two bispyridyl ligands, N,N´-bis(3-pyridylmethyl)-diphthalic diimide (**1.84**) and N,N´-bis(3-pyridylmethyl)-oxydiphthalic diimide (**1.85**; Figure

1.10).[131] The coordination polymers $[Cd(1.84)_{1.5}(NO3)_2]_n.nCHCl_3$ (**1.86**) and $[Cd(1.85)_2(NO_3)_2]_n.nEtOH$ (**1.87**) have either a 2D (6,3) brick-wall network with **1.84** or a 1D chain of layered double bridging units with solely angular **1.85**. The connection of the diimide moieties supplemented by the rich hydrogen bonding prevents interpenetration in 3D networks.

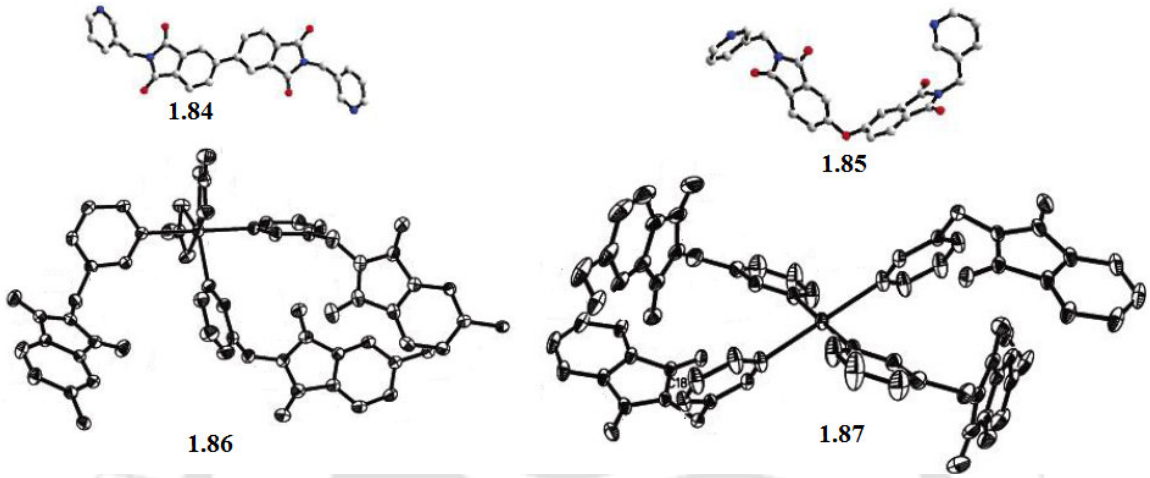

Figure 1.10: Structures of two ligand **1.84** and **1.85** and their Cd(II) coordination polymers.

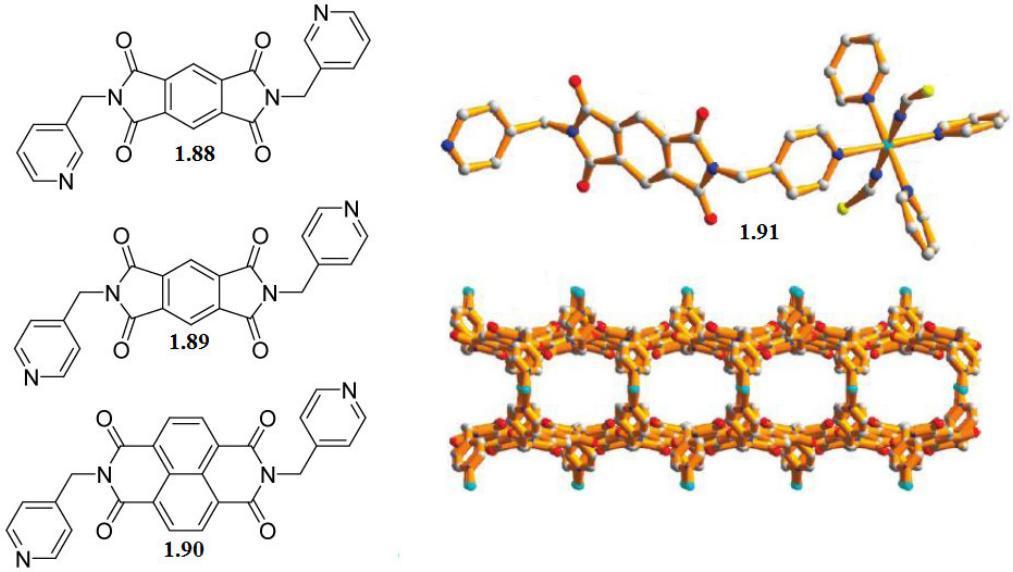

Figure 1.11: Structures of ligands **1.88**, **1.85**, **1.90** along with the Co(II) complex of **1.89**.

Recently, Li et al reported structural diversity in a series of Mn(II), Cd(II), and Co(II) complexes with pyridine donor diimide ligands, namely, N,N´-bis(4-pyridylmethyl)-pyromellitic diimide, **1.88**, N,N´-bis(3-pyridylmethyl)-pyromellitic diimide, **1.89**, N,N´-bis(4-pyridylmethyl)-naphthalene diimide, **1.90**.[132] A representative example of $\{[Co(1.89)_2(NCS)_2].3(HCCl_3)\}_n$, **1.91**, is shown in Figure 1.11, depicting the coordination environment and formation of channels between 3-fold interpenetrating diamondoid networks. The complex **1.91** shows a highly selective sorption behaviour toward CO_2, which can be a promising candidate as adsorbents for CO_2/N_2 separation.

Assembly of a 1D coordination polymer through in situ formation of a pyridine donor naphthalene diimide ligand by double C-C coupling on $CHCl_3$ under solvothermal conditions is also reported.[133] The original ligand, N,N´-bis(4-pyridylmethyl)naphthalenediimide (**1.92**), react with $Mn(CF_3CO_2).2H_2O$ and NaSCN in a CH_3OH-$CHCl_3$ mixture under solvothermal conditions, afforded red crystals of 1D coordination polymer (**1.93**), namely, $\{[Mn(NCS)_4(Lig)].2.5H_2O\}_n$, in which the new ligand (Lig) was formed apparently via a metal/ligand in situ reaction (Figure 1.12).

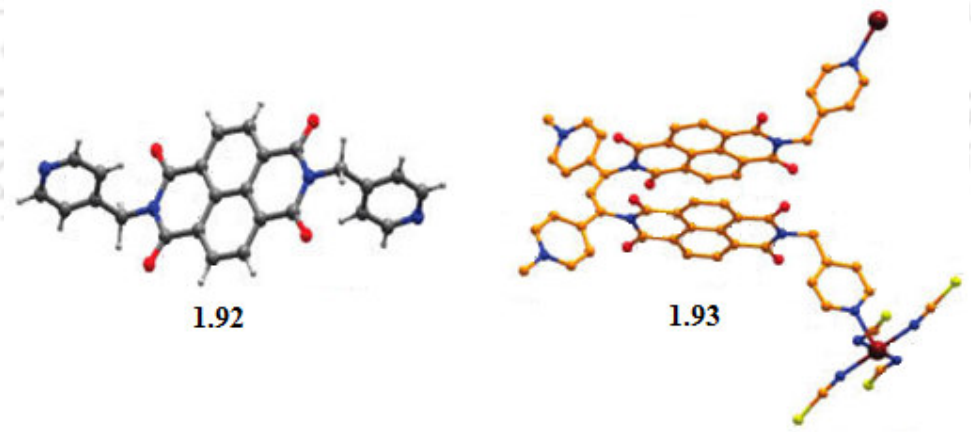

Figure 1.12: Structures of ligand **1.92** and Mn(II) coordination polymer (**1.93**) formed with a new ligand in situ reaction.

1.8 Pharmaceutical applications of cyclic imides

Naphthalimides, (1*H*-benzo[*de*]isoquinoline-1,3-(2*H*)-diones), consisting of a flat, π-deficient aromatic or heteroaromatic system, are a class of compounds known to have wide-ranging biological activities, such as antitrypanosomal activity,[134] analgesic activity,[135] sensor

activity,[136] photobiological activity,[137] serotonin 5-HT_{1A} and 5-HT_7 binding activity,[138] antinociceptive activity,[139] 5-HT_3 receptor antagonists[140,141] fluorescence probe[142] and antitumor activity against both murine and human tumor cells.[143-145] In particular, naphthalimide analogs have been considered as a promising group of anticancer agents by intercalating deoxyribonucleic acid (DNA), e.g., amonafide, mitonafide, bisnafide (DMP-840), and elinafide (LU-79553) have reached the clinical trials stage for the treatment of solid tumors and exhibited excellent antitumour activity against advanced breast cancer.[146-151]

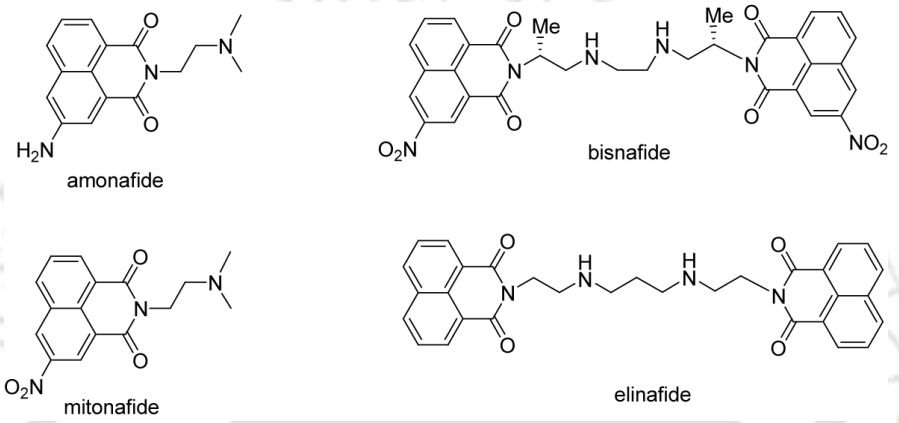

Recently, three excellent reviews have been described on naphthalimides, *i.e.*, Brana et al reported the synthesis and anticancer activity of naphthalimides,[152] Ingrassia et al provided detailed insight into the analysis of the mechanisms of action and clinical trials of naphthalimides as anticancer agents.[153] Min and Hui investigated the relationships between the structures of the naphthalimides such as mononaphthalimides, bisnaphthalimides, naphthalimide- heterocycle conjugates; and their antitumour activity in detail.[154]

Kamal et al reported DNA-binding ability and antitumour activity of pyrrolo[2,1 *c*][1,4]benzodiazepine–naphthalimide hybrids (**1.94**) with different alkylamide spacers. When the carbon chain increased from two to three, there was a substantial increase in the DNA-binding affinity.[155] Kamal et al further studied a series of pyrrolobenzodiazepine-naphthalimide conjugates tethered through a piperazine ring system, and evaluated for their anticancer activity against a number of cell lines.[156] These new conjugates exhibited very high DNA binding affinity and cytotoxic activity.[157] Some new coumarin linked naphthalimide conjugates (**1.95**) were synthesized and evaluated for the anticancer activity against selected human tumour cell lines of lung, breast, oral and prostrate cancers.[158]

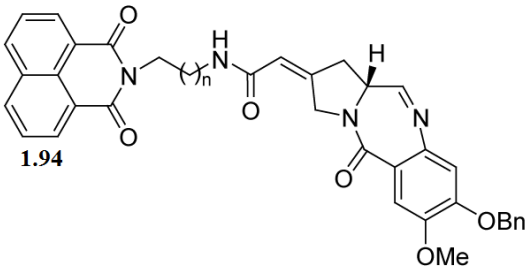

1.94

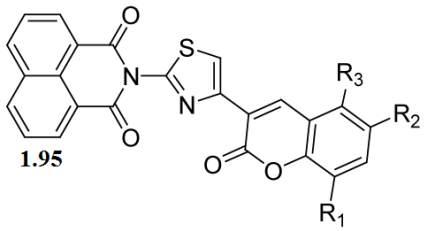

1.95

$R_1 = R_2 = R_3 = H$
$R_1 = OMe, R_2 = R_3 = H$
$R_2 = Cl, R_1 = R_3 = H$

1.9 Scope of the present work

Foregoing discussion has shown that cyclic imides have extensively been studied for various applications. They are important as protecting groups for the amine functionality and as optical materials. Various cyclic imides undergo photochemical reactions as photo induced single electron transfer (SET) with a wide variety of electron donors and also show environment sensitive fluorescence properties which can make them useful for biochemical studies. The dipolar nature and electron deficient properties of cyclic imides make them versatile for supramolecular and host-guest chemistry. They are useful materials for anion and cation sensing as well as for molecular recognition. The metal-organic frameworks constructed from imides containing pyridine and carboxylate groups have been recognized as photoluminescent material and selective gas adsorbent. Imide derivatives have also been used in pharmaceutical applications as a potential class of antineoplastic agents and as antifolate thymidylate synthase inhibitors.[159,160]

Further to this, molecular recognition of imides is of interest in chromatographic resolutions,[161] thymine receptors,[162] liquid crystals,[163] molecular tapes and sheet,[164] as well as theoretical[165] and experimental[166] evaluations of secondary effects in hydrogen bonding. For example, imide derivatives bind to adenine derivative and capable of extracting it in non-aqueous solvents like chloroform from water due to the complementary N-H···N and N-H···O hydrogen bonds between the receptor and the adenine derivative.[167] The self complementary hydrogen bonding in imides is also utilized in chiral chromatographic separation of heterocyclic drugs such as barbiturates, gluterimides and hydantoins.[168] A resorcarene derivative functionalized with phthalimide unit, self assembles through complementary N-H···N and N-H···O hydrogen bonds

and reversibly encapsulates different N-protected amino acid esters giving a method for enantio separation technique.[169,170] A poly-ureidophthalimide (**1.96**) is synthesized in a single condensation step, which folds into a chiral, helical architecture proved by circular dichroism spectroscopy.[171] The helix is sustained by virtue of intramolecular hydrogen bonding between amide N-H group of urea and the imide carbonyl group. The cooperativity of donor-acceptor interactions in the formation of zipper-shaped artificial duplexes (**1.97**) between electron rich 1,5-dihydroxynaphthalene or 1,4-dihydroxybenzene with electron deficient pyromellitic diimide units is reported and studied by ^{1}H-NMR binding investigations.[172]

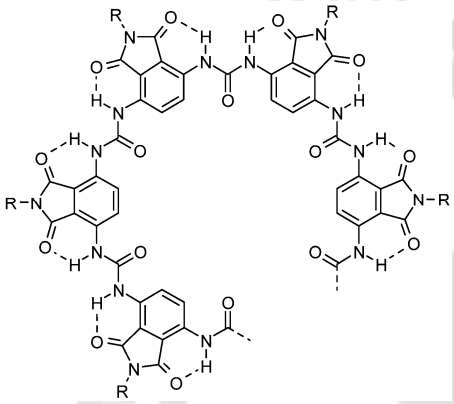

1.96

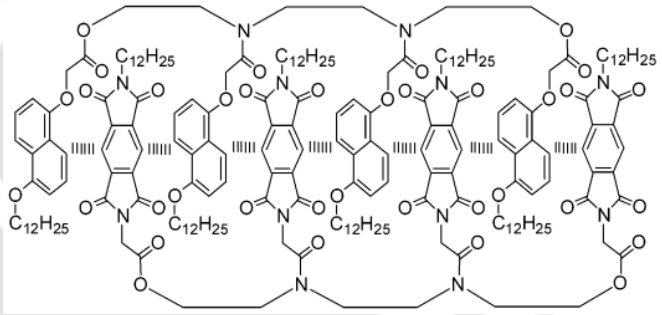

1.97

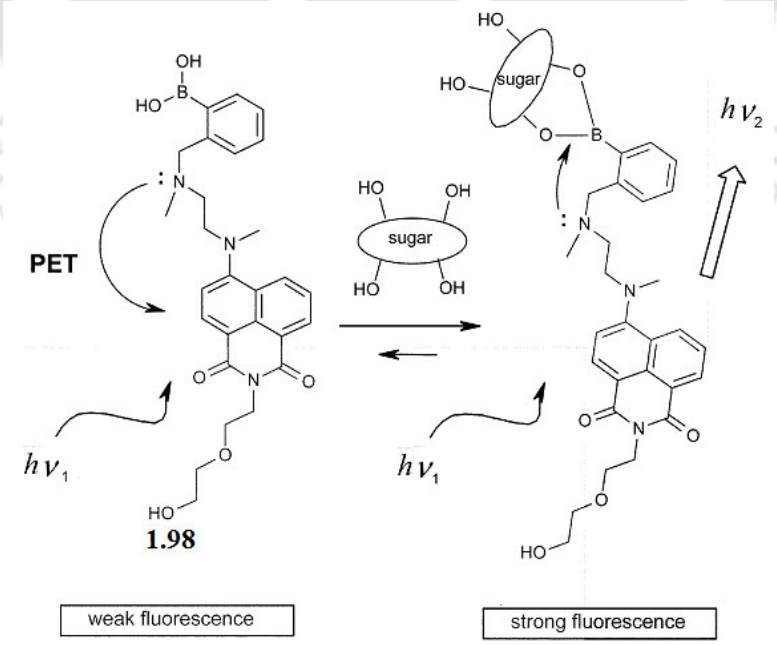

1.98

Scheme 1.37.

The optical sensing of naphthalimide derivatives is well known. In 1998, de Silva and coworkers[173] applied a naphthalimide dye to detect thiols *via* irreversible Michael addition and in 2002 Lakowicz and coworkers introduced N-phenylboronic acid derivatives of 1,8-naphthalimide for glucose detection.[174] Trup and coworkers presented an improved water-soluble fluororophore for the optical detection of saccharides by combining the functional naphthalimide core with the well-known ability of boronic acids to bind to the diol moiety of saccharides (**1.98**; Scheme 1.37).[175]

Core substituted naphthalene diimides (cNDI) are finding use in a range of biomimetic and bioinspired artificial systems including electron and energy transfer systems, in synthetic multifunctional pores and as transmembrane channels.[176-178] The bichromophoric models such as **1.99** have been synthesized for studying highly efficient fluorescence resonance energy transfer (FRET) (Scheme 1.38). Such photophysical processes are highly desirable for unraveling binding and folding events in biomaterials amongst others.[179]

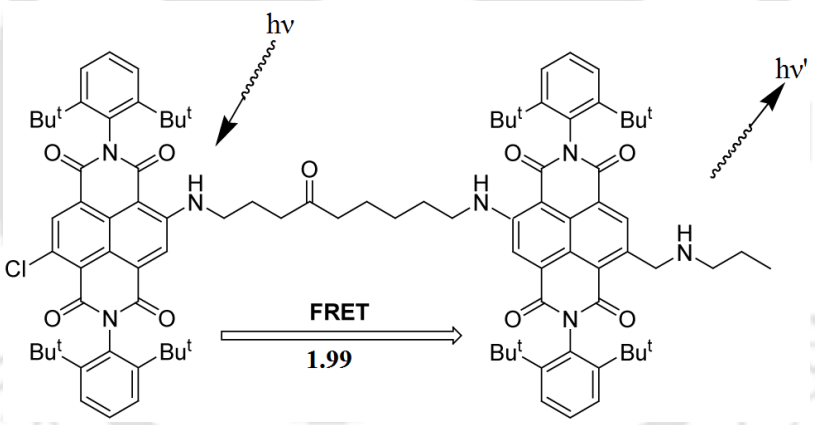

Scheme 1.38.

Naphthalene diimides applied as thin films on thiol-enhanced gold contacts as well as air-stable organic semiconductors with high electron mobility have been used in the fabrication of solution-cast n-channel field effect transistors.[180] Cyano cNDI semiconductors for air-stable, flexible and optically-transparent n-channel organic field-effect transistors have also been recently prepared with excellent results, comparable to that available using perylene dyes.[181]
Finally, metal ion coordination to such cyclic imides led to interesting supramolecular architecture in terms of their topology and dimensionality. Phthalimide protected dipeptide derived from glycilglycine is reported earlier to form β-pleated sheets in its transition metal

complexes.[182] Zaworotko and coworkers reported MOF based on the assembly of cubohemioctahedra as secondary building unit using rigid bezene-1,3-dicarboxylic acid tethered by naphthalene diimide units.[183] Naphthalimide based flexible homochiral and enantiopure ligands have also been reported recently to coordinate with metal ion in the formation of dimeric and tetrameric supramolecular assemblies which are supported by strong π…π stacking interactions.[126,127]

There is thus definite scope to study the supramolecular features of imide tethered functional groups for molecular recognition and host-guest chemistry. Looking at the potential of the cyclic imides in prospect of photochemical and photophysical properties; their ease of synthesis and readily accommodated synthetic modification which make them amenable for various applications such as anion and cation sensing, molecular recognition, supramolecular and host-guest chemistry and coordination chemistry; we have studied supramolecular features of various cyclic imides tethered carboxylic acids in the presence of organic guest or upon coordination with metal ions to obtain interesting supramolecular assemblies. In the present work, we have applied "bottom-up" approach to synthesize various cyclic imide derivatives. A variety of aspects of imide chemistry including host-guest self assembled networks, polymorphism, molecular recognition, organic gelation, solvatochromism and metal-organic frameworks are studied. A fair amount of work is devoted to understand the role of non-covalent interactions and properties of host-guest self assembled networks derived from cyclic imides. The nono-dimensional assemblies as well as selective host-guest binding may be the guiding factor for separation techniques and novel electronic properties. It may be expected that the structural variations in the extended networks of hydroxyl or carboxylic acid compounds can be brought about by anchoring such compounds to a dipolar unit such as phthalimide unit. Phthalimide has the ability to control weak interactions in host-guest systems

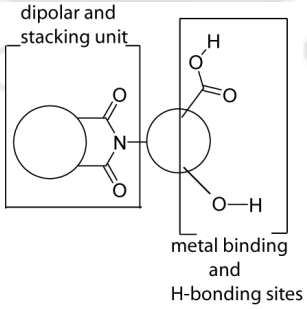

Scheme 1.39.

by participation of the carbonyl groups in hydrogen bond interactions coupled with dipolar interaction of the ring. The dipolar interactions controls π-stacking in the supramolecular assemblies of 1,8-naphthalimide compounds or it's metal complexes. Further, there is also a good amount of interest to use flexible carboxylate ligands for the synthesis of coordination polymers. For these reasons, we have chosen a few compounds which have phthalimide or naphthalimide units at one end and hydroxyl or carboxylic acid at another end (Scheme 1.39); to see the effect of dipolar interactions toward the tuning of structural patterns in the presence of organic guest molecules or metal centres. Therefore, we prepared some crystalline products as host-guest complexes or metal complexes from transition metal (II) salts with these compounds, whose structural features show the consequence of dipolar interaction in the packing of these complexes.

References:

(1) Challis, B. C.; Challis, J. A. *The Chemistry of Amides* (Ed: J. Zabicky), Wiley Interscience, New York, **1970**.

(2) Pinto, B. M. *Acyclic Organonitrogen Stereodynamics* (Eds: J. B. Lambert, Y. Takeuchi), VCH Publishers, New York, **1992**.

(3) Bennet, J.; Somayaji, V.; Brown, R. S.; Santrasiero, B. D. *J. Am. Chem. Soc.* **1991**, *113*, 7563.

(4) Greenburg, T.; Thomas, D.; Bevilacqua, C. R.; Coville, M.; Ji, D.; Tsai, J.-C.; Wu, G. *J. Org. Chem.* **1992**, *57*, 7093.

(5) Valat, P.; Wientgens, V.; Kossanyi, L. B.; Demeter, A.; Berces, T. *J. Am. Chem. Soc.* **1992**, *114*, 946.

(6) Baumstark, L.; Dotrong, M.; Oakley, M. G.; Stark, R. R.; Boykin, D. W. *J. Org. Chem.* **1987**, *52*, 3640.

(7) Kanaoka, Y. *Acc. Chem. Res.* **1978**, *11*, 407.

(8) Howard, K. A.; Koch, T. H. *J. Am. Chem. Soc.* **1975**, *97*, 7288.

(9) Gane, P. A. C.; Boles, M. O. *Acta. Cryst.* **1979**, *B35*, 2664.

(10) Barrett, D. M. Y.; Kahwa, I. A.; Mague, J. T.; Mcpherson, G. L. *J. Org. Chem.* **1995**, *60*, 5946.

(11) Wright, W. W.; Hallden-Abberton, M. *Polyimides in Ullmann's Encyclopedia of Industrial Chemistry*, **2002**, Wiley-VCH, Weinheim.

(12) Ackermann, P.; Margot, P.; Müller, F. *Fungicides, Agricultural in Ullmann's Encyclopedia of Industrial Chemistry*, **2002**, Wiley-VCH, Weinheim.

(13) Nicolaou, K. C. *Angew. Chem., Int. Ed.* **1993**, *32*, 1377.

(14) Mitsunobu, O.; Yamada, Y. *Bull. Chem. Soc. Japan* **1967**, *40*, 2380.

(15) Mitsunobu, O. *Synthesis*, **1981**, 1.

(16) Sheehan, J. C.; Bolhofer, V. A. *J. Am. Chem. Soc.* **1950**, 72, 2786.

(17) Reddy, P. Y.; Kondo, S.; Toru, T.; Ueno, Y. *J. Org. Chem.*, **1997**, *62*, 2652.

(18) Chandrasekhar, S.; Takhi, M.; Uma, G. *Tetrahedron Lett.*, **1997**, *38*, 8089.

(19) Le, Z.-G.; Chen, Z.-C.; Hu, Y.; Zheng, Q.-G. *Synthesis*, **2004**, 208.

(20) Mitsunubu, M.; Wade, M.; Sano, T.; *J. Am. Chem. Soc.* **1972**, 94, 697.

(21) Sen, S. E.; Roach, S. L.; *Synthesis*, **1995**, 756.

(22) Cheney, M. L.; McManus, G. J.; Perman, J. A.; Wang, Z.; Zaworotko, M. J. *Cryst. Growth Des.* **2007**, *7*, 616.

(23) Mamada, M.; Pérez-Bolívar, C.; Anzenbacher Jr., P. *Org. Letters* **2011**, *13*, 4882.

(24) Greene, T. W.; Wuts, P. G. M. *Protecting groups in organic synthesis,* 3rd ed., John Wiley & Sons Inc., New York, **1980**.

(25) Ing, H. R.; Manske, R. H. F. *J. Chem. Soc.* **1926**, 2348.

(26) Khan, N. M. *J. Org. Chem.* **1995**, *60*, 4536.

(27) Hendrickson, J. *Tetrahedron,* **1975***, 31*, 2517.

(28) Gibson, M.S.; Bradshaw, R.W. *Angew. Chem. Int. Ed. Engl.* **1968**, *7*, 919.

(29) Osby, J. O.; Martin, M. G.; Ganem, B. *Tetrahedron Lett.* **1984**, *25*, 2093.

(30) Havlik, S. E.; Simmons, J. M.; Winton, V. J.; Johnson, J. B. *J. Org. Chem.*, **2011**, *76*, 3588.

(31) Coyle, J. D. *In Synthetic Organic Photochemistry;* Horspool, W. M., Ed.; Plenum: New York, **1984**; pp 259-284.

(32) Yoon, U. C. Mariano, P. S. *Acc. Chem. Res.* **2001**, *34*, 523.

(33) Oelgemöller, M.; Griesbeck, A. G. *J. Photochem. Photobiol. C Photochem. Rev.* **2002**, *3*, 109.

(34) Griesbeck, A. G.; Henz, A.; Peters, K.; Peters, E. M.; von Schering, H. G. *Angew. Chem., Int. Ed. Engl.* **1995**, *34*, 474.

(35) Takahashi, Y.; Miyashi, T.; Yoon, U. C.; Oh, S. W.; Mancheno, M.; Su, Z.; Falvey, D. F.; Mariano, P. S. *J. Am. Chem. Soc.* **1999**, *121*, 3926.

(36) Yoon, U. C.; Kim, D. U.; Lee, C. W.; Choi, Y. S., Lee, Y.-J.; *J. Am. Chem. Soc.* **1995**, *117*, 2698.

(37) Yoon, U. C.; Kim, J. W.; Ryu, J. Y.; Cho, S. J.; Oh, S. W.; Mariano, P. S. *J. Photochem. Photobiol. A* **1997**, *106*, 145.

(38) Yoon, U. C.; Oh, S. W.; Lee, C. W. *Heterocycles* **1995**, 41, 2665.

(39) Yoon, U. C.; Oh, S. W.; Lee, J. H.; Park, J. H.; Kang, K. T.; Mariano, P. S. *J. Org. Chem.* **2001**, *66*, 939.

(40) Yoon, U. C.; Oh, S. W.; Lee, S. M.; Cho, S. J.; Gamlin, J.; Mariano, P. S. *J. Org. Chem.* **1999**, *64*, 4411.

(41) Yoon, U. C.; Kim, D. U.; Kim, J. C.; Lee, J. G.; Mariano, P. S.; Lee, Y. J.; Ammon, H. L. *Tetrahedron Lett.* **1993**, *34*, 5855.

(42) Yoon, U. C.; Cho, S. J.; Lee, Y. J.; Mancheno, M. J.; Mariano, P. S. *J. Org. Chem.* **1995**, *60*, 2353.

(43) Yoon, U. C.; Lee, C. W.; Oh, S. W.; Mariano, P. S. *Tetrahedron* **1999**, *55*, 11997.

(44) Maruyama, K.; Kubo, Y. *J. Org. Chem.* **1981**, *46*, 3612.

(45) Lee, Y. J.; Ling, R.; Mariano, P. S.; Yoon, U. C.; Kim, D. U.; Oh, S. W. *J. Org. Chem.* **1996**, 61, 3304.

(46) Kanaoka, Y. *Acc. Chem. Res.* **1978**, *11*, 407.

(47) Kanaoka, Y.; Migita, Y.; Koyama, K.; Sato, Y.; Nakai, H.; Mizoguchi, T. *Tetrahedron Lett.* **1973**, 1193.

(48) Kanaoka, Y.; Koyama, K.; Flippen, J. L.; Karle, I. L.; Witkop, B. *J. Am. Chem. Soc.* **1974**, 96, 4719.

(49) Machida, M.; Takechi, H.; Kanaoka, Y. *Synthesis* **1982**, 1078.

(50) Sato, Y.; Nakai, H.; Ogiwara, H.; Mizoguchi, T.; Migita, Y.; Kanaoka, Y. *Tetrahedron Lett.* **1973**, 4565.

(51) Sato, Y.; Nakai, H.; Mizoguchi, T.; Kawanishi, M.; Hatanaka, Y.; Kanaoka, Y. *Chem. Pharm. Bull.* **1982**, *30*, 1263.

(52) Yoon, U. C.; Lee, S. J.; Lee, K. J.; Cho, S. J.; Lee, C. W.; Mariano, P. S. *Bull. Korean Chem. Soc.* **1994**, *15*, 154.

(53) Yoon, U. C.; Cho, S. J.; Oh, J. H.; Lee, J. G.; Kang, K.T.; Mariano, P. S. *Bull. Korean Chem. Soc.* **1991**, *12*, 241.

(54) Griesbeck, A.G.; Oelgemöller, M.; Lex, J.; Haeuseler, A.; Schmittel, M. *Eur. J. Org. Chem.* **2001**, 1831.

(55) Coyle, J. D.; Bryant, L. R. B.; Cragg, J. E.; Challiner, J. F.; Haws, E. J. *J. Chem. Soc., Perkin Trans. 1* **1985**, 1177.

(56) Coyle, J. D.; Patel, P. *J. Chem. Res. Synopsis* **1985**, 102.

(57) Close, M.; Coyle, J. D.; Haws, E. J.; Perry, C. J. *J. Chem. Res. Synopsis* **1997**, 115.

(58) Kubo, Y.; Tojo, S.; Suto, M.; Toda, R.; Araki, T. *Chem. Lett.* **1984**, *13*, 2075.

(59) Kubo, Y.; Suto, M.; Tojo, S.; Araki, T. *J. Chem. Soc. Perkin Trans. I* **1986**, 771.

(60) Malval, J.-P.; Suzuki, S.; Morlet-Savary, F.; Allonas, X.; Fouassier, J.-P.; Takahara, S.; Yamaoka, T. *J. Phys. Chem. A* **2008**, *112*, 3879.

(61) Malval, J.-P.; Morlet-Savary, F.; Allonas, X.; Fouassier, J.-P.; Suzuki, S.; Takahara, S.; Yamaoka, T. *Chem. Phys. Lett.* **2007**, *443*, 323.

(62) Saotome, M.; Takano, S.; Tokushima, A.; Ito, S.; Nakashima, S.; Nagasawa, Y.; Okada, T.; Miyasaka, H. *Photochem. Photobiol. Sci.* **2005**, *4*, 83.

(63) Ortica, F.; Scaiano, J. C.; Pohlers, G.; Cameron, J. F.; Zampini, A. *Chem. Mater.* **2000**, *12*, 414.

(64) Suyama, K.; Nakao, S.; Shirai, M. *J. Photopol. Sci. Technol.* **2005**, *18*, 141.

(65) Duan, L.; Xu, Y.; Qian, X.; Zhang, Y.; Liu, Y. *Tetrahedron Lett.* **2009**, *50*, 22.

(66) Matsugo, S.; Kawanishi, S.; Yamamoto, K.; Sugiyama, H.; Matsuura, T.; Saito, I. *Angew. Chem., Int. Ed. Engl.* **1991**, *30*, 1351.

(67) Reszka, K. J.; Takayama, M.; Sik, R. H.; Chignell, C. F.; Saito, I. *Photochem. Photobiol.* **2005**, *81*, 573.

(68) Abraham, B.; McMaster, S.; Mullan, M.; Kelly, L. A. *J. Am. Chem. Soc.* **2004**, *126* 4293.

(69) Liu, B.; Tian, H. *J. Mater. Chem.* **2005**, *15*, 2681.

(70) Gunnlaugsson, T.; Kruger, P. E.; Lee, T. C.; Parkesh, R.; Pfeffer, F. M.; Hussey, G. M. *Tetrahedron Lett.* **2003**, *44*, 6575.

(71) Gunnlaugsson, T.; Kruger, P. E.; Jenson, P.; Pfeffer, F. M.; Hussey, G. M. *Tetrahedron Lett.* **2003**, *44*, 8909.

(72) Pfeffer, F. M.; Buschgens, A. M.; Barnett, N. W.; Gunnlaugsson, T.; Kruger, P. E. *Tetrahedron Lett.* **2005**, *46*, 6579.

(75) Pfeffer, F. M.; Seter, M.; Lewcenko, N.; Barnett, N. W. *Tetrahedron Lett.* **2006**, *47*, 5241.

(76) Yoon, J.; Qian, X.; Kim, J. S.; Lee, C.; Han, S. J.; Kim, N. H.; Kim, S.; Xu, Z. *Tetrahedron Lett.* **2007**, *48*, 9151.

(77) Kluciar, M.; Ferreira, R.; Castro, B. D.; Pischel, U. *J. Org.Chem.* **2008**, *73*, 6079.

(78) Pischel, U.; Remon, P.; Ferreira, R. *J. Phys. Chem. C* **2009**, *113*, 5805.

(79) Guha, S.; Saha, S. *J. Am. Chem. Soc.* **2010**, *132*, 17675.

(80) Bhosale, S. V.; Bhosale, S. V.; Kalyankar, M. B.; Langford, S. J. *Org. Lett.* **2009**, *11*, 5418.

(81) de Silva, A. P.; Gunaratne, H. Q. N.; Habibjiwan, J. I.; McCoy, C. P.; Rice, T. E.; Soumillion, J. P. *Angew. Chem., Int. Ed.* **1995**, *34*, 1728.

(82) Gunnlaugsson, T.; McCoy, C. P.; Morrow, R. J.; Phelan, C.; Stomeo, F. *Arkivoc* **2003**, *8*, 216.

(83) He, H.; Mortellaro, M. A.; Leiner, M. J. P.; Fraatz, R. J.; Tusa, J. K. *J. Am. Chem. Soc.* **2003**, *125*, 1468.

(84) (a) Parkesh, R.; Lee, T. C. Gunnlaugsson, T. *Org. Biomol. Chem.* **2007**, *5*, 310. (b) Gunnlaugsson, T.; Lee, T. C.; Parkesh, R. *Org. Biomol. Chem.* **2003**, *1*, 3265.

(85) Tamanini, E.; Katewa, A.; Sedger, L. M.; Todd, M. H.; Watkinson, M. *Inorg. Chem.* **2009**, *48*, 319.

(86) Parkesh, R.; Lee, T. C.; Gunnlaugsson, T. *Tetrahedron Lett.* **2009**, *50*, 4114.

(87) Tamanini, E.; Flavin, K.; Motevalli, M.; Piperno, S.; Gheber, L. A.; Todd, M. H.; Watkinson, M. *Inorg. Chem.* **2010**, *49*, 3789.

(88) Xu, Z. C.; Qian, X. H.; Cui, J. N. *Org. Lett.* **2005**, *7*, 3029.

(89) Xu, Z.; Yoon, J.; Spring, D. R. *Chem. Commun.* **2010**, *46*, 2563.

(90) Xu, Z.; Baek, K.-H.; Kim, H. N.; Cui, J.; Qian, X. H.; Spring, D. R.; Shin, I.; Yoon, J. *J. Am. Chem. Soc.* **2010**, *132*, 601.

(91) Wang, J.; Xiao, Y.; Zhang, Z.; Qian, X.; Yang, Y.; Xu, Q. *J. Mater. Chem.* **2005**, *15*, 2836.

(92) Xu, Z.; Qian, X.; Cui, J.; Zhang, R. *Tetrahedron* **2006**, *62*, 10117.

(93) Lu, C.; Xu, Z.; Cui, J.; Zhang, R.; Qian, X. *J. Org. Chem.* **2007**, *72*, 3554.

From chem. Soc precious

(94) Chen, T.; Zhu, W.; Xu, Y.; Zhang, S.; Zhang, X.; Qian, X. *Dalton Trans.* **2010**, *39*, 1316.

(95) Xu, Z.; Zheng, S.; Yoon, J.; Spring, D. R. *Analyst* **2010**, *135*, 2554.

(96) Silva, A. P. D.; Gunaratne, H. Q. N.; Gunnlaugsson, T.; Lynch, P. L. M. *New J. Chem.* **1996**, *20*, 871.

(97) Claessens, G.; Stoddart, J. F. *J. Phys. Chem.* **1997**, *10*, 254.

(98) Barooah, N.; Sarma, R. J.; Baruah, J. B. *Cryst. Growth Des.* **2003**, *3*, 639.

(99) Pantos, G. D.; Pengo, P.; Sanders, J. K. M. *Angew. Chem., Int. Ed.* **2007**, *46*, 194.

(100) Pantos, G. D.; Wietor, J.-L.; Sanders, J. K. M. *Angew. Chem., Int. Ed.* **2007**, *46*, 2238

(101) Blacker, A. J.; Jazwinski, J.; Lehn, J.-M.; Cesario, M.; Guilhem, J.; Pascard, C. *Tetrahedron Lett.* **1987**, *28*, 6057.

(102) Iwanaga, T.; Nakamoto, R.; Yasutake, M.; Shinmyozu, T. *Angew. Chem., Int. Ed.* **2006**, 45, 3643.

(103) Esteban-Gomez, D.; Fabbrizzi, L.; Licchelli, M.; Sacchi, D.; *J. Mater. Chem.* **2005**, *15*, 2670.

(104) Esteban-Gomez, D.; L. Fabbrizzi, L.; Licchelli, M. *J. Org. Chem.* **2005**, *70*, 5717.

(105) Johnstone, K.; Bampos, N.; Gunter, M. J.; Sanders, J. K. M. *Chem. Commun*. **2003**, 1396.

(106) Kaiser, G.; Jarrosson, T.; Otto, S.; Ng, Y.-F.; Sanders, J. K. M. *Angew. Chem., Int. Ed.* **2004**, *43*, 1959.

(107) Pascu, S. I.; Jarrosson, T.; Naumann, C.; Otto, S.; Kaiser, G.; Sanders, J. K. M. *New J. Chem.* **2005**, *29*, 80.

(108) Vignon, S. A.; Jarrosson, T.; Iijima, T.; Tseng, H.-R.; Sanders, J. K. M. Stoddart, J. F. *J. Am. Chem. Soc.* **2004**, *126*, 9884.

(109) Janiak, C. *J. Chem. Soc., Dalton Trans.* **2000**, 3885.

(110) Reger, D. L.; Elgin, J. D.; Semeniuc, R. F.; Pellechia, P. J.; Smith, M. D. *Chem. Commun.* **2005**, 4068.

(111) Reger, D. L.; Semeniuc, R. F.; Elgin, J. D.; Rassolov, V.; Smith, M. D. *Cryst. Growth Des.* **2006**, *6*, 2758.

(112) Reger, D. L.; Elgin, J. D.; Smith, M. D; Simpson, B. K. *Polyhedron* **2009**, *28*, 1469.

(113) Reger, D. L.; Debreczeni, A.; Reinecke, B.; Rassolov, V.; Smith, M. D.; Semeniuc, R. F. *Inorg. Chem.* **2009**, 48, 8911.

(114) Reger, D. L.; Debreczeni, A.; Smith, M. D. *Inorg. Chim. Acta* **2010**, *364*, 10.

(115) Reger, D. L.; Debreczeni, A.; Horger, J. J.; Smith, M. D. *Cryst. Growth Des*. **2011**, *11*, 4068.

(116) Barooah, N.; Sarma, R. J.; Baruah, J. B. *CrystEngComm* **2006**, *8*, 608.

(117) Degenhardt, C. F.; Lavin, J. M.; Smith, M. D.; Shimizu, K. D.; *Org. Letters* **2005**, *7*, 4079.

(118) Rasberry, R. D.; Smith, M. D.; Shimizu, K. D. *Org. Letters* **2008**, *13*, 2889.

(119) Rathore, R.; Lindeman, S. V.; Kochi, J. K. *J. Am. Chem. Soc.* **1997**, *119*, 9393.

(120) Mukhopadhyay, P.; Iwashita, Y.; Shirakawa, M.; Kawano, S.; Fujita, N.; Shinkai, S. Angew. Chem., Int. Ed. **2006**, *45*, 1592.

(121) Colquhoun, H. M.; Williams, D. J.; Zhu, Z. *J. Am. Chem. Soc.* **2002**, *124*, 13346.

(122) Iwanaga, T.; Nakamoto, R.; Yasutake, M.; Shinmyozu, T. *Angew. Chem., Int. Ed.* **2006**, 45, 3643.

(123) Tomasulo, M.; Naistat, D. M.; White, A. J. P.; Williams, D. J.; Raymo, F. M.; *Tetrahedron Lett.* **2005**, *46*, 5695.

(124) Pantos, G. D.; Pengo, P.; Sanders, J. K. M. *Angew. Chem., Int. Ed.* **2007**, 46, 194.

(125) Lehn, J.-M. *Angew. Chem., Int. Ed.* **1988**, *27*, 89.

(126) Reger, D. L.; Horger, J.; Smith, M. D.; Long, G. J. *Chem. Commun.* **2009**, 6219.

(127) Reger, D. L.; Horger, J. J.; Smith, M. D. *Chem. Commun.* **2011**, *47*, 2805.

(128) Perman, A. J.; Dubois, K.; Nouar, F.; Zoccali, S.; Woltas, L.; Eddaoudi, M.; Larsen, R. W.; Zaworotko, M. J. *Cryst. Growth Des.* **2009**, *9*, 5021.

(129) Zhang, Z.; Wojtas, L.; Zaworotko, M. J. *Cryst. Growth Des.* **2011**, *11*, 1441.

(130) (a) Tzeng, B. C.; Chiu, T. H.; Chen, B. S.; Lee, G. H. *Chem.-Eur. J.* **2008**, *14*, 5237. (b) Ding, B.; Yi, L.; Wang, Y.; Cheng, P.; Liao, D. Z.; Yan, S. P.; Jiang, Z. H.; Song, H. B.; Wang, H. G. *Dalton Trans.* **2006**, 665. (c) Li, J. R.; Tao, Y.; Yu, Q.; Bu, X. H. *Chem. Commun.* **2007**, 1527.

(131) Lu , X.-Q.; Jiang, J.-J.; Zhang, L.; Chen, C.-L.; Su, C.-Y.; Kang, B.-S. *Cryst. Growth Des.* **2005**, *5*, 419.

(132) Li, G-B.; Liu, J-M.; Cai, Y-P.; Su, C-Y. *Cryst. Growth Des.* **2011**, *11*, 2763.

(133) Li, G-B.; Liu, J-M.; Yu, Z-Q.; Wang, W.; Su, C-Y. *Inorg Chem.* **2009**, *48*, 8659.

(134) Muth, M.; Hoerr, V.; Glaser, M.; Ponte-Sucre, A.; Moll, H.; Stich, A.; Holzgrabe, U. *Bioorg. Med. Chem. Lett.*, **2007**, *17*, 1590.

(135) Andricopulo, A. D.; Muller, L. A.; Cechinel, V.; Cani, G. S.; Roos, J. F.; Correa, R.; Santos, A. R. S.; Nunes, R. J.; Yunes, R. A. *FARMACO* **2000**, *55*, 319.

(136) Grabchev, I.; Staneva, D.; Betcheva, R. *Polym. Degrad. Stabil*. **2006**, *91*, 2257.

(137) Xu, Y. F.; Qian, X. H.; Yao, W.; Mao, P.; Cui, J. N. *Bioorg. Med. Chem.* **2003**, *11*, 5427.

(138) Kowalski, P.; Kowalska, T.; Bojarski, A. J.; Duszynska, B. *J. Heterocyclic Chem*. **2007**, *44*, 889.

(139) De Souza, M. M.; Correa, R.; Cechinel, V.; Grabchev, I.; Bojinov, V. *Pharmazie* **2002**, *57*, 430.

(140) Langlois, M.; Soulier, J. L.; Rampillon, V.; Gallais, C.; Bremont, B.; Shen, S.; Yang, D.; Giudice, A.; Sureau, F. *Eur. J. Med. Chem*. **1994**, *29*, 925.

(141) Langlois, M.; Soulier, J. L.; Bremont, B.; Shen, S.; Rampillon, V.; Giudice, A. *Bioorg. Med. Chem. Lett.* **1992**, *2*, 691.

(142) Kawai, K.; Kawabata, K.; Tojo, S.; Majima, T. *Bioorg. Med. Chem. Lett.* **2002**, *12*, 2363.

(143) Brana, M. F.; Castellano, J. M.; Moran, M.; Devega, M. J. P.; Perron, D.; Conlon, D.; Bousquet, P. F.; Romerdahl, C. A.; Robinson, S. P. *Anti-Cancer Drug Design* **1996**, *11*, 297.

(144) Brana, M. F.; Castellano, J. M.; Moran, M.; Devega, M. J. P.; Qian, X. D.; Romerdahl, C. A.; Keilhauer, G. *Eur. J. Med. Chem*. **1995**, *30*, 235.

(145) Gupta, R.; Liu, J. X.; Xie, G. J.; Lown, J. W. *Anti-Cancer Drug Design* **1996**, *11*, 581-96.

(146) Costanza, M. E.; Berry, D.; Henderson, I. C.; Ratain, M. J.; Wu, K.; Shapiro, C.; Duggan, D.; Kalra, J.; Berkowitz, I.; Lyss, A. P. *Clin. Cancer Res*. **1995**, *1*, 699.

(147) Kreis, W.; Chan, K.; Budman, D. R.; Allen, S. L.; Fusco, D.; Mittelman, A.; Hock, K.; Akerman, S.; Calabro, A.; Puccio, C.; Spigelman, M. *Cancer Invest*. **1996**, *14*, 320-7.

(148) Thompson, J.; Pratt, C. B.; Stewart, C. F.; Avery, L.; Bowman, L.; Zamboni, W. C.; Pappo, A. *Invest. New Drugs* **1998**, *16*, 45.

(149) Bousquet, P. F.; Brana, M. F.; Conlon, D.; Fitzgerald, K. M.; Perron, D.; Cocchiaro, C.; Miller, R.; Moran, M.; George, J.; Qian, X. D.; Keilhauer, G.; Romerdahl, C. A. *Cancer Res.* **1995**, *55*, 1176.

(150) Villalona-Calero, M. A.; Eder, J. P.; Toppmeyer, D. L.; Allen, L. F.; Fram, R.; Velagapudi, R.; Myers, M.; Amato, A.; Kagen-Hallet, K.; Razvillas, B.; Kufe, D. W.; Von Hoff, D. D.; Rowinsky, E.K. *J. Clin. Oncol.* **2001**, *19*, 857.

(151) Brana, M. F.; Cacho, M.; Ramos, A.; Dominguez, M. T.; Pozuelo, J. M.; Abradelo, C.; Rey-Stolle, M. F.; Yuste, M.; Carrasco, C.; Bailly, C. *Org. Biomol. Chem.* **2003**, *1*, 648-54.

(152) Brana, M. F.; Romas, A. *Curr. Med. Chem. Anti-Cancer Agents* **2001**, *1*, 237.

(153) Ingrassia, L.; Lefranc, F.; Kiss, R.; Mijatovic, T. *Curr. Med. Chem.* **2009**, *16*, 1192.

(154) Lv, M.; Xu, H. *Curr. Med. Chem.* **2009**, *16*, 4797.

(155) Kamal, A.; Srinivas, O.; Ramulu, P.; Ramesh, G.; Kumar, P. P. *Bioorg. Med. Chem. Lett.*, **2003**, *13*, 3577.

(156) Kamal, A.; Ramu, R.; Tekumalla, V.; Khanna, G. B. R.; Barkume, M. S.; Juvekar, A. S.; Zingde, S. M. *Bioorg. Med. Chem.*, **2008**, *16*, 7218.

(157) Kamal, A.; Adil, S.F.; Tamboli, J.R.; Siddardha, B.; Murthy, U. S. N. *Lett. Drug Des. Discov.*, **2008**, *5*, 261.

(158) Kamal, A.; Adil, S. F.; Tamboli, J. R.; Siddardha, B.; Murthy, U. S. N. *Lett. Drug Des. Discov.*, **2009**, *6*, 201.

(159) Sami, S. M.; Dorr, R. T.; Alberts, D. S.; Remers, W. A. *J. Med. Chem.* **1993**, 36 765.

(160) Costi, M. P.; Tondi, D.; Rinaldi, M.; Barlocco, D.; Cignarella, G.; Santi, D. V. *J. Med. Chem.* **1996**, 31, 1011.

(161) Feibush, B.; Figueroa, A.; Charles, R.; Onan, K. D.; Feibush, P.; Karger, B. L. *J. Am. Chem. Soc.* 1986, *108,* 3310.

(162) Hamilton, A. D.; Van Engen, D. *J. Am. Chem. Soc.* 1987, *109,* 5035.

(163) Fouquey, C.; Lehn, J.-M.; Levelut, A.-M. *Adv. Mater.* 1990, *2*, 254.

(164) Zerkowski, J. A.; Seto, C. T.; Wierda, D. A,; Whitesides, G. M. J. *Am. Chem. Soc.* 1990, 112, 9025-9026.

(165) Jorgensen, W.; Pranata, J. *J. Am. Chem. Soc.* **1990**, *112*, 2008.

(166) Jeong, K. S.; Tjivikua, T.; Rebek, J. Jr. *J. Am. Chem.* Soc. **1990**, *112*, 3215.

(167) Park, T. K.; Schroeder, J.; Rebek, Jr. J. *J. Am. Chem. Soc.* **1991**, 113, 5125.

(168) Askew, B.; Ballester, P.; Buhr, C.; Jeong, K. S.; Jones, S.; Parris, K.; Williams, K.; Rebek, Jr. J. *J. Am. Chem. Soc.* **1989**, 111, 1082.

(169) Hayashida, O.; Sebo, L.; Rebek, Jr. J. *J. Org. Chem.* **2002**, *67*, 8291.

(170) Ajami, D.; Iwasawa, T.; Rebek, Jr. J. *Proc. Natl. Acad. Sci. USA* **2006**, *103*, 8934.

(171) Van Grop, J. J.; Vekemans, J. A. J. M.; Meijer, E. W. *Chem. Commun.* **2004**, 60.

(172) Zhou, Q.-Z.; Jiang, X.-K.; Shao, X.-B.; Chen, G.-J.; Jia, M.-X.; Li, Z.-T. *Org. Lett.* **2003**, *5*, 1955.

(173) Silva, A. P. D.; Gunaratne, H. Q. N.; Gunlaugsson, T. *Tetrahedron Lett.* **1998**, *39*, 5077.

(174) DiCesare, N.; Adhikari, D. P.; Heynekamp, J. J.; Heagy, M. D. Lakowicz, J. R. *J. Fluoresc.*, **2002**, *12*, 147.

(175) Trupp, S.; Schweitzer, A.; Mohr, G. J. *Org. Biomol. Chem.*, **2006**, *4*, 2965.

(176) Bhosale, S.; Sission, A. L.; Talukdar, P.; Furstenberg, A.; Banerji, N.; Vauthey, E.; Bollot, G.; Mareda, J.; Roger, C.; Wurthner, F.; Sakai, N.; Matile, S. *Science* **2006**, *313*, 84.

(177) Tanaka, H.; Litvinchuk, S.; Tran, D.-H.; Bollt, G.; Mareda, J.; Sakai, N.; Matile, S. *J. Am. Chem. Soc.* **2006**, *128*, 16000.

(178) Gorteau, V.; Bollot, G.; Mareda, J.; Perez-Velasco, A.; Matile, S. *J. Am. Chem. Soc.* **2006**, *128*, 14788.

(179) Wurthner, F.; Ahmed, S.; Thalacker, C.; Debaerdemaeker, T. *Chem.–Eur. J.* **2002**, *8*, 4742.

(180) Rodrigues, M. A.; Demets, G. J. F.; Politi, M. J. *J. Mater. Chem.* **2002**, *12*, 1250.

(181) Jones, B. A.; Facchetti, A.; Marks, T. J.; Wasielewski, M. R. *Chem. Mater.* **2007**, *19*, 2703.

(182) Barooah, N.; Sarma, R. J.; Baruah, J. B. *Eur. J. Inorg. Chem.* **2006**, 2942.

(183) Cairns, A. J.; Perman, J. A.; Wojtas, L.; Kravtsov, V. C.; Alkordi, M. H.; Eddaoudi, M.; Zaworotko, M. J. *J. Am. Chem. Soc.* **2008**, *130*, 1560.

Chapter 2

Host-guest complexes of cyclic imides containing hydroxy benzoic acids with aromatic N-heterocycles

Rational design of molecular assemblies using organic functional solids to generate a variety of supramolecular architectures has gained impressive research interest in the field of crystal engineering and supramolecular chemistry.[1] Host-guest crystalline materials are of special interest in solid state due to their different physical properties from corresponding hosts[2] which also makes them useful for pharmaceutical applications.[3] In particular, host-guest microporous materials with channels and cavities are important because they have possible applications in the areas of heterogeneous catalysis,[4d] size selective separation,[4e] gas absorption[4a,b,c] and biomimetics.[4f] In the field of supramolecular chemistry, cyclic imide derivatives have been proved as versatile scaffolds to design the crystals of specific molecular arrangements.[5] Cyclic imides attached to aromatic rings possess dipolar nature and this effect provide extra stability to the packing arrangement.[6] From this point of view, imides containing π-stacking synthons such as naphthalimides or naphthalene diimides combined with carboxylic acid or hydroxyl functional groups draw special interest.[7] These multifunctional molecules create extended network solids by self-assembly through hydrogen bonding interactions of the functional groups along with the π…π stacking interactions of the naphthalimide rings. The hydrogen bonds between carboxylic acids and simple aromatic amines may be of different types. Some possible hydrogen bond motifs arising from interactions of carboxylic acid with pyridine and quinoline are shown in Scheme 2.1, and some of those motifs are already available in the literature.[8] These interactions either lead to co-crystals or ionic salts which are useful in pharmaceutical chemistry[9] as well as in the synthesis of porous materials.[10] Packing effect as well as pKa of an acid and a base influence the formation of corresponding carboxylate salts or co-crystals.[11] Steric factors also play an important role in stabilization of these motifs.[5b,11c] Depending on the association of parent carboxylic acids in cyclic hydrogen bonds, it is likely that such hydrogen bond motifs may originate from cleavage of cyclic dimeric carboxylic acid by inclusion of a base such as pyridine or quinoline. It is anticipated that free rotation of naphthalimide or naphthalene diimides

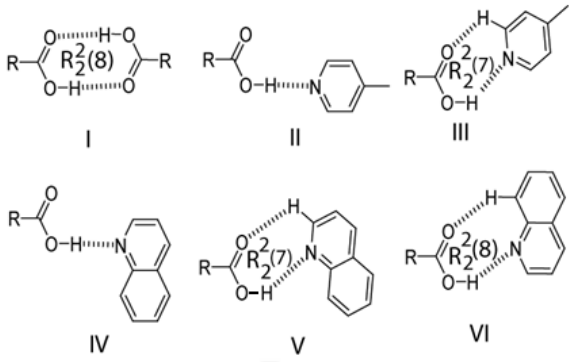

Scheme 2.1: Some hydrogen bonded motifs showing interactions of pyridine and quinoline with a carboxylic acid.

aromatic rings around the C-N bond would provide an environment to adjust hydrogen bond motifs with geometry guided by the dipolar nature of the imide rings. Further, it may be noted that the two carbonyl groups of the imide would participate in weak interactions to guide the orientation of the carboxylic acid groups. Thus, to establish these motifs (as shown in Scheme 2.1) in solid-state assembly, we have studied the structures of host-guest complexes of pyridine/bipyridine and quinoline with some of the aromatic hydroxy carboxylic acids that are tethered by naphthalimide or naphthalene diimide. Analogous motifs derived from interactions of pyridine or quinoline with formic acid are constructed and their corresponding energies are calculated by density functional theory (DFT) using diffuse functions. The cyclic imide compounds used for the preparation of host-guest complexes are shown in Scheme 2.2.

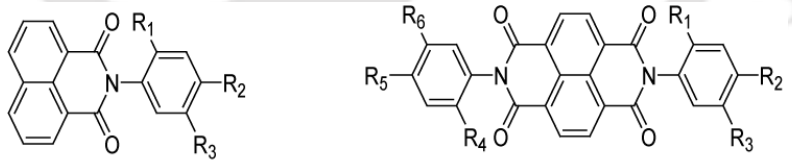

R_1 = COOH, R_2 = OH, R_3 = H; **2.1**
R_1 = OH, R_2 = COOH, R_3 = H; **2.2**
R_1 = OH, R_2 = H, R_3 = COOH; **2.3**

R_1, R_4 = COOH; R_2, R_5 = OH; R_3, R_6 = H; **2.4**
R_1, R_4 = OH; R_2, R_5 = COOH; R_3, R_6 = H; **2.5**
R_1, R_4 = OH; R_2, R_5 = H; R_3, R_6 = COOH; **2.6**

Scheme 2.2: Structures of host molecules.

We believe that present study would help to ascertain the role of directional interactions and the type of assemblies that can be form from trifunctional molecules containing both hydroxyl and carboxylic acid groups tethered by a π-stacking imide synthons (as shown in Scheme 2.3). Such study would not only provide information on the assembling process but would also be able to

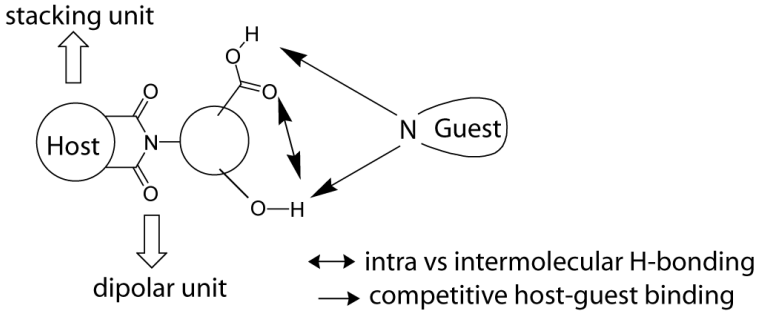

Scheme 2.3: Illustration of host-host or host-guest interactions

distinguish the de-protonation processes of the hydroxyl or carboxylic acid groups to form their corresponding salt. For this reason, hydroxy carboxylic acid can be a choice due to the additional hydrogen bonding site of hydroxyl group for N-heterocycle guests. Further, the incorporation of naphthalimide ring with such functional groups would make the system more complicated which may lead to some unexpected bonding pattern. The hydrocarboxylic acids can be associated with intramolecular and intermolecular O-H···O interactions, whether retention or cleavage of such motifs would contribute in the formation of new kind of structural patterns.

The host compounds **2.1**-**2.6** are prepared by cyclocondensation reactions of 1,8-naphthalic anhydride and 1,4,5,8-naphthalenetetracarboxylic dianhydride with respective amino hydroxy benzoic acids. Various host-guest complexes of these cyclic imide hydroxy carboxylic acids with pyridine or bipyridine are prepared and are shown in Scheme 2.4 with their host-guest stoichiometry. Crystallization of compounds **2.1** and **2.5** with pyridine solvent led to the formation of crystals of pyridine solvates (**2.1a and 2.5a**). The crystals of pyridine solvates of **2.2** could not obtained under the similar crystallization conditions, however, when we added 4,4′-bipyridine (bpy) in a pyridine solution of **2.2**, we obtained co-crystal of compound **2.2** with

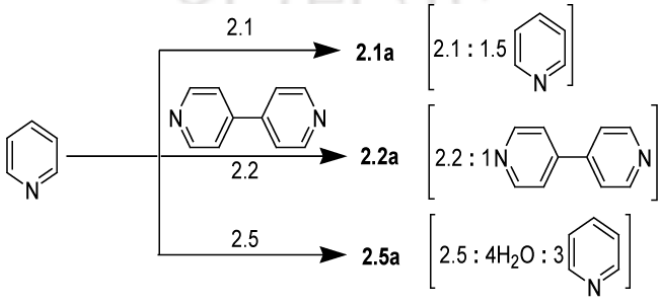

Scheme 2.4: Host-guest complexes of pyridine/bipyridine showing host-guest stoichiometry.

bpy (**2.2a**) in 1:1 host-guest ratio. Salt formation is not observed in these structures and intermolecular interactions between the guest pyridine/bpy and –COOH/-OH groups of host molecules either lead to the formation of solvates or co-crystal. Various types of intermolecular hydrogen bonding interactions are found to responsible for the formation of channels filled by guest molecules in all these host-guest 3D supramolecular structures. Moreover, two different types of hydrogen bond motifs between the –COOH group of host molecules and guest molecules, namely, discrete O-H···N interactions and a combination of O-H···N and C-H···O interactions making cyclic $R_2^2(7)$ hydrogen bond motif, are observed in the structures of these host-guest complexes.

Single crystal X-ray structure analysis reveals that solvate **2.1a** crystallizes in triclinic P-1 space group, asymmetric unit of this has two molecules of host **2.1** with one and half of the guest pyridine molecule. The guest pyridine molecule which appears as its half in the asymmetric unit, is disordered across an inversion centre sharing the nitrogen and carbon atoms at 1 and 4 position of pyridine ring with half occupancies. The hydrogen atom attached to –COOH group of host molecule is also disordered and shared between the two same oxygen atoms of two –COOH groups by O-H···O (O2-H2···O2; $d_{D\cdots A}$ 2.47Å, <D-H···A 180.00º) interaction (Figure 2.1a). The hydrogen atom located on disordered pyridine ring is also shared with this oxygen atom by N-H···O (N2-H26···O2; $d_{D\cdots A}$ 3.22Å, <D-H···A 121.79º) interaction which also participates in bifurcated donor hydrogen bonding and further interacts with another oxygen atom of –COOH group by N-H···O (N2-H26···O1; $d_{D\cdots A}$ 2.75Å, <D-H···A 138.78º) interaction. Another symmetry nonequivalent guest pyridine molecule also interact with the –COOH group, -OH group and carbonyl oxygen atom of the host molecule by donor-acceptor C-H···O (C21-H21···O2; $d_{D\cdots A}$ 3.45Å, <D-H···A 145.07º and C20-H20···O4; $d_{D\cdots A}$ 3.47Å, <D-H···A 171.21º) and O-H···N (O3-H3A···N3; $d_{D\cdots A}$ 2.77Å, <D-H···A 168.15º) interactions, respectively. The host molecules also assemble in the lattice through C-H···O (C11-H11···O5; $d_{D\cdots A}$ 3.21Å, <D-H···A 137.31º and C15-H15···O4; $d_{D\cdots A}$ 3.47Å, <D-H···A 137.86º) interactions exist between the carbonyl oxygen and naphthalimide rings. These interactions result in the construction of 2D layers of host molecules containing channels of approximate 11×9 Å dimensions in the lattice. The 2D layers are further connected to each other via C-H···π ($d_{C5\ldots\pi}$ 3.54Å) interactions creating a 3D host-guest architecture of **2.1a** in the crystal lattice (Figure 2.1b). The channels formed inside the 2D layers of the host molecules are filled by both symmetry nonequivalent guest pyridine molecules as viewed along a axis (Figure 2.1b, 2.1c). Earlier in the case of pyridine solvates of various naphthalimide tethered carboxylic acids, we have demonstrated that the guest molecule interacts

with the host molecule either making a cyclic $R_2^2(7)$ hydrogen bond motifs or via a discrete O-H···N interaction.[5i]

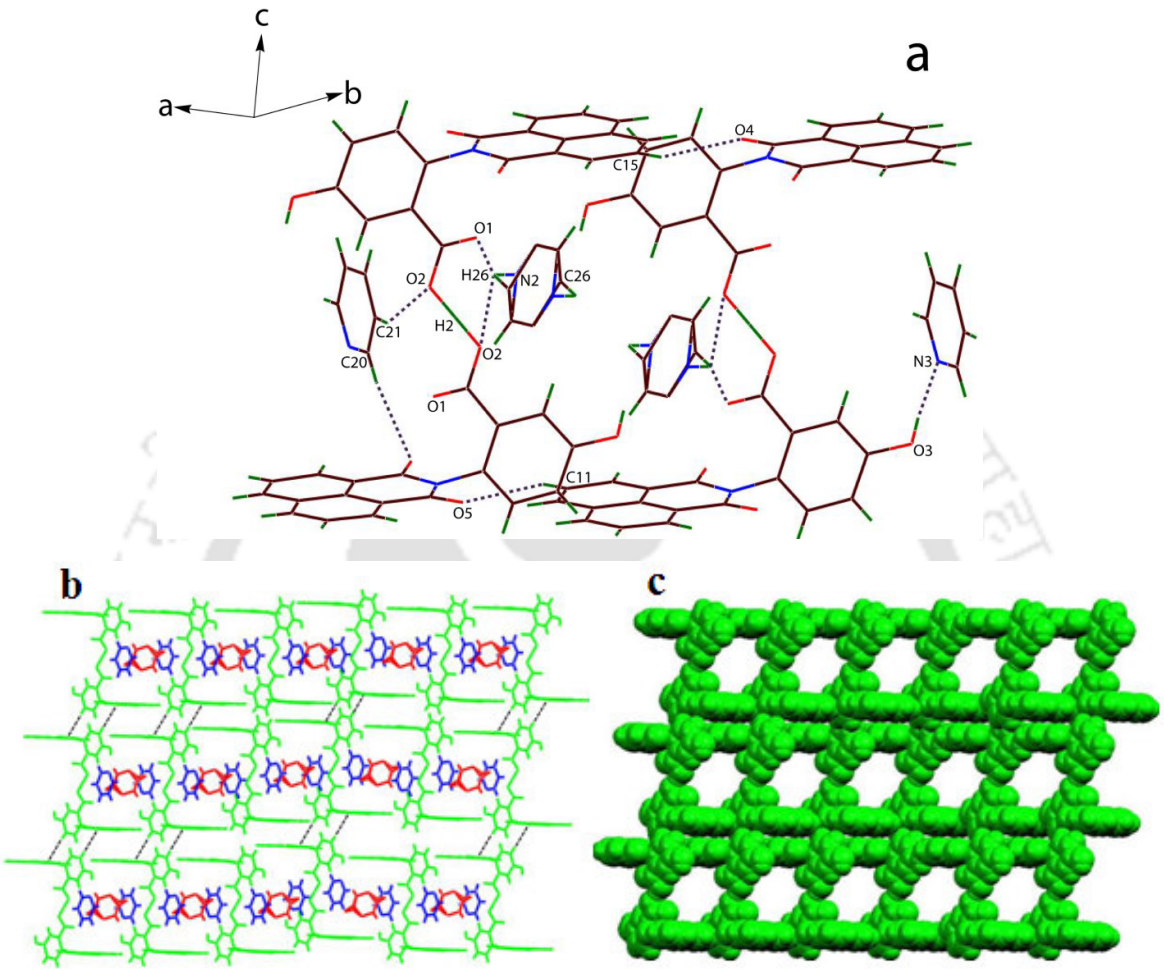

Figure 2.1. (a) Weak interactions in the host-guest assembly of **2.1a**. (b) Formation of 3D channel architecture where 2D separated layers of host molecules (green) are sustained by C-H···π interactions containing both the symmetry nonequivalent guest pyridine molecules (red and blue) inside the channels (along a axis). (c) Space filling model after removal of pyridine molecules inside the channels.

The co-crystal **2.2a** crystallized in triclinic P-1 space group, posseses one molecule of host **2.2** and one molecule of guest bpy in its crystallographic asymmetric unit. In the structure of **2.2a**, guest bpy molecule loses its planarity and both the aromatic rings are twisted at an angle of 32^0 with respect to each other. The guest bpy molecule is found to associate with host molecules via both donor and acceptor host-guest interactions (Figure 2.2a). Both the nitrogen atoms of bpy

interact with –COOH and –OH functional groups of host molecule via acceptor O-H···N (O2-H2···N2; $d_{D\cdots A}$ 2.60Å, <D-H···A 173.97º and O3-H3···N3; $d_{D\cdots A}$ 2.70Å, <D-H···A 152.88º, respectively) interactions and its aromatic ring also interacts with naphthalimide ring of host molecule via acceptor C-H···π ($d_{C15\ldots\pi}$ 3.57Å) interaction. The aromatic rings of guest bpy molecule are also found to display four different donor hydrogen bonds with host molecule, namely, C20-H20···O2 ($d_{D\cdots A}$ 3.55Å, <D-H···A 164.63º) and C24-H24···O5 ($d_{D\cdots A}$ 3.09Å, <D-H···A 112.04º) interactions with –COOH group and carbonyl oxygen, respectively, making a cyclic $R_2^2(16)$ hydrogen bond motif, C26-H26···O3 ($d_{D\cdots A}$ 3.38Å, <D-H···A 156.29º) interaction with –OH group and C28-H28···π ($d_{C28\ldots\pi}$ 3.50Å) interaction with aromatic ring of host molecule. Moreover, the π...π interactions between the naphthalimide rings of host molecules and one of the aromatic rings of guest molecule are also observed in the lattice. No

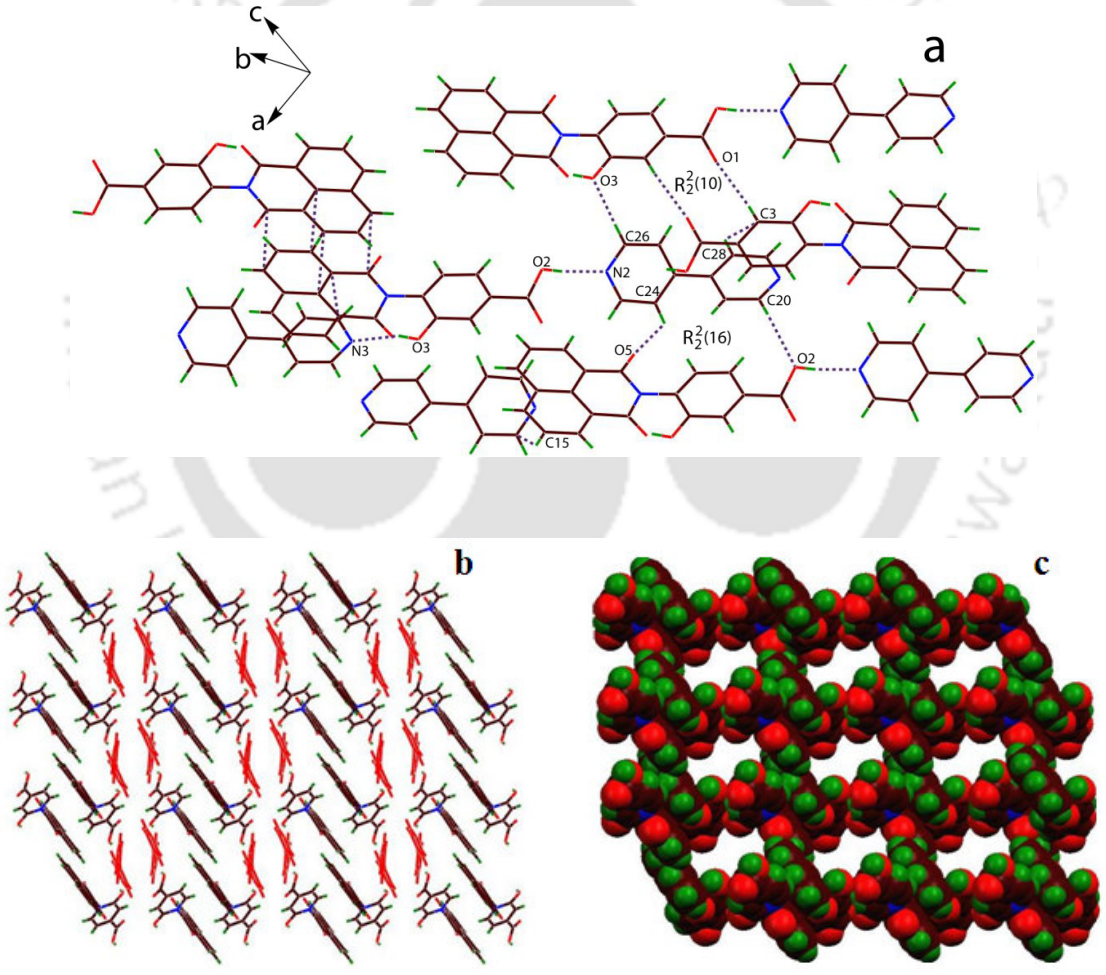

Figure 2.2. (a) Weak interactions among the host and guest bpy molecules in **2.2a**. (b) Crystal packing arrangement showing 3D channels along b axis. (c) Space filling model after removal of guest bpy (red) molecules inside the channels.

interactions between the guest molecules are observed, however, the host molecules are found to interact with each other by a combination of two similar C-H···O (C3-H3A···O1; $d_{D\cdots A}$ 3.62Å, <D-H···A 175.04º) interactions between the oxygen atom of –COOH groups and hydrogen atom of aromatic ring, forming a cyclic $R_2^2(10)$ motif in the lattice. Strong π...π contact between the naphthalimide rings of host molecules are also observed in the hydrogen bonded network of **2.2a**. All the intermolecular host-host and host-guest hydrogen bond interactions can be taken in account for the construction of 3D supramolecular channel network of **2.2a** in the crystal lattice. The channels of approximate 16×10 Å dimensions are created by repeated 3D hexameric assemblies of host molecules. The guest molecules are encapsulated inside these assemblies filling the channels as viewed along a axis (Figure 2.2b, 2.2c). Bipyridine or terpyridines are used to make porous building blocks with aromatic carboxylic acids.[12]

The solvate **2.5a** crystallized in triclinic P-1 space group, included half molecule of **2.5** lying on the inversion centre, one and half molecules of guest pyridine and two molecule of solvent water in its crystallographic asymmetric unit. The guest pyridine molecule which appears as its half in the asymmetric unit, is disordered across an inversion centre and disposed in the lattice such that the nitrogen and carbon atoms at 1 and 4 positions of the pyridine rings are shared with half occupancies (Figure 2.3a). This symmetric arrangement produces two sets of symmetry nonequivalent guest pyridine (total three) and two sets of symmetry independent water molecules (total four) in the lattice. One set of lattice water molecules interact with –COOH and –OH groups of host molecule via donor-acceptor O-H···O (O6-H6A···O1; $d_{D\cdots A}$ 2.75Å, <D-H···A 162.40º and O3-H3A···O6; $d_{D\cdots A}$ 2.62Å, <D-H···A 169.89º) interactions and assemble two host and two lattice water molecules in a 1D layered arrangement forming repeated supramolecular cavities in the lattice. The cavities formed along the a axis contain disorder pyridine (from one set) and another set of water molecules interacting with each other via N-H···O (N5-H20A···O7; $d_{D\cdots A}$ 2.93Å, <D-H···A 172.10º) interactions. No interactions between the host molecules or same guest molecules are observed in the crystal lattice of **2.5a**. Another set of guest pyridine molecules are associated with –COOH group of host molecules by a combination of donor-acceptor C-H···O (C19-H19···O1; $d_{D\cdots A}$ 3.15Å, <D-H···A 119.00º) and O-H···N (O2-H2···N2; $d_{D\cdots A}$ 2.68Å, <D-H···A 172.75º) interactions making cyclic $R_2^2(7)$ hydrogen bond motifs and further interacts with –OH and carbonyl group of host molecules through donor C-H···O (C18-H18···O3; $d_{D\cdots A}$ 3.43Å, <D-H···A 134.89º and C17-H17···O5; $d_{D\cdots A}$ 3.09Å, <D-H···A 117.58º) interactions. These interactions assemble the 1D layers into 3D supramolecular host-guest

network. The 3D network created by host-guest interactions also form channels of approximate 16×6 Å dimensions in the lattice along c axis. These channels created between the 3D layers of host molecules are filled by both sets of guest water and pyridine molecules (Figure 2.3b, 2.3c). We have also shown earlier that different orientations of the weak interactions lead to polymorphic structures in pyridine solvates of naphthalene diimide tethered carboxylic acids.[11c]

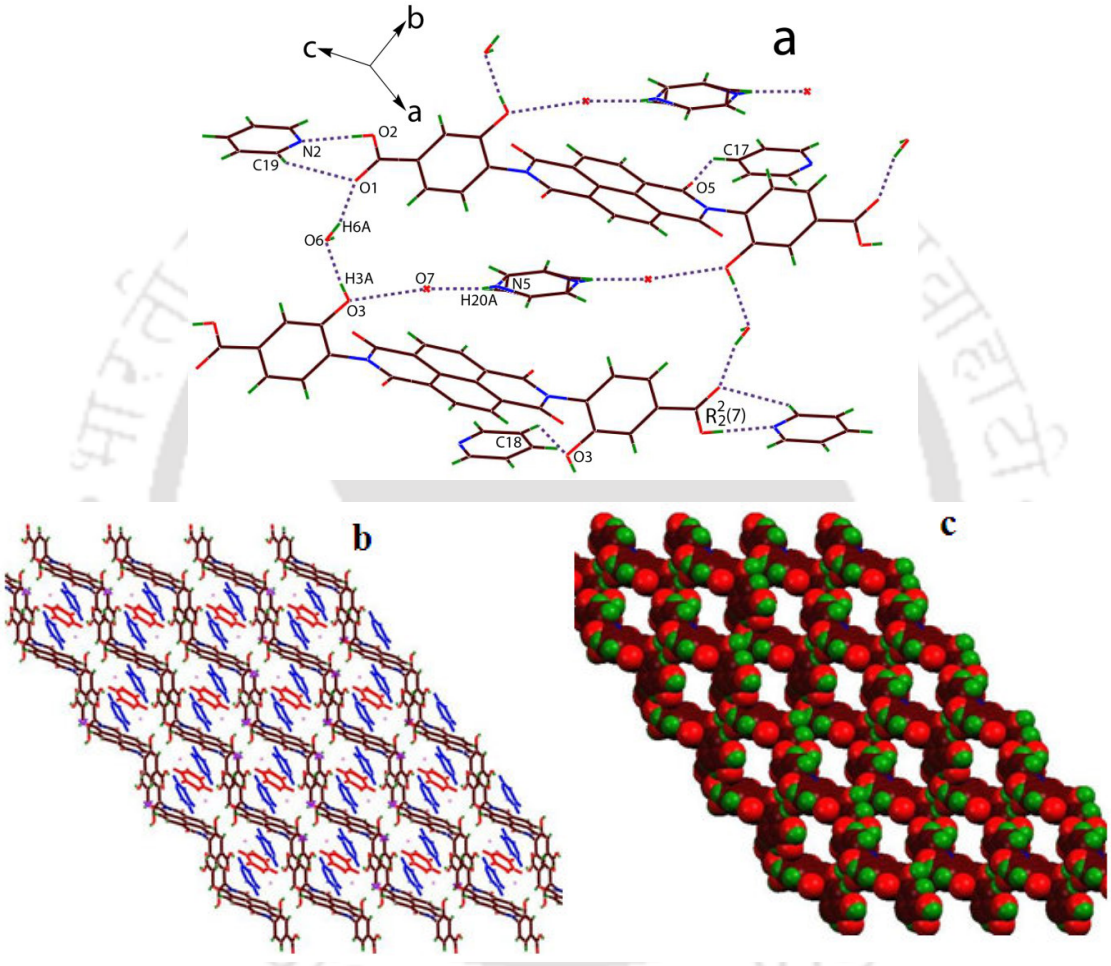

Figure 2.3. (a) Host-guest weak interactions forming 1D supramolecular cavity in the structure of **2.5a**. (b) Formation of 3D channels (along c axis) containing guest pyridine and water molecules inside the channels in the supramolecular architecture of **2.5a**. (c) Space filling model after removal of guest molecules inside the channels.

Since two different types of hydrogen bond motifs (**II** and **III**, as shown in Scheme 2.1) are observed between the -COOH groups and pyridine/bipyridine in the structures of these host-guest complexes; we performed DFT calculations on analogous motifs derived from formic acid

and pyridine to establish these motifs in the solid state. Optimized structures of pyridine/formic acid motifs at the B3LYP/6-31+G* level of theory are shown in Figure 2.4.

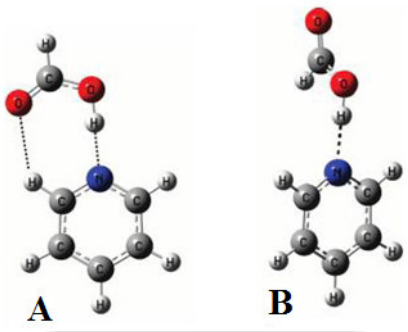

Figure 2.4. Optimized structures of pyridine/formic acid motifs at two different orientations.

In structure 2.4A, both the formic acid and pyridine molecules are coplanar (with a dihedral angle H-O-C-O = 0^0 in formic acid), which facilitates the formation of two short range interactions viz. O-H···N ($d_{H\cdots A,}$ 1.73 Å) and C-H···O ($d_{H\cdots A,}$ 2.45 Å) interactions. However, in the case of structure 2.4B, the two molecules lie at an angle 90^0 to each other, which allows the formation of only one O-H···N ($d_{H\cdots A,}$ 1.78 Å) interaction, and consequently the structure 2.4B is found to be less stable than 2.4A. To obtain a optimized structure with pyridine/formic acid at an angle 90^0 to each other, as shown in Figure 2.4B, we used H-O-C-O=180^0, and calculated energy difference between the two conformers of the acid molecule (with H-O-C-O = 0^0 and with H-O-C-O = 180^0) and subtracted it from the interaction energy of 2.4B to obtain relative stability of 2.4A (E2.4A – E2.4B) because a stable structure like 2.4A was obtained only when the formic acid was used with H-O-C-O=0^0. Relative stability of 2.4A calculated with different basis functions is shown in Table 2.1. It is observed that with lower level basis functions, the relative stability of 2.4A is found to be ~0.15 kcal/mol, whereas highly polarization and diffuse basis function, 6-31++G** gives this value -0.31 kcal/mol. Diffuse double-ζ basis function AUG-cc-pVDZ shows the highest relative stability, that is, -0.61 kcal/mol. The importance of such small interaction energies in crystal lattice is well documented.[13] Such a small difference in energy accounts the probability of formation of both structures depicted in Figure 2.4. The structures of **2.1a** and **2.2a** have discrete types of hydrogen bonds, whereas **2.5a** has a cyclic type; these results combined with the narrow energy differences between the cyclic and discrete structure suggest that the interplay of these weak interactions occurs in the packing pattern and such an

effect with steric requirements decide the formation of different types of hydrogen bond motifs in the solid-state structures of these systems.

Table 2.1. Stability of 2.4A with different basis sets (in kcal/mol).

Basis sets	Relative stability of 2.4A
6-31+G*	-0.16
6-31++G*	-0.13
6-31++G**	-0.31
AUG-cc-pVDZ	-0.61

Powder X-ray diffraction (PXRD) patterns of all these host-guest crystalline materials are recorded, which are almost the same as that simulated patterns from the single-crystal data, revealing the phase purity of the bulk samples (Figure 2.15-2.17). To examine the host-guest ratios in the pyridine solvates, thermogravimetric analyses (TGAs) are carried out (Figure 2.18 and 2.19). Solvate **2.1a** loses 27.6% weight in two steps between 85 and 140^0C which corresponds to the loss of one and half equivalent of pyridine molecules (calcd 26.3%). In solvate **2.5a**, the weight loss between 25 and 55^0C is accounted for the loss of lattice water molecules, further 29.4% weight loss, corresponds to three equivalent of pyridine molecules, occurs from **2.5a** in the temperature range 90-160^0 (calcd 30.5%).

The solvates of compounds **2.3, 2.4 and 2.6** with quinoline **(2.3a, 2.4a and 2.6a)** are also prepared and shown in Scheme 2.5 with their host-guest stoichiometry. All these structures exhibit host-guest O-H···N interactions and the salt formation is also not observed in these structures. The guest quinoline molecules are found to associate with host molecules via different types of weak interactions in the structures of **2.3a, 2.4a and 2.6a**. The 3D supramolecular architectures of these various structures create different types of channels in their crystal lattices which are filled by guest molecules.

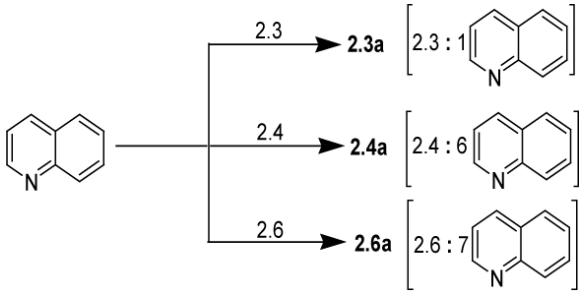

Scheme 2.5. Various solvates of quinoline showing host-guest ratio.

The solvate **2.3a** crystallized in monoclinic $P2_1/c$ space group, containing one molecule of host **2.3** and one guest quinoline molecule in its crystallographic asymmetric unit. The hydrogen atom attached with –COOH group of the host molecule acts as disordered hydrogen in the structure of **2.3a** and is shared with guest quinoline molecule via N-H···O (N2-H2···O2; $d_{D\cdots A}$ 2.54Å, <D-H···A 172.41º) interaction (Figure 2.5a). Another oxygen atom of –COOH group of host molecule form intermolecular bifurcated acceptor hydrogen bond with the aromatic ring of another host molecule by the combination of O-H···O (O3-H3A···O2; $d_{D\cdots A}$ 2.62Å, <D-H···A 176.99º) and C-H···O (C4-H4···O1; $d_{D\cdots A}$ 3.22Å, <D-H···A 127.11º) hydrogen bonds generating a $R_2^1(6)$ motif in the lattice. Carbonyl groups and naphthalimide rings of the host molecules also interact to each other via C-H···O (C15-H15···O4; $d_{D\cdots A}$ 3.23Å, <D-H···A 127.65º) interactions and create a 2D arrangement of host-guest molecules. Further to this, aromatic rings of guest quinoline molecule interact with the oxygen atoms of –OH group and carbonyl group of host molecules via O···π ($d_{O3}\ldots_{\pi}$ 3.21Å and $d_{O5}\ldots_{\pi}$ 3.21Å) interactions. Consequently, individual 2D layers pack together to construct a 3D intermolecular hydrogen bonded host-guest channel network in the lattice where repeated hexameric assemblies of host molecules are involved in the formation of a individual channel of approximate 14×5 Å dimension. The channels formed by repeated 3D hexameric assemblies of host molecules, accommodate the guest quinoline molecules as viewed along a axis (Figure 2.5b, 2.5c).

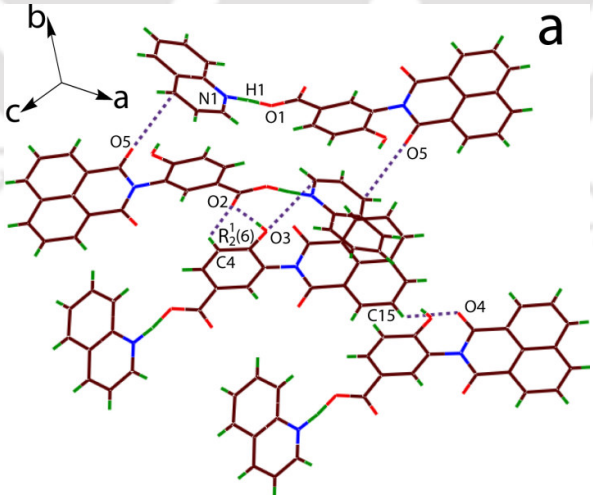

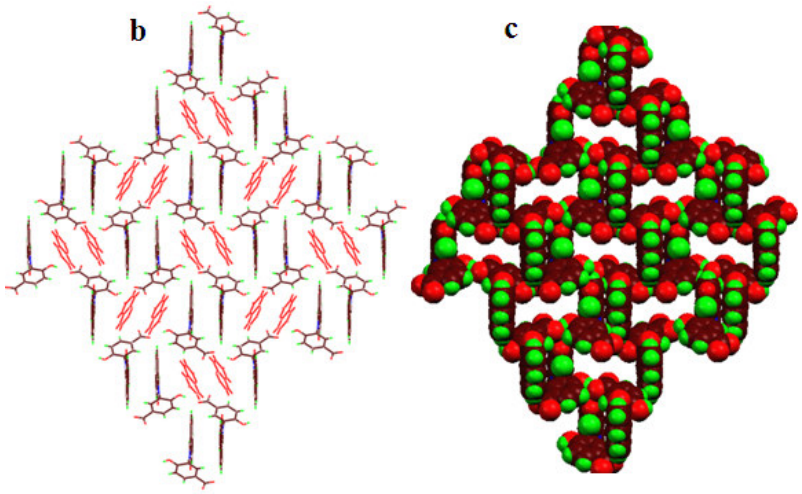

Figure 2.5. (a) Intermolecular interactions in a part of crystal structure of **2.3a**. (b) 3D hexameric assemblies of host molecules creating channels along the a axis. (c) Space filling model after removal of guest molecules inside the channels.

The solvate **2.4a** crystallized in triclinic P-1 space group and it contains half molecule of **2.4** lying on the inversion centre with three symmetry nonequivalent guest quinoline molecules in its crystallographic asymmetric unit. In the crystal lattice of **2.4a**, all the three symmetry independent quinoline molecules are found to associate with host molecule via different weak interactions (Figure 2.6a). First set of quinoline molecule form a cyclic $R_2^1(6)$ hydrogen bond motif interacting with –OH and aromatic ring of host molecule by the combination of acceptor O-H···N (O3-H3A···N2; $d_{D\cdots A}$ 2.79Å, <D-H···A 175.27º) and C-H···N (C3-H3···N2; $d_{D\cdots A}$ 3.42Å, <D-H···A 131.35º) interactions. This quinoline molecule also demonstrates some other weak interactions namely, donor C16-H16···O5 ($d_{D\cdots A}$ 3.08Å, <D-H···A 132.13º) and acceptor C3-H3A···π ($d_{C3\ldots\pi}$ 3.69Å) interactions with the carbonyl group and aromatic ring of host molecule, respectively. Another set of quinoline molecule participate in the formation of a discrete O-H···N (O2-H2···N3; $d_{D\cdots A}$ 2.60Å, <D-H···A 172.30º) hydrogen bond with the –COOH group of host molecule. Third set of quinoline molecules do not facilitate by O-H···N interactions but interact with the oxygen atoms of –COOH and carbonyl groups of host molecule via discrete donor C-H···O (C37-H37···O1; $d_{D\cdots A}$ 3.60Å, <D-H···A 162.96º and C35-H35···O4; $d_{D\cdots A}$ 3.32Å, <D-H···A 133.61º, respectively) interactions. The host molecules do not enclose any weak interaction between them. The guest quinoline molecules belong to first and third set interact with each other only via C-H···π ($d_{C19\ldots\pi}$ 3.75Å) interaction. The C-H···O interactions between the host molecules and first set of quinoline molecules, aggregate them in a 1D layer. Further,

creation of 3D channel-like supramolecular structure occurs in the lattice by the other interactions experienced between host and quinoline molecules. Second and third set of quinoline molecules do not participate in the channel formation. However, the channels (approximate 20×11 Å dimensions) created by the combination of first set of quinoline and host molecules, accommodate the second and third set of quinoline molecules as viewed along the a axis (Figure 2.6b, 2.6c). A quinoline solvate of dopamine based pyromellitic diimide host is reported to create channels in the lattice in which two sets of symmetry non-equivalent guest molecules are found to involve in the construction of channels whereas third set of guest molecules take position inside the channels.[5j]

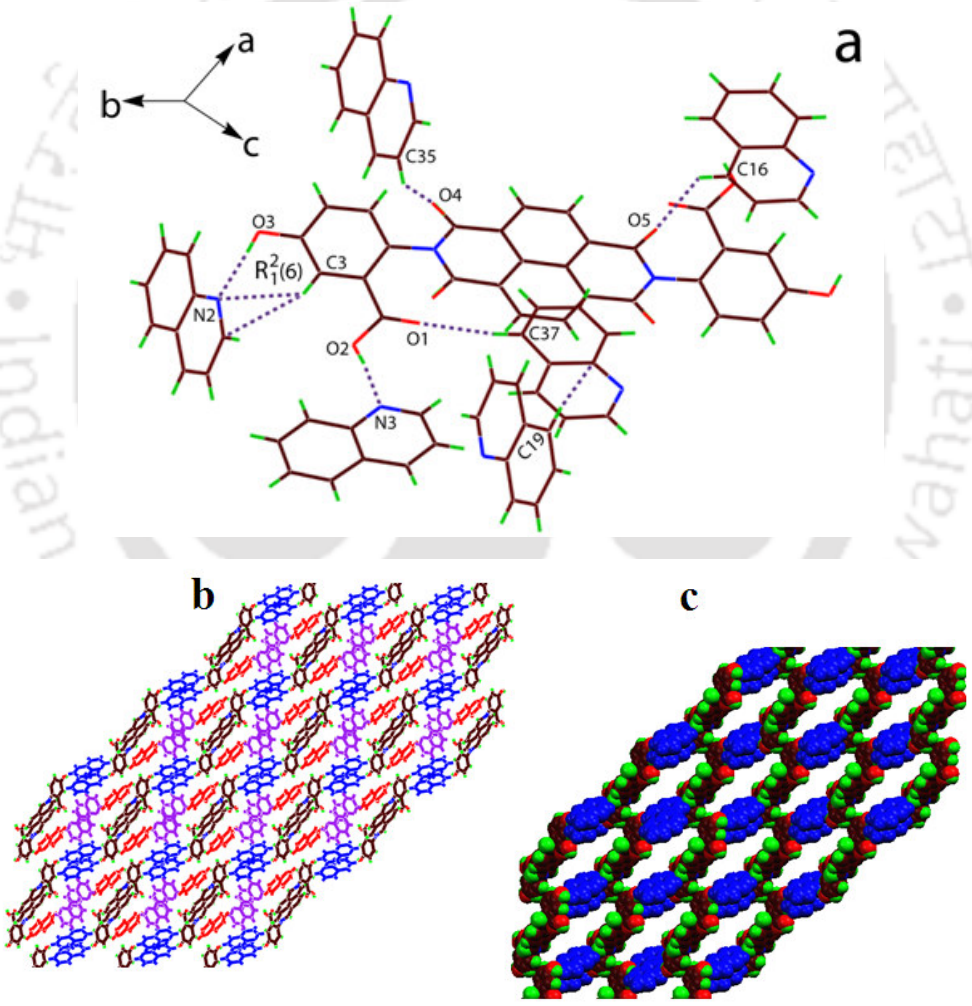

Figure 2.6. (a) Host-guest interactions in a part of crystal structure of **2.4**. (b) 3D supramolecular architecture containing two different sets of guest molecules inside the channels (along a axis). (c) Space filling model after removal of guest quinoline (blue and red) molecules inside the channels.

The solvate **2.6a** crystallized in triclinic P-1 space group and it contains half molecule of **2.6** lying on the inversion center with three and half symmetry nonequivalent guest quinoline molecules in the crystallographic asymmetric unit. The guest quinoline molecule which appears as its half in the asymmetric unit, is disordered and maintains a symmetric structure with respect to an inversion center. The disordered structure is formed by sharing two nitrogen atoms with half occupancies with two carbon atoms at two opposite sites. In the crystal lattice of **2.6a**, the host molecules do not interact with each other any kind of weak interaction (Figure 2.7a). Likely, no interaction between the disorder quinoline and host molecule is observed in the lattice. Remaining three symmetry independent quinoline molecules have different types of interactions with host molecule. First set of quinoline molecule has three different types of interactions with host molecule; two donor C-H···O (C17-H17···O2; $d_{D\cdots A}$ 3.31Å, <D-H···A 157.20º and C15-H15···O5; $d_{D\cdots A}$ 3.23Å, <D-H···A 148.53º) interactions with the –COOH and carbonyl groups, respectively, and one acceptor O-H···N (O3-H3A···N2; $d_{D\cdots A}$ 2.68Å, <D-H···A 155.05º) interaction with –OH group. Second set of quinoline molecule forms a cyclic $R_2^2(7)$ hydrogen bond motif with –COOH group by the combination of donor-acceptor O-H···N (O1-H1···N4; $d_{D\cdots A}$ 2.65Å, <D-H···A 170.87º) and C-H···O (C33-H33···O2; $d_{D\cdots A}$ 3.32Å, <D-H···A 126.80º) interactions. Third set of quinoline molecule interacts with carbonyl group of host molecule via donor C-H···O (C30-H30···O4; $d_{D\cdots A}$ 3.45Å, <D-H···A 157.52º) interaction, simultaneously showing strong π···π contacts with the naphthalene ring of host molecule. These host-guest interactions are found to responsible for the formation of 2D layered network of host and guest molecules in the lattice. These 2D layers are further grown along a axis via guest-guest C-H···π ($d_{C45\ldots\pi}$ 3.44Å) interactions experienced between the disordered and second set of quinoline molecules. Thus, a 3D supramolecular host-guest architecture is constructed in the lattice which contains 2D rectangular channels of approximate 11×11 Å dimension along a axis. The channels are formed by the layered arrangement of host and first set of quinoline molecules. Third set of quinoline molecules are sandwiched inside these channels via weak interactions. The disordered and second sets of guest molecules do not take part in the formation of channels but participate in the enhancement of supramolecular architecture from 2D to 3D through weak interactions in the crystal lattice (Figure 2.7b, 2.7c). However, the quinoline solvates of naphthalene diimide tethered carboxylic acids are found to form pseudopolymorphic structures via different types of host-guest interactions,[11c] but the formation of channels in these structures

may be attributed to the role of additional O-H···N interactions exist between the –OH group of host molecule and guest quinoline molecules.

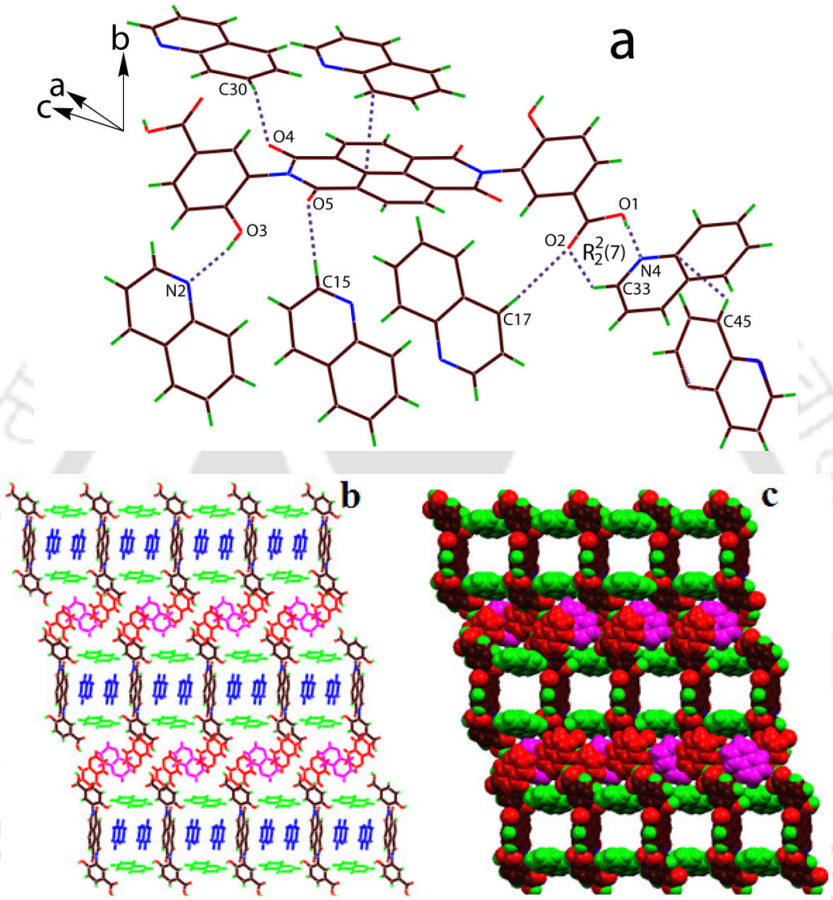

Figure 2.7. (a) Host-guest interactions in a part of crystal structure of **2.6a**. (b) 3D host-guest channels architecture containing a set of guest molecules inside the channels. (c) Space filling model after removal of guest quinoline molecules inside the channels.

DFT calculations were also carried out on the energy of different hydrogen bond motifs arise by the interactions between formic acid and quinoline molecule. Although, the salt formation was not observed in the hydrogen bond motifs formed by the interaction of carboxylic acids and pyridine/quinoline in our systems, however calculations based on DFT show that the salt formation between pyridine and formic acid is not a favourable process but it may occur in case of quinoline and formic acid. Optimized structures of quinoline/formic acid motifs at the B3LYP/6-31+G* level of theory are shown in Figure 2.8.

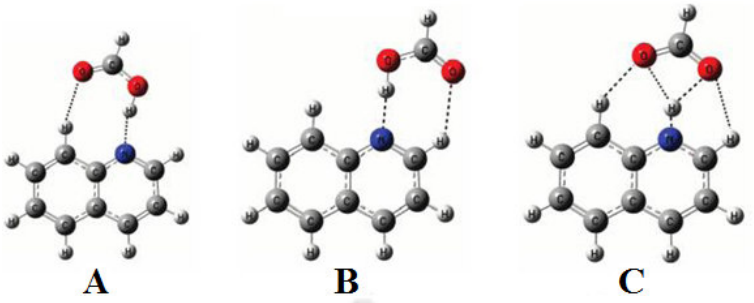

Figure 2.8. Optimized structure of solvates (A, B) and salt (C) of formic acid with quinoline.

It is observed that two different short-range O-H···N ($d_{H\cdots A,}$ 1.76 Å in 2.8A; $d_{H\cdots A,}$ 1.73 Å in 2.8B) and C-H···O ($d_{H\cdots A,}$ 2.35 Å in 2.8A; $d_{H\cdots A,}$ 2.44 Å in 2.8B) interactions exist in structure 2.8A and 2.8B. The interactions between quinoline and formic acid are exocyclic in 2.8A, while these interactions are endocyclic in 2.8B. The optimized structure of quinolinium carboxylate salt (Figure 2.8C) clearly shows that the two ions are in the same plane. The N-H bond length is found to be 1.06 Å, which is much longer than the typical N-H covalent bond length (0.80 Å). The interaction distance between the H atom of quinolinium cation and the two O atoms of carboxylate anion are 1.81 and 1.99 Å, which shows the formation of the moderately strong hydrogen bond between them. Two C-H···O interactions with $d_{H\cdots A}$ (Å) 2.18 and 2.45 are also exist there. Among the three structures, 2.8B is found to be the most stable. Different levels of calculations show that the stability of 2.8B compared to 2.8A lies in the range -0.57 kcal/mol to -0.63 kcal/mol (Table 2.2) which also affects the order of N···H bond distances in structures 2.8A and 2.8B (2.8A, 1.76 Å > 2.8B, 1.73Å).

Table 2.2. Stability of different hydrogen bond motifs (in kcal/mol).

Basis sets	Stability of 2.8B over 2.8A	Stability of 2.8B over 2.8C
6-31+G*	-0.57	-13.65
6-31++G*	-0.58	-13.65
6-31++G**	-0.63	-14.87
AUG-cc-pVDZ	-0.64	-14.94

The formation of quinolinium carboxylate salt (2.8C) is possible, but it is quite unstable compared to 2.8A or 2.8B. The range of stability of 2.8B compared to 2.8C with different basis

sets is found to be -13.65 kcal/mol to -14.94 kcal/mol (Table 2.2). This theoretical data suggest that there are geometrical requirements, which are over and above the conventional pKa values of an acid under consideration to make solvates or deprotonated species in solid-state assembly.[14]

The PXRD patterns of the quinoline solvates **2.3a**, **2.4a**, **2.6a** are shown in Figure 2.20, 2.21 and 2.22, respectively, in the Experimental Section. All of the peaks of different solvates can be correlated nearly with their respective simulated PXRD patterns of single crystal X-ray structures. The small deviations are attributed to loss of solvent molecules leading to loss of crystallinity. TGAs on quinoline solvates are also carried out (Figure 2.23-2.25). Solvate **2.3a** shows one step weight loss of 28.1% weight between 145 and 185^{0}C corresponds to one equivalent of quinoline molecule (calcd 27.9%). Weight loss of six guest quinoline molecules occurs in two steps from **2.4a**. In first step, 39.0% weight loss corresponds to four equivalent of quinoline molecules occurs between 115 and 150^{0}C (calcd 39.3%). In second step, 31.9% weight loss occurs from the residue of the first step for remaining two guest quinoline molecules between 210 and 245^{0}C (calcd 32.4%). For the solvate **2.6a**, a continuous weight loss due to the seven equivalent of quinoline molecules takes place in the temperature range 115-275^{0}C corresponding to a weight loss of 58.7% (calcd 62.6%).

In conclusion, supramolecular structural features of host-guest complexes of pyridine/bipyridine and quinoline with a few trifunctional molecules that contained both hydroxyl and carboxylic acid groups tethered by a π-stacking naphthalimide or naphthalene diimide tectons are studied. Various types of intermolecular hydrogen bonding interactions are found to responsible for the formation of channels filled by guest molecules in all these host-guest 3D supramolecular architectures. Despite of two different functional groups that are capable of getting deprotonated, none of them resulted in salt formation with pyridine and quinoline, but participated in supramolecular interactions and provided the directional properties to host-guest systems. It is also clear from this study that stability of the channels which are filled by guest molecules, are guided by various types of intermolecular host-guest interactions. We could distinguish two different classes of channels, namely, the one are those constructed by the self assembly of hosts containing the guest molecules within them. Another category includes the channels formed by the combination of both host and guest molecules containing additional guest molecules inside them. Since the guest molecules studied here are relatively bigger in size than conventional solvent molecules, we could identify the symmetry associated with the guest molecules and found that there are symmetry non-equivalent guests in certain cases, for example, a system

which embedded six molecules of quinoline namely **2.4a**, has two symmetry non-equivalent guest molecules within the channel. The structures of **2.4a** and **2.6a** contain higher number of guest molecules and serve as excellent storage systems for quinoline molecules by organic hosts. It is observed that the discrete as well as cyclic types of hydrogen bonds are involved with the host-guest O-H···N interactions. DFT calculations on energy of different formic acid/pyridine and formic acid/quinoline motifs suggest that the energy differences between these motifs are very small and within the limit of very weak hydrogen bonds. Thus, their formation is controlled by the other weak interactions present in the crystal lattices. Such small energy difference also accounts for the formation of both types of structural patterns in pyridine/bipyridine complexes depending on the steric requirements. DFT calculations show that the salt formation between pyridine and formic acid is not a favorable process but it may occur in case of quinoline and formic acid.

Experimental Section:

Computational Details:

We have considered motifs derived from formic acid with pyridine or quinoline as model system for calculation of energy. The geometries of the models have been calculated with DFT[15] using the combined Becke's three-parameter exchange functional and the gradient-corrected functional of Lee, Yang and Parr (B3-LYP functional)[16] at 6-31+G* levels. This functional has been demonstrated to predict reliable geometries for hydrogen bonded systems.[17] Single point calculations at the 6-31+G*, 6-31++G** and B3LYP/AUG-cc-pVDZ[18] level were performed on the fully optimized geometries using B3LYP/6-31+G*. All calculations are performed using the Gaussian03 program.[19] The choice of this basis set is based on the consideration to obtain reliable properties for hydrogen-bonded systems, and it is essential to employ basis sets that possess sufficient diffuseness and angular flexibility.[20] This basis set 6-31++G** is sufficient to predict reliable properties for hydrogen-bonded systems. All calculations are carried out in the gas phase.

Detailed synthetic methodologies are given below. Analytical data as well as spectroscopic data are listed along with each compound. The instrumental details are given in Appendix.

Synthesis and characterization of compounds and their host-guest complexes:

2-(1,3-Dioxo-1*H*,3*H*-benzo[de]isoquinolin-2-yl)-5-hydroxy-benzoic acid; **2.1**: A solution of 1,8-naphthalic anhydride (0.990 g, 5 mmol) and 2-amino-5-hydroxy-benzoic acid (0.765 g, 5 mmol)

in N,N-dimethylformamide (15 mL) was refluxed for 5 hrs. The reaction mixture was cooled to room temperature, poured into ice cooled water (50 mL) and stirred for 15 min. A brown colored precipitate of the product was formed, which was filtered and air dried. Yield: 86%; IR (KBr, cm^{-1}): 3293 (s), 1720 (s), 1693 (s), 1623 (m), 1582 (s), 1499 (w), 1382 (m), 1293 (m), 1250 (s), 1208 (s), 824 (w), 780 (m), 665 (w). ^{1}HNMR (400 MHz, DMSO-d^6): 10.07 (s, 1H), 8.49 (m, 4H), 7.89 (t, 2H, *J* = 8.0 Hz), 7.48 (s, 1H), 7.26 (d, 1H, *J* = 8.4 Hz), 7.10 (d, 1H, *J* = 8.4 Hz). ESI-MS: 334.127 [M + H^+].

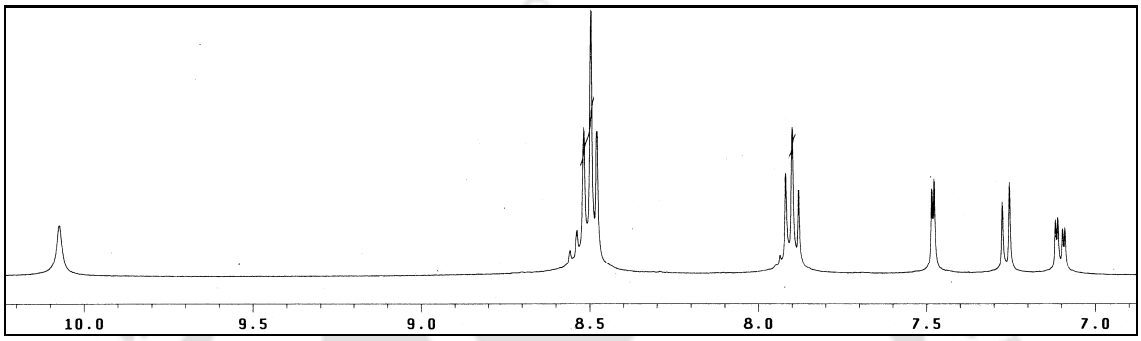

Figure 2.9: ^{1}HNMR spectra of compound **2.1**.

4-(1,3-Dioxo-1*H*,3*H*-benzo[de]isoquinolin-2-yl)-3-hydroxy-benzoic acid; **2.2**: Compound **2.2** was also obtained by the cyclo-condensation reaction of 1,8-naphthalic anhydride and 4-amino-3-hydroxy-benzoic acid with the similar procedure as used for **2.1**. Yield: 84%; IR (KBr, cm^{-1}): 3397 (m), 1774 (w), 1737 (m), 1693 (s), 1651 (s), 1621 (s), 1589 (s), 1513 (w), 1437 (m), 1379 (m), 1358 (m), 1302 (w), 1270 (w), 1243 (s), 1121 (m), 1012 (w), 960 (w), 893 (w), 784 (m), 764 (m). ^{1}HNMR (400 MHz, DMSO-d^6): 10.11 (s, 1H), 8.51 (m, 4H), 7.90 (t, 2H, *J* = 7.6 Hz), 7.56 (s, 1H), 7.50 (d, 1H, *J* = 8.0 Hz), 7.10 (d, 1H, *J* = 8.4 Hz). ESI-MS: 334.106 [M + H^+].

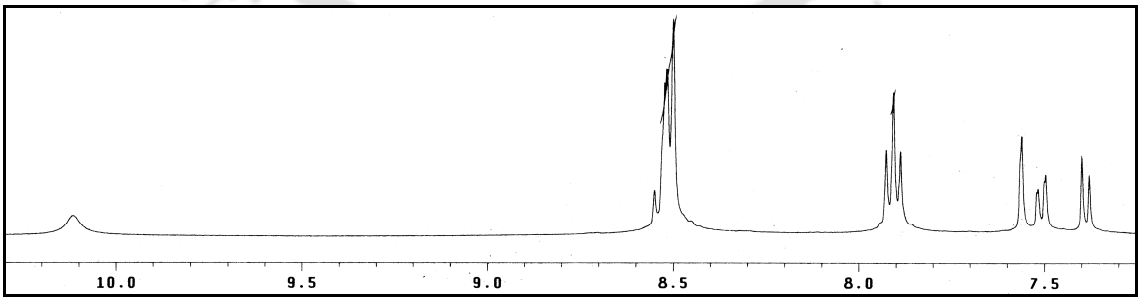

Figure 2.10: ^{1}HNMR spectra of compound **2.2**.

3-(1,3-Dioxo-1*H*,3*H*-benzo[de]isoquinolin-2-yl)-4-hydroxy-benzoic acid; **2.3**: Compound **2.3** was synthesized by the cyclo-condensation reaction of 1,8-naphthalic anhydride and 3-amino-4-

hydroxy-benzoic acid with the similar procedure as used for **2.1**. Yield: 87%; IR (KBr, cm^{-1}): 3292 (s), 1774 (w), 1711 (s), 1698 (s), 1644 (m), 1608 (s), 1589 (m), 1510 (w), 1438 (w), 1376 (m), 1297 (m), 1270 (s), 1236 (s), 1191 (w), 1013 (w), 778 (m), 662 (w). ^{1}HNMR (400 MHz, DMSO-d^6): 10.61 (s, 1H), 8.49 (m, 4H), 7.89 (m, 4H), 7.07 (d, 1H, J = 8.8 Hz). ESI-MS: 334.132 [M + H^+].

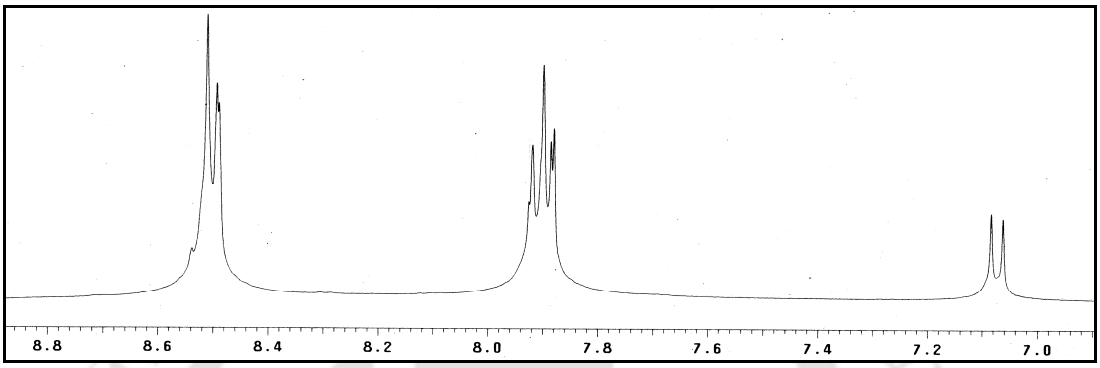

Figure 2.11: ^{1}HNMR spectra of compound **2.3**.

5-hydroxy-2-[7-(2-carboxy-4-hydroxy-phenyl)-1,3,6,8-tetraoxo-3,6,7,8-tetrahydro-1*H*-benzo[*lmn*][3,8]phenanthrolin-2-yl]-benzoic acid, **2.4**: A solution of 1,4,5,8-naphthalenetetracarboxylic dianhydride (1.34 g, 5 mmol) and 2-amino-5-hydroxy-benzoic acid (1.530 g, 10 mmol) in N,N-dimethylformamide (20 mL) was refluxed for 3 hrs. The reaction mixture was cooled to room temperature, poured into ice cooled water (100 mL) and stirred for 15 min. A yellow colored precipitate of the product was filtered and air dried. Yield: 90%; IR

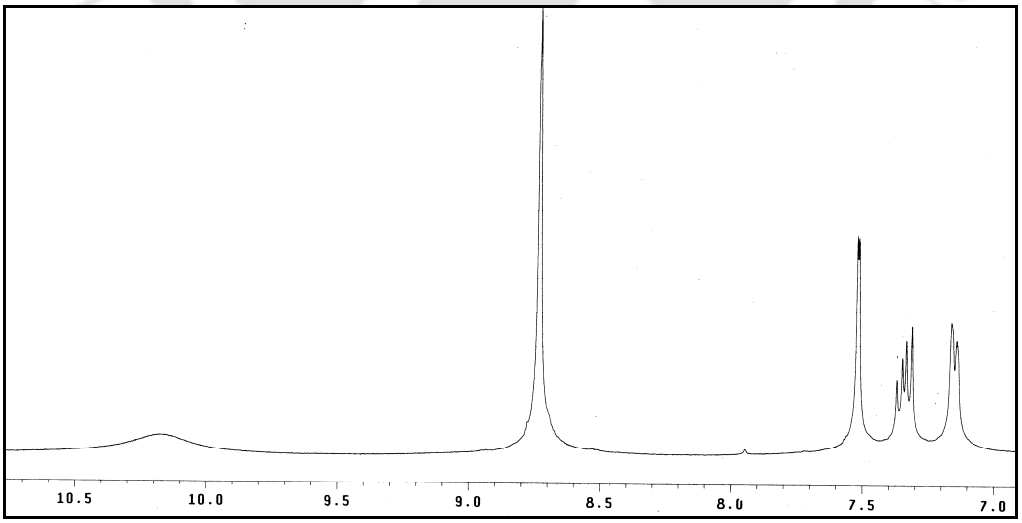

Figure 2.12: ^{1}HNMR spectra of compound **2.4**.

(KBr, cm^{-1}): 3419 (m), 1736 (s), 1705 (s), 1657 (s), 1606 (m), 1583 (m), 1505 (w), 1454 (w), 1374 (m), 1361 (m), 1292 (w), 1260 (s), 1205 (s), 1154 (w), 1065 (w), 986 (w), 881 (w), 771 (m), 746 (m). ^{1}HNMR (400 MHz, DMSO-d^6): 10.17 (s, 2H), 8.73 (s, 4H), 7.52 (s, 2H), 7.33 (dd, 2H, *J* = 8.8 Hz), 7.15 (d, 2H, *J* = 8.4 Hz). ESI-MS: 584.112 [M + H^+].

3-hydroxy-2-[7-(4-carboxy-2-hydroxy-phenyl)-1,3,6,8-tetraoxo-3,6,7,8-tetrahydro-1*H*-benzo[*lmn*][3,8]phenanthrolin-2-yl]-benzoic acid; **2.5**: A red colored precipitate of the product **2.5** was obtained by the cyclo-condensation reaction of 1,4,5,8-naphthalenetetracarboxylic dianhydride and 4-amino-3-hydroxy-benzoic acid with the similar procedure as used for **2.4**. Yield: 90%; IR (KBr, cm^{-1}): 3341 (m), 1712 (s), 1673 (s), 1603 (m), 1580 (m), 1426 (m), 1355(s), 1254 (s), 1113 (w), 981 (w), 950 (w), 885 (w), 839 (m), 768 (m), 751 (m), 704 (w). ^{1}HNMR (400 MHz, DMSO-d^6): 10.20 (s, 2H), 8.74 (s, 4H), 7.58 (s, 2H), 7.54 (d, 2H, *J* = 8.8 Hz), 7.46 (d, 2H, *J* = 8.0 Hz). ESI-MS: 584.124 [M + H^+].

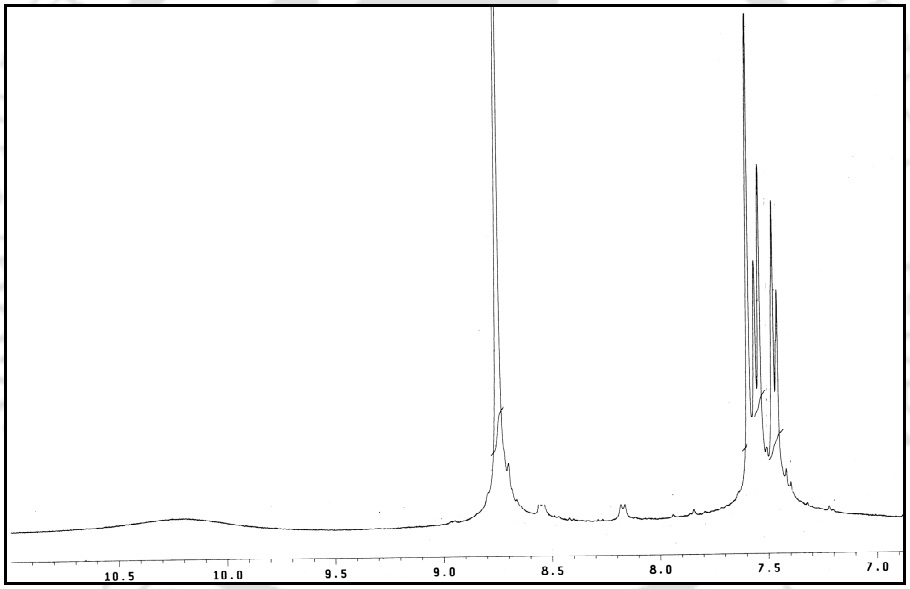

Figure 2.13: ^{1}HNMR spectra of compound **2.5**.

4-hydroxy-2-[7-(3-carboxy-6-hydroxy-phenyl)-1,3,6,8-tetraoxo-3,6,7,8-tetrahydro-1*H*-benzo[*lmn*][3,8]phenanthrolin-2-yl]-benzoic acid; **2.6**: The product **2.6** was obtained by the cyclo-condensation reaction of 1,4,5,8-naphthalenetetracarboxylic dianhydride and 3-amino-4-hydroxy-benzoic acid as pink solid with the similar procedure as used for **2.4**. Yield: 90%; IR (KBr, cm^{-1}): 3300 (m), 1707 (s), 1668 (s), 1611 (s), 1582 (m), 1514 (w), 1451 (m), 1352(s), 1296 (m), 1260 (s), 1252 (s), 1212 (m), 1123 (w), 1087 (w), 985 (w), 841 (w), 768 (m), 648 (w).

^{1}HNMR (400 MHz, DMSO-d^6): 10.62 (s, 2H), 8.72 (s, 4H), 8.00 (s, 2H), 7.93 (d, 2H, *J* = 8.4 Hz), 7.09 (d, 2H, *J* = 8.8 Hz). ESI-MS: 584.095 [M + H$^+$].

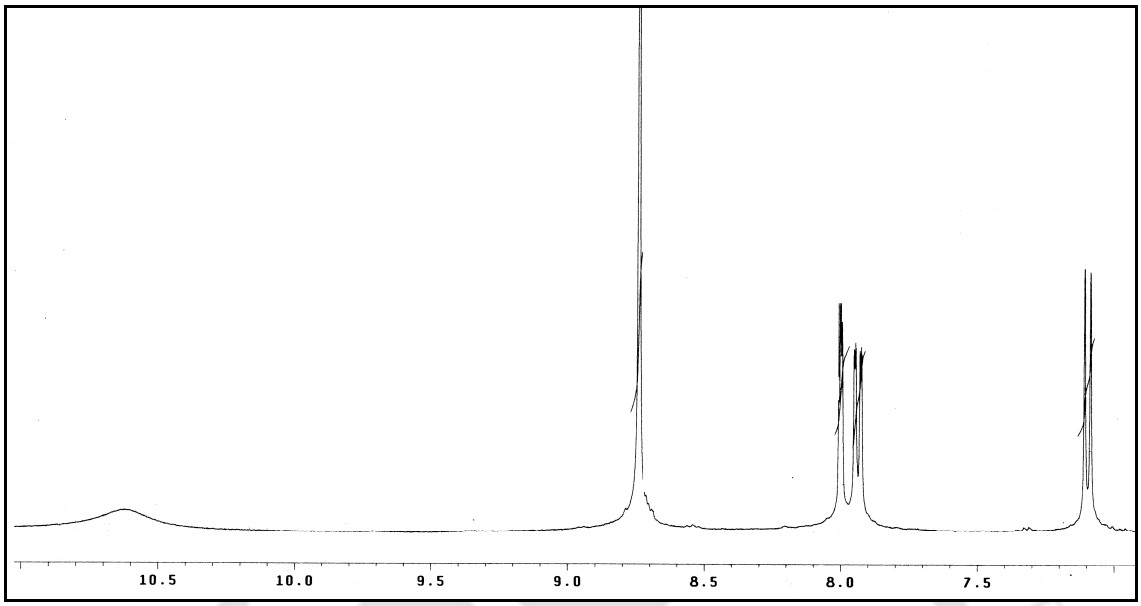

Figure 2.14: ^{1}HNMR spectra of compound **2.6**.

Solvate 2.1a: The crystals of solvate **2.1a** were obtained as colourless plates from a solution of compound **2.1** in pyridine. IR (KBr, cm^{-1}): 3294 (m), 1719 (s), 1694 (s), 1651 (s), 1624 (m), 1591 (m), 1500 (w), 1438 (w), 1381 (m), 1361 (m), 1292 (m), 1248 (s), 1208 (s), 1065 (w), 823 (w), 781 (m), 750 (m). ^{1}HNMR (400 MHz, DMSO-d^6): 10.07 (s, 1H), 8.57 (d, 3H, *J* = 2.8 Hz), 8.50 (t, 4H, *J* = 7.6 Hz), 7.90 (t, 2H, *J* = 7.6 Hz), 7.78 (t, 2H, J = 7.2 Hz), 7.49 (s, 1H), 7.38 (t, 3H, *J* = 6.0 Hz), 7.27 (d, 1H, *J* = 8.4 Hz), 7.11 (d, 1H, *J* = 8.0 Hz).

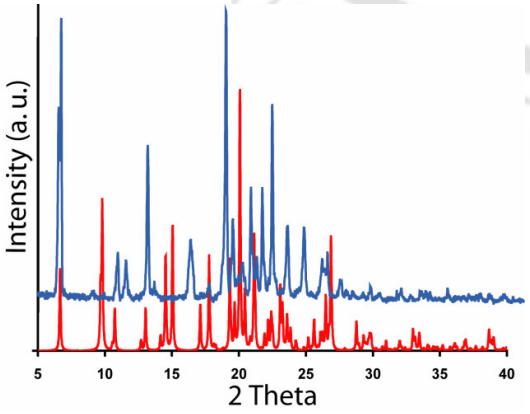

Figure 2.15: Simulated (below) and experimental (above) PXRD patterns of solvate **2.1a**.

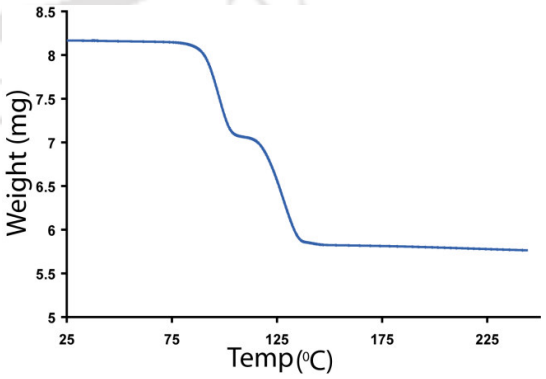

Figure 2.18: TGA curve of solvate **2.1a**.

Co-crystal 2.2a: A solution of compound **2.2** in pyridine and a solution of bpy in ethanol were mixed together in 1:1 ratio; red block crystals of **2.2a** were obtained after 15 days from the solution. IR (KBr, cm^{-1}): 3444 (m), 1774 (w), 1737 (m), 1688 (s), 1650 (s), 1589 (s), 1437 (m), 1378 (m), 1357 (m), 1243 (s), 1120 9m), 1013 (m), 959 (w), 897 (w), 815 (m), 782 (m), 764 (m). ^{1}HNMR (400 MHz, DMSO-d^{6}): 10.13 (s, 1H), 8.71 (s, 4H), 8.50 (d, 4H, *J* = 7.6 Hz), 7.90 (t, 2H, *J* = 7.6 Hz), 7.80 (s, 4H), 7.56 (s, 1H), 7.50 (d, 1H, *J* = 8.0 Hz), 7.38 (d, 1H, *J* = 8.4 Hz).

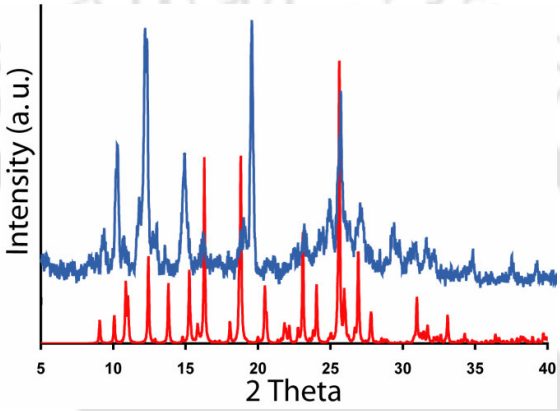

Figure 2.16: Simulated (below) and experimental (above) PXRD patterns of co-crystal **2.2a**.

Solvate 2.5a: Compound **2.5** was dissolved in pyridine and left undisturbed for seven days. The crystals of **2.5a** were obtained as red blocks. IR (KBr, cm^{-1}): 3430 (m), 1714 (m), 1673 (s), 1582 (m), 1426 (m), 1358 (s), 1255 (s), 1214 (m), 1200 (m), 1092 (w), 981 (w), 949 (w), 883 (w), 840 (w), 768 (m), 753 (m). ^{1}HNMR (400 MHz, DMSO-d^{6}): 10.19 (s, 2H), 8.74 (s, 4H), 8.57 (s, 6H), 7.74 (t, 3H, J = 7.2 Hz), 7.59 (s, 2H), 7.54 (d, 2H, *J* = 8.4 Hz), 7.46 (d, 2H, *J* = 8.0 Hz), 7.37 (s, 6H).

Solvate 2.3a: The solvate **2.3a** was obtained by crystallization of compound **2.3** from quinoline solution as brown block crystals. IR (KBr, cm^{-1}): 3445 (m), 1698 (s), 1662 (s), 1589 (s), 1501 (m), 1434 (m), 1355 (s), 1291 (m), 1241 (s), 889 (w), 849 (w), 809 (m), 787 (m), 735 (w), 670 (w). ^{1}HNMR (400 MHz, DMSO-d^{6}): 10.63 (s, 1H), 8.90 (d, 2H, *J* = 2.8 Hz), 8.72 (s, 1H), 8.42 (d, 2H, *J* = 7.6 Hz), 7.88 (m, 5H), 7.76 (t, 2H, *J* = 7.2 Hz), 7.61 (t, 1H, J = 7.6 Hz), 7.52 (dd, 2H, *J* = 4.4 Hz), 7.10 (d, 1H, *J* = 8.4 Hz).

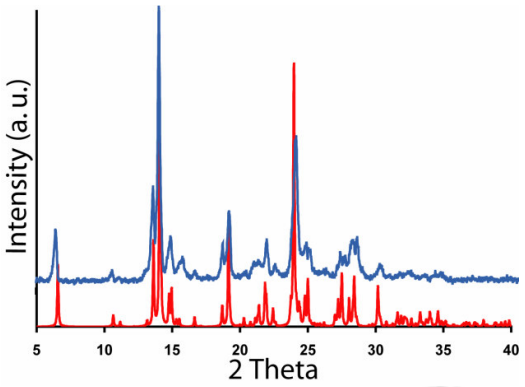

Figure 2.17: Simulated (below) and experimental (above) PXRD patterns of solvate **2.5a**.

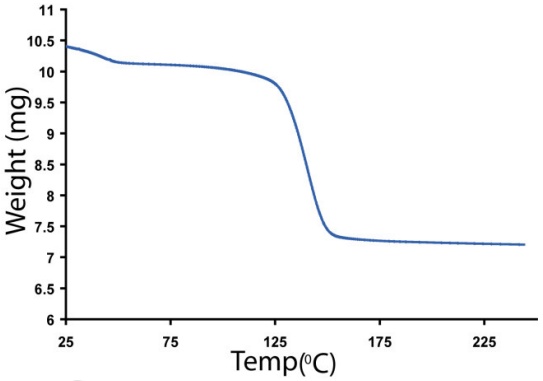

Figure 2.19: TGA curve of solvate **2.5a**.

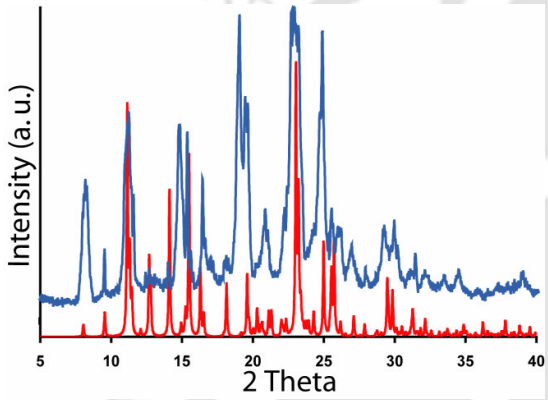

Figure 2.20: Simulated (below) and experimental (above) PXRD patterns of solvate **2.3a**.

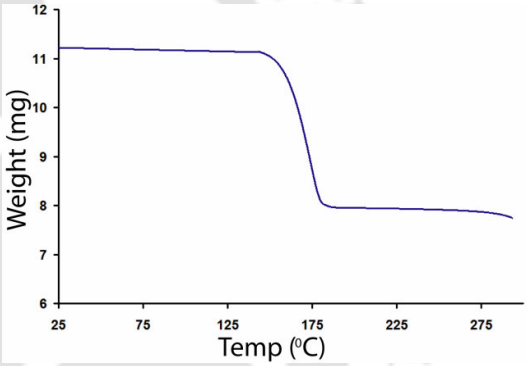

Figure 2.23: TGA curve of solvate **2.3a**.

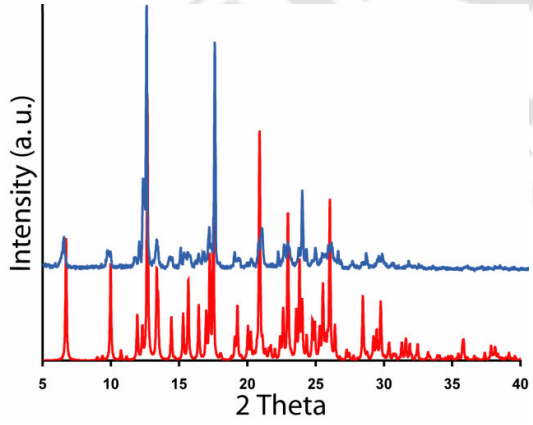

Figure 2.21: Simulated (below) and experimental (above) PXRD patterns of solvate **2.4a**.

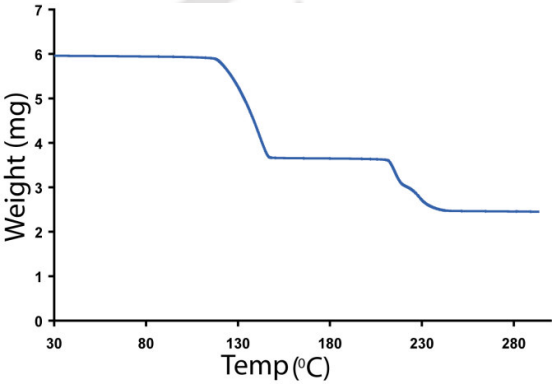

Figure 2.24: TGA curve of solvate **2.4a**.

Solvate 2.4a: A solution of compound **2.4** in pyridine and quinoline resulted in the formation of crystals of solvate **2.4a** as red blocks. IR (KBr, cm^{-1}): 3444 (m), 1706 (s), 1667 (s), 1530 (m), 1363 (s), 1289 (m), 1256 (s), 1222 (m), 1146 (w), 1124 (w), 771 (m). ^{1}HNMR (400 MHz, DMSO-d^{6}): 10.16 (s, 2H), 8.90 (d, 6H, *J* = 2.8 Hz), 8.71 (s, 4H), 8.36 (d, 6H, *J* = 8.0 Hz), 8.00 (dd, 12H, *J* = 8.4 Hz), 7.76 (t, 6H, *J* = 8.0 Hz), 7.59 (t, 6H, J = 8.0 Hz), 7.33 (m, 8H), 7.32 (d, 2H, *J* = 8.4 Hz), 7.15 (d, 2H, *J* = 8.8 Hz).

Solvate 2.6a: The solvate **2.6a** was obtained from a solution of compound **2.6** in quinoline and pyridine after three days as yellow blocks. IR (KBr, cm^{-1}): 3434 (m), 1712 (s), 1681 (s), 1606 (s), 1581 (s), 1504 (m), 1447 (m), 1374 (m), 1346 (s), 1301 (s), 1248 (s), 1123 (m), 1082 (m), 981 (w), 949 (w), 810 (m), 784 (m), 765 (m). ^{1}HNMR (400 MHz, DMSO-d^{6}): 10.56 (s, 2H), 8.90 (d, 7H, *J* = 2.8 Hz), 8.51 (s, 4H), 8.50 (s, 2H), 8.36 (d, 7H, *J* = 7.6 Hz), 8.00 (dd, 14H, *J* = 8.0 Hz), 7.89 (t, 7H, *J* = 8.0 Hz), 7.76 (t, 7H, *J* = 7.6 Hz), 7.61 (t, 7H, J = 7.2 Hz), 7.52 (dd, 2H, *J* = 4.0 Hz), 7.07 (d, 2H, *J* = 8.4 Hz).

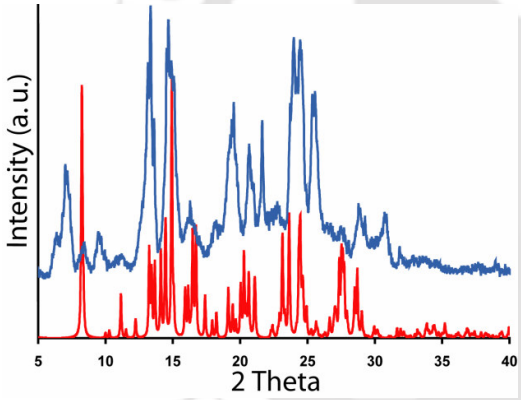

Figure 2.22: Simulated (below) and experimental (above) PXRD patterns of solvate **2.6a**.

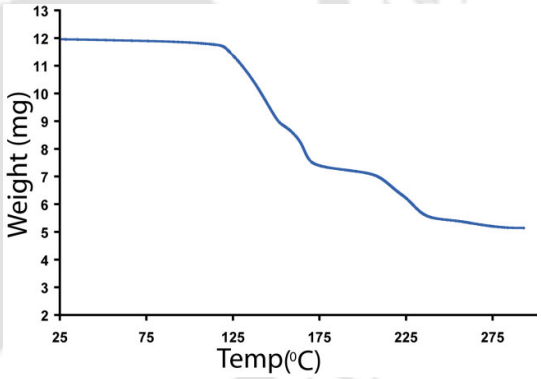

Figure 2.25: TGA curve of solvate **2.6a**.

References:

(1) (a) Etter, M. C. *Acc. Chem. Res.* **1990**, *23*, 120. (b) Huang, K.-S.; Britton, O.; Bryn, S. R.; Etter, M. C. *J. Mater. Chem.* **1997**, *7*, 713. (c) Gavezzotti, A. *Acc. Chem. Res.* **1994**, *27*, 309. (d) Desiraju, G. R. *Angew. Chem., Int. Ed.* **1995**, *34*, 2311. (e) Dunitz, J. D. *Chem. Commun.* **2003**, 545. (f) Nishio, M. *CrystEngComm* **2004**, *6*, 130. (g) Hosseini, M. W. *CrystEngComm* **2004**, *6*, 318. (h) Almarsson, Ő.; Zaworotko, M. J. *Chem. Commun.* **2004**, 1889.

(2) (a) Byrn, S. R. *Solid-State Chemistry of Drugs; Academic press:* New York, 1982. (b) Desiraju, G. R. *Science* **1996**, *278*, 404. (c) Jetti, R. K. R.; Boese, R.; Sarma, J. A. R. P.; Reddy,

L. S. R.; Vishweshwar, P.; Desiraju, G. R. *Angew. Chem., Int. Ed.* **2003**, *42*, 1963. (d) Yu, L. *J. Am. Chem. Soc.* **2003**, *125*, 6380. (e) Duntiz, J. D.; Bernstein, J. *Acc. Chem. Res.* **1995**, *28*, 193. (f) Hennigar, T. L.; MacQuarrie, D. C.; Losier, P.; Rogers, R. D.; Zaworotko, M. J. *Angew. Chem., Int. Ed. Engl.* **1997**, *36*, 972.

(3) (a) Visheswar, A. P.; McMahon, J. A.; Bis, J. A.; Zaworotko, M. J. *J. Pharm. Sci.* **2006**, *95*, 499. (b) Morissette, S. L.; Almarsson, O.; Peterson, M. L.; Remenar, J. F.; Read, M. J.; Lemmo, A. V.; Ellis, S.; Cima, M. J.; Gardner, C. R. *Adv. Drug Delivery Rev.* **2004**, *56*, 275.

(4) (a) Halder, G. J.; Kepert, C. J.; Moubaraki, B.; Murray, K. S.; Cashion, J. D. *Science* **2002**, *298*, 1762. (b) Kitaura, R.; Seki, K.; Akiyama, G.; Kitagawa, S. *Angew. Chem., Int. Ed.* **2003**, *42*, 428. (c) Yaghi, O. M.; Ơ Keeffe, M.; Ockwig, N. W.; Chae, H. K.; Eddaoudi, M.; Kim, J. *Nature* **2003**, *423*, 705. (d) Mahender, J. Y.; Dewal, B.; Shimizu, L. S. *J. Am. Chem. Soc.* **2006**, *128*, 8122. (e) Rebek, J.; Askew, B.; Ballester, P.; Buhr, C.; Jones, S.; Nemeth, D.; Williams, K. *J. Am. Chem. Soc.* **1987**, *109*, 5033. (f) Seneque, O.; Rager, M.-N.; Giorgi, M.; Reinaud, O. *J. Am. Chem. Soc.* **2000**, *122*, 6183.

(5) (a) Colquhoun, H. M.; Williams, D. J.; Zhu, Z. *J. Am. Chem. Soc*. **2002**, *124*, 13346. (b) Cheney, M. L.; McManus, G. J.; Perman, J. A.; Wang, Z.; Zaworotko, M. J. *Cryst. Growth Des.* **2007**, *7*, 616. (c) Degenhardt III, C.; Shortell, D. B.; Adams, R. D.; Shimizu, K. D. *Chem.Comm.* **2000**, 929. (d) Degenhardt, C. F.; Lavin, J. M.; Smith, M. D.; Shimizu, K. D.; *Org. Letters* **2005**, *7*, 4079. (e) Rasberry, R. D.; Smith, M. D.; Shimizu, K. D. *Org. Letters* **2008**, *13*, 2889. (f) Barooah, N.; Sarma, R. J.; Baruah, J. B. *Cryst. Growth Des.* **2003**, *3*, 639. (g) Barooah, N.; Sarma, R. J.; Baruah, J. B. *CrystEngComm* **2006**, *8*, 608. (h) Baruah, J. B.; Karmakar, A.; Barooah, N. *CrystEngComm* **2008**, *10*, 151. (i) Singh, D.; Bhattacharyya, P.; Baruah, J. B. *Cryst. Growth Des.* **2010**, *10*, 348. (j) Singh, D.; Baruah, J. B. *Cryst. Growth Des.* **2011**, *11*, 768.

(6) (a) Gawronski, J.; Kaik, M.; Kwit, M.; Rychlewska, U. *Tetrahedron* **2006**, *62*, 7866. (b) Flamigni, L.; Johnston, M. R.; Giribabu, L. *Chem. Eur. J.* **2002**, *8*, 3938.

(7) (a) Reger, D. L.; Elgin, J. D.; Semeniuc, R. F.; Pellechia, P. J.; Smith, M. D. *Chem. Commun.* **2005**, 4068. (b) Reger, D. L.; Semeniuc, R. F.; Elgin, J. D.; Rassolov, V.; Smith, M. D. *Cryst. Growth Des.* **2006**, *6*, 2758. (d) Reger, D. L.; Debreczeni, A.; Reinecke, B.; Rassolov, V.; Smith, M. D.; Semeniuc, R. F. Inorg. Chem. 2009, 48, 8911.

(8) (a) Bhogala, B. R.; Basavoju, S.; Nangia, A. *Cryst. Growth Des.* **2005**, 5, 1683. (b) Bhogala, BR.; Nangia,A. *Cryst. Growth Des.* **2003**, 3,547. (c) Blagden, N.; deMatas, M.; Gavan, P. T.; York, P. *Adv. Drug Delivery Rev.* **2007**, 59, 617. (d) Biradha, K.; Zaworotko, M. J. *Cryst. Eng.* **1998**, 1, 67.

(9) (a) Weyna, D. R.; Shattock, T.; Visweshwar, P.; Zaworotko, M. J. *Cryst. Growth Des.* **2009**, *9*, 1106. (b) Bhatt, P. M.; Ravindra, N. V.; Banerjee, R.; Desiraju, G. R. *Chem. Commun.* **2005**, 1073.

(10) (a) Rajput, L.; Biradha, K. *Cryst. Growth Des.* **2009**, 9, 40. (b) Lim, S.; Kim, H.; Selvapalam, N.; Kim, K.J.; Cho, S.J.; Seo, G.; Kim, K. *Angew. Chem., Int. Ed. Engl.* **2008**, 47, 3352.

(11) (a) Karki, S.; Friscic, T.; Jones, W. *CrystEngComm* **2009**, 11, 740. (b) Singh, W. M.; Barooah, N.; Baruah, J. B. *J. Mol. Struct.* **2008**, 875, 329. (c) Singh, D.; Baruah, J. B. *CrystEngComm* **2009**, 11, 2688.

(12) (a) Zaworotko, M. J. *Chem. Commun.* **2001**, 1. (b) Rajput, L.; Biradha, K. *Cryst. Growth Des.* **2009**, *9*, 40. (c) Etter, M. C.; Reutzel, S. M. *J. Am. Chem. Soc*. **1991**, *113*, 2586.

(13) Steiner, T. *Angew. Chem., Int. Ed.*. **2002**, *41*, 48.

(14) Mohamed, S.; Tocher, D. A.; Vickers, M.; Karamertzanis, P. G.; Price, S. L. *Cryst. Growth Des.* **2009**, *9*, 2881.

(15) (a) Ireta, J.; Neugebauer, J.; Scheffler, M. *J. Phys. Chem. A* **2004**, *108*, 5692. (b) Hohenberg, P.; Kohn, W. *Phys. Rev. B* **1964**, *136*, 864.

(16) (a) Becke, A. D. *J. Chem. Phys.* **1993**, *98*, 5648. (b) Lee, C.; Yang, W.; Parr, R. G. *Phys. Rev. B* **1988**, *37*, 785.

(17) (a) Dkhissi, A.; Adamowicz, L.; Maes, G. *J. Phys. Chem. A* **2000**, *104*, 2112. (b) Dkhissi, A.; Adamowicz, L.; Maes, G. *Chem. Phys. Lett.* **2000**, *324*, 127.

(18) Woon, D. E; Dunning, T. H., Jr. *J. Chem. Phys.* **1993**, *98*, 1358.

(19) (a) *GAUSSIAN03, Revision B.05*; Gaussian, Inc.: Pittsburgh, PA, 2003. (b) *GAUSSIAN03, Revision B.05*; Gaussian, Inc.: Pittsburgh, PA, 2003.

(20) Chalasinski, G.; Szczesniak, M. *Chem. Rev.* **1994**, *94*, 1723.

Chapter 3

Polymorphism and pseudopolymorphism in pyridine and quinoline solvates of cyclic imide carboxylic acids

We have mentioned in chapter 2 that different types of hydrogen bonds as illustrated in Scheme 2.1 are possible from interactions of pyridine and related aromatic nitrogen containing heterocyclic compounds with carboxylic acids. It is clear from that discussion that orientation of the aromatic ring/s with respect to carboxylic acid is one of the key factors to form a particular type of hydrogen bond geometry among the different types of hydrogen bonded motifs.[1] Such assemblies formed from different hydrogen bond patterns may lead to supramolecular isomerisation.[2] There is also another possibility that the guest molecules themselves participate in assembly formation, and further includes additional molecules of the guest in such assembly. Identification of such systems with different hydrogen bond motifs would lead to the design of polymorphic structures. One choice for the study of such polymorphs[3] would be to construct an assembly of guests with hosts that are dissimilarly bound to multiple numbers of guest molecules.[4] In this respect, the study on the guest binding ability of N-glycinylpyromelliticdiimide derivatives with different aromatic amines has already revealed interesting conformational features; as well as preferential deprotonation of carboxylic acids.[5] It is also a well known fact that carboxylic acids form molecular complexes with pyridine[6] and such molecular complexes have relevance in ion transport.[7] There are numerous examples of naphthalenediimide[8] or pyromelliticdiimide[9] derivatives that encapsulate planar aromatic compounds. In these examples, the encapsulation occurs through formation of primary self-assembly of host molecules, however, interaction of guest with a host can modify such assembly and make a secondary assembly for guest encapsulation. Moreover, the inclusion of solvent molecules plays an important role in tuning the geometrical alignment of the host molecules which in turn affects the Z' value (number of molecules in an asymmetric unit) in crystals and leads to pseudopolymorphs.[10] The supramolecular features associated with carboxylic acid derivatives of naphthalenene diimide and pyromellitic diimide make them attractive for such studies, as they provide weak interactions to bind an aromatic nitrogen containing heterocycle in different ways.[11] Recently,

we have established the formation of different hydrogen bond motifs between various host carboxylic acids tethered by imide units and guest amines (pyridine and quinoline). These host-guest complexes were simply prepared by crystallizing host in a guest (solvent) medium. We were also interested to observe the effect of secondary guest molecule in the formation of such types of hydrogen bond motifs. We anticipated that presence of secondary guest that can bind with host along with primary guest, may influence the structural patterns and may produce mixed solvates, polymorphs or pseudopolymorphs. Further, it may be noted that the presence of guest molecule may cause the rotation of aromatic rings around the C-N bond in atropisomeric diacids tethered by naphthalenediimide or pyromellitic diimide units which would provide syn or anti conformers of host molecules (as shown in Scheme 3.1).

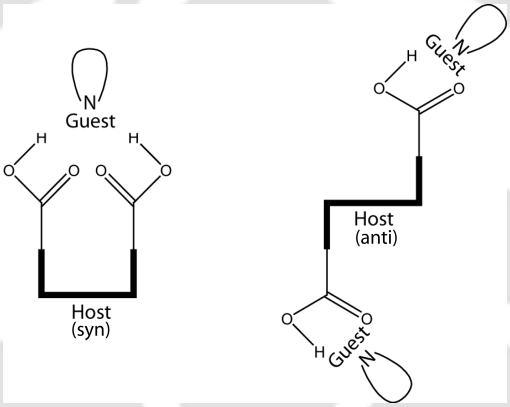

Scheme 3.1.

To expand these observations, compounds **3.1-3.3** are synthesized by the cyclocondensation reactions of 1,4,5,8-naphthalenetetracarboxylic dianhydride and pyromellitic dianhydride

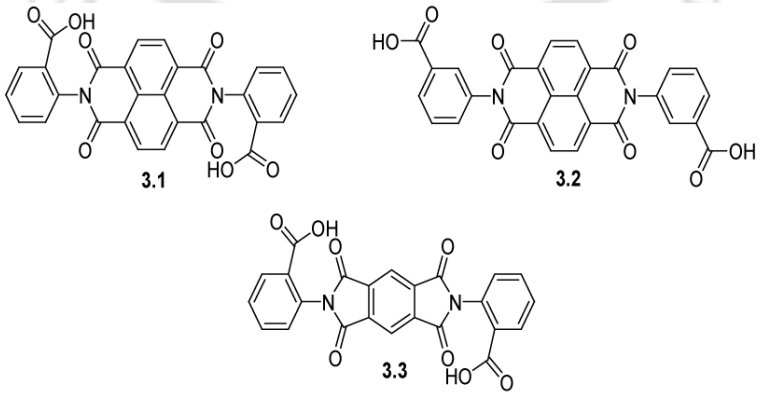

Scheme 3.2: Structures of host molecules.

with respective amino benzoic acids, respectively, (shown in Scheme 3.2) and crystallized in the presence of primary guest as well as both primary and secondary guest. In this study, we report the different ways of inclusion of guest aromatic N-heterocycles, namely, pyridine and quinoline, in the assemblies of host aromatic dicarboxylic acids tethered by naphthalenediimide and pyromellitic diimide units.

The crystallization of host **3.1** at two different conditions led to formation of two different polymorphic solvates of host **3.1** with pyridine in a ratio 1:4 (Scheme 3.3). Polymorphism is often characterized as the ability of a substance to exist as two or more crystalline phases that have different arrangements and/or conformations of the molecules in the crystal lattice[12]. Two polymorphic forms identified for these solvates have different packing patterns and crystallized in different space groups. The polymorph **3.1a** is obtained from a solution of **3.1** in pyridine, whereas the polymorph **3.1b** is obtained by crystallizing **3.1** from a mixed solvent of pyridine and benzene.

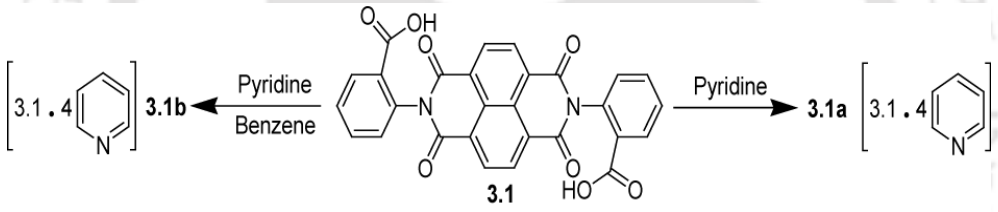

Scheme 3.3: Two different pyridine solvates (polymorphs **3.1a** and **3.1b**) of host **3.1**.

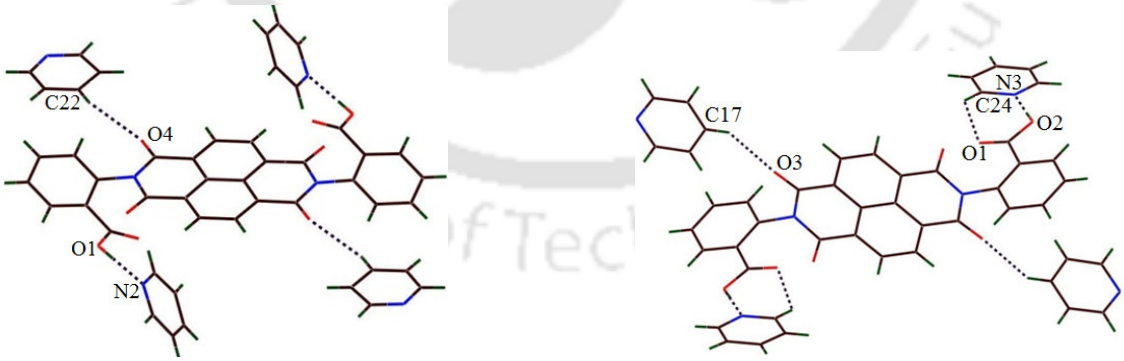

Polymorph 3.1b **Polymorph 3.1a**

Figure 3.1: Weak interactions in the host-guest assembly of **3.1a** and **3.1b**.

The polymorph **3.1a** crystallizes in monoclinic $P2_1/n$ space group. In the crystal lattice of this polymorph, the pyridine molecules are positioned in two different types of environments or in other words, two sets of independent coordinates are required to describe the orientations of pyridine molecules in the crystal lattice (Figure 3.1). One such set comprises two pyridine molecules and these two pyridine molecules are attached to the carboxylic acid groups of host molecule via cyclic $R^2_2(7)$ hydrogen bond motifs. This occurs through involvement of donor-acceptor C–H···O (C24–H24···O1; $d_{D\cdots A}$ 3.29Å, <D-H···A 122.40º) and O–H···N (O2–H2···N3; $d_{D\cdots A}$ 2.61Å, <D-H···A 175.43º) interactions. The other set is also comprised of two pyridine molecules. These two molecules of pyridine interact with the carbonyl oxygens of the host molecule via donor C-H···O (C17-H17···O3; $d_{D\cdots A}$ 3.27Å, <D-H···A 126.49º) interactions in the crystal lattice of **3.1a**.

The polymorph **3.1b** crystallizes in triclinic P-1 space group. In this polymorph, there are also two sets of pyridine molecules, two pyridines in each set (Figure 3.1). They are positioned in two independent environments in the lattice. One set of pyridine molecules are associated with carboxylic acid groups of host molecule via discrete acceptor O-H···N (O1-H1···N2; $d_{D\cdots A}$ 2.62Å, <D-H···A 171.19º) interactions. The other set of pyridine molecules require an independent coordinate for their description; this set of pyridine molecules are held with the carbonyl oxygens of host molecule through donor C-H···O (C22-H22···O4; $d_{D\cdots A}$ 3.38Å, <D-H···A 145.10º) interactions in the crystal lattice. This indicates clearly that in the structures of **3.1a** and **3.1b**, minor differences in hydrogen bonding interactions between the host and guest molecules are alleged in the formation of two polymorphs of pyridine solvates of host **3.1**. That kind of polymorphism related to solvates of organic host compounds is recently reported in the literature.[13]

The $R^2_2(8)$ type of cyclic hydrogen bonded structure is common in carboxylic acids,[9b,c,d] however, such type of hydrogen bond pattern is absent in these polymorphs. The reason for such an observation could be the hierarchy of O– H···N interactions over O–H···O interactions in these systems. The IR spectra and ^{1}HNMR spectra of the two polymorphs are identical. The peaks obtained in the PXRD patterns of both the polymorphs are different and are also consistent with the simulated peaks of single crystal X-ray structure determined at 298K (Figure 3.11). The thermogravimetric analyses reveal that the polymorph **3.1b** loses all four pyridines at 119^{0}C; whereas **3.1a** loses the pyridine molecules in two different steps (Figure 3.9 and 3.10). In the case of **3.1a**, it loses two molecules of pyridine at 102^{0}C followed by another two molecules at 142^{0}C. It must be mentioned that each of the pyridine molecules in **3.1b** is associated through weak interactions and they are lost together at a particular

temperature, whereas in the case of **3.1a**, the two pyridines molecules are associated with cyclic $R^2_2(7)$ interactions; while the other two are weakly bound pyridines. This leads to the loss of two pyridine molecules bound by discrete C-H···O interactions at relatively lower temperature, whereas the pyridines bound by a combination of C–H···O and N–H···O interactions are lost at a relatively higher temperature.

When quinoline was used as a solvent of crystallization for **3.1**, two different solvates (**3.1c** and **3.1d**) of **3.1** are obtained (Scheme 3.4); which are also the pseudopolymorphs to each other, in which the ratio of **3.1** to quinoline is 1: 5 and 1:3, respectively. The solvate **3.1c** is obtained by crystallization of **3.1** from quinoline, whereas **3.1d** is formed by crystallization of a solution of **3.1** from mixed solvent of quinoline and pyridine.

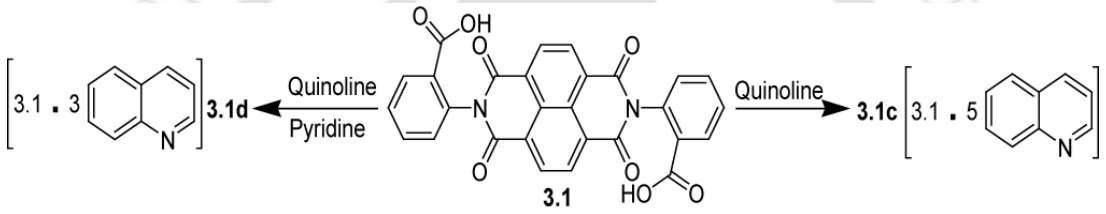

Scheme 3.4: Two different quinoline solvates (pseudopolymorphs **3.1c** and **3.1d**) of host **3.1**.

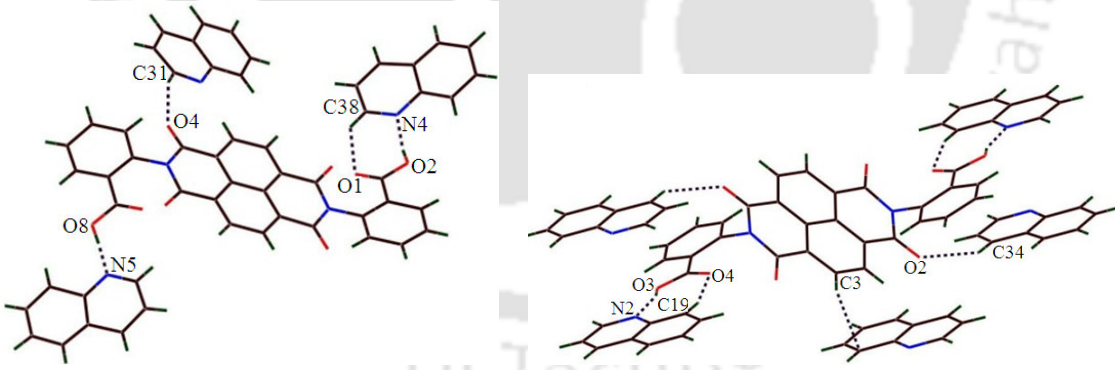

Psuedopolymorph 3.1d **Psuedopolymorph 3.1c**

Figure 3.2: A part of crystal structure of **3.1c** and **3.1d** showing host-guest interactions.

The solvates of host **3.1** with quinoline, **3.1c** crystallizes in triclinic P-1 and **3.1d** crystallizes in monoclinic $P2_1/c$ space group. In the structure of **3.1c**, one quinoline ring is disordered; thus, precise description of hydrogen bondings in this solvate is not possible. In this solvate

all the quinoline molecules are in three different environments and thus they require three sets of coordinates to describe their orientations (Figure 3.2). Among the five quinoline molecules in **3.1c**; two of them are involved in cyclic $R^2_2(8)$ type hydrogen bond through O3–H3A···N2 ($d_{D\cdots A}$ 2.66Å, <D-H···A 158.44º) and C19–H19···O4 ($d_{D\cdots A}$ 3.52Å, <D-H···A 158.57º) interactions with the carboxylic acid groups of host molecule. Another two quinoline molecules are engaged in C24–H24···O2 ($d_{D\cdots A}$ 3.23Å, <D-H···A 123.83º) interactions with the carbonyl oxygens of host molecule. The fifth quinoline molecule is held perpendicular to the naphthalimide ring of host molecule via C–H···π ($d_{C5\ldots\pi}$ 3.70Å) interaction. The solvate **3.1d** has relatively less symmetric structure with respect to **3.1c**. This solvate also requires three independent sets of coordinates to describe the orientation of three quinoline molecules (Figure 3.2). It has one carboxylic acid group bound to the quinoline through cyclic $R^2_2(7)$ hydrogen bond, involving O2–H2···N4 ($d_{D\cdots A}$ 2.62Å, <D-H···A 167.64º) and C38–H38···O1 ($d_{D\cdots A}$ 3.26Å, <D-H···A 129.57º) interactions. The other carboxylic acid group is attached to a quinoline molecule through a discrete O8–H8···N5 interaction ($d_{D\cdots A}$ 2.72Å, <D-H···A 125.70º). There is another set of quinoline molecules in the lattice which are associated through C31–H31···O4 ($d_{D\cdots A}$ 3.21Å, <D-H···A 155.98º) interactions with the carbonyl oxygens of host molecule.

Although the composition of the **3.1c** and **3.1d** is different; in each case the molecules have three symmetry independent sets of quinoline molecules in the asymmetric unit. These symmetry differences arise due to the difference in orientations of the quinoline groups in the lattices to make a stable packing pattern by optimizing the various attractive and repulsive forces. The PXRD patterns of both these pseudopolymorphs are also different to each other, showing good correlations with their simulated patterns (Figure 3.14). The thermogravimetric study on the **3.1c** shows that it loses five quinoline molecules in two steps (Figure 3.12). At first it loses two molecules of quinoline at 160^0C and the next three molecules of quinoline are lost at 190^0C. The other solvate **3.1d** loses three quinoline molecules in a single step at 185^0C (Figure 3.13). From the above discussions it is clear that in the two crystals, the solvent molecules differ in numbers but the number of coordinates required to describe the orientations of the solvents in these two solvates are same. For comparison, each repeated unit of the **3.1c** has two $R^2_2(8)$ types of hydrogen bonds between the quinolines and carboxylic acids whereas in the case of **3.1d**, the quinoline molecules are associated with the carboxylic acid groups of host molecule via discrete as well as $R^2_2(7)$ type of hydrogen bond pattern.

The crystallization conditions show that quinoline solvate of host **3.1** is formed preferentially in the presence of both pyridine and quinoline solvents, since, the pseudopolymorph **3.1c** is obtained by crystallization of **3.1** in quinoline, whereas **3.1d** is obtained by crystallization of **3.1** in a mixed solvent of quinoline and pyridine. This selective binding of quinoline over pyridine by the host **3.1** in the formation of different solvates is further substantiated by a titration experiment based on fluorescence emission of the host and its relative interactions with pyridine and quinoline. The host compound **3.1** on excitation at 330 nm emits at 400 nm, whereas a similar excitation of a dimethylsulfoxide solution of solvate **3.1a** at 330 nm shows an emission at 410 nm. The quinoline solvate **3.1c** has a very low emission at 430 nm (Figure 3.3). We have taken advantage of these facts and carried out a control experiment by monitoring the changes in fluorescence emission by adding quinoline to a solution of **3.1a** in dimethylsulfoxide. Upon addition of the quinoline, fluorescence quenching at 410 nm took place and a gradual decrease in the corresponding fluorescence emission was also found. Upon addition of excess quinoline, the emission spectra resemble the emission spectra of **3.1c**. This is reflected in the observation of a shift from 410 to 430 nm (Figure 3.3). It suggests that, as **3.1a** transforms to **3.1c**, the fluorescence intensity decreases.

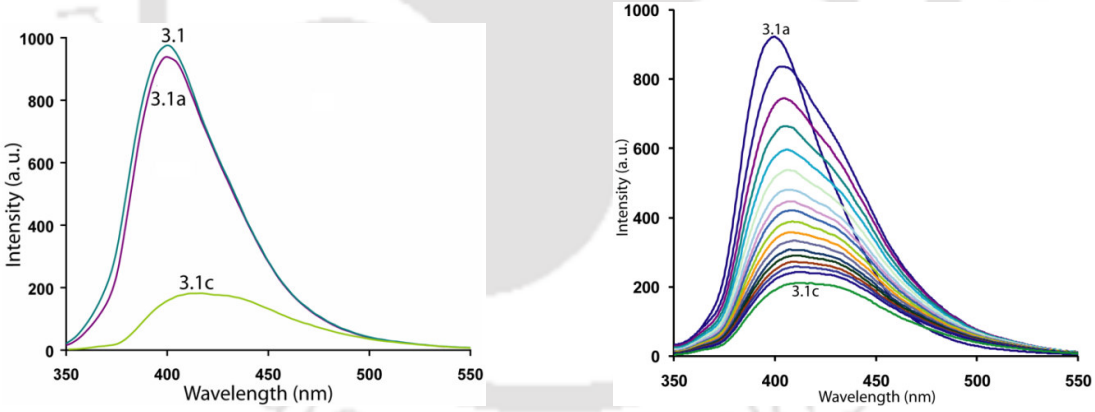

Figure 3.3: Fluorescence emissions of **3.1**, **3.1a** and **3.1c** and fluorescence titration showing quenching in the emission (λ_{ex} = 330 nm) of pyridine solvate **3.1a** (1.1×10^{-5} M in dimethylsulfoxide) on addition of quinoline (2 mL in each aliquot from 1.1×10^{-5} M solution of quinoline in dimethylsulfoxide).

This happens due to the formation of **3.1c** which has very poor fluorescence emission at this wavelength. The solvates of host **3.1** with pyridine are relatively unstable and degrade in three to four days, whereas the solvates with quinoline are stable.

The crystal structures of 1:3 solvates of host **3.2** with pyridine (**3.2a**) and the 1:3 solvate of **3.2** with quinoline (**3.2b**) are also determined (Scheme 3.5). Both the solvates show structural similarity containing disordered pyridine and quinoline molecules trapped within the cavity formed by assembly of host and guest molecules (Figure 3.4).

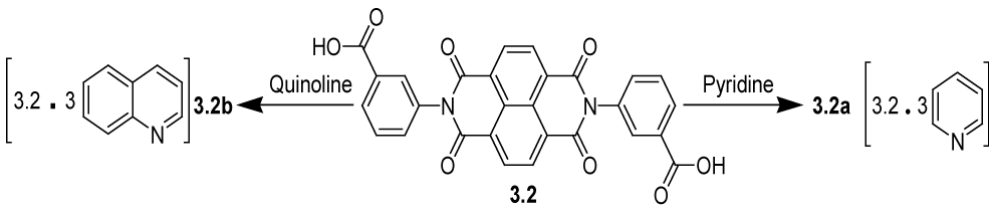

Scheme 3.5: Pyridine and quinoline solvates (**3.2a** and **3.2b**) of host **3.2**.

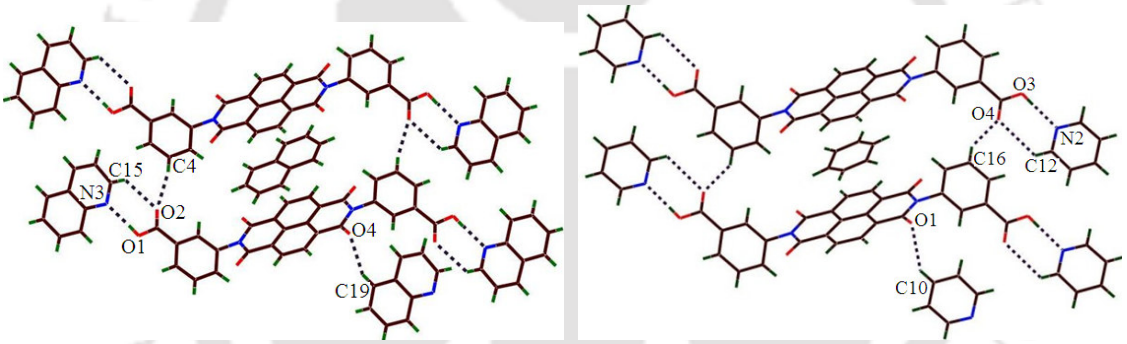

Solvate 3.2b **Solvate 3.2a**

Figure 3.4: Structures of solvates **3.2a** and **3.2b** showing encapsulation of pyridine and quinoline molecules inside the cavities formed by host-guest interactions.

Both the solvates crystallize in triclinic P-1 space group. The three pyridine molecules of the solvate **3.2a** are in two different types of environments, of which two molecules are in one set. These molecules are associated with the carboxylic acid groups of host molecule via O3–H3···N2 ($d_{D\cdots A}$ 2.60Å, <D-H···A 177.93º) and C12–H12···O4 ($d_{D\cdots A}$ 3.28Å, <D-H···A 122.43º) interactions making cyclic $R^2_2(7)$ hydrogen bond motifs. These pyridine molecules are further held in the lattice by very weak C10–H10···O1 ($d_{D\cdots A}$ 3.34Å, <D-H···A 142.41º) interactions. The third molecule is a disordered pyridine, which has an independent symmetry with respect to the other two. This pyridine molecule is disordered across an inversion centre and disposed

in the lattice such that the nitrogen and carbon atoms at1 and 4 positions of the pyridine rings are shared with half occupancies. The host molecules also interact to each other via C16–H16···O4 ($d_{D\cdots A}$ 3.36Å, <D-H···A 145.81º) interactions making dimeric assemblies in the lattice. The hydrogen bonded cavities formed in the dimeric assemblies of host molecules encapsulate the disordered pyridine molecules. The trapped molecules of the pyridine are placed above and below the naphthalene rings in the lattice and are separated by a distance of 3.9 Å. This indicates that there are no π–interactions among the naphthalene rings. The crystal structure of **3.2b** has structural similarity to the crystal structure of **3.2a**. In the structure of **3.2b**, there are two symmetry independent quinoline molecules bound to carboxylic acid groups through O1–H1···N3 ($d_{D\cdots A}$ 2.62Å, <D-H···A 176.19º) and C15–H15···O2 ($d_{D\cdots A}$ 3.28Å, <D-H···A 127.98º) hydrogen bond interactions in $R^2_2(7)$ type arrangement. These molecules further interact with the host molecule via C19–H19···O4 ($d_{D\cdots A}$ 3.34Å, <D-H···A 152.72º) interactions in the lattice. The carbonyl oxygen of the carboxylic acid group anchors another host molecule through C4–H4···O2 interaction ($d_{D\cdots A}$ 3.29Å, <D-H···A 167.51º). In this case too, assemblies are formed through these interactions in which quinoline molecules get encapsulated. The encapsulated quinoline molecules are disordered and maintain a symmetric structure with respect to an inversion center. The disodered structure is formed by sharing two nitrogen atoms and two carbon atoms with half occupancies at two opposite sites.

We have also tried to obtain polymorphs or pseudopolymorphs in the case of pyridine and quinoline solvates; **3.2a** and **3.2b**, respectively. For this purpose, the host **3.2** was crystallized with pyridine in the presence of other solvents such as benzene, toluene, hexane and tetrahydrofuran. In each case, we could be obtained only the solvate **3.2a** which was further characterized by unit cell measurement experiments. Similarly, the mixed solvents crystallization attempts were failed to obtain another polymorphic or pseudopolymorphic structures of quinoline solvate **3.2b**. The solvates **3.2a** and **3.2b** on heating lose three molecules of pyridine and three molecules of quinoline at 129 and 148^{0}C, respectively, supporting the composition of the solvates (Figure 3.15 and 3.16).

Two different solvates (pseudopolymorphs) of host **3.3** with guest pyridine molecules are obtained by varying crystallization conditions (Scheme 3.6). Crystallization of **3.3** from neat pyridine gave solvate **3.3a** whereas crystallization of **3.3** from toluene containing pyridine provided **3.3b**. Both the solvates are crystallized in same space group containing two halves of symmetry independent molecules of host **3.3** with three and two guest pyridine molecules in their crystallographic asymmetric units, respectively (Figure 3.5).

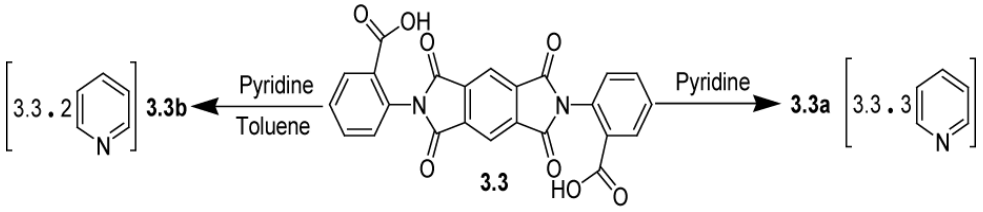

Scheme 3.6: Two different pyridine solvates (pseudopolymorphs **3.3a** and **3.3b**) of host **3.3**.

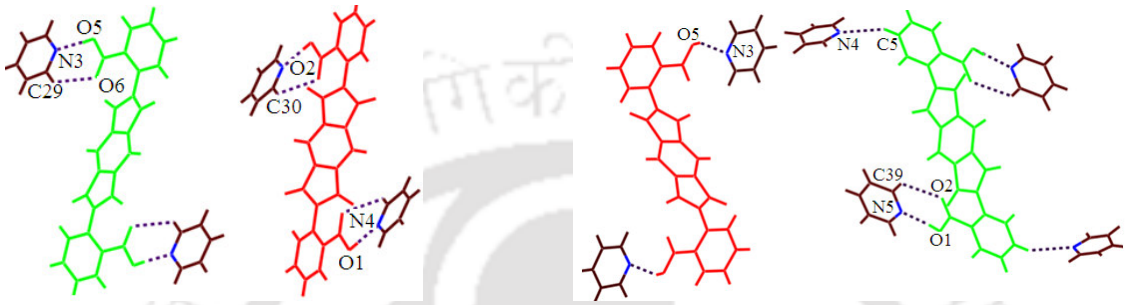

Psuedopolymorph 3.3b **Psuedopolymorph 3.3a**

Figure 3.5: Host-guest interactions in the structures of **3.3a** and **3.3b** showing two symmetry non-equivalent host molecules in each case.

Both the solvates (**3.3a** and **3.3b**) crystallize in triclinic P-1 space group. The host molecules possess inversion centers in both solvates and appear as their two symmetric halves at two symmetry independent positions in the asymmetric units. In the structure of **3.3b**, both the pyridine are held with the carboxylic acid groups of the two symmetry independent host molecules via $R^2_2(7)$ types of hydrogen bonds which are formed by O–H···N (O1–H1···N4; $d_{D\cdots A}$ 2.68Å, <D-H···A 173.60º and O5–H5A···N3; $d_{D\cdots A}$ 2.61Å, <D-H···A 173.39º) and C–H···O (C30–H30···O2; $d_{D\cdots A}$ 3.17Å, <D-H···A 118.80º and C29–H29···O6; $d_{D\cdots A}$ 3.19Å, <D-H···A 125.45º) interactions. In the solvate **3.3a**, the pyridine molecules are involved in hydrogen bonding in multiple ways. It forms the conventional $R^2_2(7)$ motif via O1–H1···N5 ($d_{D\cdots A}$ 2.68Å, <D-H···A 174.74º) and C39–H39···O2 ($d_{D\cdots A}$ 3.25Å, <D-H···A 123.40º) interactions. Another set of pyridine in the lattice is positioned in slightly oblique to the carboxylic acid, so it does not form cyclic hydrogen bond structure but has only discrete O5–H5···N3 ($d_{D\cdots A}$ 2.84Å, <D-H···A 150.43º) interaction. The third set of pyridine is weakly held in the interstices through C5–H5···N4 ($d_{D\cdots A}$ 3.47Å, <D-H···A 152.81º) interaction. The observation of the two different pyridine solvates may be attributed to the role of toluene in the crystallization process. The crystallization from neat pyridine provides more number of

solvent pyridine in the lattice as it is obvious that the pyridine being the solvent would try to make a structure via maximization of its interactions with the host. Whereas, toluene does not have heteroatom to interact with a carboxylic acid; thus it would weakly bind, eventually, there is a competition to make tight packed structure through strong O–H···N interactions by pyridine. Such process expels toluene molecules, leads to the formation of solvate with two pyridine molecules. Thermal properties of these two pyridine solvates are also different which show that solvate **3.3a** loses three pyridine molecules in a single step at 110^0C whereas solvate **3.3b** loses two pyridine molecules in one step at 160^0C (Figure 3.17 and 3.18). The peaks obtained in PXRD patterns of both the psuedopolymorphs are different to each other and match well with the peaks of their simulated patterns (Figure 3.19).

In conclusion, structural features of two polymorphs of pyridine solvates of host **3.1** are established. Two pseudopolymorphs of host **3.1** with guest quinoline molecules are also synthesized under different crystallization conditions. The preferential binding of quinoline over pyridine by the host **3.1** is observed. The host **3.2** is a isomeric dicarboxylic acid to host **3.1**, however, it forms solvates in different host-guest ratios from the solvates of host **3.1**. In the structures of pyridine and quinoline solvates of **3.2**, supramolecular cavities formed between the host molecules are sustained by trapping additional guest molecules in a similar fashion showing no interactions between host and guest in such a cavity. The host **3.3** also forms two pseudopolymorphs with guest pyridine molecules by varying crystallization conditions. We have found that the two carboxylic acid groups across the ring in all these host-guest complexes have a trans geometry. The structural features of the solvates and polymorphs show different types of hydrogen bond motifs. It makes avenues for generating a new kind of host–guest assemblies from amine, namely pyridine and quinoline, interactions with a central dicarboxylic acid molecule to encapsulate guest amine/s. The structures of solvates described here require multiple numbers of coordinate systems to describe their orientations in the crystal lattice. This point requires clear attention as the complete description of a crystal structure of a solvated molecule is dependent on the combined description of the symmetry of host and solvent molecules. Discovering the precise location of the hydrogen atoms by means of X-ray crystallography is difficult in water solvates; thus, the present systems are ideal for study of symmetry-related issues associated with solvent molecules. Moreover, the symmetry non-equivalent solvates with same Z□ value can have different orientations of the parent molecules depending on the solvent attached to it and it is the crystal packing requirement that decides such orientations and such phenomenon arises from intermolecular or intramolecular push–pull interactions of various weak interactions.

Experimental Section:

Detailed synthetic methodologies are given below. Analytical data as well as spectroscopic data are listed along with each compound. The instrumental details are given in Appendix.

Synthesis and characterization of compounds and their various solvates:

Compound **3.1**: A solution of 1,4,5,8-naphthalenetetracarboxylic dianhydride (1.34 gm, 5 mmol) and anthranilic acid (1.33 gm, 10 mmol) in N,N-dimethylformamide (25 ml) was refluxed for 3 hrs. The reaction mixture was cooled to room temperature, poured into iced water (50 ml) and stirred for 15 min. A pink coloured precipitate of the product was obtained. This was filtered and air dried. Yield: 85%; IR (KBr, cm^{-1}): 3423(m), 3169 (m), 2923 (w),2604 (w), 1715 (s), 1668 (s), 1604 (w), 1583 (m), 1454 (m), 1355 (s), 1255 (s), 1137 (m), 1077 (w), 986 (w), 865 (w), 769 (m), 730 (m), 646 (w). ^{1}HNMR (400 MHz, DMSO-d^{6}): 8.76 (s, 4H), 8.15 (d, 2H, *J* = 8.0 Hz), 7.82 (t, 2H, *J* = 7.6 Hz), 7.67 (t, 2H, *J* = 7.6 Hz), 7.57 (d, 2H, *J* = 7.6 Hz). ^{13}C NMR (DMSO-d^{6}): 165.8, 162.8, 135.7, 133.7, 131.5, 130.9, 130.8, 129.3, 128.7, 126.8. ESIMS: 507.0824 [M + H^{+}].

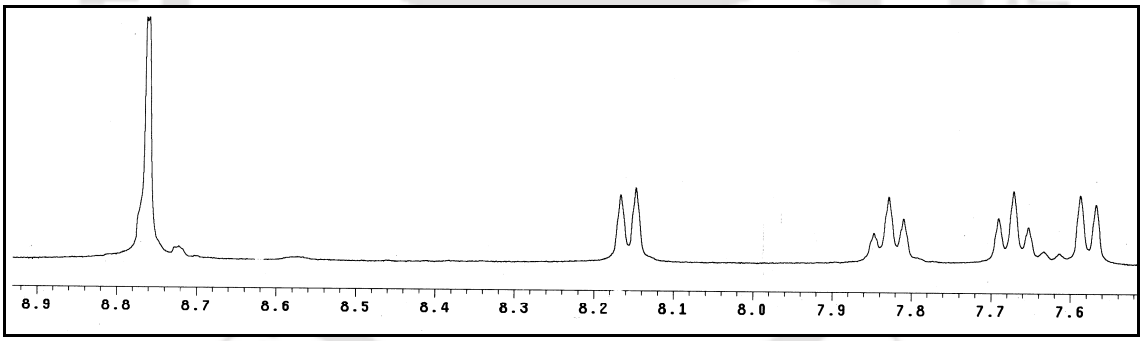

Figure 3.6: ^{1}HNMR spectra of compound **3.1**.

Compound **3.2**. Compound **3.2** was synthesized following the same procedure as described for compound **3.1**. Yield: 90%. IR (KBr, cm^{-1}) 3432 (m), 3982 (m), 2922 (m), 2675 (w), 2554 (w), 1698 (s), 1673 (s), 1581 (m), 1449 (m), 1415 (m), 1345 (s), 1305 (m),1275 (m), 1247 (s), 1194 (m), 1111 (w), 981 (w), 916 (w), 767 (m), 731 (m), 669 (w), 556 (w). ^{1}HNMR (400 MHz, DMSO-d^{6}): 8.72 (s, 4H), 8.09 (s, 2H), 8.07 (d, 2H, *J* = 7.6 Hz), 7.73 (t, 2H, *J* = 8.0 Hz), 7.69 (d, 2H, *J* = 7.2 Hz). ^{13}C NMR (DMSO-d^{6}): 166.8, 163.0, 135.9, 133.6, 131.89, 130.4, 130.3, 129.5, 129.4, 127.1, 126.7. ESI-MS: 507.0830 [M + H^{+}].

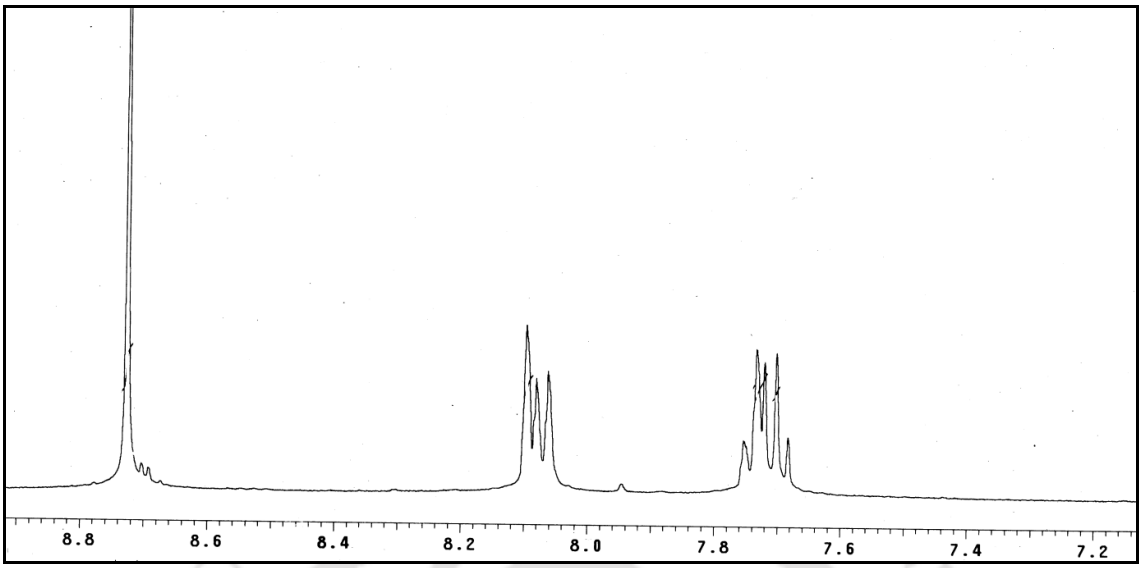

Figure 3.7: ^{1}HNMR spectra of compound **3.2**.

Compound **3.3**: A solution of pyromellitic dianhydride (1.090 gm, 5 mmol) and 2-aminobenzoic acid (1.31 gm, 10 mmol) in acetic acid (25 ml) was refluxed for 3 hrs. The reaction mixture was cooled to room temperature; a brown colored precipitate of the product was obtained, filtered and washed several times with water to remove the acetic acid and dried in open air to give **3.3** in anhydrous form. Yield: 92%. IR (KBr, cm^{-1}): 3483 (bm), 2927 (w), 2620 (w), 1777 (s), 1724 (s), 1492 (m), 1455 (m), 1380 (s), 1253 (s), 1191 (m), 1118 (s), 844 (w), 752 (m), 646 (w). ^{1}HNMR (400 MHz, DMSO-d^{6}): 8.33 (s, 2H), 8.14 (d, 2H, J = 8.0 Hz), 7.64 (t, 2H, J = 7.6 Hz), 7.52 (t, 2H, J = 7.6 Hz), 7.34 (d, 2H, J = 7.6 Hz). ^{13}C NMR (DMSO-d6): 166.1, 165.6, 137.4, 133.4, 131.5, 131.2, 130.6, 129.4, 129.0, 118.6. ESI-MS: 457.098 ($M + H^{+}$).

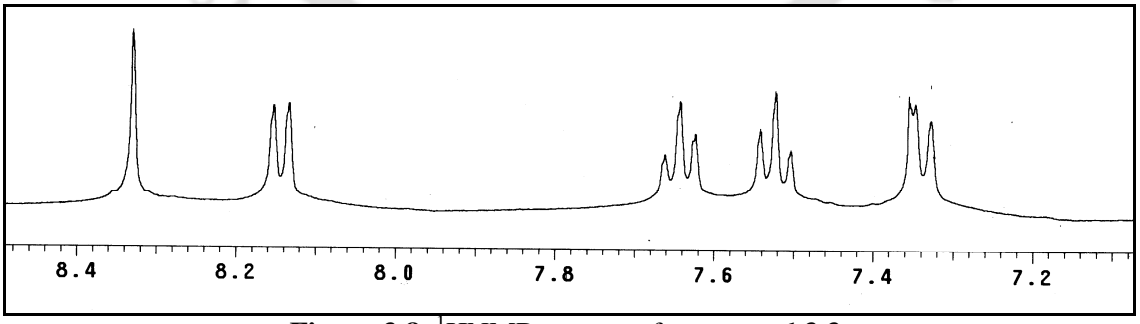

Figure 3.8: ^{1}HNMR spectra of compound **3.3**.

Solvate **3.1a**: The compound **3.1** was dissolved in pyridine and left undisturbed for three days. The crystals of **3.1a** were obtained as red blocks. IR (KBr, cm^{-1}): 3419 (m), 3138 (m),

2601 (w), 2466 (w), 1731 (s), 1704 (s), 1673 (s), 1603 (m), 1583 (m), 1490 (m), 1454 (m), 1374 (s), 1359 (s), 1255 (s),1238 (s),1153 (m), 1137 (m), 1077 (w), 987 (w), 883 (w), 866 (w), 772 (m), 729 (m), 646 (w), 630 (w). ^{1}HNMR (400 MHz, DMSO-d^{6}): 8.75 (s, 4H), 8.57 (s, 8H), 8.31 (s, 4H), 8.15 (d, 2H, *J* = 6.8 Hz), 7.78 (t, 2H, *J* =7.2 Hz), 7.66 (t, 2H, *J* = 8.0 Hz), 7.57 (d, 2H, *J* = 8.0 Hz), 7.40 (s, 8H).

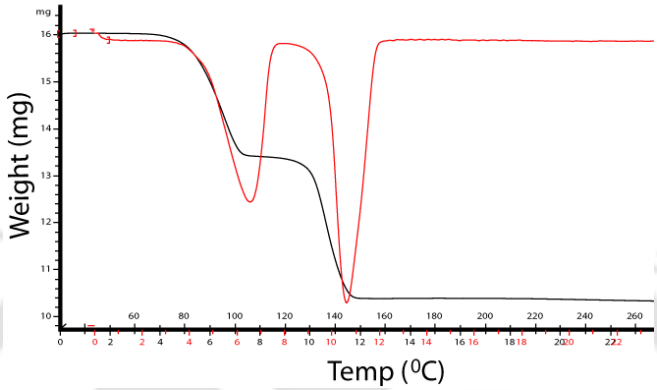

Figure 3.9: TGA curve of polymorph **3.1a**.

Solvate **3.1b**: To a solution of **3.1** (0.13 gm, 0.25 mmol) in pyridine (3 ml), benzene (1 ml) was added. The resulting mixture was kept for crystallization. The solvate **3.1b** was crystallized as small yellow blocks after three days. IR (KBr, cm^{-1}): 3445 (m), 3141 (m), 2460 (w), 1709 (s), 1673 (s), 1602 (s), 1583 (m), 1488 (m), 1452 (m), 1354 (s), 1254 (s), 1152 (m), 1078 (w), 1061 (w), 907 (w), 865 (w), 767 (m), 730 (m), 630 (w). ^{1}HNMR (400 MHz, DMSO-d^{6}): 8.75 (s, 4H), 8.59 (s, 8H), 8.31(s, 4H), 8.16 (d, 2H, *J* = 7.2 Hz), 7.78 (t, 2H, *J* = 7.6 Hz), 7.67 (t, 2H, *J* = 7.6 Hz), 7.57(d, 2H, *J* =7.6 Hz), 7.38 (s, 8H).

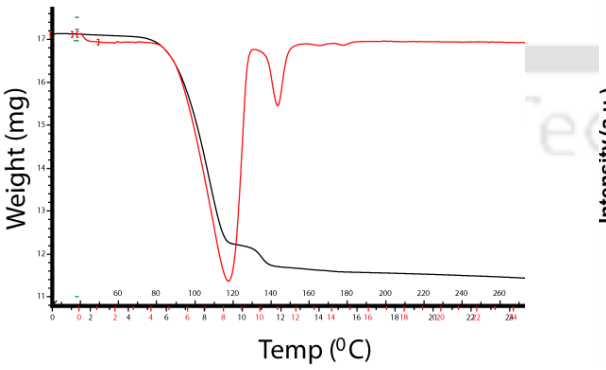

Figure 3.10: TGA curve of polymorph **3.1b**.

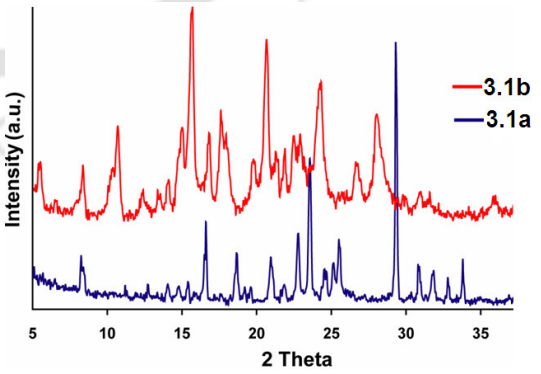

Figure 3.11: PXRD patterns of **3.1a and 3.1b**.

Solvate **3.1c**: The solvate **3.1c** was crystallized as yellow blocks from the quinoline (2 ml) solution of **3.1** (0.13 gm, 0.25 mmol). IR (KBr, cm^{-1}): 3423 (m), 3072 (w), 2377 (w), 1712 (s), 1673 (s), 1582 (m), 1500 (w), 1449 (w), 1353 (s), 1253 (s), 1142 (m), 985 (w), 808 (m), 767 (m), 731 (m), 629 (w), 537 (w). ^{1}HNMR (400 MHz, DMSO-d^{6}) 8.90 (bs, 5H), 8.75 (s, 4H), 8.36 (d, 5H, *J* = 8.0 Hz), 8.16 (d, 2H, *J* = 8.0 Hz), 8.00 (dd, 10H, *J* = 8.0 Hz), 7.82 (t, 2H, *J* = 7.6 Hz), 7.77 (t, 5H, *J* = 6.8 Hz), 7.67 (t, 2H, *J* = 7.6 Hz), 7.62 (d, 5H, *J* = 8.0 Hz), 7.58 (d, 2H, *J* = 8.0 Hz) 7.53 (dd, 5H, *J* = 4.0 Hz).

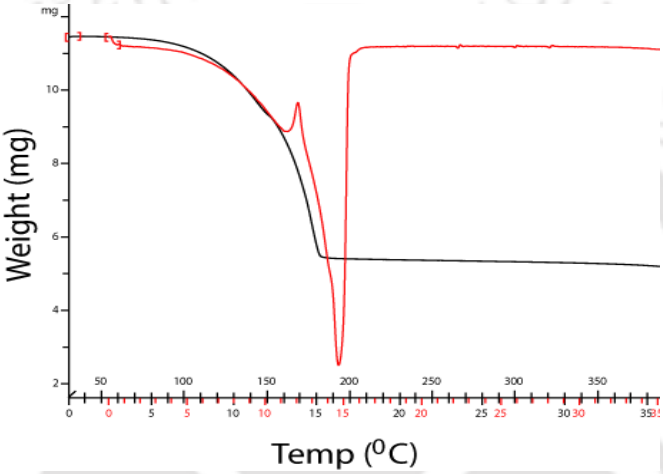

Figure 3.12: TGA curve of psuedopolymorph **3.1c**.

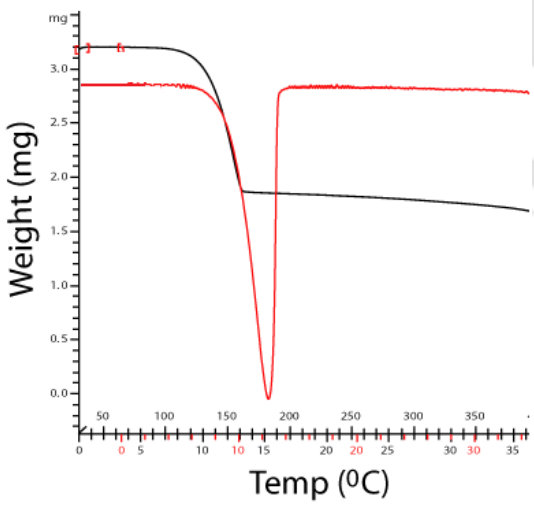

Figure 3.13: TGA curve of **3.1d**.

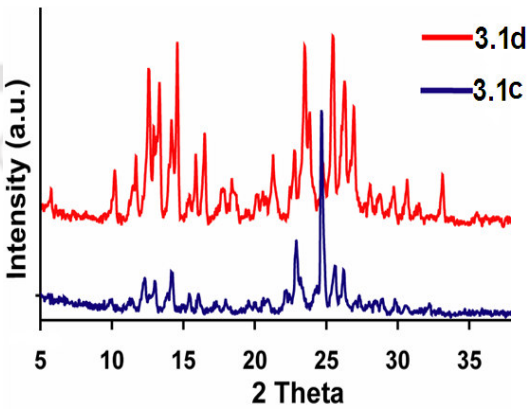

Figure 3.14: PXRD patterns of **3.1c and 3.1d**.

Solvate **3.1d**: The crystals of the solvate **3.1d** were obtained from a solution of **3.1** (0.13 gm, 0.25 mmol) in quinoline (2 ml) and pyridine (1 ml) after three days as yellow blocks. IR (KBr, cm^{-1}): 3424 (m), 3062 (m), 2437 (m), 1944 (w), 1713 (s), 1674 (s), 1582 (m), 1500 (w), 1450 (w), 1353 (s), 1317 (m), 1255 (s), 1231 (s), 1141 (w), 1125 (w), 985 (w), 863 (w), 810 (m), 787 (m), 767 (m), 731 (w), 629 (w), 537 (w). ^{1}HNMR (400 MHz, DMSO-d^{6}): 8.90 (s, 3H), 8.75 (s, 4H), 8.37 (d, 3H, *J* = 8.4 Hz), 8.15 (d, 2H, *J* = 8.0 Hz), 8.00 (dd, 6H, *J* = 8.0 Hz), 7.82 (t, 2H, *J* = 7.6 Hz), 7.77 (t, 3H, *J* = 7.2 Hz), 7.67 (t, 2H, *J* = 7.6 Hz), 7.60 (m, 5H), 7.53 (dd, 3H, *J* = 4.4 Hz).

Solvate **3.2a**: Compound **3.2** was dissolved in pyridine and left undisturbed for three days. From this solution the crystals of pyridine solvate **3.2a** were obtained in as reddish block. IR (KBr, cm^{-1}): 3384 (m), 3070 (m), 2412 (w), 1712 (s), 1680 (s), 1582 (m), 1484 (w), 1435 (m), 1346 (s), 1254 (m), 1207 (m), 1154 (m), 1060 (m), 785 (w), 735 (m), 510 (w). ^{1}HNMR (400 MHz, DMSO-d^{6}): 8.73 (s, 4H), 8.56 (d, 4H, *J* = 4.0 Hz), 8.09 (s, 2H), 8.07 (d, 2H, *J* = 7.6 Hz), 7.78 (t, 2H, *J* = 8.0 Hz), 7.73 (t, 2H, *J* = 8.0 Hz), 7.69 (d, 2H, *J* = 8.0 Hz), 7.38 (dd, 4H, *J* = 4.4 Hz).

Solvate **3.2b**: The crystals of quinoline solvate **3.2b** were obtained as yellow blocks from the quinoline solution of compound **3.2**. IR (KBr, cm^{-1}): 3424 (m), 3065 (w), 2917 (w), 2395 (w), 1712 (s), 1680 (s), 1581 (m), 1498 (w), 1446 (m), 1344 (s), 1308 (m), 1251 (s), 1151 (m), 984 (w), 810 (m), 769 (m), 735 (m), 628 (w), 507 (w). ^{1}HNMR (400 MHz, DMSO-d^{6}): 8.91 (d, 3H, *J* = 4.0 Hz), 8.72 (s, 4H), 8.37 (d, 3H, *J* = 8.0 Hz), 8.09 (s, 2H), 8.07 (d, 2H, *J* = 7.6 Hz), 8.00 (dd, 6H, *J* = 8.0 Hz), 7.74 (m, 7H), 7.62 (t, 3H, *J* = 8.0 Hz), 7.53 (dd, 3H, *J* = 4.0 Hz).

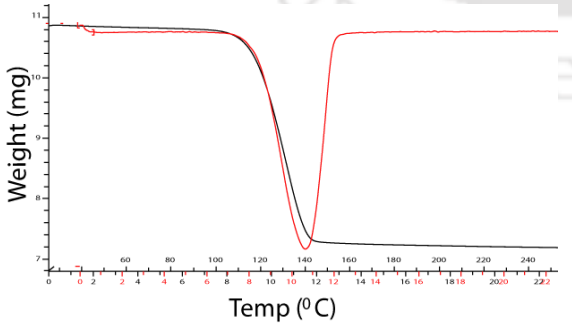

Figure 3.15: TGA curve of solvate **3.2a**.

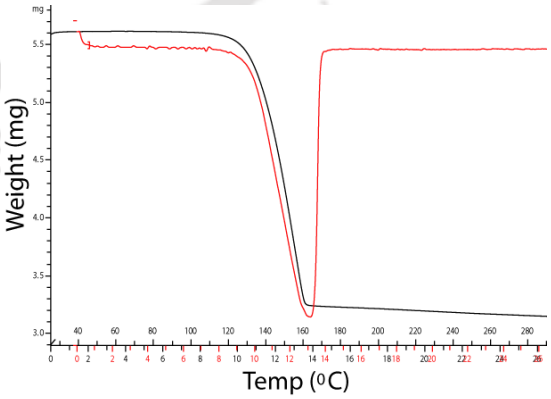

Figure 3.16: TGA curve of solvate **3.2b**.

Solvate **3.3a**: The solvate **3.3a** was obtained as colorless needles from the pyridine solution of compound **3.3**. IR (KBr, cm^{-1}): 3502 (bm), 2924 (w), 2623 (w), 1776 (s), 1720 (s), 1634 (s), 1492 (m), 1454 (m), 1384 (s), 1281 (m), 1264 (m), 1190 (m), 1121 (s), 845 (w), 754 (m), 728 (w). ^{1}HNMR (400 MHz, DMSO-d^{6}): 8.50 (s, 6H), 8.32 (s, 2H), 8.11 (d, 2H, *J* = 8.0 Hz), 7.65 (m, 5H), 7.55 (t, 2H, *J* = 8.0 Hz), 7.38 (d, 2H, *J* = 7.6 Hz), 7.24 (t, 6H, *J* = 6.0 Hz).

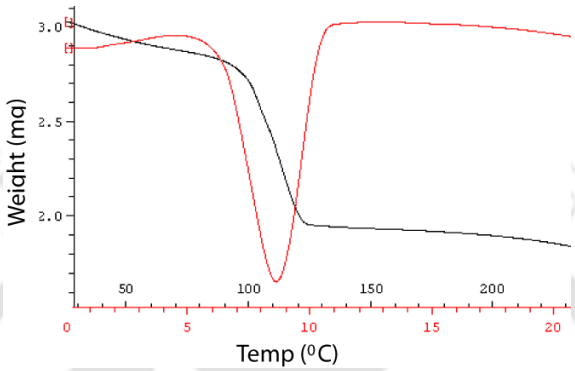

Figure 3.17: TGA curve of psuedopolymorph **3.3a**.

Solvate **3.3b**: A solution of compound **3.3** in pyridine and toluene gave the solvate **3.3b** as colourless blocks in quantitative yield. IR (KBr, cm^{-1}): 3446 (bm), 3077 (w), 2460 (w), 1778 (s), 1724 (s), 1601 (m), 1489 (m), 1453 (m), 1437 (m), 1381 (m), 1284 (m), 1189 (m), 1119 (m), 1063 (m), 1008 (w), 845 (w), 752 (m), 727 (w), 630 (w). ^{1}HNMR (400 MHz, DMSO-d^{6}): 8.57 (s, 4H), 8.50 (s, 2H), 8.11 (d, 2H, *J* = 7.6 Hz), 7.81 (m, 4H), 7.68 (t, 2H, *J* = 7.6 Hz), 7.60 (d, 2H, *J* = 7.6 Hz), 7.39 (t, 4H, *J* = 5.6 Hz).

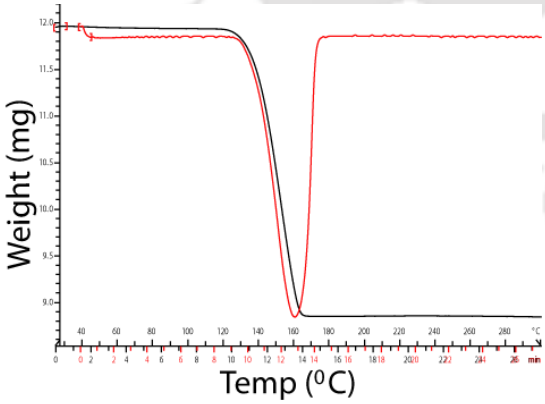

Figure 3.18: TGA curve of **3.3b**.

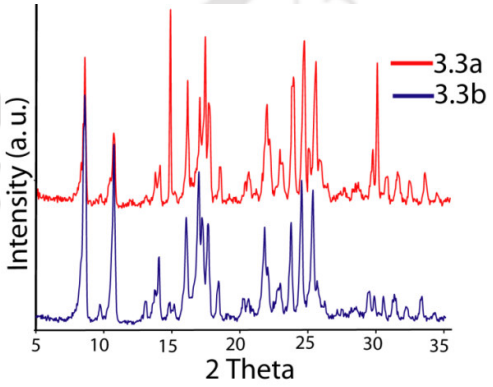

Figure 3.19: PXRD patterns of **3.3a and 3.3b**.

References:

1. (a) Aakeröy, C.B.; Baety, A.M.; Helfrich, B.A. *Angew Chem. Int Ed.* **2001**, *40*, 3240. (b) Aakeröy, C.B.; Baety, A.M.; Helfrich, B.A. *J. Am. Chem. Soc.* **2002**, *124*, 14425. (c) Aakeröy, C.B.; Baety, A.M.; Helfrich, B.A.; Nieuwenhuyzen, M.; *Cryst. Growth Des.* **2003**, *3*,159.

2. (a) Aitipamula, S.; Nangia, A. *Chem.–Eur. J.* **2005**, *11*, 6727. (b) Sarma, B.; Nath, N. K.; Bhogala, B. R.; Nangia, A. *Cryst. Growth Des.* **2009**, *9*, 1546.

3. Bernstein J. *Polymorphism in Molecular Crystals*, Oxford Science Publications, Oxford, **2002**.

4. (a) Bernal, I. in *Models, mysteries and magic of molecules* eds. Boeyens J. C.A. and Ogilvie, J.F.; Springer Netherlands, **2007**, pp 137-165. (b) Nangia, A. *Acc. Chem. Res.* **2008**, *41*, 595. (c) Parrish, D. A.; Deschamps, J. R.; Gilardi, R. D.; Butcher R. J. *Cryst Growth Des.* **2008**, *8*, 57.

5. Singh, W. M.; Barooah, N.; Baruah, J. B. *J. Mol. Struct.* **2008**, *875*, 329.

6. (a) Rychlewska, U.; Warzajtis, B.; Joachimiak, R.; Paryzek, Z. *Acta Crystallogr. Sect. B*: *Struct. Sci.* **2008**, *64*, 383. (b) Tanaka, K.; Hiratsuka T.; Urbanczyk-Lipkowska, Z. *Eur. J. Org. Chem.* **2003**, 3043. (c) Miyake, Y.; Matsuura, Y.; Sada, K.; Miyata, M. *Chem. Lett.* **1997**, 1263.

7. Kozlowski C. A.; Walkowiak, W. *Sep. Sci. Technol.* **2004**, *39*, 3127.

8 (a) Voshosale, S.V.; Jani, C.H.; Langford, S.J.; *Chem. Soc. Rev.* **2008**, *37*, 331. (b) Kishikawa, K.; Iwashima, C.; Komoto, S.; Yamaguchi, K.; Yamamoto, M. *J. Chem. Soc. Perkin. Trans. 1*, **2000**, 2217. (c) Mukhopadhyay, P.; Iwashita, Y.; Shirakawa, M.; Kawano, S.; Fujita, N.; Shinkai, S. *Angew. Chem., Int. Ed.* **2006**, *45*, 1592. (d) Lee, H.N.; Xu, Z.; Kim, S.K.; Swamy, K.M.K.; Kim, Y.; Kim, S.-J.; Yoon, J. *J. Am. Chem. Soc.* **2007**, *129*, 3828.

9 (a) Kishikawa, K.; Tsubokura, S.; Kohmoto, S.; Yamamoto, M.; Yamaguchi, K. *J. Org. Chem.* **1999**, *64*, 7568. (b) Degenhardt, C.F.; Lavin, J. M.; Smith, M.D.; Shimizu, K.D.; *Org. Letters* **2005**, *7*, 4079. (c) Degenhardt III, C.; Shortell, D. B.; Adams, R.D.; Shimizu,K.D. *Chem.Comm.* **2000**, 929. (d) Barooah, N.; Sarma, R. J.; Baruah, J. B. *CrystEngComm* **2006**, *8*, 608.

(10) (a) Threlfall, T. L. *Org. process Res. Dev.* **2000**, *4*, 384. (b) Todd, A. M.; Anderson, K. M.; Byrne, P.; Goeta, A. E.; Steed, J. W. *Cryst. Growth Des.* **2006**, *6*, 1750. (c) Cabeza, A. J.

C.; Day, G. M.; Motherwell, W. D. S.; Jones, W. *J. Am. Chem. Soc*. **2006**, *128*, 14466. (d) Davey, R. J.; Blagden, N.; Righini, S.; Alison, S.; Quayle, M. J.; Fuller, S. *Cryst. Growth Des.* **2001**, *1*, 59. (e) Babu, N. J.; Nangia, A. *Cryst. Growth Des.* **2006**, *6*, 1995.

11 (a) Rajput, L.; Biradha, K. *Cryst. Growth Des.* **2009**, *9*, 40. (b) Etter, M. C.; Reutzel, S. M.; *J. Am. Chem. Soc.* **1991**, *113*, 2586. (c) Zaworotko, M. J.; *Chem. Commun*. **2001**, 1.
(d) Cheney, M. L.; McManus, G. J.; Perman, J. A.; Wang, Z. Zaworotko, M. J. *Cryst. Growth Des.* **2007**, *7*, 616.
(12) Grant, D. J. W. *Theory and origin of polymorphism.* In H. G. Brittain (ed.) *Polymorphism in Pharmaceutical Solids.* Marcel Dekker, Inc., New York, **1999**, pp 1-34.
(13) (a) Guo, J.; Ulrich, J. *Cryst. Res. Technol.* **2010**, *45*, 267. (b) Suzuki, M.; Kobayashi, K. *Cryst. Growth Des.* **2011**, *11*, 1814.

Chapter 4

Gel formation in cyclic imide carboxylic acids and solvent dependent fluorescence emission in cyclic imide heterocycles

In this chapter, we present studies on the gel formation of some carboxylic acids tethered by various cyclic imides as low molecular weight organogelators. The organogelators are a family of low molecular weight organic molecules that can form gels in polar or apolar organic solvents at low concentrations. The subject of organogels has generated enormous interest due to their unique features and potential applications for new soft organic materials,[2] template synthesis,[3] drug delivery,[4] separations and biomimetics.[5] In gels formed by polymeric gelators, the networks arise from the entanglement and interaction of covalently bonded chains, whereas in gels formed by low molecular weight gelators, the networks are held together by multiple noncovalent interactions. The phthalimide derivatives in the form of polymeric imides form gels.[6] Although there are a large number of examples in which small molecules such as 1,3:2,4-di-O-benzylidene-d-sorbitol (DBS),[7] cholesterol derivatives,[8] bolaform amides,[9] symmetrical dialkylamides,[10] symmetrical bisureas,[11] and N-n-octyl-D-gluconamide,[12] are used as organic gelators; gels from monomeric naphthalimide and phthalimide derivatives have not been reported yet. Shinkai and Würthner reported perylene bisimides (PBI) π-functional organic compounds as a versatile low molecular weight organogelators which have ability to form organogels in various organic solvents.[13]

These studies prompted us to investigate some potentially important mono and diimide derivatives having gel-forming ability. For this purpose, compounds **4.1**-**4.5** are synthesized by the condensation reactions of 5-amino-isophthalic acid with different cyclic anhydrides (shown in Scheme 4.1).

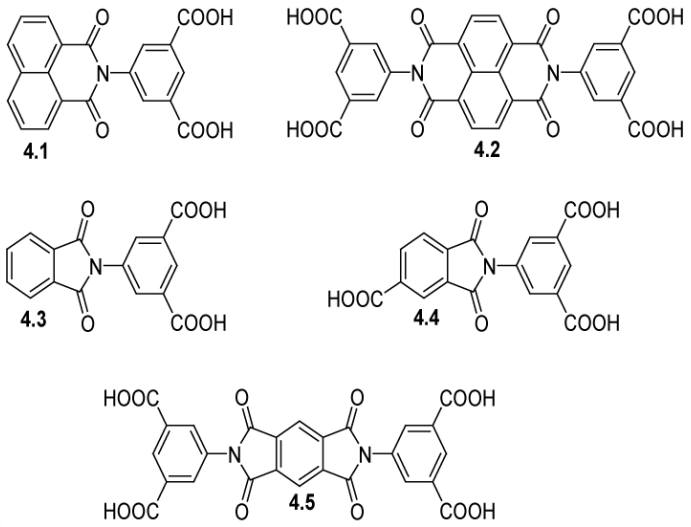

Scheme 4.1. Structures of some imides that form gels.

When these imides **4.1-4.5** are dissolved in DMSO followed by addition of water; they form gels. A series of gels are prepared and the conditions for their formation and their properties are listed in Table 4.1. In a typical experiment, **4.3** is dissolved in DMSO (0.83 wt %, w/v) by heating and water was added in a resultant clear solution. A transparent thermo-reversible gel is formed after a few minutes upon cooling at room temperature under ambient conditions. The gels of other imides are prepared following the same procedure as describe for **4.3**, only differences being in the amount of gelators and co-solvent. The ratio of gelling solvents DMSO and water is used 5:2 in the gels of compound **4.1** and **4.2** where as 3:2 in the case of other gels to get the maximum stability of gels. To estimate the thermal stability of the gels, critical gel concentrations (wt %, w/v) and critical gel temperature (gel to sol melting temperature, T_{gel}) are recorded (Table 4.1). These data show that the gel formed by compound **4.3** is most stable gel which has lower critical gel concentration and higher critical gel temperature. Dastidar et al reported a series of adducts of N,N'-bis-(pyridyl) urea-dicarboxylic acid as low molecular weight organic gelator.[14] These adducts were found to be good hydrogelators of pure water with low gelator concentration in 1.2-3.0 wt% range. The critical gel temperature of these gels vary from 64-98^{0}C. The gelation ability of a series of simple derivatives of 2,6-pyridinedicarboxylic acid that lack large aliphatic groups is also reported in water/DMSO mixtures.[15] The gels obtained with these derivatives display unusual high gel-to-sol transition temperatures; at the gelator

concentrations of 1-10 wt%, the transition temperature exceeds 150°C. The gels were observed to be thermoreversible, transparent, and stable over long periods.

Table 4.1: Gel formation of various imides

Compounds	DMSO:Water	Wt% (gm/lit)	T_{gel} (^{0}C)
4.1	5:2	2.00	65
4.2	5:2	2.77	74
4.3	3:2	0.83	84
4.4	3:2	1.46	68
4.5	3:2	1.13	70

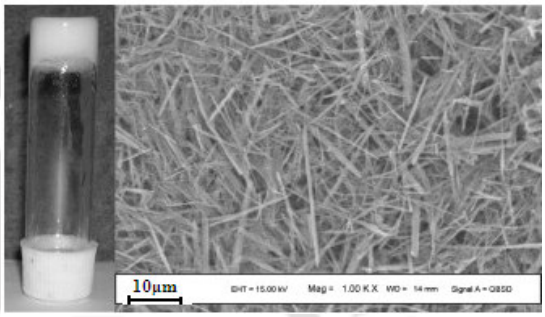

Figure 4.1: SEM of gel **4.1**

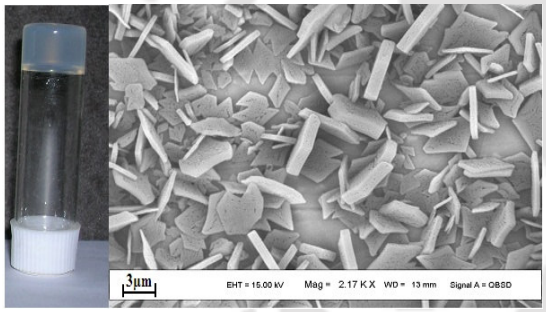

Figure 4.2: SEM of gel **4.3**

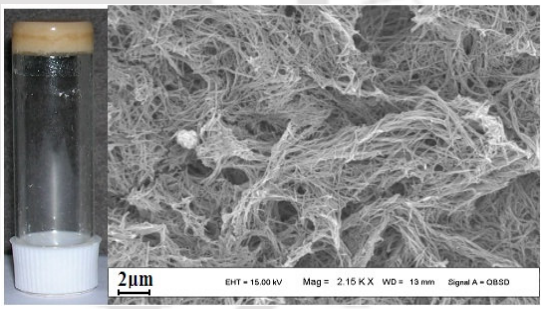

Figure 4.3: SEM of gel **4.4**

The scanning electron micrograph (SEM) of each gel was recorded to predict the morphologies of xerogels (dried gels). The representative SEM images of some of the gel are shown in Figure 4.1-4.3. SEM analyses show that the gel prepared by compound **4.1** has short thick fibre-like structure varying from 10 to 40 µm in length and from 0.5–1.0 µm in width. The morphology of the other gels varies and they have network structures or plate-like structures of micron size. The gel of **4.3** has plate-shaped structures with 2–8 µm length and 0.7–2.0 µm width. On the other hand, the gel of **4.4** has interconnected fiber networks with width of about 0.25–0.40 µm. The macroscopic properties of similar kind of organogelators have been investigated by various physico-chemical measurements such as optical microscopy, electron microscopy (e.g., SEM,

TEM), atomic force microscopy (AFM), X-ray diffraction, dynamic light scattering, small angle neutron scattering, etc. It is believed that the gelator molecules form some kind of 3D fibrous aggregates via spontaneous self-assembly process involving various intermolecular interactions and the bulk solvents are immobilized within such 3D network causing gelation. SEM of gels of pyridinedicarboxylic acid derivatives in aqueous DMSO show the presence of thin, straight fibres that are 10 μm long and weakly interconnected.[15] The morphological characteristics of the xerogels of the N,N'-bis-(pyridyl) urea-dicarboxylic acid gelators show a mixture of plate shaped and 1D slender fibers or a complicated 3D network of fibers of tape morphology and intertwined network of 1D fibers.[14] In all the cases, the fibers are ~10 μm long and the thickness varied from submicron to 10 μm. The gelation properties of PBI dye, which is able to gelate a multitude of organic solvents at rather low concentration (~0.2 wt%), can be attributed to the presence of hydrogen bonds between the benzamide functional groups that enforce the strong π-π stacking interactions between PBI units leading to gelation.[13c] AFM of PBI gel shows the helical fibres with 3.1 nm of height, 8.0 nm of width and several micrometers in length.

Single crystal structure information on a gelator molecule is important to understand the supramolecular architecture of the meta-stable gel fiber in its native (gel) form.[16] However, it is virtually impossible to determine the crystal structure of a gel fiber; Dastidar reported first example of crystal structure of a pyridyl urea based low molecular weight organic gelator molecule which was crystallized from its gelling solvents such as ethylene glycol and water.[17] The supramolecular assembly of the gelator molecule and the interacting solvents in the crystal lattice displays microporous architecture with channels that contained both solvent molecules through hydrogen bonding interactions with the gelator molecules. We have also tried to crystallize the gelator molecules in a mixture of DMSO and water solvents but could not be achieved the suitable single crystals of any gelator molecule with both of its gelling solvents. However, the compound **4.3** was crystallized in DMSO and the formation of a 1:1 solvate of **4.3** with DMSO was characterized by determining its crystal structure. The structure of the solvate is shown in Figure 4.4a. Generally, carboxylic acids are strongly hydrogen bonded amongst themselves, but it is very interesting to note that the solvate of **4.3** with DMSO is devoid of O–H···O interactions amongst the carboxylic acid groups. However, it displays a hydrogen bond O2–H2···O4 interaction ($d_{D\cdots A}$ 2.59Å, <D-H···A, 175.0º) between the oxygen atom of DMSO and the –OH of one of the carboxylic acid groups. This compound forms sheet-like structure in

which the DMSO molecules are between the two layers of the imides. The DMSO molecules themselves have weak S···O ($d_{D\cdots A}$ 2.59Å, 3.31 Å) interactions (Figure 4.4b). The layers grow along the crystallographic a axis. This arrangement leads to a highly porous structure, which, possibly on addition of water, results in a strong hydrogen bonded network leading to formation of the gel. The mechanism of gelation of well known family of dipicolinic acid derivatives is proposed to arise from the base-assisted deprotonation of the carboxylic functionality, leading to the formation of the sodium chelate of the monodeprotonated ligand as the key gelling species.[15] Electrostatic interactions and hydrogen bonds are thus believed to account to some extent for the formation of extended structures in which dipicolinic acid species self-assemble with the help of bridging water molecules. Xu et al reported naphthalene based β-aminoacids and N-(fluorenylmethoxycarbonyl) amino acids hydrogelators for biomedical applications in which 3D fibril network is proposed to sustain by hydrogen bond network and π-π interactions.[18]

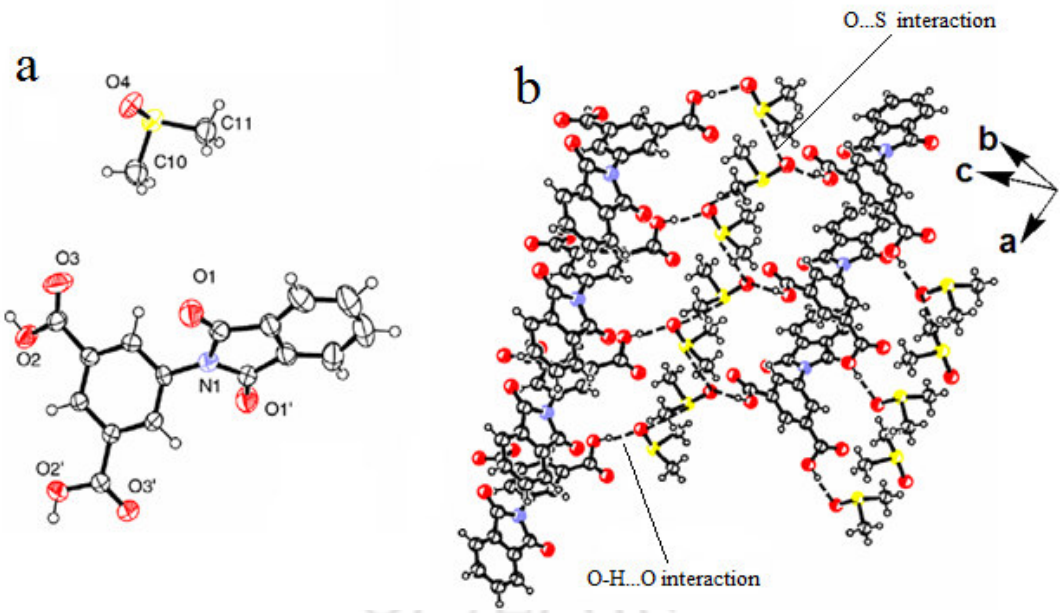

Figure 4.4: (a) ORTEP diagram of 1:1 DMSO solvate of **4.3** (20% thermal ellipsoid). (b) Weak interactions leading to sheet-like structure.

Most of the compounds such as **4.1**,[19a] **4.2**[19b] and **4.3**[19c,d] are already reported in literature; however, in this study we have shown their gel formation abilities.

A number of cyclic imide compounds having isoquinoline backbone are also synthesized and their solvent dependent fluorescence emission properties are studied as a part of this chapter. The

organic compounds having fluorophores that are sensitive to environment are of great importance in chemistry and biology.[20] The fluorescence emission spectra of some heterocyclic compounds such as benzo[de]benzo[4,5]imidazo[2,1-a]isoquinoline (Scheme 4.2) are sensitive to environment[21] and some of such heterocyclic compounds are used as organic photoconductive materials.[22] So, the functionalization of such heterocyclic compounds is expected to form derivatives that may possess interesting optical properties.[23] Heterocyclic compounds having more numbers of delocalized aromatic rings in conjugation to each other would lead to better as well as novel optical properties.[22] With an interest to identify and characterize and also to understand optical properties of compounds bearing fluorophores that are sensitive to environment, we have synthesized a few heterocyclic compounds as shown in Scheme 4.2. We have studied fluorescence emission of these compounds and compared with some of their derivatives.

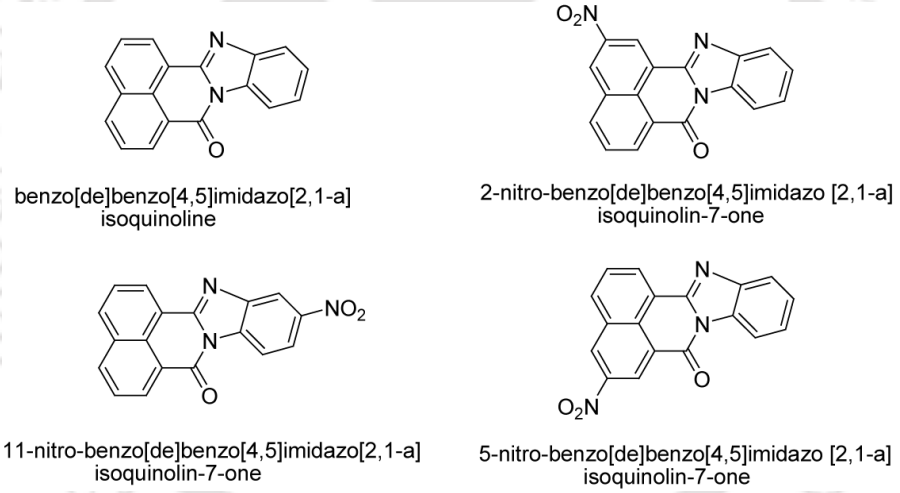

Scheme 4.2: Structures of heterocycles.

In this study we observed that the condensation reaction of 1,8-naphthalic anhydride with 4-nitro 1,2-diaminobenzene led to the formation of cyclic imide heterocyclic compound **4.7** in acetic acid solvent[24] whereas the same reaction using N,N-dimethylformamide (DMF) solvent provided cyclic imide derivative **4.6** (Scheme 4.3).

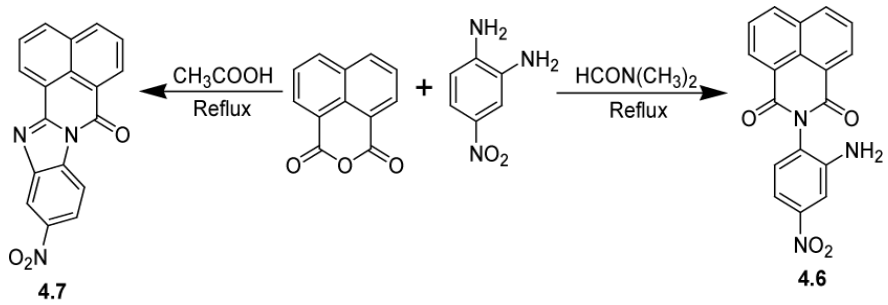

Scheme 4.3: Solvation controlling reaction path in the formation of two different product.

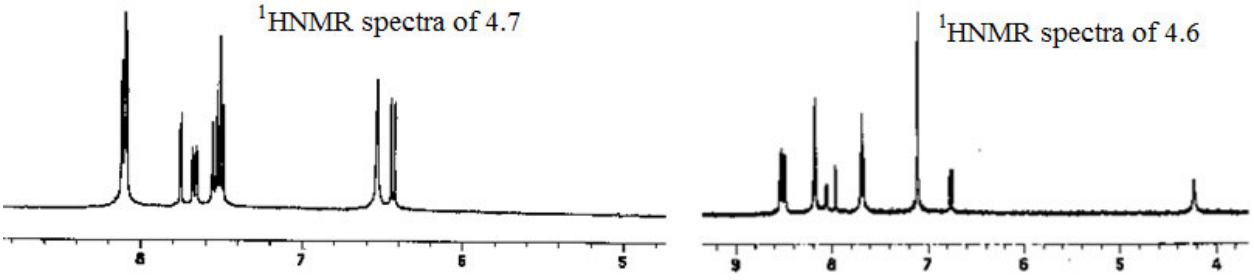

Figure 4.5: ^{1}HNMR spectra of compound **4.6** and **4.7**.

Whilst trying to understand this reaction, we found that the reaction of 1,8-naphthalic anhydride with 4-nitro-1,2-diaminobenzene was dependent completely on the solvent. The spectroscopic data of compound **4.7** were compared with its earlier reported one.[24] Compound **4.6** was isolated as a solvate of DMF, the structure of which is shown in Figure 4.5. The solvates of dicarboxylic acids with DMF and DMSO are common in literature and some of them show interesting optical properties.[25] In this solvate, the DMF molecules is held with parent molecule by strong hydrogen bond, N3–H3a···O7 ($d_{D\cdots A}$ 2.86Å, <D-H···A, 161.33º) and by the π…π interaction between the 1,8-naphthalimide ring and the lone pair of the nitrogen atom of the DMF. The presence of the π…π interaction is established by the distance of separation 3.35 Å. This distance is well within the admissible limit for π…π interactions. The compound shows IR absorptions for carbonyl stretching at 1771 cm^{-1} and at 1740 cm^{-1} due to the carbonyl groups of the DMF and the imide ring, respectively. It also demonstrates a strong absorption at 3446 cm^{-1} for the NH_2 group. The C–H group of DMF is appeared at 2923 cm^{-1}, whilst the nitro group stretching is observed at 1304 cm^{-1}. In solution also, DMF unit is tightly bound to the parent molecule and in the ^{1}HNMR, the methyl signals are appeared as two singlets at δ 2.50 and δ 2.34 ppm. The observation of the

two singlets suggests two different environments for the methyl groups attached to the nitrogen atom of DMF. Thus, the sluggish reaction in DMF solvent is attributed to complementary hydrogen bonding ability of compound **4.6** with DMF.

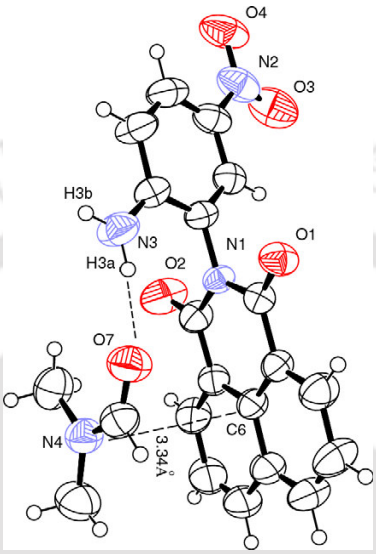

Figure 4.6: Crystal structure of DMF solvate of compound **4.6** (50% thermal ellipsoids).

Synthesis of heterocycles: Based on above observation (Scheme 4.3), the heterocyclic compounds **4.9** and **4.10** were prepared by the reactions as depicted in Scheme 4.4 and 4.5. The condensation of 1,8-naphthalic anhydride with 4-nitro 1,2-diaminobenzene in acetic acid gave 11-nitro-benzo[de]benzo[4,5]imidazo[2,1-a]isoquinolin-7-one (**4.7**). Although this reaction is expected to give two isomeric products, we obtained a single isomer. This could be due to the fact that such cyclization process passes through imide intermediates. It has already shown that only one imide isomer is formed in this reaction before cyclization (Scheme 4.3). This was shown by trapping the intermediate imide derivative in DMF solvent.[26] The formation of specific imide in this reaction may be attributed to the ease of attack of the amino group at *p*-position to the nitro group of 4-nitro-1,2-diaminobenzene; this group is less sterically crowded between the two possible amino groups supposed to be attack on the ring of 1,8-naphthalic anhydride, leading to the formation of only one isomer. The reduction of the nitro group of the compound **4.7** resulted in the formation of the corresponding amine **4.9**.

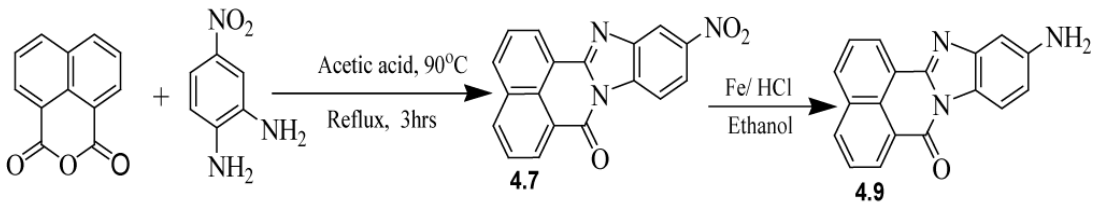

Scheme 4.4. Synthesis of heterocycles **4.7** and **4.9**.

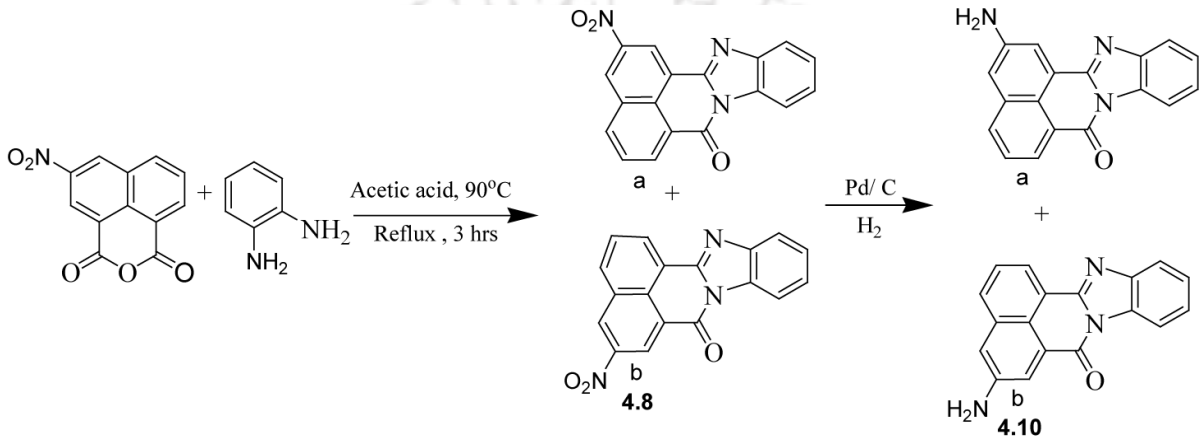

Scheme 4.5. Synthesis of heterocycles **4.8** and **4.10**.

Similarly, the condensation reaction of 3-nitro-1,8-naphthalic anhydride with 1,2-diaminobenzene gave a mixture of isomeric products; namely 2-nitro-benzo[de]benzo[4,5]imidazo[2,1-a]isoquinolin-7-one (**4.8a**) and 5-nitro-benzo[de]benzo[4,5]imidazo[2,1-a]isoquinolin-7-one (**4.8b**). We could not separate the two isomers by conventional chromatographic techniques such as preparative TLC or column chromatography. The ^{1}HNMR chemical shift and the integration values of the mixture of isomers suggest the formation of an almost equimolar mixture of the two isomers. In an earlier report, it was suggested that similar reaction under sonication in presence of alumina resulted only one isomer[27] but in our case we have failed to obtain pure isomer through the reaction condition described herein and the isomeric product separation of **4.8** was not successful. However, We were also synthesized successfully only one isomer by the condensation reaction of 3-nitro-1,8-naphthalic anhydride with 1,2-diaminobenzene under solvothermal condition by solvent drop

grind method using acetic acid solvent in an autoclave at 250^0C. The ^{1}HNMR spectra of one isomer obtained from this reaction, along with the mixture of isomers are shown in Figure 4.6. It has eight peaks in aromatic region and tallies the structure of **4.8a**. The assignment of the ^{1}HNMR to this compound is on the assumption that the simulated ^{1}HNMR of other isomer **4.8b** shows proton signals at relatively high chemical shift than the isomer **4.8a**.

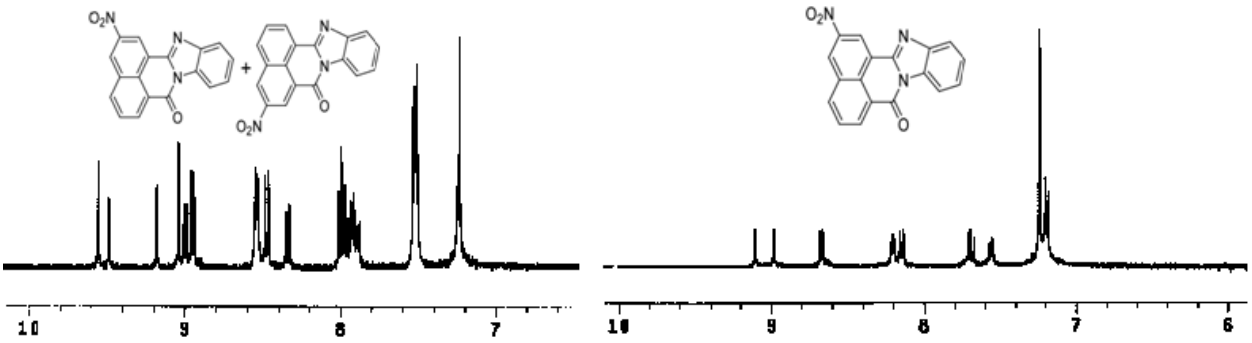

Figure 4.7: ^{1}HNMR spectra of mixture of isomers (**4.8a** and **4.8b**) and a single isomer (**4.8a**).

Since, the optical properties of these two isomers and derivatives are indistinguishable, we proceeded to take the mixture of isomers for optical study described in the next section. The reduction of the nitro group of these isomers (**4.8**) was carried out by hydrogen gas with a catalytic amount of palladized carbon to prepare two isomeric amine derivatives **4.10** (Scheme 4.5). The amino group of compound **4.9** was further functionalized to obtain various derivatives **4.11-4.14** as illustrated in Scheme 4.6. Methyl and acyl derivatives (**4.15**-**4.18**) of compound **4.10** were also synthesized by similar procedures (Scheme 4.7).

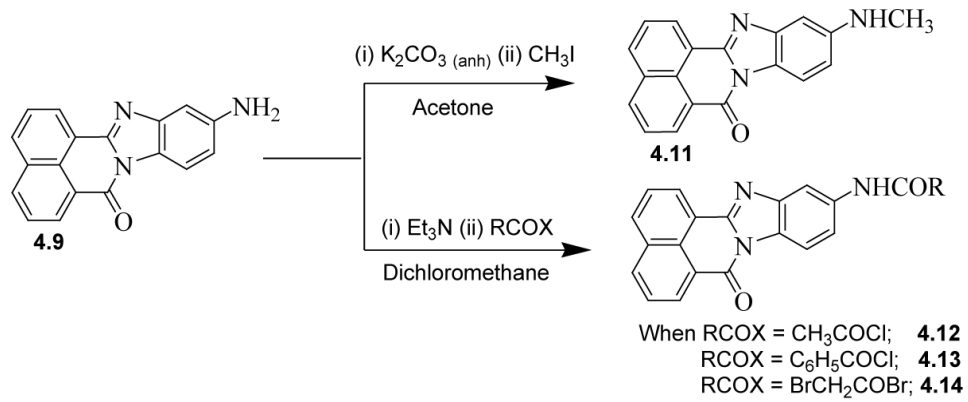

Scheme 4.6. Synthesis of various derivatives of **4.9**.

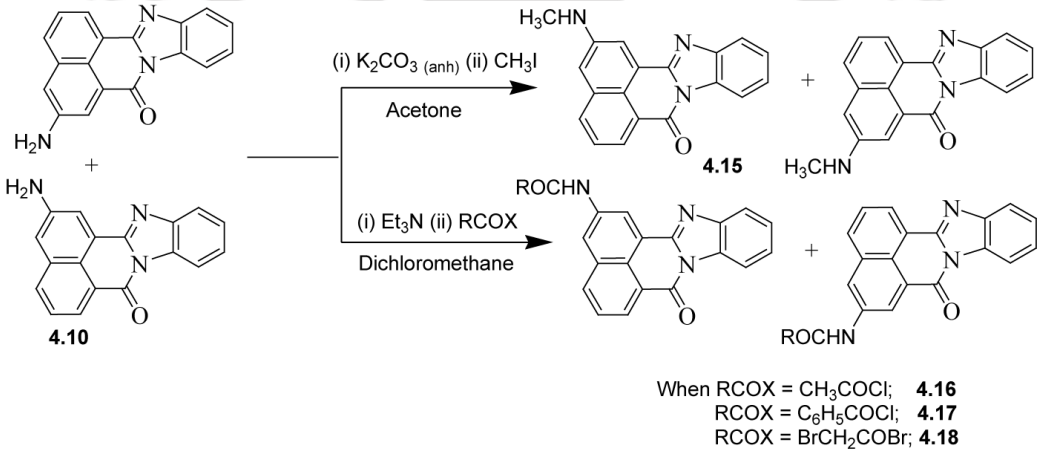

Scheme 4.7. Synthesis of various derivatives of **4.10**.

Optical properties: The compounds **4.9** and **4.10** show solvatochromic property and the absorption features of **4.9** and **4.10** are different in different solvents, which are listed in Table 4.2. The compounds **4.9** and **4.10** are derived from a planar aromatic ring system which is derived from 1,8-naphthalic anhydride. The imides derived from naphthalic anhydride are useful

Table 4.2: Effect of solvent on the visible spectra of **4.9** and **4.10**.

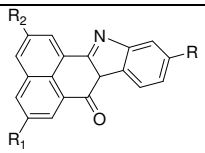	Solvent	λmax (nm)	ε /$M^{-1}cm^{-1}$
R = NH_2, R_1, R_2 = H (**4.9**)	Dichloromethane	430	1.27×10^4
R = NH_2, R_1, R_2 = H (**4.9**)	Methanol	437	1.02×10^4
R = NH_2, R_1, R_2 = H (**4.9**)	Acetonitrile	444	0.95×10^4
R = H, R_1, R_2 = H/NH_2 (**4.10**)	Dichloromethane	427	1.12×10^4
R = H, R_1, R_2 = H/NH_2 (**4.10**)	Acetonitrile	432	1.00×10^4
R = H, R_1, R_2 = H/NH_2 (**4.10**)	Methanol	438	0.96×10^4

as fluorescence probe and their applications are decided to a large extent by the presence of tether connecting two similar or dissimilar molecules.[27] The compounds **4.9** and **4.10** have reasonable fluorescence emission properties on excitation at appropriate wavelengths. The UV-visible absorption spectra as well as fluorescence emission spectra of several derivatives of **4.9** are recorded and listed in Table 4.3. Between the nitro and amino groups, the later shifts the fluorescence emission towards higher wavelength. Whereas, in the case of substituted amines it is observed that the substituent attached on nitrogen leads the emission to higher wavelength. Among the N-substituent compounds **4.11**-**4.14**, the highest shift is observed for the N-benzoylated derivative **4.13**. It is attributed to the fact that benzoate group participates on delocalization of electrons with the aromatic ring of the heterocycle. The fluorescence emission spectra of various derivatives of mixture of 2-amino-benzo[de]benzo[4,5]imidazo[2,1-a] isoquinolin-7-one and 5-amino-benzo[de]benzo[4,5]imidazo[2,1-a]isoquinolin-7-one (**4.10**) were also recorded and the emission wavelength and quantum yields are listed in Table 4.3. Although the compound **4.10** is a mixture of two isomers, in none of the cases, we could obtain any distinguishable fluorescence emission feature of the two isomers. The observed shifts and intensity changes in various substituents of **4.9** and **4.10** predominantly occur from the electronic effect caused to the overall electronic environment by the presence of the substituents. It is important to note that the emission spectra of naphthalimide fluorophores having amine groups are proton responsive[28] and such compounds have relevance in recognition of anions.[29]

Table 4.3: The visible spectra and fluorescence emission (λ_{ex} = 410 nm) of derivatives of **4.9** and **4.10**.

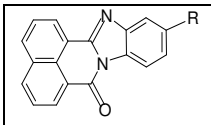	λmax/nm (dichloromethane)	ε /$M^{-1}cm^{-1}$ (dichloromethane)	λ_{em}/nm (dichloromethane)	Φ (dichloromethane)
R = NO_2	390	19772	463	0.134
R = NH_2	430	12727	508	0.252
R = $NHCH_3$	395	6818	515	0.060
R = $NHCOCH_3$	397	6136	545	0.350
R = $NHCOC_6H_5$	401	8409	546	0.452
R=$NHCOCH_2Br$	393	10909	518	0.343
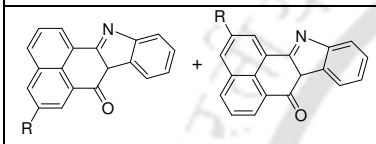				
R=NH_2	427	11,212	491	0.288
R=$NHCH_3$	375	18,909	538	0.156
R=$NHCOCH_3$	401	10,303	493	0.290
R=$NHCOC_6H_5$	401	19,181	493	0.324
R=$NHCOCH_2Br$	395	10,393	495	0.215

In the case of compound **4.9**, the fluorescence emission of parent compound in dichloromethane solution is observed at 508 nm upon excitation at 410 nm. The compound **4.9** is found to be fluorescence inactive in methanol. Accordingly, the fluorescence emission of the **4.9** observed from dichloromethane solution also gets quenched on addition of methanol (Figure 4.7a). The protonation causes shift in the fluorescence emission to a lower wavelength from the emission of parent compound **4.9**. For example, the parent compound **4.9** in dichloromethane on excitation at 410 nm emits at 514 nm, and the same solution emits at 508 nm and 498 nm, respectively, on addition of one or two equiv of HCl (Figure 4.7b).

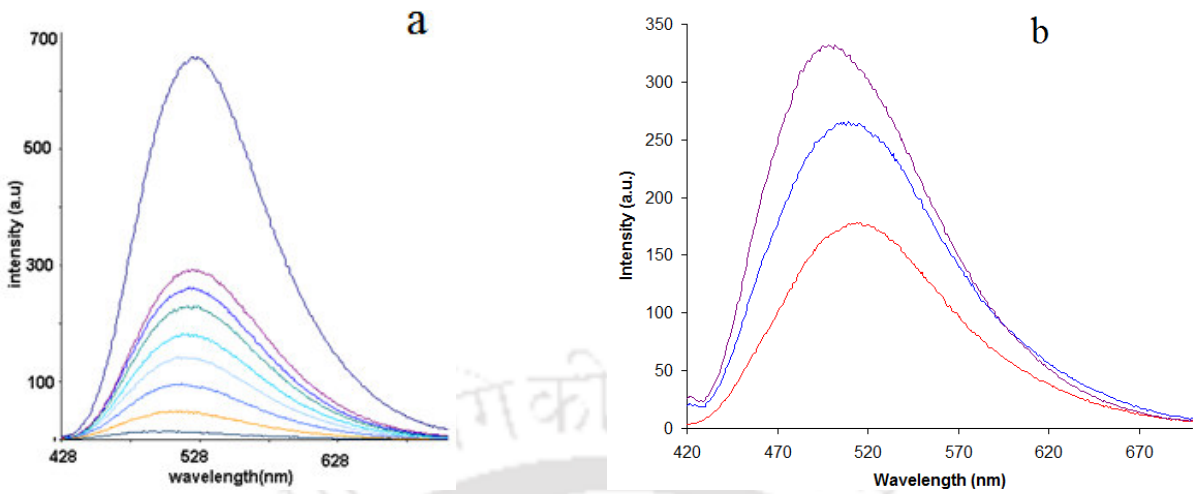

Figure 4.8: (a) Effect of the addition of methanol to a solution of **4.8** in dichloromethane (λ_{ex} = 410 nm). (b) Fluorescence emission spectra of **4.8** in dichloromethane and on addition of one mole equiv of HCl and two mole equiv of HCl (in each cases 3 ml of 1.1×10^{-5} M solution).

The emission spectra of **4.10** are also highly solvent dependent. A solution of **4.10** on excitation at 410 nm in dichloromethane, acetonitrile, and methanol shows fluorescence emission at 491nm (Φ = 0.458), 527 nm and 562 nm, respectively, (Figure 4.8a). Such large characteristic shifts in emission spectra make it possible to distinguish these three solvents. From the Table 4.2, it is clear that the compound **4.10** shows very small solvatochromicity in visible spectra, whereas, the same compound shows a large shift in emission spectra on change of solvents. This suggests that a polar excited state capable of forming exciplex with different solvents is involved in fluorescence emission. Addition of methanol to dichloromethane solution of **4.10** changes its fluorescence emission; initially, the emission occurring due to excitation at 410 nm decreases but the emission shifts to a higher wavelength and on gradual addition of methanol it once again increases and reaches the emission wavelength that corresponds to the observed emission wavelength from a methanolic solution of **4.10** (Figure 4.8b). Similarly the addition of methanol to an acetonitrile solution of **4.10** shifts the fluorescence emission to higher wavelength (Figure 4.8c). The compound **4.10** also shows proton responsive fluorescence emission which is dependent on the hydrogen ion concentrations.

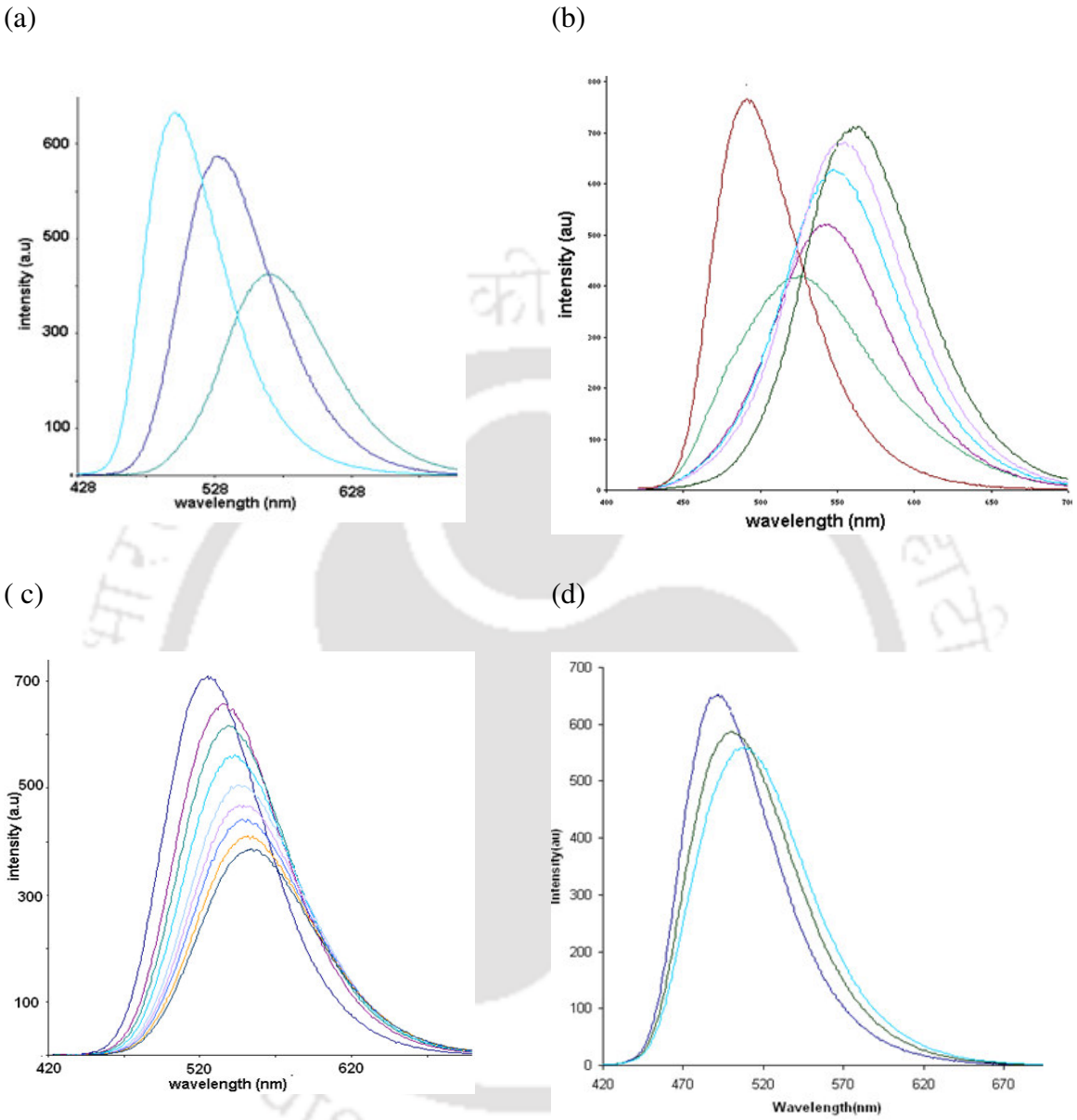

Figure 4.9: (a) The fluorescence emission (λ_{ex} = 410 nm) of **4.10** in dichloromethane, acetonitrile and methanol (in each cases 3 ml of 1.1×10^{-5} M solution of **4.10**) (b) of **4.10** on addition of different aliquots of methanol to a dichloromethane solution of **4.10** (c) of **4.10** on addition of different aliquots of methanol to an acetonitrile solution of **4.10** (d) of **4.10** in dichloromethane, and on addition of one mole equiv of HCl and two mole equivalent of HCl.

For example, treatment of a solution of **4.10** with HCl (one equiv) causes a change of fluorescence emission from 491 to 501 nm and on addition of two equiv of the acid, the emission occurs at 510 nm (Figure 4.8d). These results suggest that the protonation effects the delocalization of electrons of the amino group, which in turn contributes to the changes in the emission spectra of these compounds. The solvato-emissive properties can be attributed to the stabilization of polar exited by polar solvent, whereas the proton responsive nature is attributed to the hydrogen bonding by protic solvent and protonation by mineral acid. Similar properties are seen in receptors of carboxyilic acids.[30]

In conclusion, a series of new class of low molecular weight organogelators is prepared and their gel formation properties are described. We observed that water plays a crucial role in the formation of strong hydrogen bonded networks with these compounds leading to the formation of gels. The role of solvents in deciding the course of the reaction of 4-nitro-1,2-diaminobenzene with 1,8-naphthalic anhydride is reported. The heterocyclic compounds derived from planar aromatic ring show solvato-emissive properties. A large shift in fluorescence emission wavelength is observed on introduction of amino group at different positions of benzo[de]benzo[4,5]imidazo[2,1-a]isoquinolin-7-one. Different organic solvents such as dichloromethane, acetonitrile, methanol can be distinguished from the emission wavelengths of the **4.10** in these solvents. Depending on the position of an amino group in the rings and on protonation of the amino groups at different positions, the fluorescence emissions shifts to higher or lower wavelength.

Experimental Section:

Determination of fluorescence quantum yield:

Fluorescence quantum yields were determined by calibrating the perylene (Φ = 0.94) with fluorescence excitation at 410 nm as standard. The fluorescence quantum yield were calculated by using the following formula:[31]

$$\frac{(\text{Quantum yield})_{\text{sample}}}{(\text{Quantum yield})_{\text{standard}}} = \frac{\text{Absorption of standard (Area under the graph of emission spectra)}_{\text{sample}}}{\text{Absorption of sample (Area under the graph of emission spectra)}_{\text{standard}}}$$

Detailed synthetic methodologies are given below. Analytical data as well as spectroscopic data are listed along with each compound. The instrumental details are given in Appendix.

Synthesis and characterization of various compounds:

Compounds **4.1**-**4.5**: Compounds **4.1**-**4.5** were synthesized by refluxing a solution of 5-amino-isophthalic acid with different cyclic anhydrides for 4 hrs in the temperature range 90-120^{0}C. The solvents used in these condensation reactions were DMF (in the case of formation of product **4.1** and **4.2**) and acetic acid (for the formation of product **4.3**, **4.4** and **4.5**). The precipitates of the pure product were obtained in these reactions which were filtered, washed with water several times and air dried.

Compound **4.1**: Yield: 86%; IR (KBr, cm^{-1}): 3445 (m), 2924 (w), 2560 (w), 1702 (s), 1673 (m), 1587 (w), 1411 (w), 1338 (w), 1286 (m), 937 (w), 774 (w), 696 (w). ^{1}HNMR (400 MHz, DMSO-d^6): 7.92 (t, 2H, J = 8 Hz), 8.24 (s, 2H), 8.52 (m, 5H). ESI-MS: 361.867 (M + H$^+$).

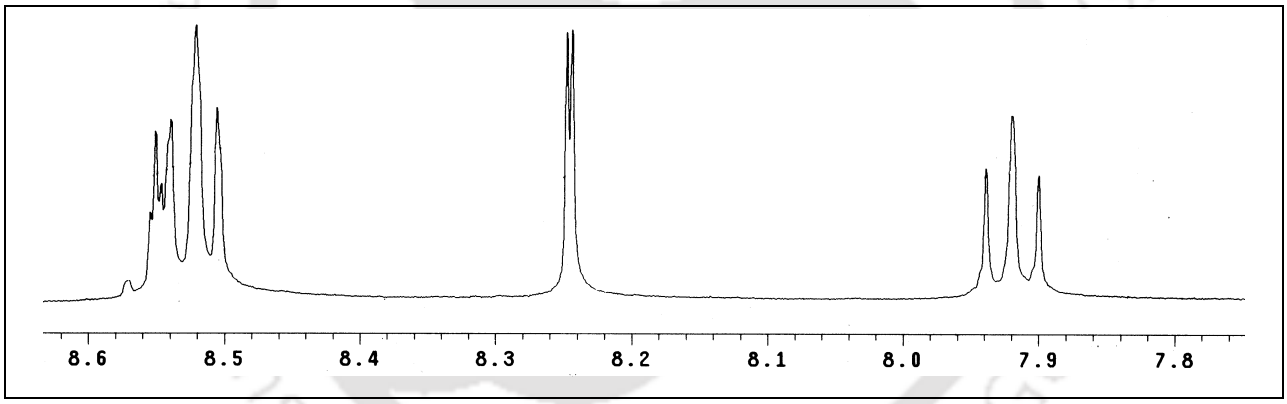

Figure 4.10: ^{1}HNMR spectra of compound **4.1**.

Compound **4.2**: Yield: 85%; IR (KBr, cm^{-1}): 3424 (m), 2925 (w), 1710 (s), 1680 (s), 1581 (w), 1450 (w), 1350 (m), 1251 (s), 1169 (s), 1122 (w), 1012 (w), 769 (w), 741 (w), 646 (w). ^{1}HNMR (400 MHz, DMSO-d^6): 8.31 (s, 4H), 8.58 (s, 2H), 8.73 (s, 4H). ESI-MS: 596.832 (M + H$^+$).

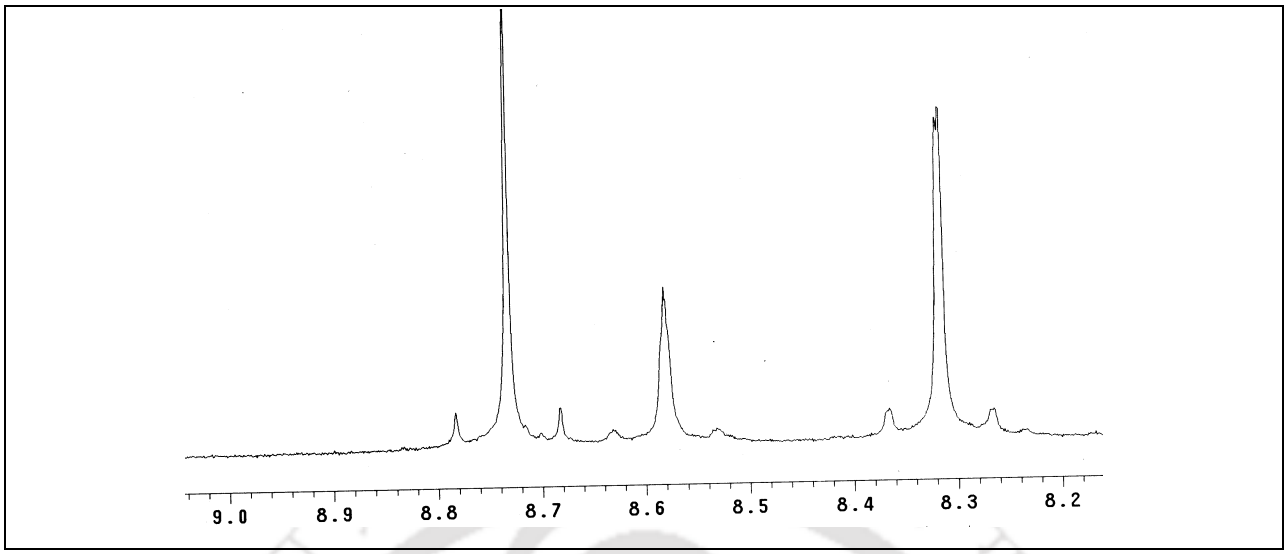

Figure 4.11: ^{1}HNMR spectra of compound **4.2**.

Compound **4.3**: Yield: 95%; IR (KBr, cm^{-1}): 3445 (m), 2925 (w), 2549 (w), 1728 (s), 1605 (m), 1416 (m), 1382 (s), 1281 (m), 1226 (m), 1112 (w), 1081 (w), 875 (w), 759 (w), 711 (m), 641 (w), 530 (w). ^{1}HNMR (400 MHz, DMSO-d^{6}): 7.91 (dd, 2H, J = 5.6 Hz), 7.99 (dd, 2H, J = 5.6 Hz), 8.29 (s, 2H), 8.49 (s, 1H). ESI-MS: 312.102 ($M + H^{+}$).

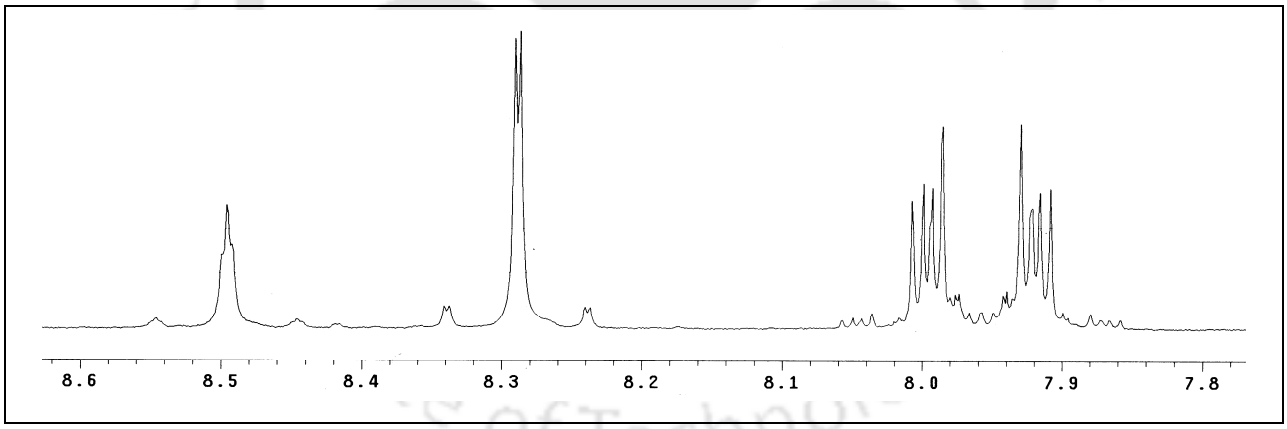

Figure 4.12: ^{1}HNMR spectra of compound **4.3**.

Compound **4.4**: Yield: 95%; IR (KBr, cm^{-1}): 3427 (s), 2890 (w), 1726 (s), 1383 (m), 1249 (m), 1095 (w), 724 (w). ^{1}HNMR (400 MHz, DMSO-d^{6}): 7.94 (s, 1H), 8.10 (d, 1H, J = 2.0 Hz), 8.31 (s, 2H), 8.41 (d, 1H, J = 2.0 Hz), 8.50 (s, 1H). ESI-MS: 365.042 ($M + H^{+}$).

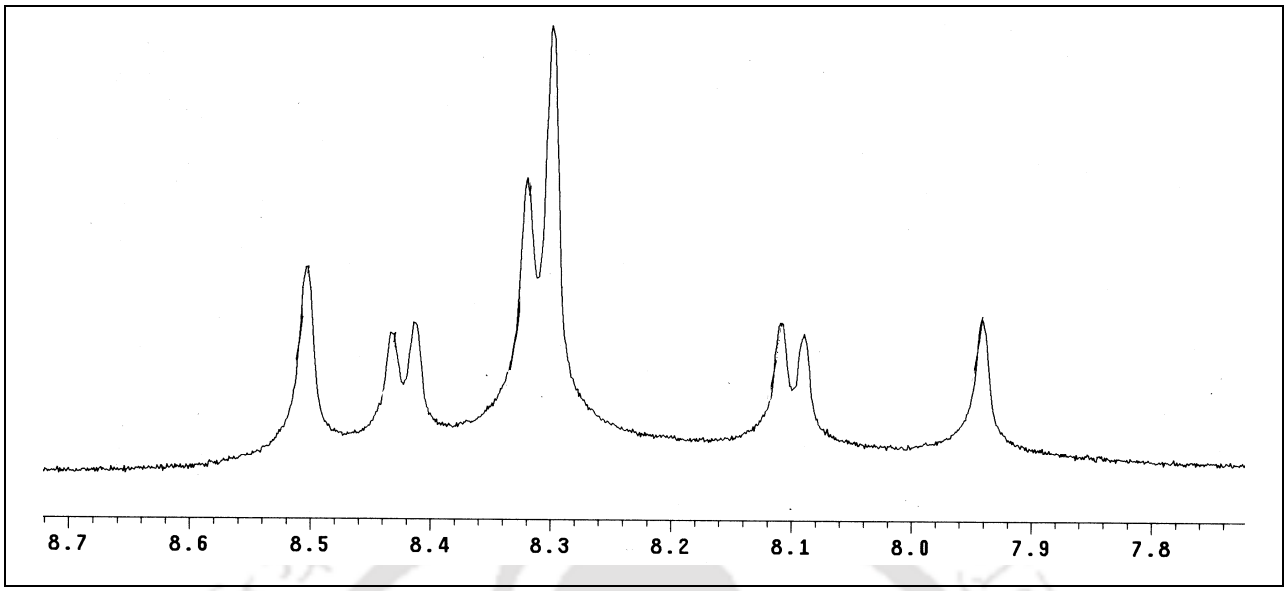

Figure 4.13: ^{1}HNMR spectra of compound **4.4**.

Compound **4.5**: Yield: 90%; IR (KBr, cm^{-1}): 3422 (m), 2924(w), 1731(s), 1604 (w), 1376 (s), 1239 (m), 1115 (w), 1013 (m), 950 (w), 757 (w), 675 (w). ^{1}HNMR (400 MHz, DMSO-d^{6}): 8.31 (s, 4H), 8.42 (s, 2H), 8.54 (s, 2H). ESI-MS: 545.934 ($M + H^{+}$).

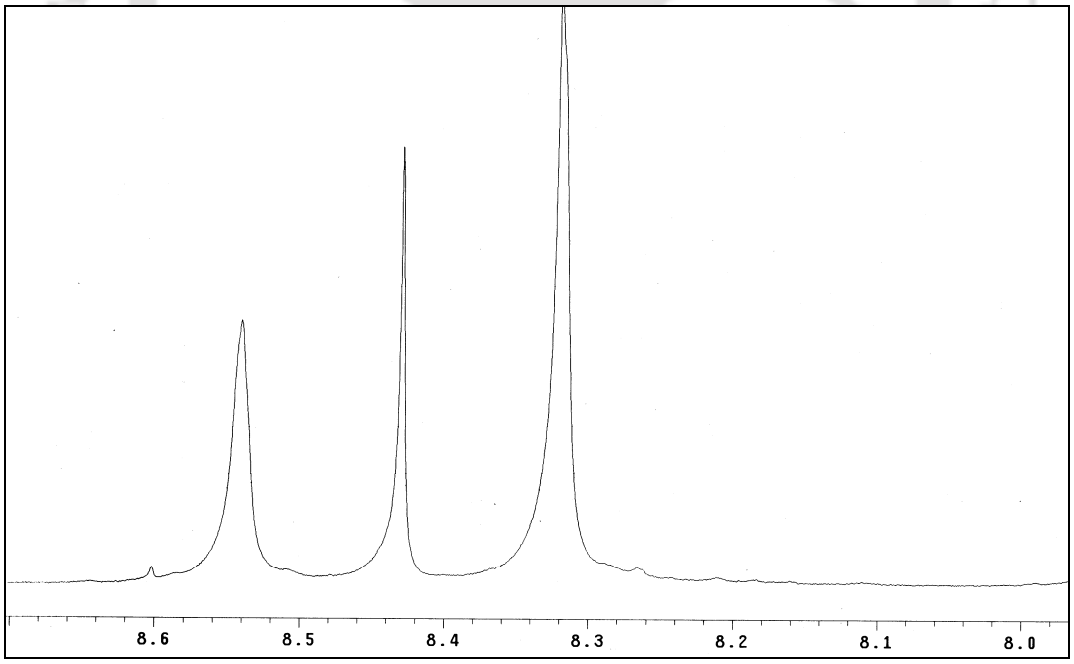

Figure 4.14: ^{1}HNMR spectra of compound **4.5**.

Compound **4.6**: A solution of 1,8-naphthalic anhydride (0.990 g, 5 mmol) and 4-nitro 1,2-diaminobenzene (0.765 g, 5 mmol) was refluxed in DMF (10 ml) at 90^0C for 3 hrs. The reaction mixture was cooled affording crystalline product **4.6** in 98% yield. IR (KBr, cm^{-1}): 3446 (s), 1740 (s), 1771 (s), 1580 (m), 1304 (s), 1013 (s), 775 (s). ^{1}HNMR (400 MHz, DMSO-d^6): 8.50 (dd, 2H, *J* = 3.6 Hz), 8.17 (d, 2H, *J* = 4.8 Hz), 8.05 (d, 1H, *J* = 8.8 Hz), 7.96 (s, 1H), 7.68 (t, 2H, *J* = 8.4 Hz), 6.75 (d, 1H, *J* = 4.8 Hz), 4.23 (s, 2H). ESI-MS: 334.175 ($M + H^+$).

Compound **4.7**: A solution of 1,8-naphthalic anhydride (0.99 gm, 5 mmol) and 4-nitro 1,2 diaminobenzene (0.77 gm, 5 mmol) was refluxed in acetic acid (10 mL) for 4 hrs. The reaction mixture was cooled and water (20 mL) was added to the reaction mixture and stirred for 20 minutes. The precipitate was filtered and washed several times with water to remove acetic acid. The product was air-dried to obtain the product in 77% yield. IR (KBr, cm^{-1}): 1699 (s), 1517 (s), 1335 (s), 1237 (m), 1156 (w), 1043 (w), 752 (m) 567 (w). ^{1}HNMR (400 MHz, $CDCl_3$): 8.10 (t, 2H, *J* = 6.4 Hz), 7.75 (d, 1H, *J* = 2.4 Hz), 7.67 (d, 1H, *J* = 2.4 Hz), 7.65 (d, 1H, *J* = 2.4 Hz), 7.51 (dd, 2H, *J* = 8.0 Hz), 6.53 (s, 1H), 6.47 (d, 1H, *J* = 8.8 Hz). ESI-MS: 316.176 ($M + H^+$).

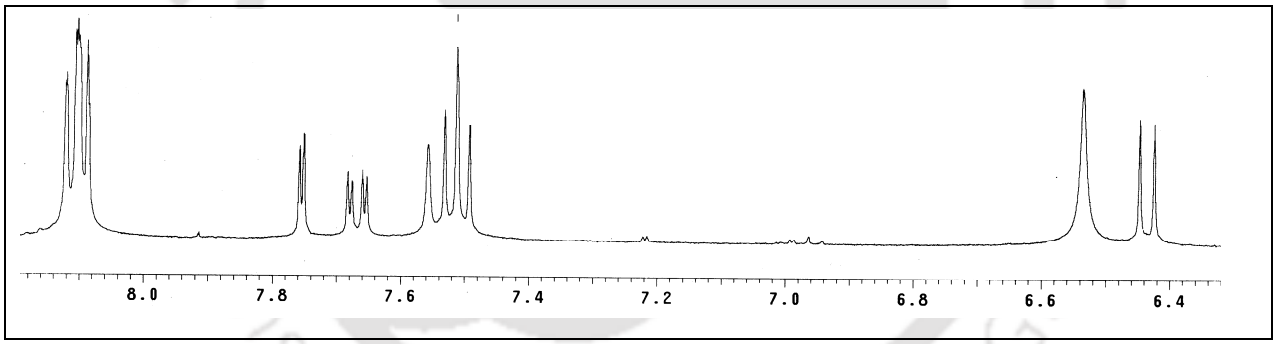

Figure 4.15: ^{1}HNMR spectra of compound **4.7**.

Compound **4.8**: A mixture of two isomers (**4.8a** and **4.8b**) of compound **4.8** was obtained following the same procedure as described for compound **4.7**. Yield: 80%. IR (KBr, cm^{-1}): 3444 (m), 3067 (m), 1696 (s), 1596 (m) 1531 (m), 1443 (w) 1343 (s) 1234 (m), 1152 (w), 1039 (w), 751 (m) 557 (w). ^{1}HNMR (400 MHz, $CDCl_3$): 9.55 (d, 1H, *J* = 4 Hz) 9.48 (d, 1H, *J* = 4 Hz), 9.18 (d, 1H, *J* = 4 Hz), 9.0 (d, 1H, *J* = 4 Hz), 8.98 (d, 1H, *J* = 8 Hz), 8.95 (d, 1H, *J* = 8 Hz), 8.54 (m, 2H), 8.48 (d, 1H, *J* = 8 Hz), 8.35 (d, 1H, *J* = 8Hz) 7.99 (t, 2H, *J* = 8Hz), 7.91-7.94 (m, 2H), 7.50-7.53 (m, 4H). ESI-MS: 316.181 ($M + H^+$).

Compound **4.9:** To a solution of **4.7** (0.32 gm, 1 mmol) in ethanol /water (2:1, 20 mL) iron powder (35 mmol) and aqueous HCl (10%, 5 mL) were added. The mixture was kept at 90° C for 2 hrs. The reaction mixture was brought to room temperature; water (10 mL) was added to the reaction mixture and filtered. The solid product obtained was washed with water and the product was purified by preparative thin layer chromatography. Yield: 55%. IR (KBr, cm^{-1}): 3232 (w), 3363 (s), 1589 (m), 1621 (s), 1697 (s). ^{1}HNMR (400 MHz, $CDCl_3$): 8.76 (m, 2H), 8.26 (d, 1H, *J* = 8.4 Hz), 8.1 (d, 1H, *J* = 8 Hz), 7.9 (d, 1H, *J* = 2.4 Hz), 7.8 (m, 2H), 7.66 (d, 1H, *J* = 8.4 Hz), 6.85 (d, 1H, *J* = 8.4 Hz), 5.0 (s, 2H). ^{13}C NMR ($CDCl_3$): 158.9, 145.8, 137.4, 134.3, 134.2, 131.6, 130.8, 129.7, 129.5, 129.3, 127.4, 125.9, 125.7, 123.1, 120.2, 120.1, 118.5, 115.3. ESI-MS: 286.186 ($M + H^+$).

Compound **4.10:** To a solution of mixture of two isomers of **4.8** (1.58 gm, 5 mmol) in tetrahydrofuran (20 mL), palladized carbon (10%, 0.1 g) was added. The mixture was stirred under hydrogen atmosphere (50 psi) for 24 hrs, filtered, and the solvent was removed from filtrate under reduced pressure to get the desired product. The yield after purification is 85%. IR (KBr, cm^{-1}): 3448 (w), 3362 (s), 2924 (m), 2851 (m), 1690 (s), 1627 (s), 1550 (w), 1448 (w), 1352 (s), 1330 (s), 1166 (w), 1050 (w), 872 (w), 764 (w). ^{1}HNMR (400 MHz, $CDCl_3$): 8.48-8.56 (m, 4H), 8.25 (d, 1H, *J* = 3Hz), 8.18 (d, 1H, *J* = 3 Hz), 7.96 (d, 1H, *J* = 8 Hz), 7.83-7.85 (m, 2H), 7.62-7.67 (m, 2H), 7.43-7.48 (m, 4H), 7.35 (d, 1H, *J* = 3 Hz), 4.2 (s, 2H). ^{13}C NMR ($CDCl_3$): 158.1, 145.4, 134.2, 133.3, 130.0, 128.2, 127.8, 127.4, 125.9, 125.6, 125.4, 123.9, 122.4, 120.1, 118.0, 116.1, 115.7, 112.5. ESI-MS: 286.196 ($M + H^+$).

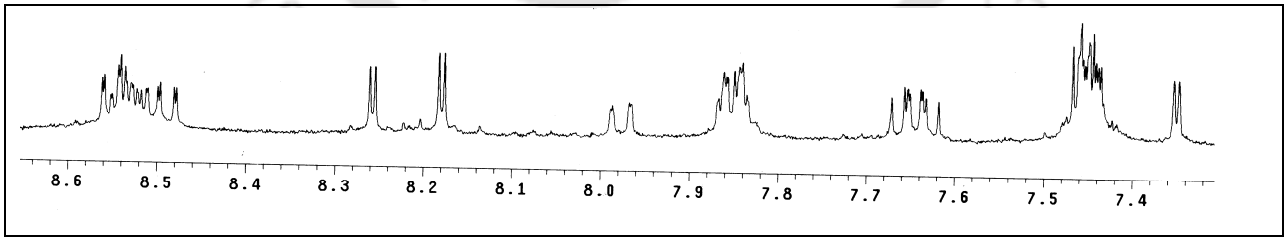

Figure 4.16: ^{1}HNMR spectra of compound **4.10**.

Compounds **4.11-4.14:** Compound **4.9** was converted to corresponding N-methyl (**4.11**), N-acetyl (**4.12**), N-benzoyl (**4.13**) and N- bromoacetyl derivatives (**4.14**) by reactions with suitable reagents as follows:

Compound **4.11:** A mixture of compound **4.9** (0.1 gm, 0.35 mmol) and anhydrous potassium carbonate was refluxed in dry acetone with methyl iodide (0.08 g, 0.53 mmol) for 24 hrs. The reaction mixture was evaporated, water and dichloromethane were added, the organic layer was separated and the product was extracted from the dichloromethane by evaporation. The compound was further purified by TLC. Yield: 25 %. IR (KBr, cm^{-1}) : 3390 (s), 2924 (s), 2853 (m), 1693 (s), 1621 (s), 1502 (s), 1318 (m). ^{1}HNMR (400 MHz, DMSO-d^6) : 8.65 (d, 1H, *J* = 7.2 Hz), 8.16 (d, 1H, *J* = 8.4 Hz), 7.98 (d, 1H, *J* = 8.4 Hz), 7.82 (d, 1H, *J* = 2.8 Hz), 7.7 (m, 4H), 6.86 (dd, 1H, *J* = 2.8 Hz), 3.0 (s, 3H). ESI-MS: 300.113 ($M + H^+$).

Compounds **4.12**-**4.14**: The compound **4.9** (0.06 g, 0.2 mmol) was mixed with RCOX (for **4.12**, **4.13**; R = CH_3, Ph and X = Cl respectively, whereas for **4.14**; R = $BrCH_2CO$- and X = Br) and triethylamine (0.4 mL) in dry dichloromethane. The mixture was stirred overnight at room temperature. On adding 40 mL water to the reaction mixture, the solid products in pure form were obtained in quantitative yield.

Compound **4.12**: IR (KBr, cm^{-1}): 3302 (s), 2923 (s), 2852 (m), 1702 (s), 1662 (s), 1597 (m). ^{1}HNMR (400 MHz, DMSO-d^6): 10.26 (s, 1H), 8.9 (s, 1H), 8.72 (d, 2H, *J* = 8 Hz), 8.54 (d, 1H, *J* = 8.4 Hz), 8.38 (d, 1H, *J* = 8.4 Hz), 7.94 (m, 2H), 7.8 (d, 1H, *J* = 8.8 Hz), 7.64 (d, 1H, *J* = 8.4 Hz), 2.1 (d, 3H, *J* = 8.6 Hz). ^{13}C NMR (DMSO-d^6): 168.36, 159.80, 149.87, 143.65, 139.15, 137.20, 135.48, 132.10, 131.67, 131.13, 127.40, 127.08, 126.67, 122.54, 119.92, 117.46, 116.94, 114.97, 109.60, 105.87, 24.09. ESI-MS: 328.124 ($M + H^+$).

Compound **4.13**: IR (KBr, cm^{-1}): 3301 (m), 3071 (m), 1703 (s), 1601 (m), 1699 (s). ^{1}HNMR (400 MHz, DMSO-d^6) 10.57 (s, 1H), 8.7 (d, 1H, *J* = 3.6Hz), 8.52 (d, 1H, *J* = 7.6 Hz), 8.36 (d, 1H, *J* = 7.2 Hz), 8.15 (d,1H, *J* = 4.8 Hz), 8.04 (d, 1H, *J* = 4.8 Hz), 7.94 (d, 2H, *J* = 4.8 Hz), 7.9 (s, 1H), 7.83 (d, 1H, *J* = 7.2, Hz), 7.63 (d, 2H, *J* = 4.8 Hz), 7.57 (s, 1H), 7.51(d, 2H, *J* = 4.8 Hz). ^{13}C NMR (DMSO-d^6): 165.47, 159.95, 148.63, 139.49, 136.70, 135.34, 134.95, 131.68, 131.43, 130.97, 129.26, 128.38, 127.77, 127.28, 126.95, 126.08, 122.52, 119.99, 119.24, 118.73, 114.96, 111.11, 107.21. IR (KBr, cm^{-1}): 3301 (m), 3071 (m), 1703 (s), 1601 (m), 1699 (s). ESI-MS: 390.122 ($M + H^+$).

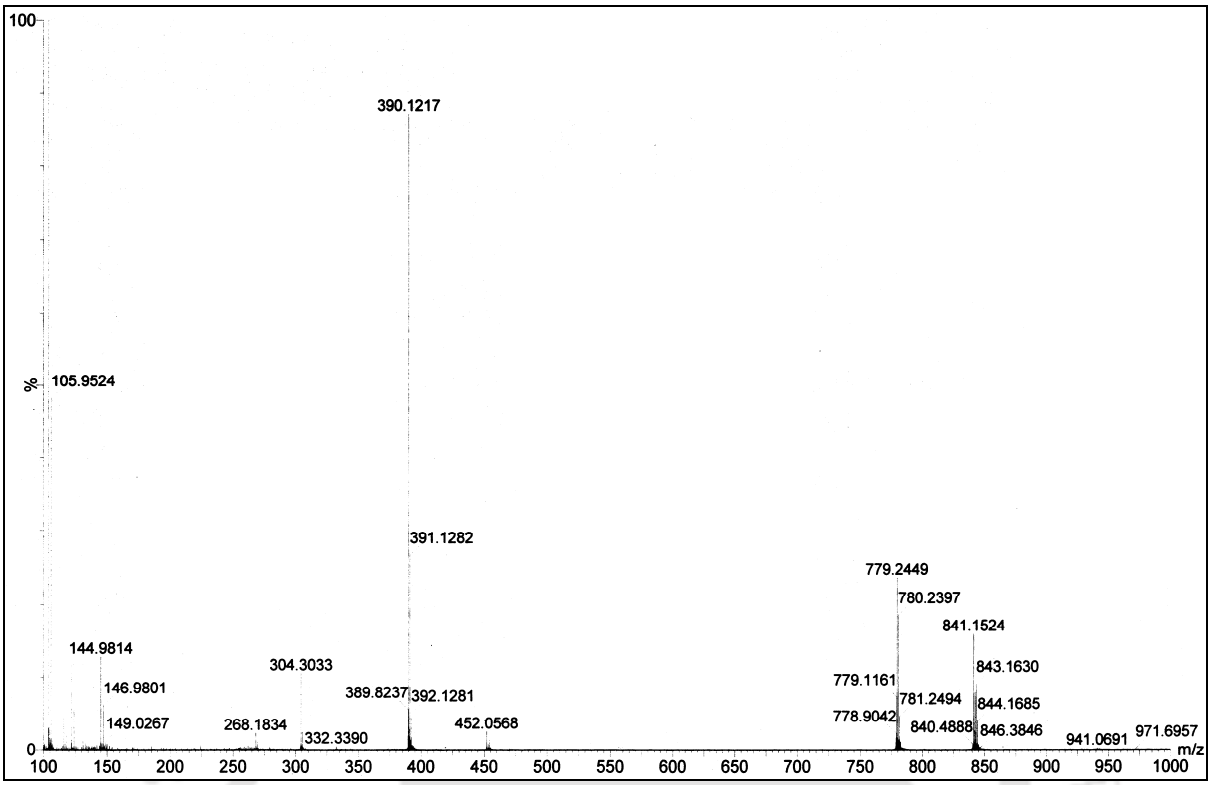

Figure 4.17: Mass spectra of compound **4.13**.

Compound **4.14**: IR (KBr, cm^{-1}): 3253 (s), 2959 (s), 1698 (m), 1654 (s), 1737 (s), 1591 (m), 1233 (m). ^{1}HNMR (400 MHz, DMSO-d^{6}): 10.72 (s, 1H), 8.9 (s, 1H), 8.7 (d, 2H, *J* = 8 .4 Hz), 8.53 (d, 1H, *J* = 8.4 Hz), 8.37 (d, 1H, *J* = 8.4 Hz), 7.9 (m, 2H), 7.8 (m, 1H), 7.65 (d, 1H, *J* = 8.4 Hz), 4.1 (s, 2H). ^{13}C NMR (DMSO-d^{6}): 170.89, 159.96, 148.54, 136.49, 136.13, 135.50, 132.39, 131.80, 131.26, 127.37, 127.09, 126.24, 122.52, 119.80, 119.47, 119.20, 118.25, 117.58, 106.51, 62.02. ESI-MS: 405.984 and 407.983 ($M + H^{+}$).

Compounds **4.15**-**4.18**: The compounds **4.15**-**4.18** were synthesized from compound **4.10** by identical procedures that are described for compounds **4.11**-**4.14**, respectively.

Compound **4.15:** Yield: 28%; IR (KBr, cm^{-1}): 3445 (s), 2924 (m), 2852 (w), 2357 (w), 1622 (s), 1430 (m), 1327 (s), 1231 (m), 1159 (w), 927 (w), 842 (w), 763 (m). ^{1}HNMR (400 MHz, $CDCl_3$): 8.53 (m, 4H), 8.43 (d, 1H, *J* = 6.4 Hz), 8.39 (d, 1H, *J* = 2.8 Hz), 8.32 (d, 1H, *J* = 2.8 Hz), 8.00 (d, 1H, *J* = 8.0 Hz), 7.85 (m, 4H), 7.62 (m, 2H), 7.45 (m, 4H), 7.21 (d, 1H, *J* = 2.4 Hz), 7.10 (d, 1H, *J* = 2.4 Hz), 3.07 (d, 6H, *J* = 6.8 Hz). ESI-MS: 300.108 ($M + H^{+}$).

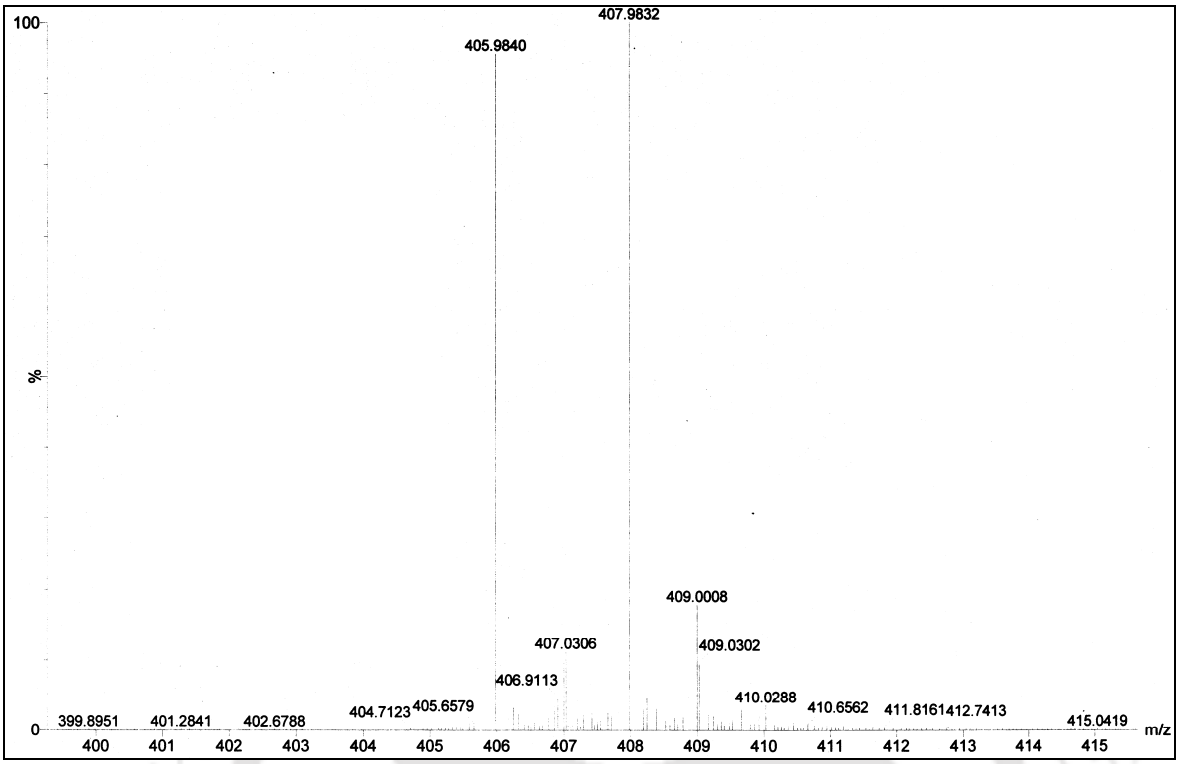

Figure 4.18: Mass spectra of compound **4.14**.

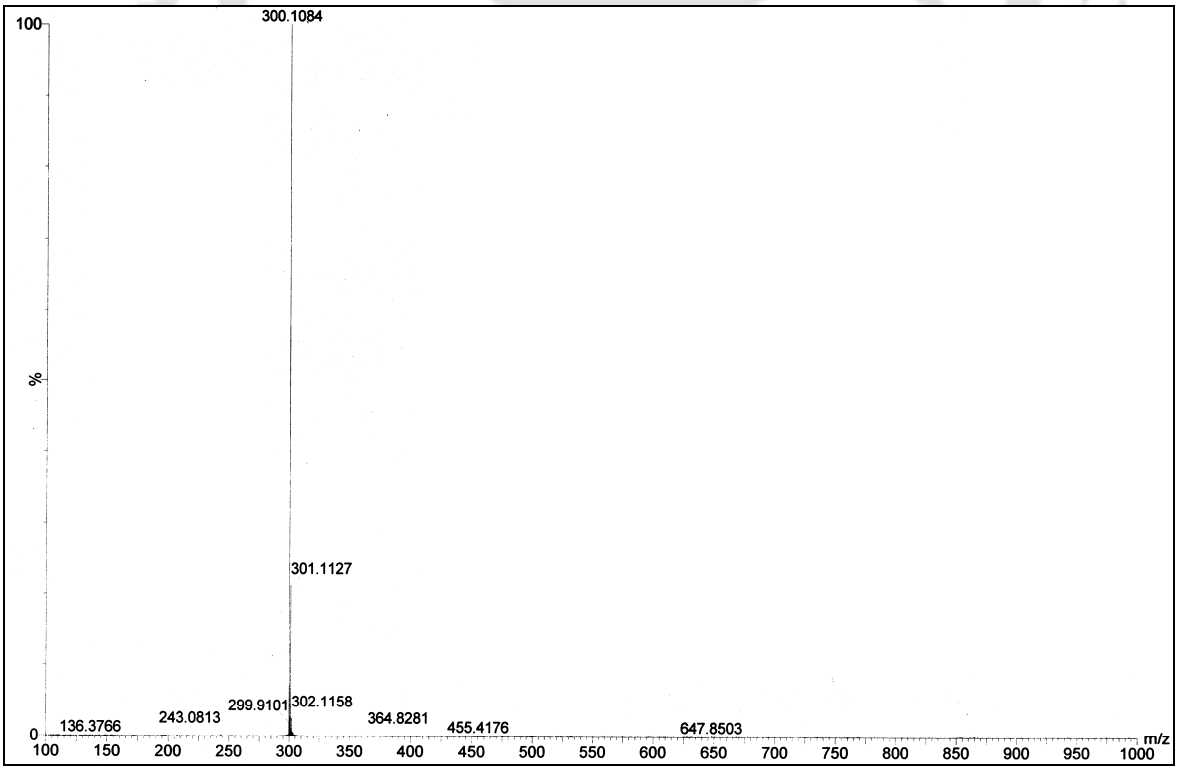

Figure 4.19: Mass spectra of compound **4.15**.

Compound **4.16**: Yield: 82%; IR (KBr, cm^{-1}): 3433(s), 2983(m), 2738(w), 2678(w), 1657s 1558(m), 1347(m), 1262(m), 1161(w), 1035(m), 878(w), 767(m). ^{1}HNMR (400 MHz, $CDCl_3$): 9.92 (s, 1H), 9.85 (s, 1H), 8.43 (s, 1H), 8.28 (d, 2H, *J* = 4.0 Hz), 8.26 (s, 1H), 8.15 (d, 1H, *J* = 4.0 Hz), 8.08 (d, 1H, *J* = 7.2 Hz), 8.00 (t, 2H, *J* = 5.6 Hz), 7.73 (d, 1H, *J* = 8.4 Hz), 7.60 (d, 1H, *J* = 7.2 Hz), 7.34 (m, 2H), 7.28 (t, 2H, *J* = 8.0 Hz), 6.98 (dd, 4H, *J* = 3.6 Hz), 2.08 (s, 4H). ^{13}C NMR (DMSO-d^6): 169.07, 159.96, 148.61, 143.17, 138.27, 134.72, 132.42, 131.31, 129.19, 127.24, 125.37, 124.98, 122.78, 122.18, 120.17, 119.68, 119.45, 118.42, 115.11, 45.31. ESI-MS: 328.122 ($M + H^+$).

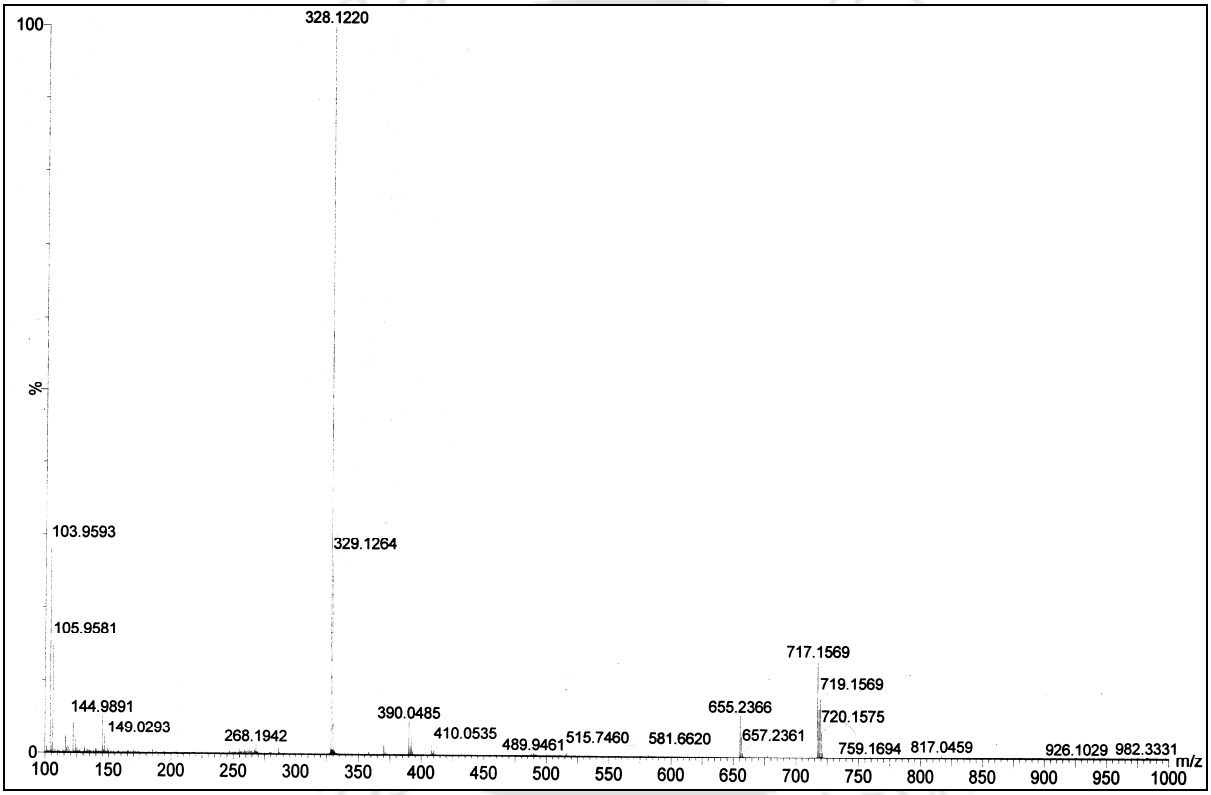

Figure 4.20: Mass spectra of compound **4.16**.

Compound **4.17**: Yield: 84%; IR (KBr, cm^{-1}): 3394 (s), 3054 (w), 2923 (w), 1788 (m), 1705 (s), 1657(m), 1543 (s), 1351 (m), 1243 (s), 1174 (m), 1040 (m), 877 (w), 750 (w), 705 (m). ^{1}HNMR (400 MHz, $CDCl_3$): 10.24 (s, 1H), 10.18 (s, 1H), 8.72 (s, 1H), 8.58 (s, 1H), 8.22 (d, 1H, *J* = 7.2 Hz), 8.10 (dd, 2H, *J* = 3.6 Hz), 7.87 (d, 1H, *J* = 8.4 Hz), 7.70 (t, 4H, *J* = 8.0 Hz), 7.59 (d, 4H, *J* = 6.4 Hz), 7.40 (dd, 2H, *J* = 6.0 Hz), 7.31 (t, 2H, *J* = 7.6 Hz), 7.15 (m, 5H), 7.04 (m, 5H). ^{13}C NMR (DMSO-d^6): 168.19, 166.55, 163.12, 143.54, 138.25, 135.79, 134.58, 133.59, 132.59,

131.50, 131.06, 130.84, 129.91, 129.81, 129.20, 128.39, 128.25, 125.59, 120.04, 115.04. ESI-MS: 390.107 ($M + H^+$).

Compound 4.18: Yield: 80%; IR (KBr, cm^{-1}): 3437 (s), 3274 (s), 1697 (s), 1673 (s), 1599 (m), 1552 m(), 1492 (w), 1431 (m), 1347 (m), 1050 (w), 868 (w), 766 (m), 677 (w). ^{1}HNMR (400 MHz, $CDCl_3$): 10.44 (s, 1H), 10.38 (s, 1H), 8.46 (s, 1H), 8.37 (s, 1H), 8.31 (s, 2H), 8.22 (d, 1H, *J* = 7.6 Hz), 8.16 (d, 1H, *J* = 7.2 Hz), 8.03 (t, 1H, *J* = 6.8 Hz), 7.79 (d, 1H, *J* = 8.4 Hz), 7.66 (d, 1H, *J* = 8.0 Hz), 7.35 (m, 3H), 7.14 (m, 2H), 7.05 (dd, 4H, *J* = 3.2 Hz), 3.64 (s, 4H). ^{13}C NMR (DMSO-d^6): 172.39, 160.47, 149.38, 143.77, 138.21, 135.57, 133.05, 132.03, 130.23, 128.05, 126.15, 125.76, 123.81, 123.01, 120.82, 120.21, 119.89, 115.86, 62.67. ESI-MS: 405.978 and 407.975 ($M + H^+$).

References:

(1) (a) Esch, J. V.; Feyter, S. D.; Kellogg, R. M.; Schryver, F. D.; Feringa, B. L. *Chem.-Eur. J.* **1997**, *3*, 1238. (b) Esch, J. V.; Schoonbeek, F.; Loos, M. D.; Kooijman, H.; Spek, A. L. Kellogg, R. M.; Feringa, B. L. *Chem.-Eur. J.* **1999**, *5*, 937. (c) Hanabusa, K.; Yamada, M.; Kimura, M.; Shirai, H. *Chem. Mater.* **1999**, *11*, 649. (d) Ryu, S. Y.; Kim, S.; Seo, J.; Kim, Y. W.; Kwon, O. H.; Jang, D. J.; Park, S. Y. *Chem. Commun.* **2004**, 70. (e) Bommel, K. J. C. V.; Pol, C. V. D.; Muizebelt, I.; Friggeri, A.; Heeres, A.; Meetsma, A.; Feringa, B. L.; Esch, J. V. *Angew. Chem., Int. Ed.,* **2004**, *43*, 1663. (f) Beginn, U.; Tartsch, B. *Chem. Commun.* **2001**, 1924. (g) Boileau, S.; Bouteiller, L.; Laupretre, F.; Lortie, F. *New J. Chem.* **2000**, *24*, 845.

(2) (*a*) Terech, P.; Weiss, R. G. *Chem. Rev.*, **1997**, *97*, 3133. (*b*) Esch, J. H. V.; Feringa, B. L. *Angew. Chem., Int. Ed.* **2000**, *112*, 2351.

(3) Rees, G. D.; Robinson, B. H. *Adv. Mater.* **1993**, *5*, 608.

(4) Haering, G.; Luisi, P. L. *J. Phys. Chem.* **1986**, *90*, 5892.

(5) Hafkamp, R. J. H.; Kokke, P. A.; Danke, I. M. *J. Chem. Soc., Chem. Commun.* **1997**, *6*, 545.

(6) Liaw, D.-J.; Hsu, P.-N.; Chen, J.-J.; Liaw, B.-Y.; Hwang, C.-Y. *J. Polym. Sci., Part A: Polym. Chem.* **2001**, *39*, 1557.

(7) Yamasaki, S.; Tsutsumi, H. *Bull. Chem. Soc. Jpn.* **1994**, *67*, 906.

(8) Lin, Y.-C.; Weiss, R. G. *Macromolecules* **1987**, *20*, 414.

(9) Hanabusa, K.; Tanaka, R.; Suzuki, M.; Kimura, M.; Shirai, H. *Adv. Mater.* **1997**, *9*, 1095.

(10) Hanabusa, K.; Yamada, M.; Kimura, M.; Shirai, H. *Angew. Chem., Int. Ed.* **1996**, *35*, 1949.

(11) Simic, V.; Bouteiller, L.; Jalabert, M. *J. Am. Chem. Soc.* **2003**, *125*, 13148.

(12) (a) Hafkamp, R. J. H.; Feiters, M. C.; Nolte, R. J. M. *J. Org. Chem.* **1999**, *64*, 412. (b) Yabuuchi, K.; Rowan, A. E.; Nolte, R. J. M.; Kato, T. *Chem. Mater.* **2000**, *12*, 440.

(13) (a) Sugiyasu, K.; Fujita N.; Shinkai, S. *Angew. Chem., Int. Ed.,* **2004**, *43*, 1229. (b) Würthner, F.; Hanke, B.; Lysetska, M.; Lambright G.; Harms, G. S. *Org. Letters* **2005**, *7*, 967. (c) Li, X-Q.; Stepanenko, V.; Chen, Z.; Prins, P.; Siebbeles, L. D. A.; Würthner, F. *Chem. Commun.* **2006**, 3871.

(14) Adarsh, N. N.; Krishna Kumar, D.; Dastidar, P. *Tetrahedron* **2007**, *63*, 7386.

(15) Müller, W. M.; Müller, U.; Mieden-Gundert, G.; Vögtle, F.; Lescanne, M.; Heuzè, K.; D'Alèo, A.; Fages, F. *Eur. J. Org. Chem.* **2002**, 2891.

(16) (a) Krishna Kumar, D.; Jose, D. A.; Dastidar P.; Das, A. *Langmuir* **2004**, *20*, 10413. (b) Ballabh, A.; Trivedi, D. R.; Dastidar, P. *Chem. Mater.* **2003**, *15*, 2136. (c) Trivedi, D. R.; Ballabh, A.; Dastidar, P.; Ganguly, B. *Chem.-Eur. J.* **2004**, *10*, 5311. (d) Dastidar, P.; Okabe, S.; Nakano, K.; Iida, K.; Miyata, M; Tohnai, N.; Shibayama, M. *Chem. Mater.* **2005**, *17*, 741.

(e) Luboradzki, R.; Gronwald, O.; Ikeda, M.; Shinkai, S.; Reinhoudt, D. N. *Tetrahedron* **2000**, *56*, 9595. (b) Tamaru, S.-I.; Luboradzki, R.; Shinkai, S. *Chem. Lett.* **2001**, 336.

(17) Kumar, D. K.; Jose, D. A.; Das, A.; Dastidar, P. *Chem. Commun.* **2005**, 4059.

(18) (a) Zhang, Y.; Gu, H.; Yang, Z.; Xu, B. *J. Am. Chem. Soc.* **2003**, *125*, 13680. (b) Yang, Z.; Gu, H.; Zhang, Y.; Wang, L.; Xu, B. *Chem. Commun.* **2004**, 208. (c) Yang, Z.; Lianga, G.; Xu, B. *Chem. Commun.* **2006**, 738.

(19) (a) Kazuharu, N.; Wakida, M.; Suzuki, K.; Yamada, Y.; Asao, T. *PCT Int. Appl.,* **2000**; 129 pp. Coden: PIXXD2 WO 2000001672 A1 2000013. (b) Crains, A. J.; Perman, J. A.; Wojtas, L.; Kravstov, V. Ch.; Alkordi, M. H.; Eddaoudi, M.; Zaworotko, M. J. *J. Am. Chem. Soc.* **2008**, *130*, 1560 (c) Oelgemoller, M.; Haeuseler, A.; Schmittel, M.; Griesbeck, A. G.; Lex, J.; Inoue, Y. *J. Chem. Soc., Perkin Trans.* **2002**, 676. (d) Diakoumakos, C. D.; Mikroyanniidis, J. A. *Polymer* **1994**, *35*, 1986.

(20) (a) Kolosov, D.; Adamovich, V.; Djurovich, P.; Mark, E.T.; Adachi, C. *J. Am. Chem. Soc.* **2002**, *124*, 9945. (b) Hoeben, J. M.; Jonkheijm, P.; Meijer, E.W.; Schenning, P.H.J. *Chem. Rev.* **2005**, *105*, 1491. (c) Callan, J.; deSilva, A.P.; Magri, D. *Tetrahedron* **2005**, *61*, 8551. (d) Zhu,

W.; Hu, C.; Chen, K.; He, J.; Songs, Q.; Hou, X. *J. Mater. Chem.* **2002**, *12*, 1262. (e) Guo, X.; Qian, X.; Jia, L. *Tetrahedron Lett.* **2004**, *45*, 113.

(21) (a) Tamuly, C.; Barooah, N.; Laskar, M.; Sarma, R. J.; Baruah, J. B. *Supramolecular Chem.* **2006**, *18*, 605. (b) Galunov, N. Z.; Krasovitskii, B. M.; Lyubenko, O. N.; Yermolenko, I. G.; Patsenker, I. D.; Doroshenko, A. O. *J. Lumin.* **2003**, *102*, 119. (c) Brana, M. F.; Ramos, A. *Curr. Med. Chem.* **2001**, *1*, 237.

(22) Law, K-Y. *Chem. Rev.* **1993**, *93*, 449.

(23) Langthals, H.; Jaschke, H. *Chem.-Eur. J.* **2006**, *12*, 2815.

(24) (a) Arient, J.; Marhan, J. *Collect. Czech. Chem. Commun*. **1963**, *28*, 1292. (b) Banerji, K. D.; Sen, K. K.; Mazumdar, A. K. D. *J. Ind. Chem. Soc*. **1976**, *53*, 1159.

(25) (a) Yang, C.; Wong, W. T.; Cui, Y.-D.; Chen, X.-M.; Yang, Y.-S. *Sci. China, Ser. B* **2003**, *46*, 331; (b) Yang, C.; Wong, W. T. *J. Mater. Chem.* **2001**, 2898.

(26) Singh, D.; Baruah, J. B. *Tetrahedron Lett.* **2008**, *49*, 4374.

(27) Pourjavadi, A.; Marandi, G.B. *J. Chem. Res.* **2001**, 485.

(28) Bhosale, S.; Jani, C.H.; Langford, S.J. *Chem. Soc. Rev.* **2008**, *37*, 331.

(29) Gunnalaugsson, T.; Kruger, P.D.; Jensen, P.; Pfeffer, F.M.; Hussey, G. M. *Tetrahedron Lett.* **2003**, *44*, 8909.

(30) Karmakar, A.; Baruah, J.B. *Supramolecular Chem.* **2008**, *20*, 667.

(31) Lakowicz, J. R. *Principles of Fluorescence Spectroscopy*, 2nd Ed. Kluwer Academic/ Plenum Publishers, New York, 1999, pp 52-53.

Chapter 5

Supramolecular aspects of transition metal complexes of cyclic imides tethered carboxylic acids

Design and synthesis of transition metal complexes with structural diversities have attracted considerable research interest as far as the dimensionality and topology of the species are concerned. The assemblies of metal-organic materials (MOMs) are not only governed by strong and highly directional metal-coordination bonds but also directed by various weak non covalent forces such as hydrogen bonding, π…π, C-H…π, and anion…π interactions,[1] especially, the less directional π…π interactions are widely explored to design superstructures with novel properties in the field of crystal engineering.[2] Among the different MOMs, metal carboxylates have attracted much attention because of the versatile coordination binding modes of carboxylate group along with hydrogen bond donor and acceptor properties in making complexes with various dimensionalities.[3] In the case of carboxylate ligands, benzene-1,3-dicarboxylic acid,[4] benzene-1,4-dicarboxylic acid,[5] and benzene-1,3,5-dicarboxylic acid[6] have been widely utilized. Metal carboxylates with flexible ligands have also been studied for the formation of coordination networks possessing permanent porosity and high thermal stability, which are useful for ionic exchange,[7] separation,[8] chemisorption,[9] gas storage,[10] catalysis,[11] magnetism,[12] optoelectronics,[13] and luminescence properties.[14] However, much work in this direction is required to have control over constructions of voids in a predictable manner.[15] Amino acids and its derivatives with flexible coordination modes have been explored in the generation of different coordination frameworks with potential application in material science and biology.[16] N-protected amino acids play significant role in biology as they are a part of some natural proteins and peptides.[17] We have discussed earlier the role of weak interactions in the formation of supramolecular networks of N-phthaloylglycinato and 4-carboxy-N-phthaloylglycinato complexes of transition metals.[18] Reger et al reported a series of Cu(II) carboxylate dimers with flexible carboxylate ligands derived from propionic acid and butanoic acid tethered by 1,8-naphthalimide unit.[19] The supramolecular networks in these dimers are sustained by strong π…π stacking interactions of

electron deficient naphthalimide units. We were also interested to elucidate the role of weak interactions in the construction of supramolecular architectures of metal complexes that can be built from bifunctional ligands bearing both the carboxylate donor group and different π-stacking aromatic imide units. For this purpose, we have chosen two bifunctional ligands (**L1H** and **L2H**, Scheme 5.1) in which carboxylate donor groups are separated from π-stacking aromatic imide tectons through flexible hydrophobic spacer and studied the structures of their supramolecular complexes upon incorporation of different metal centers. The assemblies of these metal-organic materials are governed partially or completely by supramolecular interactions.

This chapter deals with the syntheses, characterization, supramolecular structural features and photoluminescence properties of transition metal complexes of conformational flexible methyl cyclohexane carboxylic acids that are tethered by phthalimide (**L1H**) and naphthalimide (**L2H**) units.

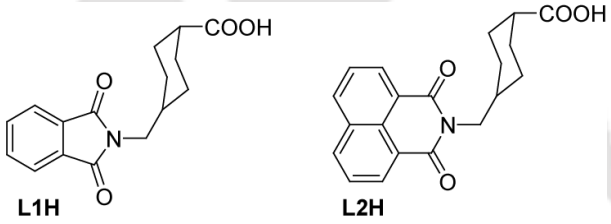

Scheme 5.1: Structures of organic ligands **L1H** and **L2H**.

L1H and **L2H** are synthesized by condensation reactions of trans-4-(aminomethyl)cyclohexanecarboxylic acid with corresponding anhydrides. These two bifunctional ligands that contained both the carboxylate donor groups and π-stacking aromatic imide unit, are incorporated into the construction of various transition metal complexes after deprotonation of acid group. A series of mononuclear metal carboxylates of L1 with Mn(II), Cu(II), Zn(II) and Cd(II) is prepared under solution state similar reaction conditions (Scheme 5.2). The carboxylate group of L1 coordinates to M(II) centers in monodentate coordination modes possessing 1:2 metal to ligand ratios in the square-pyramidal (for complex **5.2**) and octahedral geometries (for complex **5.1**, **5.3** and **5.4**) of complexes **5.1-5.4**. These complexes show identical infrared spectra with the absorption bands of asymmetric and symmetric vibrations of carboxyl groups of L1 respectively appearing at 1543-1576 and 1395-1398 cm^{-1} which confirms the monodentate coordination modes of L1 in each of the complexes.[20] In our

previous studies, we observed that the carboxylate groups of ligands N-phthaloylglycine and 4-carboxy-N-phthaloylglycine remained as monodentate carboxylates in their mononuclear transition M(II) complexes.[18] Moreover, a dinuclear Ag(I)[21] and a tetranuclear Sn(IV)[22] complexes of ligand N-phthaloylglycine are also reported in which the carboxylate groups of ligands coordinate to the metal centers in monodentate fashion.

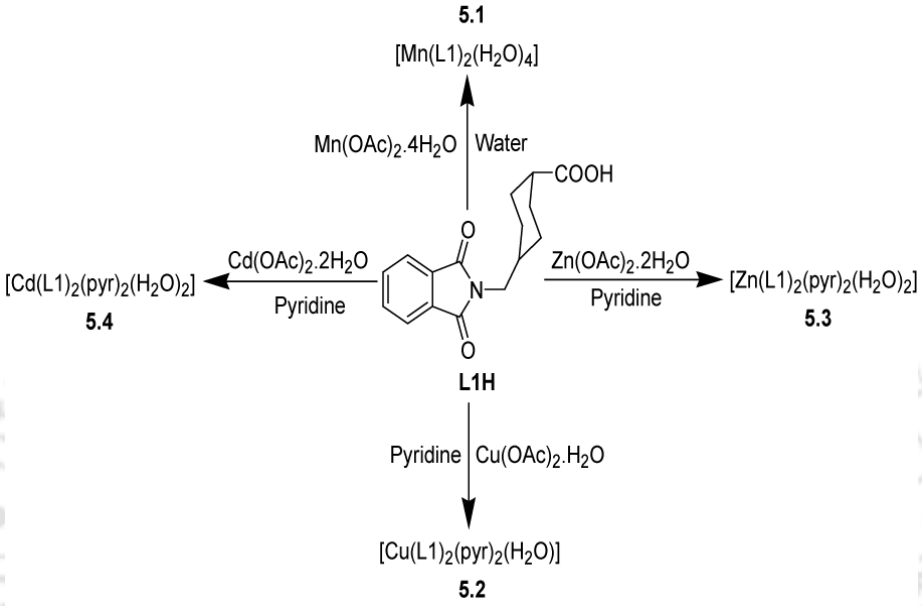

Scheme 5.2: Synthesis of mononuclear transition M(II) complexes of L1.

Single crystal X-ray analysis revealed that complex **5.1** having composition $[Mn(L1)_2(H_2O)_4]$ crystallizes in monoclinic $P2_1/c$ space group, possesses inversion centre and appears as its half in the crystallographic asymmetric unit. Octahedral geometry of six coordinated Mn(II) complex **5.1** is satisfied by two crystallographic equivalent oxygen atoms of two monodentate carboxylate groups of L1 (Mn1-O1 2.136(2) Å) and two pairs of crystallographic equivalent oxygen atoms of four water ligands (Mn1-O5 2.210(3) Å, Mn1-O6 2.202(3) Å). The free oxygen atom of carboxylate group of L1 is involved in intermolecular bifurcated acceptor hydrogen bonding with one of the coordinated waters and cyclohexyl ring via O-H···O (O5-H5A···O2; $d_{D\cdots A}$ 2.70, <D-H···A 160.00) and C-H···O (C2-H2···O2; $d_{D\cdots A}$ 3.59, <D-H···A 160.44) interactions, respectively (Figure 5.1a). The coordinated oxygen atom also form an acceptor O-H···O (O6-H6C···O1; $d_{D\cdots A}$ 2.82, <D-H···A 167.84) hydrogen bond with another coordinated water. Along with these interactions, one of the carbonyl oxygen atoms interacts with cyclohexyl ring via acceptor C-

H···O (C5-H5···O4; $d_{D...A}$ 3.29, <D-H···A 136.15) interaction, making a 1D layered structural arrangement. Another carbonyl oxygen also interact with phthalimide ring via acceptor C-H···O (C11-H11···O3; $d_{D...A}$ 3.34, <D-H···A 147.78) interaction which further induces C-H···π (dc_6…π 3.38) interactions between the methylene hydrogen atoms and phthalimide rings. Consequences of these later interactions grow the 1D layers to 2D sheet arrangements. Beside that, the phthalimide rings also interact to each other via C-H···π (dc_{11}…π 3.53) interactions which resulted in the construction of 3D zigzag supramolecular architecture of complex **5.1** as viewed along a axis (Figure 5.1b).

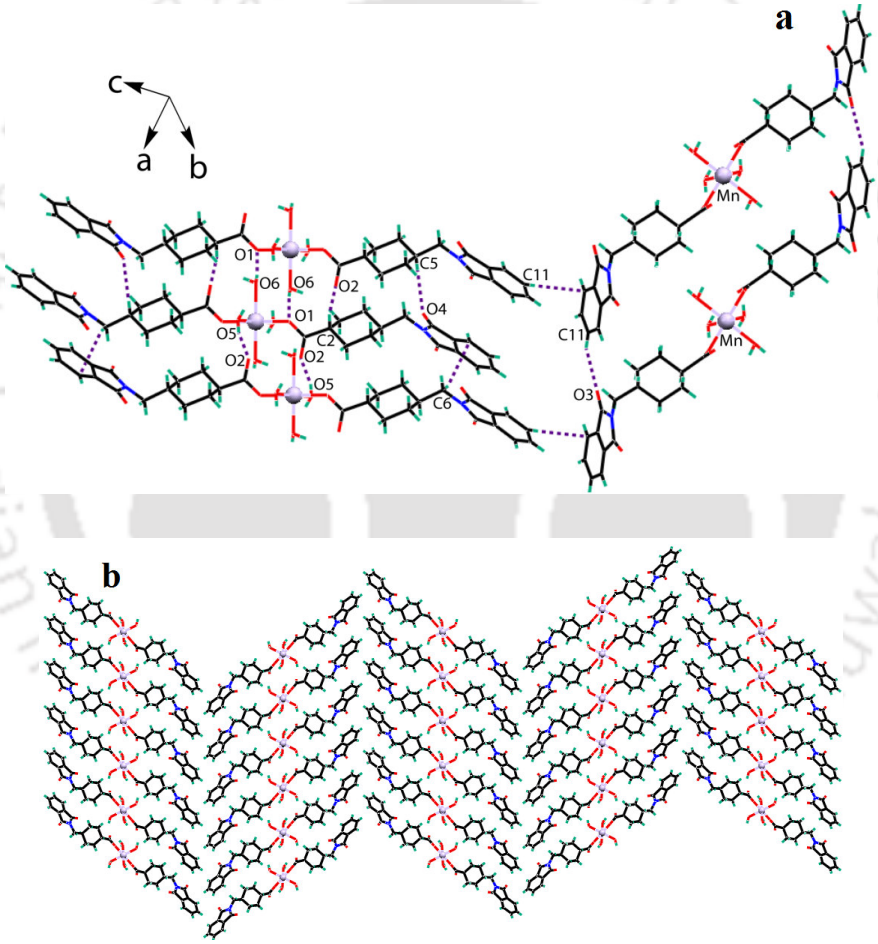

Figure 5.1: (a) A part of crystal structure of complex **5.1** showing weak interactions. (b) Formation of a 3D zigzag supramolecular architecture via intermolecular hydrogen bonding interactions.

In our previous report, we have shown the formation of β-pleated sheet structures in transition metal complexes of N- phthaloylglycylglycine dipeptide ligand that have similar compositions and coordination environments as observed in case of complex **5.1**.[23] Similar mononuclear M(II) complexes of 4-carboxy-N-phthaloylglycinato ligand are also reported earlier in which octahedral geometries around the M(II) centers are satisfied by two monodentate carboxylates and four aqua ligands.[18c] These complexes are found to be self assembled in the lattice through hydrogen bonding and C-H…π interactions.

The complex **5.2** having composition $[Cu(L1)_2(pyr)_2(H_2O)]$ is crystallized in monoclinic C2/c space group; possesses inversion centre and appears as its half in the crystallographic asymmetric unit. Square pyramidal geometry around the one Cu(II) center of five coordinated complex **5.2** is satisfied by two crystallographic equivalent oxygen atoms of two monodentate carboxylates groups of L1 (Cu1-O1 1.976(11) Å), two crystallographic equivalent nitrogen atoms of two pyridine ligands (Cu1-N2 2.029(16) Å) and one oxygen atom of water ligand (Cu1-O5 2.151(19) Å). The equatorial positions of square pyramidal geometry are occupied by two carboxylate groups and two pyridine ligands at trans disposition to each other, respectively, whereas the water ligand takes the axial position (Figure 5.2a). Free oxygen atom of coordinated carboxylate group of L1 remains involved in trifurcated acceptor hydrogen bonding with coordinated water, coordinated pyridine and with phthalimide ring via O-H···O (O5-H5A···O2; $d_{D\cdots A}$ 2.60, <D-H···A 170.34), C-H···O (C21-H21···O2; $d_{D\cdots A}$ 3.63, <D-H···A 172.20) and C-H···O (C11-H11···O2; $d_{D\cdots A}$ 3.47, <D-H···A 142.49) interactions, respectively. Simultaneously, carbonyl oxygen atom and coordinated pyridine hydrogen atom interact with phthalimide ring via O···π (do_4…π 3.16) and C-H···π (dc_{17}…π 3.68) interactions which create a 2D layered structural arrangement. The phthalimide rings of these 2D layers are further connected by strong π…π interactions; constructing a 3D supramolecular architecture containing channels among the 2D layers of architecture. The coordinated pyridine molecules takes position inside the channels as viewed along b axis (Figure 5.2b). The complex **5.2** can be compared to corresponding Cu(II) complex of N-phthaloylglycine ligand where square pyramidal geometry around the metal centre is completed by two monodentate carboxylates and two pyridine ligands occupying the basal plane and another pyridine occupying the axial position of square pyramid.[18a] Crystal structure of this complex shows that the interplanar distance of separation between the phthalimide units of

N-phthaloylglycine ligand is 3.180 Å which indicates strong π-stacking among the aromatic imide units.

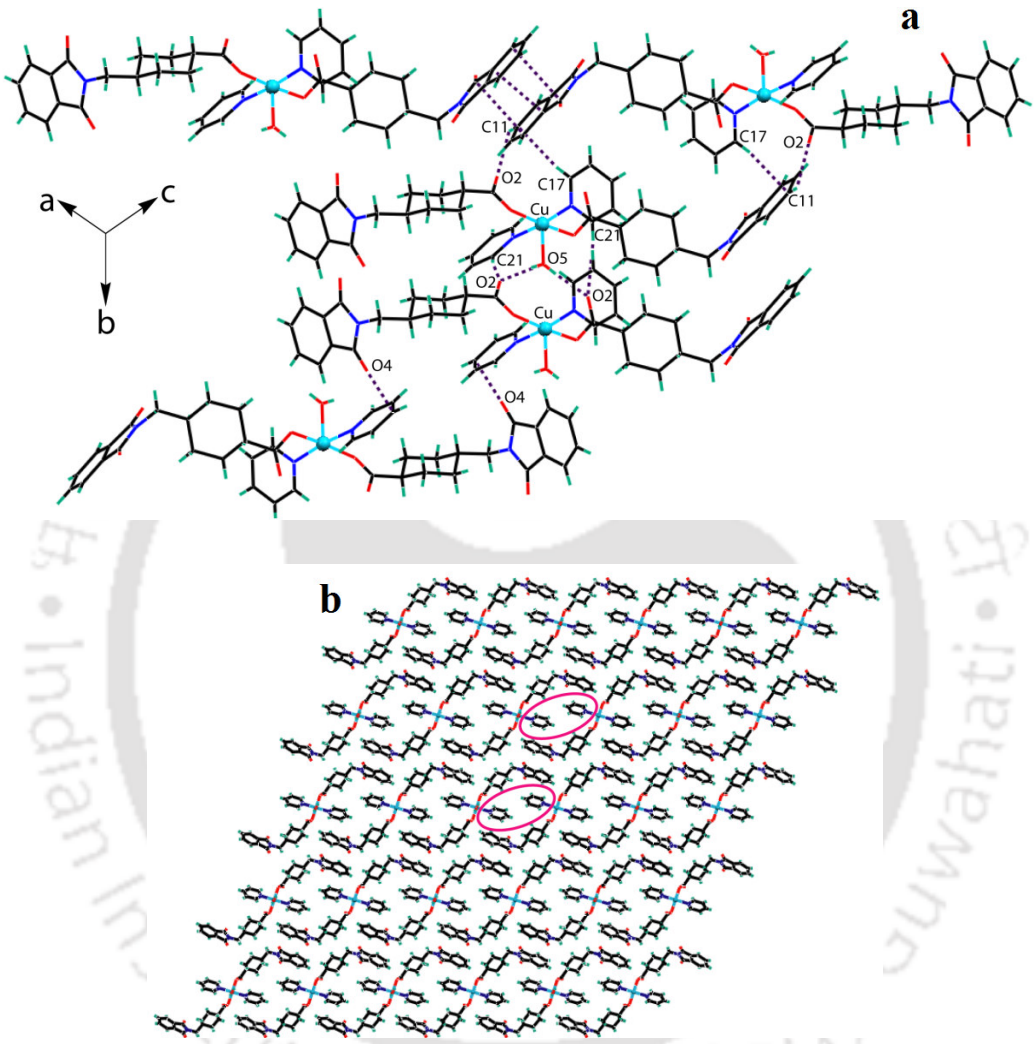

Figure 5.2: (a) Various weak interactions among the units of complex **5.2**. (b) 3D supramolecular channel network of complex **5.2** containing coordinated pyridine rings (shown by red circles) inside the channels (along b axis).

The complex **5.3** having composition $[Zn(L1)_2(pyr)_2(H_2O)_2]$ is crystallized in triclinic P-1 space group; also possesses inversion centre and appears as its half in the crystallographic asymmetric unit. The complex **5.3** has a near octahedral geometry around the Zn(II) metal centre with two monodentate carboxylate groups of crystallographic equivalent L1 (Zn1-O1 2.102(11) Å) and

two water ligands (Zn1-O5 2.103(12) Å) in trans orientation to each other, respectively, occupying the equatorial positions. The remaining two crystallographic equivalents pyridine ligands (Zn1-N2 2.267(15) Å) occupy the axial positions in the octahedral geometry (Figure 5.3a). In the crystal lattice of **5.3**, both the oxygen atoms of coordinated carboxylate group take part in intermolecular hydrogen bonding interactions. Free oxygen of the carboxylate group forms bifurcated acceptor hydrogen bond with cyclohexyl ring via two C-H···O (C2-H2···O2; $d_{D\cdots A}$ 3.45, <D-H···A 147.10 and C15-H15A···O2; $d_{D\cdots A}$ 3.53, <D-H···A 142.81) interactions whereas coordinated oxygen atom interacts with coordinated water through acceptor O-H···O (O5-H5B···O1; $d_{D\cdots A}$ 2.76, <D-H···A 170.63) interaction, making a 1D zigzag layered structure.

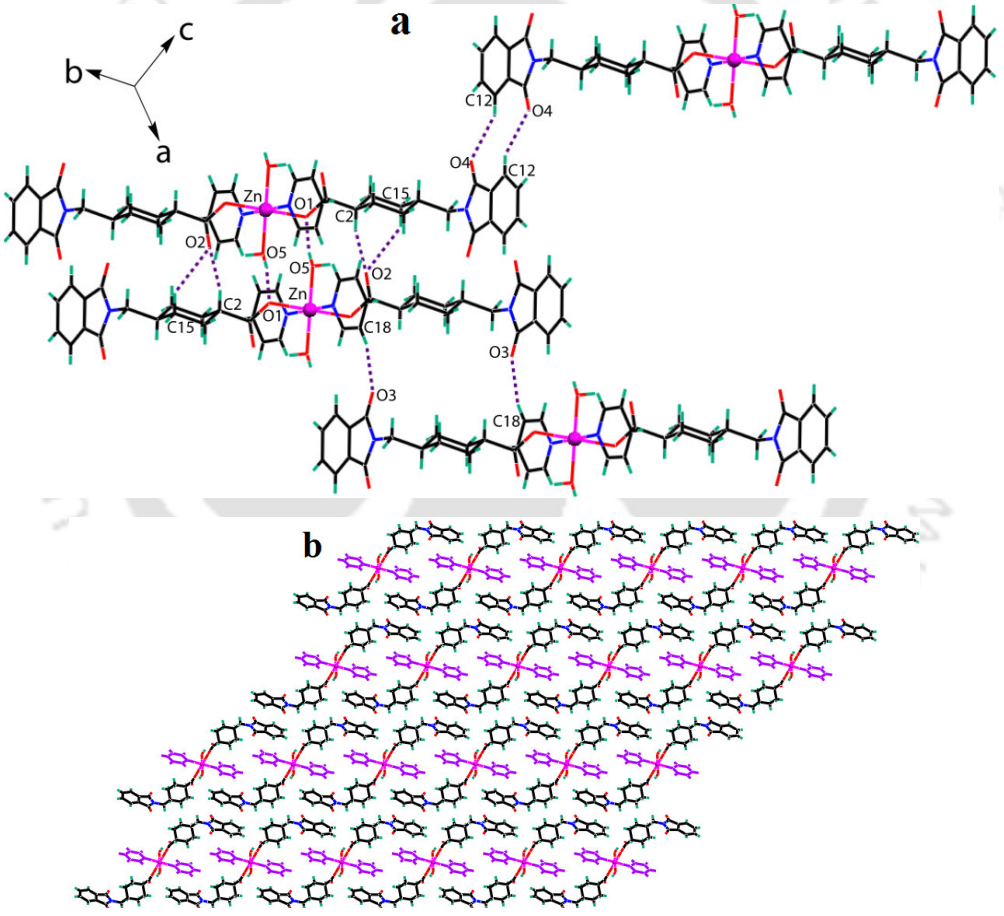

Figure 5.3: (a) Intermolecular interactions in a part of crystal structure of complex **5.3**. (b) Formation of 3D supramolecular channel network of complex **5.3** containing coordinated pyridine molecules (purple) inside the channels along a axis.

Further, both the carbonyl oxygen atoms of L1 interact with coordinated pyridine and aromatic phthalimide ring via C-H···O (C18-H18···O3; $d_{D\cdots A}$ 3.60, <D-H···A 165.37 and C12-H12···O4; $d_{D\cdots A}$ 3.39, <D-H···A 143.70) interactions, overall making a 3D supramolecular network creating channels in the lattice. Similar to the structure of **5.2**, the coordinated pyridine molecules are situated inside the channels as viewed along a axis (Figure 5.3b).

The complex **5.4** also crystallizes in triclinic P-1 space group. Structural features of **5.4** are similar to **5.3**, exhibiting some minor differences in intermolecular hydrogen bonding interactions (Figure 5.4). In contrast to the structure of **5.3**, the free oxygen atom of carboxylate group of L1 interact with cyclohexyl ring via only an acceptor C-H···O interaction (C2-H2···O2; $d_{D\cdots A}$ 3.51, <D-H···A 147.60) whereas coordinated oxygen atom engages in bifurcated acceptor hydrogen bond interacting with coordinated water and coordinated pyridine via two different O-H···O (O5-H5A···O1; $d_{D\cdots A}$ 2.72, <D-H···A 169.90) and C-H···O (C21-H21···O1; $d_{D\cdots A}$ 3.60, <D-H···A 175.70) interactions in the crystal lattice of **5.4**. Analogous mononuclear $[Co(L)_2(pyr)_2(H_2O)_2]$ and $[Ni(L')_2(pyr)_2(H_2O)_2]$ (where L = *o*-nitrobenzoic acid and L' = *p*-nitrobenzoic acid) complexes are reported. The coordinated water molecules are involved in strong hydrogen bonding with carboxyl groups of nitrobenzoates through O-H···O interactions in these complexes. Some other weak interactions such as C-H···O and π…π interactions are found to be responsible in the construction of 3D supramolecular networks.[24]

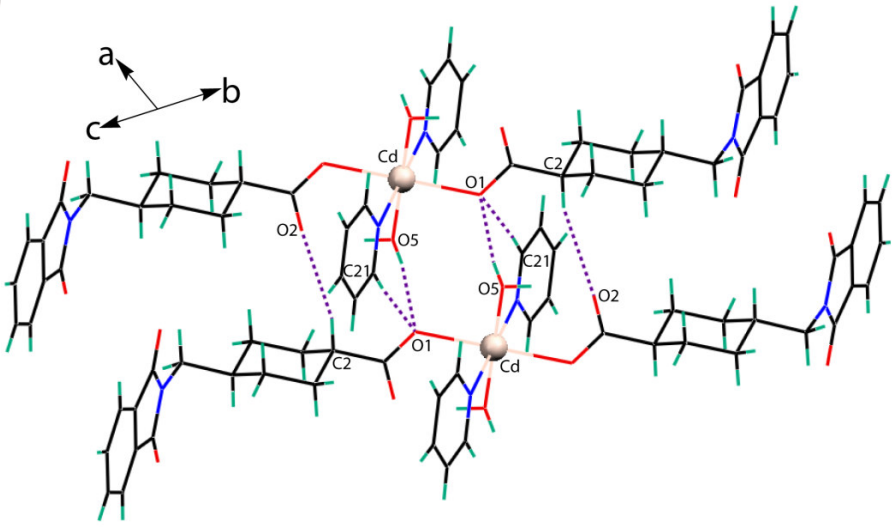

Figure 5.4: Intermolecular interactions in the structure of complex **5.4** showing some minor differences with the structure of complex **5.3**.

Three mononuclear transition metal complexes of conformationally flexible methyl cyclohexane carboxylic acid that is tethered by naphthalimide unit (**L2H**), are also synthesized under solution state similar reaction conditions. The reaction conditions used in the preparation of mononuclear Co(II), Cu(II) and Cd(II) complexes of L2 are summarized in Scheme 5.3. The M(II) to ligand (L2) ratios in all these complexes is 1:2 where carboxylate groups of L2 show monodentate (for complex **5.5** and **5.7**) and chelating coordination modes (for complex **5.6**) in the octahedral geometries of complexes **5.5-5.7**. The Infrared spectra of the complexes **5.5** and **5.7** are similar to each other showing the characteristic bands of carboxyl groups of L2 at 1588-1589 and 1438-1440 for the asymmetric and symmetric vibrations, respectively. Complex **5.6** exhibits the absorption bands of asymmetric and symmetric vibrations of carboxyl group at 1589 and 1490 cm^{-1}, respectively. These values suggest the monodentate coordination modes of L2 in complexes **5.5** and **5.7** whereas chelating coordination mode in complex **5.6**.[20] The four carboxylate groups from four separate ligands coordinate with two Cu(II) atoms in bridging coordination modes in earlier reported dimeric Cu(II) paddlewheel complexes of flexible N-(3-propanoic acid)-1,8-naphthalimide and N-(4-butanoic acid)-1,8-naphthalimide ligands.[19]

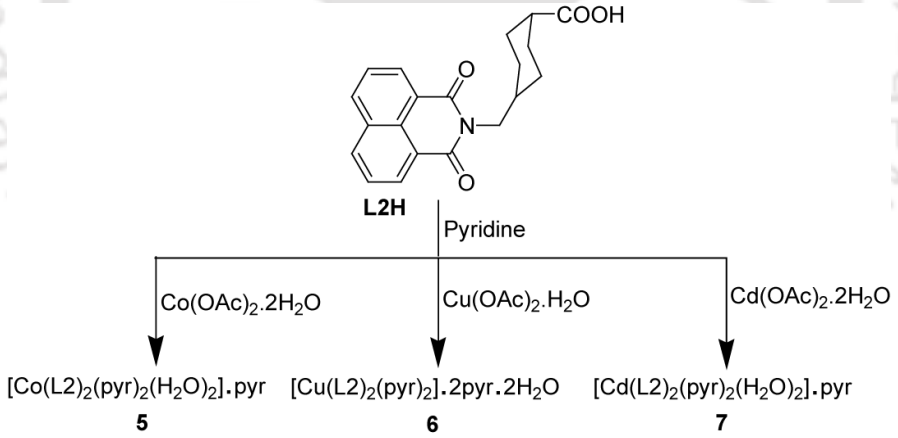

Scheme 5.3: Synthesis of mononuclear transition M(II) complexes of L2.

The complex **5.5** having composition $[Co(L2)_2(pyr)_2(H_2O)_2].pyr$ crystallizes in monoclinic $P2_1/c$ space group, also possesses inversion centre and appears as its half in the crystallographic asymmetric unit. The octahedral geometry of six coordinated complex **5.5** is satisfied by two crystallographic equivalent pyridine ligands (Co1-N2 2.228(6) Å) coordinated axially, along with two monodentate carboxylate groups of two crystallographic equivalent L2 (Co1-O2

2.095(4) Å) and two water ligands (Co1-O5 2.082(4) Å) coordinated equatorially (Figure 5.5a). Both the lattice and coordinated pyridine molecules are disordered in the crystal structure of complex **5.5**. Coordinated pyridine molecules are disposed in the lattice such that the two carbon atoms at each 2 and 3 position of pyridine ring are shared with half occupancies. The lattice pyridine molecule is also disordered across an inversion center sharing the nitrogen and carbon atoms at 1 and 4 position of pyridine ring with half occupancies. The Free oxygen atom of coordinated carboxylate group takes part in bifurcated acceptor hydrogen bonding with cyclohexyl ring via two C-H···O (C2-H2···O1; $d_{D\cdots A}$ 3.40, <D-H···A 148.52 and C19-H19A···O1; $d_{D\cdots A}$ 3.53, <D-H···A 141.53) interactions whereas the coordinated oxygen atom form an

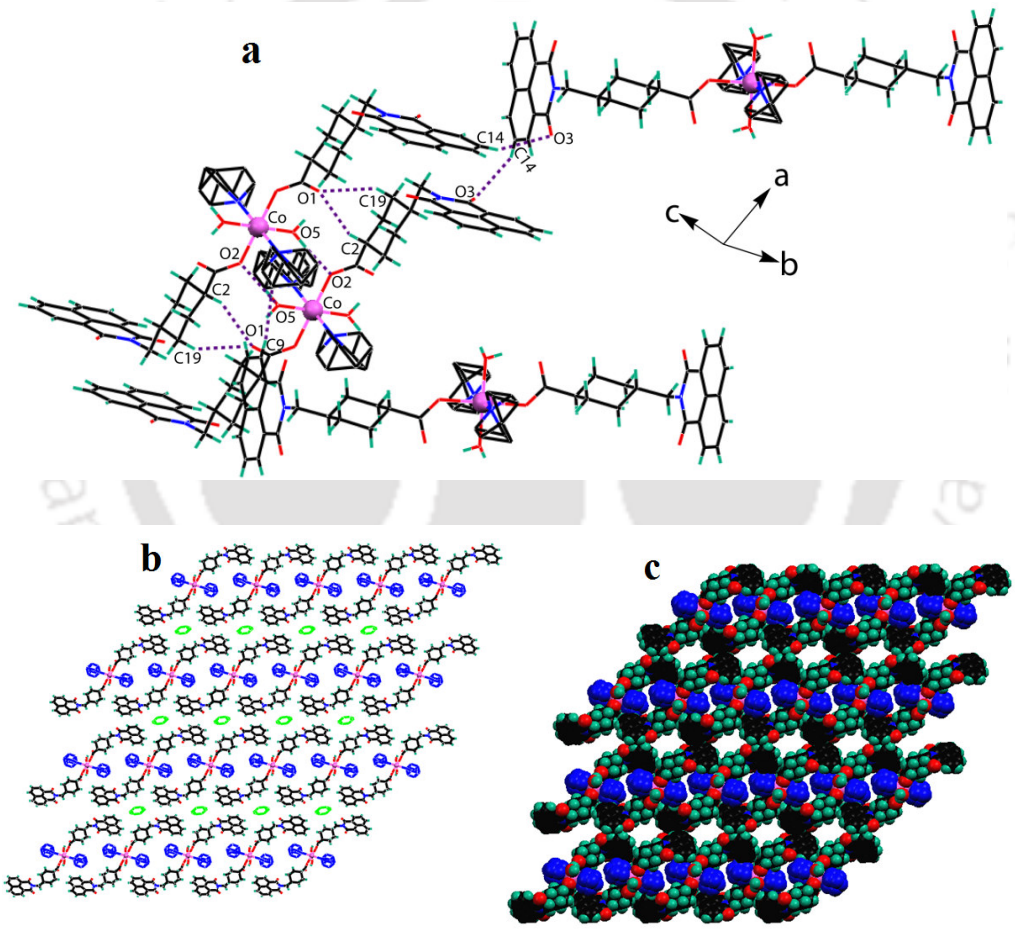

Figure 5.5: Weak intermolecular interactions in a part of the crystal structure of complex **5.5** (b) A 3D supramolecular architecture of **5.5** showing channels and voids containing coordinated and lattice pyridine molecules, respectively, along b axis. (c) Space filling model after removal of lattice pyridine molecules from the voids.

acceptor O-H···O (O5-H5B···O2; $d_{D\cdots A}$ 2.72, <D-H···A 174.88) hydrogen bond with coordinated water molecule. The 1D layer formed by these interactions further assemble in another dimension by C-H···π (dc_9…π 3.57) interactions experienced between the naphthalimide rings and coordinated pyridine molecules. This arrangement leads to the formation of channels in discrete 2D arrays of units of complex **5.5** in the lattice. Apart from that, naphthalimide rings also interact to each other via intermolecular C-H···O (C14-H14…O3; $d_{D\cdots A}$ 3.48, <D-H···A 151.66) interactions, further generating a 3D supramolecular network which is sustained by large solvent voids as viewed along b axis (Figure 5.5b). The voids created between the discrete 2D layers are filled by disordered lattice pyridine molecules. Since the Co(II) complex shows monodentate binding mode with the carboxylate group of L2, its coordination may be compared with the supramolecular construction that is made by analogous carboxy-phosphonate complex reported in the literature. We have found that coordinated water molecules are involved in tight packed structure in complex **5.5** and the voids are filled by lattice pyridine molecules in its 3D supramolecular network, whereas, the supramolecular assembly reported from carboxylate phosphate has interesting S-shape voids filled by water molecules.[25]

The complex **5.6** having composition $[Cu(L2)_2(pyr)_2].2pyr.2H_2O$ crystallizes in monoclinic $P2_1/c$ space group, also possesses inversion centre and appears as its half in the crystallographic asymmetric unit. The complex **5.6** has a distorted octahedral geometry around the Cu(II) metal centre with two trans chelating carboxylate groups of two crystallographic equivalent L2 ligands (Cu1-O1 1.951(3) Å, Cu1-O2 2.760(3) Å) at equatorial positions and two crystallographic equivalent pyridine ligands (Cu1-N2 2.002(3) Å) at axial positions (Figure 5.6a). One of the carbonyl oxygen atoms of L2 interacts with cyclohexyl ring via C-H···O (C2-H2···O4; $d_{D\cdots A}$ 3.34, <D-H···A 140.71) interaction whereas another carbonyl oxygen participate in bifurcated acceptor hydrogen bonding with cyclohexyl ring and lattice pyridine molecule via two C-H···O (C19-H19B···O3; $d_{D\cdots A}$ 3.60, <D-H···A 176.32 and C28-H28···O3; $d_{D\cdots A}$ 3.42, <D-H···A 146.03) interactions creating 2D helical chains of complex **5.6** in the crystal lattice. The lattice pyridine molecule further interacts with one of the hydrogen atoms of the lattice water molecule via donor O-H···N (O5-H5A···N5; $d_{D\cdots A}$ 2.87, <D-H···A 157.76) interaction. Another hydrogen atom of the lattice water molecule also encloses donor O-H···O (O5-H5B···O2; $d_{D\cdots A}$ 2.73, <D-H···A 110.64) hydrogen bond with one of the oxygen atoms of coordinated carboxylate group. The oxygen atom of this lattice water simultaneously engages in bifurcated acceptor hydrogen

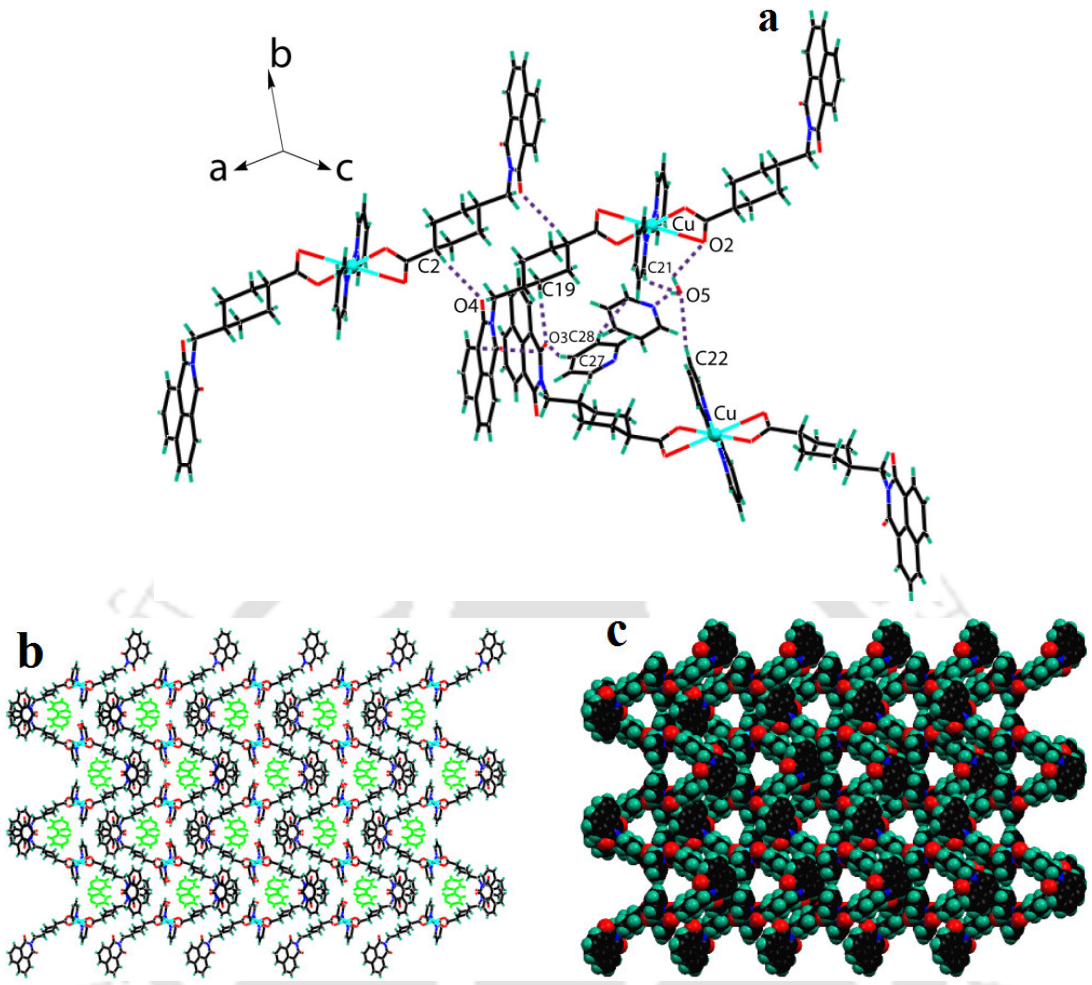

Figure 5.6: (a) A part of crystal structure of **5.6** showing weak interactions. (b) Formation of a 3D helical supramolecular network containing channels in the lattice along c axis. (c) Space filling model after removal of lattice water pyridine molecules inside the channels.

bonding with coordinated pyridine molecule via two C-H···O (C21-H21···O5; $d_{D\cdots A}$ 3.44, <D-H···A 140.33 and C28-H28···O3; $d_{D\cdots A}$ 3.52, <D-H···A 168.70) interactions. Consequence of these interactions emerges in the formation of 3D helical supramolecular network containing channels in the crystal lattice of **5.6** as viewed along c axis (Figure 5.6b). The channels created in the lattice are filled by lattice pyridine molecules which also interact to each other via C-H···π ($dc_{27}\ldots\pi$ 3.64) interactions in the lattice. The lattice water molecules remains packed in between the 2D helical chains of this supramolecular architecture. Crystal structure of 1:1 pyridine inclusion compound of dibenzotetraaza[14]annulene Cu(II) complexe is reported which revealed

a pleated-sheet like structural arrangement of host, with molecule of pyridine enclathrated within supramolecular cavities via weak aromatic edge to face C-H…π interactions.[26]

The complex **5.7** having composition $[Cd(L2)_2(pyr)_2(H_2O)_2].pyr$ crystallizes in triclinic P-1 space group, also possesses inversion centre and appears as its half in the crystallographic asymmetric unit. The structure of complex **5.7** is similar to the complex **5.5** having same coordination environment around the Cd(II) metal center (Cd1-N2 2.397(2) Å, Cd1-O1 2.289(16) Å, Cd1-O5 2.302(19) Å) as observed in complex **5.5** (Figure 5.7a). In the structure of **5.7**, guest pyridine molecule is also disordered across an inversion center as it is found in the

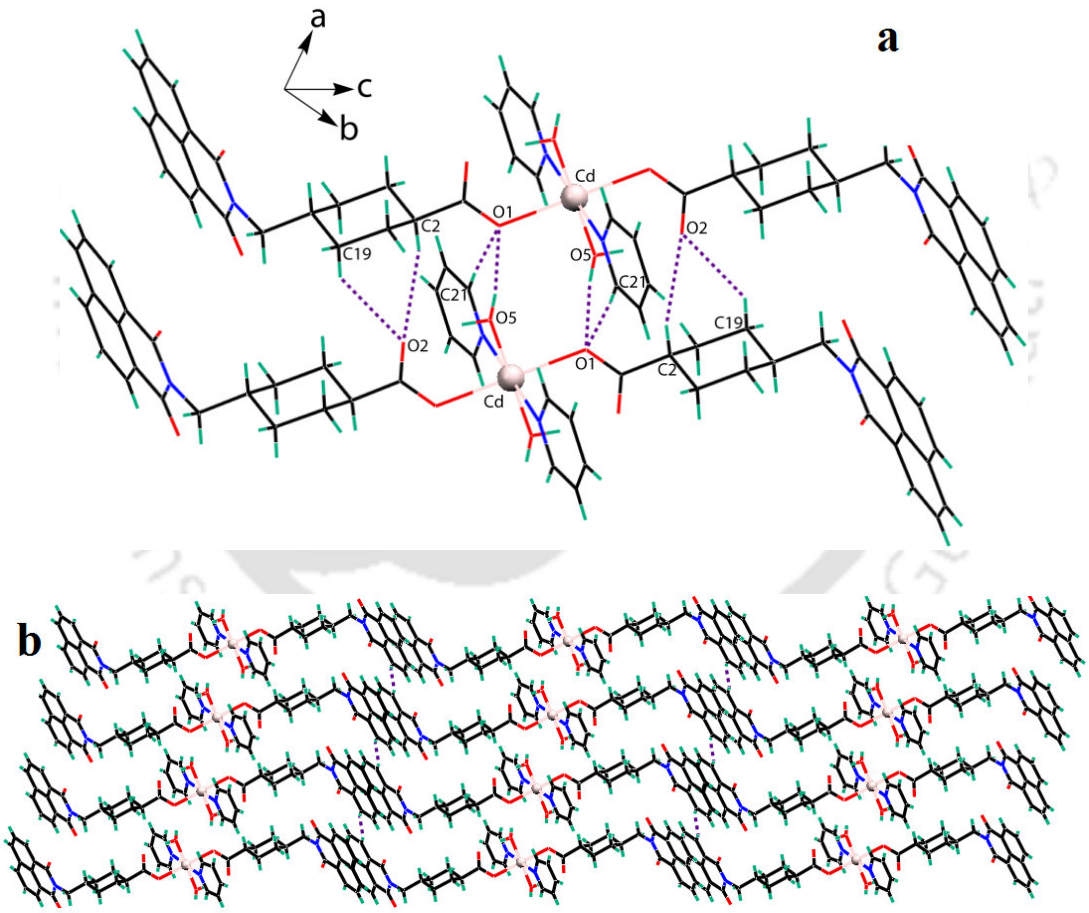

Figure 5.7: (a) Weak interactions in a part of crystal structure of complex **5.7**. (b) Formation of 2D supramolecular zigzag sheets where 1D supramolecular layers are sustained by H…H contacts.

case of complex **5.5** and does not show any weak interaction with host. The coordinated oxygen atom of carboxylate group contributes in bifurcate acceptor hydrogen bonding with coordinated water and coordinated pyridine molecule via O-H···O (O5-H5B···O2; $d_{D\cdots A}$ 2.73, <D-H···A 110.64) and C-H···O (C19-H19B···O3; $d_{D\cdots A}$ 3.60) interactions, respectively. The free oxygen atom of carboxylate group also participate in bifurcated hydrogen bonding with cyclohexyl ring via two C-H···O (C19-H19B···O3; $d_{D\cdots A}$ 3.60, <D-H···A 176.32 and C28-H28···O3; $d_{D\cdots A}$ 3.42, <D-H···A 146.03) interactions. These interactions make a stacked arrangement of units of complex **5.7** above each other and assemble the structure into an infinite 1D polymeric layered array. The naphthalimide rings in such 1D layers further interact with each other via short H···H contacts to generate 2D zigzag supramolecular sheet architecture in the crystal lattice of **5.7** as viewed along the b axis (Figure 5.7b).

PXRD patterns and Thermogravimetric analyses (TGAs) of the complexes: The PXRD patterns of complexes **5.1-5.7** are shown in Figure 5.12-5.18 in the Experimental Section. All of the peaks of the seven compounds can be indexed nearly to their respective simulated PXRD patterns, which indicate that each of the seven compounds is pure phase. The small deviations in some cases are attributed to loss of solvent molecules leading to loss of crystallinity. To examine the thermal stability of the seven complexes, thermogravimetric analyses (TGAs) were carried out (Figure 5.19-5.25). The samples were heated upto 500^0C under N_2 atmosphere. For the complex **5.1**, one step weight loss due to the four coordinated water molecules takes place in the temperature range 65-120^0C corresponding to a weight loss of 9.46% (calcd 10.2%).[18a] Decomposition of organic ligands began at 275^0C for complex **5.1** and ended at about 460^0C. TGA curve of complex **5.2** shows weight loss of coordinated water and pyridine molecules in two steps. In first step, 11.28% weight loss occurs, corresponding to one molecule of pyridine and one molecule of water between 80 and 125^0C (calcd 12.00%). In second step, 10.26% weight loss occurs from the residue of the first step for remaining coordinated pyridine molecule between 135 and 185^0C (calcd 11.1%). Further weight loss in the temperature range 285-400^0C is accounted for the decomposition of organic ligands. Complex **5.3** shows a gradual weight loss of 21.78% between 55 and 250^0C corresponding to the loss of the two coordinated water and two coordinated pyridine molecules (calcd 23.3 wt %). Decomposition of organic ligands for this complex occurs in the temperature range 315-450^0C. Similarly, TGA curve of Complex **5.4** also

shows a gradual weight loss of 20.33% between 65 and 275^{0}C corresponding to the loss of the two coordinated water and two coordinated pyridine molecules (calcd 22.0 wt %), followed by the degradation of organic ligands in the temperature range 330-470^{0}C. A large number of literature is available showing thermal analyses for coordinated water and pyridine molecules with different metal centers, however, loss of these molecules also dependent on the coordination environments and supramolecular interactions and temperature ranges vary from one complex to another. In complexes **5.1**-**5.4**, thermal properties can be correlated with literature data.[27]

In the case of complex **5.5**, the first weight loss of 8.0 wt% in the range of 95-170^{0}C corresponds to the loss of one lattice pyridine molecule (calcd 7.9 wt %). The second loss occurs in the range 220-330^{0}C corresponding to weight loss of 20.36% of the residue from the first step due to the loss of coordinated two water and two pyridine molecules (calc. 20.4%). The decomposition of coordinated organic ligands occurred at about 375^{0}C. The TGA curve of complex **5.6** shows a continuous weight loss of 25.58% between 115 and 250^{0}C corresponding to the loss of the two lattice water and two lattice pyridine molecules along with two coordinated pyridine molecules (calcd 25.8 wt %). Further weight loss in the temperature range 280-450^{0}C is attributed to the decomposition of organic ligands. For the complex **5.7**, the first step within the range 130-170^{0}C corresponds to a weight loss of 8.74% (calcd 7.9%) due to the loss of one lattice pyridine molecule, and the second step, 200-270^{0}C, is due to the loss of coordinated two water and two pyridine molecules (weight loss of 19.98% of the residue from the first step; calcd 21.0%). The organic framework of complex **5.7** starts to be decomposed when the temperature is higher than 370^{0}C. In the complex **5.7**, the first weight loss is assumed to be the loss of lattice pyridine molecule at relatively low temperature. The relatively high temperature for the loss of coordinated water or coordinated pyridine molecules implies that hydrogen bonding interactions occur in the crystal packing. Crystal structure analysis confirms clearly that both the coordinated water and coordinated pyridine molecules are involved in intermolecular O-H$\cdots$O and C-H$\cdots$O interactions, respectively, whereas, lattice pyridine molecule is not participated in any kind of interaction. A similar assumption can be made for complex **5.5** where coordinated water and coordinated pyridine molecules are engaged in intermolecular O-H$\cdots$O and C-H$\cdots\pi$ interactions, respectively, but, lattice pyridine molecule is not involved in hydrogen bond interactions. However, in the case of complex **5.6**, we could not predict the loss of lattice pyridine and coordinated pyridine molecules at two different temperature ranges. In contrast to the structures

of **5.5** and **5.7**, the structure of **5.6** revealed the fact that the lattice pyridine molecules are strongly hydrogen bonded with host molecule whereas coordinated pyridines are not engaged in intermolecular host-host interactions. The lattice water molecules are also tightly held with host molecule which is probably the reason of a gradual weight loss for all coordinated and lattice solvent molecules in a particular temperature range.

Photoluminescence properties of M(II) complexes: Metal carboxylates have been reported to have the ability to adjust the emission wavelength of organic materials through incorporation of metal centers, especially for the d^{10} metal centers.[28] So, it gives us an impetus to make an investigation on the luminescence properties of metal carboxylates in view of potential applications as photoactive materials. The photoluminescence properties of M(II) complexes **5.1-5.7** along with the free organic ligands **L1H** and **L2H** are studied in the solid state at room temperature.

The emission spectra of the free organic ligand **L1H** and its four metal complexes with Mn(II), Cu(II), Zn(II), and Cd(II), respectively, are shown in Figure 5.8.

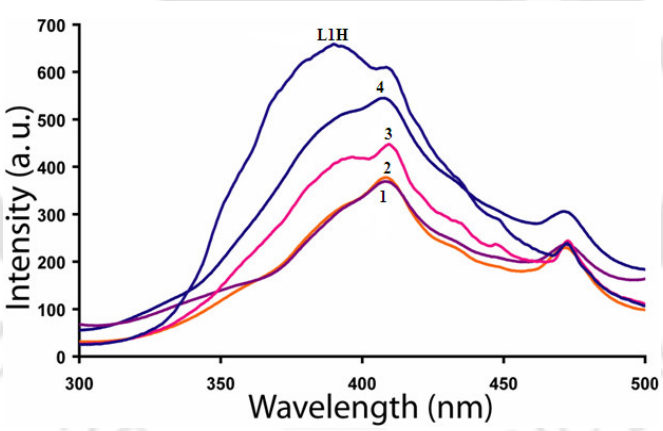

Figure 5.8. The solid state photoluminescence spectra of free organic ligand **L1H** and its four M(II) complexes (λ_{ex} = 280 nm) at room temperature.

Upon excitation at 280 nm, three photoluminescence emission bands at 390 nm, 410 nm, and 472 nm are observed for free organic ligand **L1H**. No significant differences are detected in the emission peaks of free ligand and its M(II) complexes except the intensities of emission peaks (λ_{ex} = 280 nm in each case). The emission peaks obtained for **L1H** and its different M(II) complexes may be attributed to the intraligand $\pi \rightarrow \pi^*$ transition.[29] However, it is found that the

relative intensities of the three peaks in the emission spectra of **L1H** and complexes **5.1-5.4** are different, which indicates that the intraligand transitions of **L1H** have been enhanced or weakened to different extents because of the introduction of different metal ions in these structures. The emission spectra of the free organic ligand **L2H** and its three metal complexes with Cu(II), Co(II) and Cd(II), respectively, are shown in Figure 5.9.

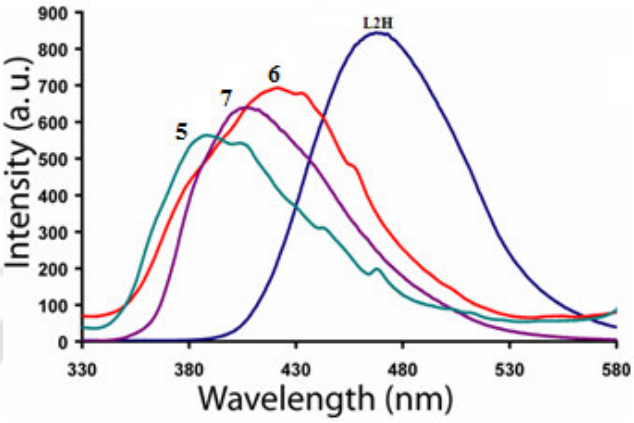

Figure 5.9. The solid state photoluminescence spectra of free organic ligand **L2H** and its three M(II) complexes (λ_{ex} = 310 nm) at room temperature.

L2H shows a strong photoluminescence emission band at 470 nm (λ_{ex} = 310 nm) which may be assigned as intraligand $\pi \rightarrow \pi^*$ transition.[29] The photoluminescence band in the emission spectra of complexes **5.5**, **5.6** and **5.7** are blue shifted as compared with that of free **L2H** and observed at 388 nm, 422 nm and 407 nm, respectively, which may be ascribed to the ligand-to-metal charge transfer (LMCT) transitions[30] (λ_{ex} = 310 nm in each case). The emission spectra of complexes **5.5**-**5.7** are also different from each other, which is probably due to the differences of M(II) centers and different coordination modes of ligands around them.

In conclusion, by using two conformational flexible bifunctional ligands that contained both the carboxylate donor group and π-stacking aromatic imide unit, we have prepared a series of metal-organic materials in which the building blocks are organized in supramolecular assemblies by various hydrogen bonds as well as C-H…π and π…π stacking interactions. In these complexes, the carboxylate groups of L1 and L2 are found to coordinate with M(II) centers in monodentate coordination modes, except the complex **5.6**, which consists of chelating carboxylate group of L2. Coordination environments around the metal centers and subtle differences in weak interactions affect the dimensionality and features of supramolecular architectures. It is observed

that both the highly directional covalent bonds and weak non-covalent forces play significant role to assemble these complexes in diverse supramolecular architectures. In the case of M(II) complexes of L1; **5.1** shows a zigzag 3D architecture whereas other complexes exhibit supramolecular 3D channels like structures containing the coordinated pyridine rings inside these channels. In the case of M(II) complexes of L2; coordination environments around the M(II) centers are same in the complexes **5.5** and **5.7**, however, former is composed of 3D architecture containing channels and voids of different dimensionality whereas later reveals 2D sheet structure. The 3D architecture of complex **5.6** is sustained by helical channels which are filled by lattice water and pyridine molecules. The solid state photoluminescence shows that the emission properties of M(II) complexes of L1 are due to the intraligand transitions whereas M(II) complexes of L2 demonstrate LMCT transitions in their emission spectra.

Experimental Section:

Detailed synthetic methodologies are given below. Analytical data as well as spectroscopic data are listed along with each compound. The instrumental details are given in Appendix.

Synthesis and characterization of compounds and their M(II) complexes:

Compound L1H: A solution of phthalic anhydride (0.740 g, 5 mmol) and trans-4-(aminomethyl)cyclohexanecarboxylic acid (0.785 g, 5 mmol) in acetic acid (20 mL) was refluxed for 3 hrs. The reaction mixture was cooled to room temperature, poured into ice cooled water (50 mL) and stirred for 15 min. A white colored crystalline product was obtained. This was filtered and dried in open air. Yield: 85%; IR (KBr, cm^{-1}): 3406 (w), 2915 (m), 2854 (m), 2528 (w), 1769 (w), 1712 (s), 1596 (s), 1538 (w), 1433 (m), 1399 (s), 1360 (m), 1331(m), 1304 (m), 1249 (m), 1223 (m), 1197 (s), 1158 (m), 1061 (m), 983 (w), 805 (m), 772 (m). ^{1}HNMR (400 MHz, $CDCl_3$): 7.82 (dd, 2H, *J* = 2.8Hz), 7.69 (dd, 2H, *J* = 3.2Hz), 3.52 (d, 2H, *J* = 6.8Hz), 2.24 (t, 1H, *J* = 12.0Hz), 2.00 (d, 2H, *J* = 10.8Hz), 1.78 (d, 3H, *J* = 6.8Hz), 1.37 (q, 2H, *J* = 8.4Hz), 1.07 (q, 2H, *J* = 10.4Hz). ^{13}C NMR ($CDCl_3$): 168.9, 150.4, 145.9, 134.1, 132.2, 123.4, 121.8, 43.9, 43.2, 36.6, 30.0, 28.5. ESI-MS: 288.156 [M + H^+].

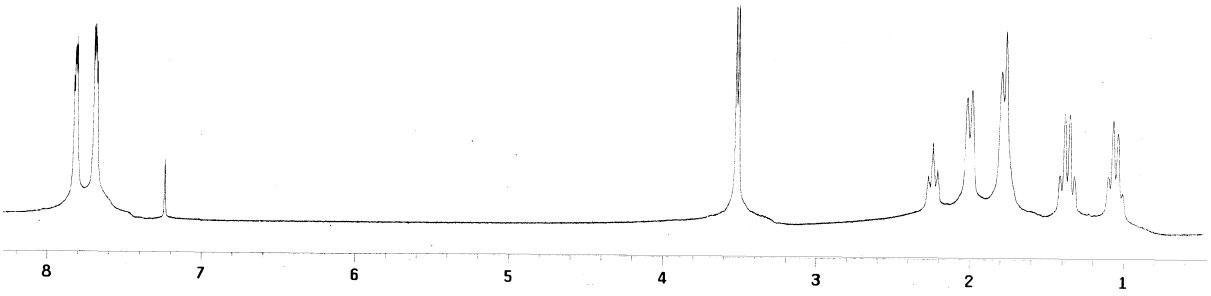

Figure 5.10: ^{1}HNMR spectra of compound **L1H**.

Compound L2H: A solution of 1,8-naphthalic anhydride (0.990 g, 5 mmol) and trans-4-(aminomethyl)cyclohexanecarboxylic acid (0.785 g, 5 mmol) in N,N-dimethylformamide (15 mL) was refluxed for 5 hrs. The reaction mixture was cooled to room temperature, poured into ice cooled water (30 mL) and stirred for 15 min. A brown colored precipitate of the product was formed, which was filtered and air dried. Yield: 82%; IR (KBr, cm^{-1}): 3501 (s), 2946 (s), 2855 (m), 1725 (s), 1695 (s), 1651 (s), 1590 (m), 1442 (w), 1389 (w), 1354 (m), 1316 (w), 1255 (m), 1237 (m), 1198 (m), 1176 (m), 1074 (w), 1030 (w), 973 (w), 935 (w), 776 (m). ^{1}HNMR (400 MHz, $CDCl_3$): 8.57 (d, 2H, *J* = 7.2Hz), 8.19 (d, 2H, *J* = 8.0Hz), 7.73 (d, 2H, *J* = 7.2Hz), 4.05 (d, 2H, *J* = 6.8Hz), 2.26 (t, 1H, *J* = 9.2Hz), 2.00 (d, 2H, *J* = 13.2Hz), 1.82 (d, 3H, *J* = 14.0Hz), 1.34 (q, 2H, *J* = 12.0Hz), 1.18 (q, 2H, *J* = 11.2Hz). ^{13}C NMR ($CDCl_3$): 164.76, 134.16, 131.58, 127.16, 122.76, 45.89, 43.01, 36.24, 30.06, 28.44. ESI-MS: 338.185 [M + H^+].

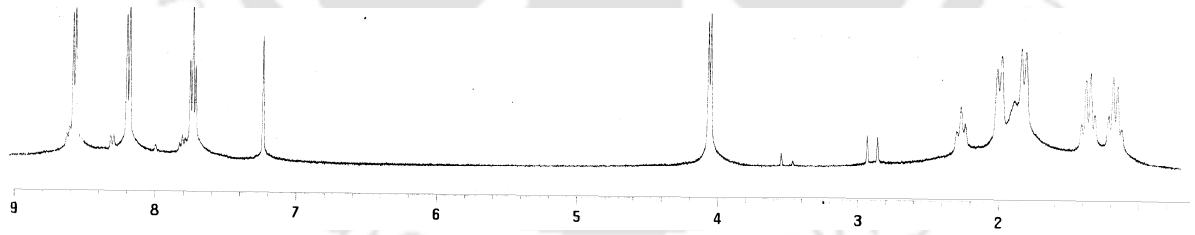

Figure 5.11: ^{1}HNMR spectra of compound **L2H**.

Complex 5.1: To a solution of **L1H** (0.144 gm, 0.5 mmol) in methanol, $Mn(OAc)_2.4H_2O$ (0.061 gm, 0.25 mmol) was added and the reaction mixture was stirred for about 30 minutes at room temperature. The precipitate obtained in the reaction mixture, was filtered and dissolved in water. Colourless block crystals of the product **5.1** were obtained after five days. Yield: 65%; Elemental anal calcd for $C_{32}H_{40}N_2O_{12}Mn$: C, 54.94; H, 5.76; N, 4.00%. Found: C, 54.90; H, 5.70; N,

4.10%. IR (KBr, cm^{-1}): 3270 (w), 2941 (s), 1774 (w), 1712 (s), 1543 (s), 1425 (s), 1397 (s), 1361 (s), 1277 (m), 1155 (w), 1055 (m), 926 (w), 766 (w), 723 (m), 621 (w).

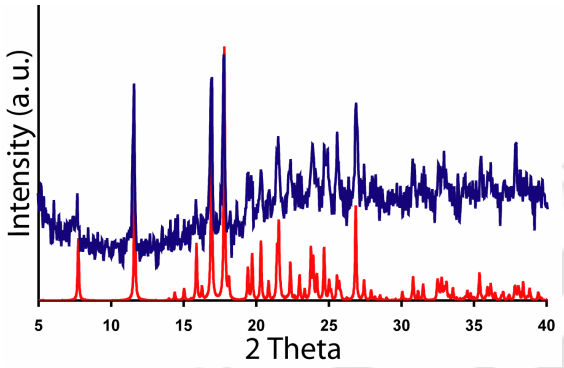

Figure 5.12: Simulated (below) and experimental (above) PXRD patterns of complex **5.1**.

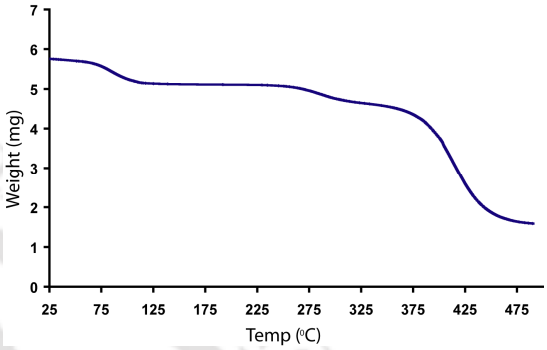

Figure 5.19: TGA curve of complex **5.1**.

Complex 5.2: Needle shaped blue crystals of the product **5.2** were obtained by the reaction of **L1H** (0.144 gm, 0.5 mmol) and $Cu(OAc)_2.H_2O$ (0.050 gm, 0.25 mmol) with the similar procedure as used for **5.1** only difference being it's recrystallization solvent (pyridine). Yield: 68%; Elemental anal calcd for $C_{42}H_{44}N_4O_9Cu$: C, 62.10; H, 5.46; N, 6.90%. Found: C, 62.07; H, 5.43; N, 6.96%. IR (KBr, cm^{-1}): 3150 (w), 2926 (s), 2859 (m), 1772 (w), 1705 (s), 1605 (m), 1576 (s), 1446 (w), 1395 (s), 1360 (m), 1052 (m), 931 (w), 723 (m), 692 (w).

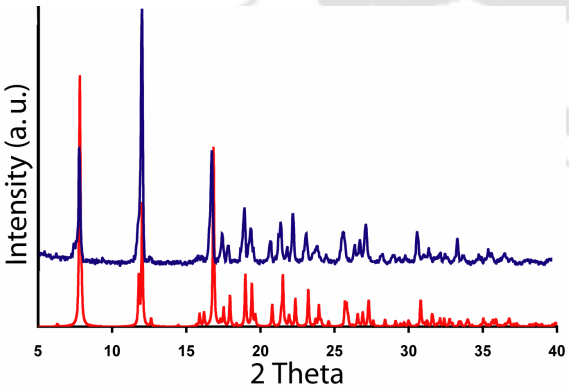

Figure 5.13: Simulated (below) and experimental (above) PXRD patterns of complex **5.2**.

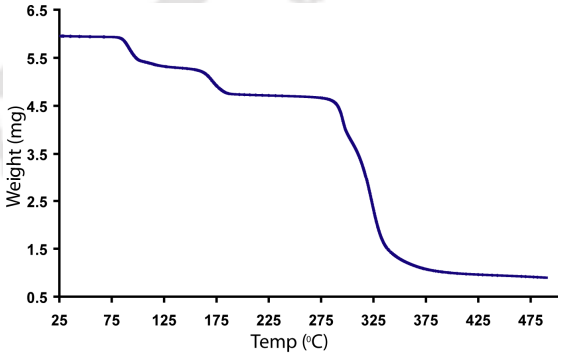

Figure 5.20: TGA curve of complex **5.2**.

Complex 5.3: Colorless good quality crystals of the product **3** were obtained by the reaction of **L1H** (0.144 gm, 0.5 mmol) and $Zn(OAc)_2.2H_2O$ (0.055 gm, 0.25 mmol) with the similar procedure as used for **5.2**. Yield: 72%; Elemental anal calcd for $C_{42}H_{46}N_4O_{10}Zn$: C, 60.61; H, 5.57; N, 6.73%. Found: C, 60.54; H, 5.56; N, 6.80%. IR (KBr, cm^{-1}): 3214 (w), 2928 (s), 2859 (m), 1771 (w), 1704 (s), 1553 (m), 1434 (m), 1398 (s), 1361 (m), 1278 (w), 1151 (w), 1055 (w), 935 (w), 719 (m), 531 (w).

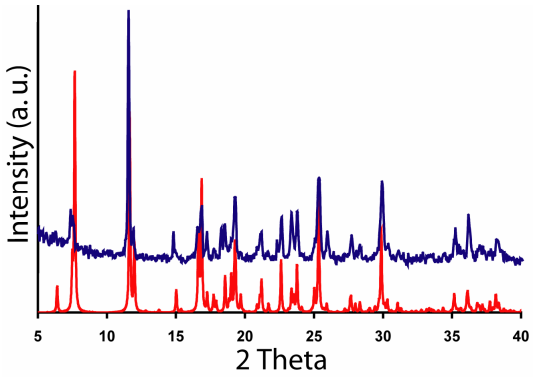

Figure 5.14: Simulated (below) and experimental (above) PXRD patterns of complex **5.3**.

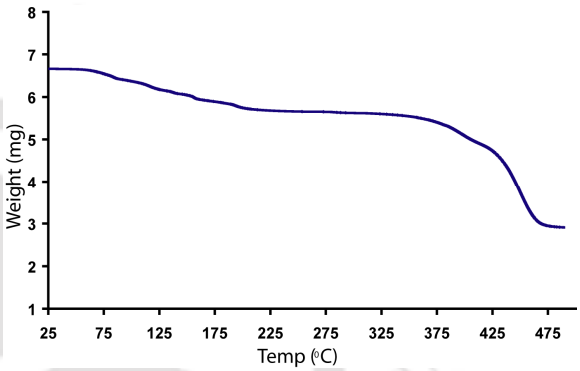

Figure 5.21: TGA curve of complex **5.3**.

Complex 5.4: Brown colored block crystals of the product **5.4** were obtained by the reaction of **L1H** (0.144 gm, 0.5 mmol) and $Cd(OAc)_2.2H_2O$ (0.065 gm, 0.25 mmol) with the similar procedure as used for **5.2**. Yield: 73%; Elemental anal calcd for $C_{42}H_{46}N_4O_{10}Cd$: C, 57.37; H, 5.27; N, 6.37%. Found: C, 57.32; H, 5.21; N, 6.48%. IR (KBr, cm^{-1}): 3148 (w), 2926 (s), 2858 (m), 1772 (w), 1704 (s), 1562 (s), 1435 (w), 1396 (s), 1361 (m), 1277 (m), 1151 (w), 1054 (w), 934 (w), 720 (m), 625 (w).

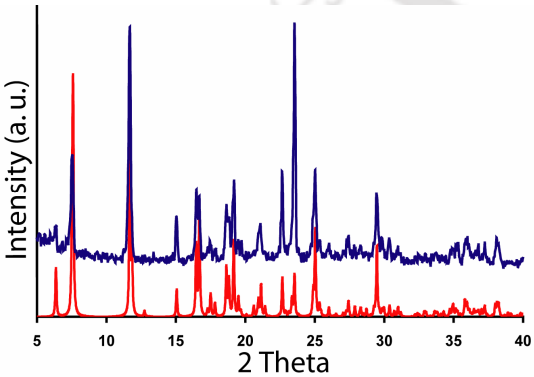

Figure 5.15: Simulated (below) and experimental (above) PXRD patterns of complex **5.4**.

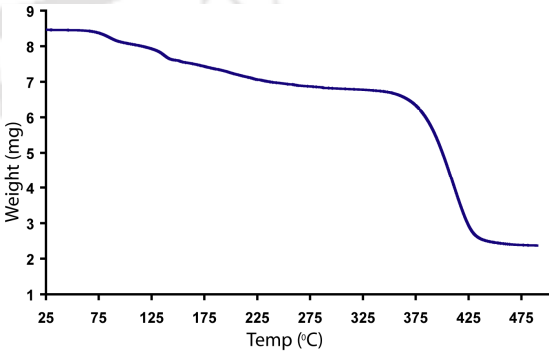

Figure 5.22: TGA curve of complex **5.4**.

Complex 5.5: To a solution of **L2H** (0.167 gm, 0.5 mmol) in N,N-dimethylformamide and ethanol (1:3), $Co(OAc)_2.2H_2O$ (0.062 gm, 0.25 mmol) was added. After stirring this reaction mixture for about 30 minutes at room temperature, a brown colour precipitate was obtained, which was filtered and dissolved in pyridine. Needle shaped crystals of the product **5.5** were obtained from pyridine solution. Yield: 55%; Elemental anal calcd for $C_{55}H_{55}N_5O_{10}Co$: C, 65.73; H, 5.52; N, 6.97%. Found: C, 65.21; H, 5.16; N, 7.22%. IR (KBr, cm^{-1}): 3408 (w), 2922 (s), 2852 (m), 1698 (m), 1657 (s), 1589 (s), 1555 (m), 1440 (s), 1415 (s), 1385 (s), 1346 (s), 1284 (w), 1237 (m), 1177 (w), 1070 (w), 936 (w), 779 (m), 699 (w).

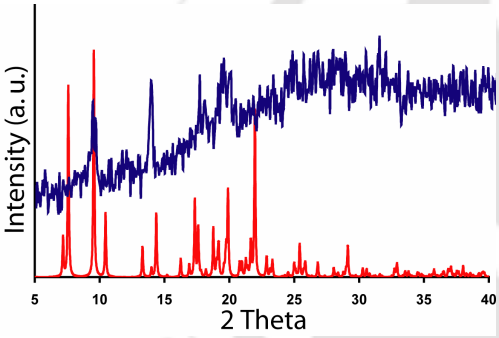

Figure 5.16: Simulated (below) and experimental (above) PXRD patterns of complex **5.5**.

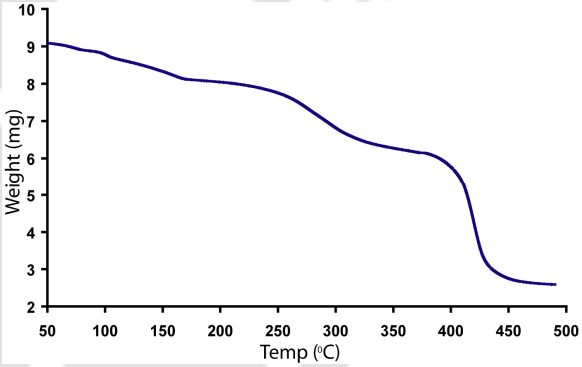

Figure 5.23: TGA curve of complex **5.5**.

Complex 5.6: Blue needle shaped crystals of the product **5.6** were obtained by the reaction of **L2H** (0.167 gm, 0.5 mmol) and $Cu(OAc)_2.H_2O$ (0.050 gm, 0.25 mmol) with the similar procedure as used for **5.5**. Yield: 58%; Elemental anal calcd for $C_{60}H_{60}N_6O_{10}Cu$: C, 66.19; H, 5.55; N, 7.72%. Found: C, 66.03; H, 5.42; N, 7.90%. IR (KBr, cm^{-1}): 3418 (w), 2924 (s), 2853 (m), 1698 (m), 1659 (s), 1589 (s), 1490 (s), 1386 (s), 1344 (s), 1281 (w), 1237 (m), 1178 (w), 1073 (w), 933 (w), 819 (w), 779 (m), 698 (w).

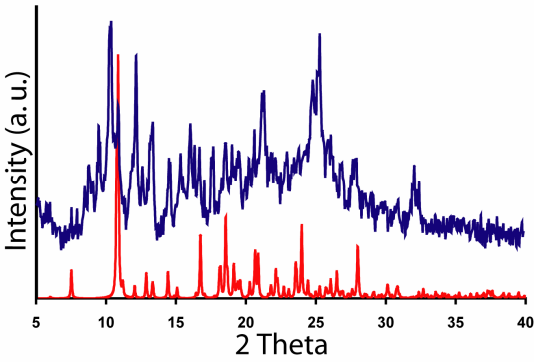

Figure 5.17: Simulated (below) and experimental (above) PXRD patterns of complex **5.6**.

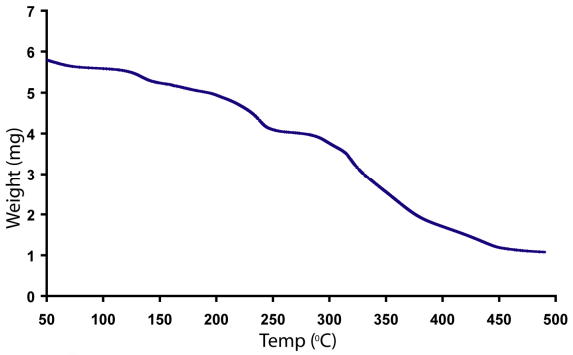

Figure 5.24: TGA curve of complex **5.6**.

Complex 5.7: Brown colored block crystals of the product **5.7** were obtained by the reaction of **L2H** (0.167 gm, 0.5 mmol) and $Cd(OAc)_2.2H_2O$ (0.065 gm, 0.25 mmol) with the similar procedure as used for **5.5**. Yield: 60%; Elemental anal calcd for $C_{55}H_{55}N_5O_{10}Cd$: C, 62.41; H, 5.24; N, 6.62%. Found: C, 62.35; H, 5.28; N, 6.77%. IR (KBr, cm^{-1}): 3434 (w), 2924 (s), 2853 (m), 1698 (m), 1656 (s), 1588 (m), 1537 (s), 1438 (s), 1385 (s), 1349 (s), 1284 (w), 1238 (m), 1177 (w), 1071 (w), 936 (w), 779 (m), 698 (w).

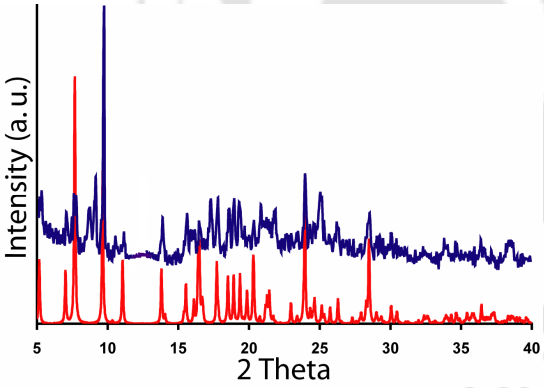

Figure 5.18: Simulated (below) and experimental (above) PXRD patterns of complex **5.7**.

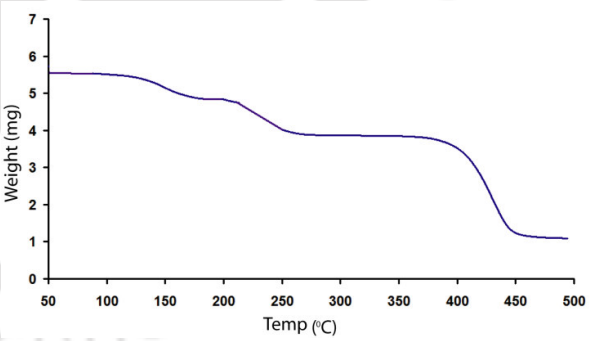

Figure 5.25: TGA curve of complex **5.7**.

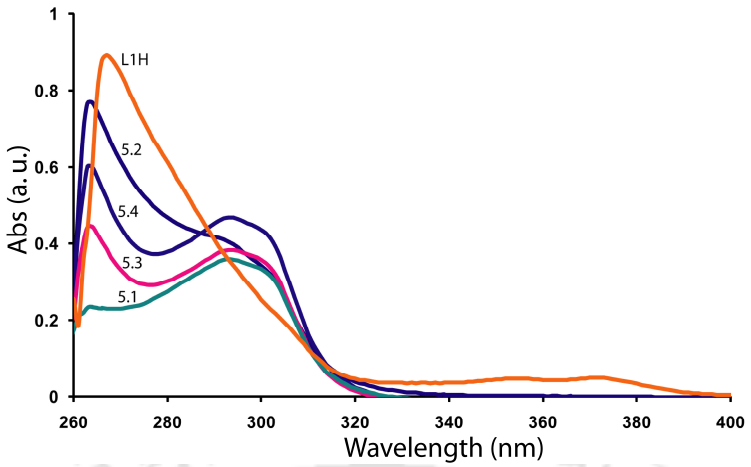

Figure 5.26: UV-Vis spectra of **L1H** showing absorbance peak at 267 nm and its different M(II) complexes showing two absorbance peaks at 263 and 293 nm in DMF (1.1×10^{-5} in each case).

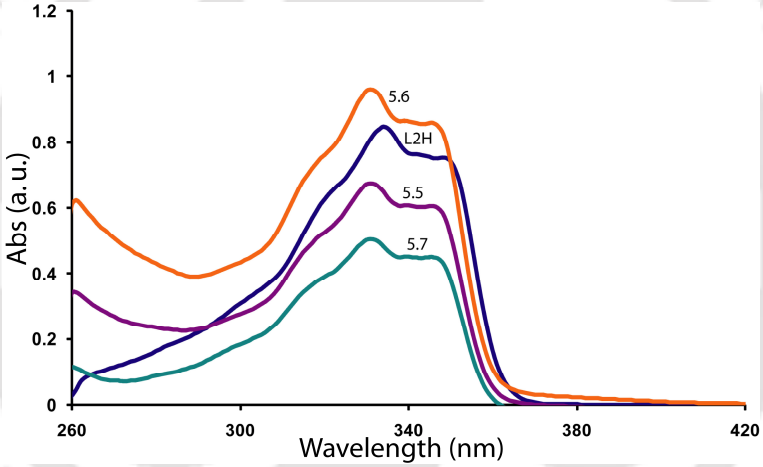

Figure 5.27: UV-Vis spectra of **L2H** and its different M(II) complexes showing two absorbance peaks in the region 330-335 and 345-350 nm in DMF (1.1×10^{-5} in each case).

.

References:

(1) (a) Allen, M. T.; Burrows, A. D.; Mahon, M. F. *J. Chem. Soc., Dalton Trans.* **1999**, 215. (b) Aaker□y, C. B.; Schultheiss, N.; Desper, J. *Inorg. Chem.* **2005**, *44*, 4983.(c) Janiak, C. *J. Chem. Soc., Dalton Trans.* **2000**, 3885, (d) Roesky, H.W.; Andruh, M. *Coord. Chem. Rev.* **2003**, *236*, 91. (e) Zaman, M. B.; Udachin, K. A.; Ripmeester, J. A. *Cryst. Growth Des.* **2004**, *4*, 585. (f) Schottel, B. L.; Chifotides, H. T.; Shatruk, M.; Chouai, A.; Pérez, L. M.; Bacsa, J.; Dunbar, K. R.

J. Am. Chem. Soc. **2006**, *128*, 5895. (g) Noro, S.; Kitaura, R.; Kondo, M.; Kitagawa, S.; Ishii, T.; Matsuzaka, H.; Yamashita, M. *J. Am. Chem. Soc.* **2002**, *124*, 2568.

(2) (a) Blake, A. J.; Champness, N. R.; Cooke, P. A.; Nicolson, J. E. B. *Chem. Commun.* **2000**, 665. (b) Reger, D. L.; Semeniuc, R. F.; Silaghi-Dumitrescu, I.; Smith, M. D. *Inorg. Chem.* **2003**, *42*, 3751. (c) Reger, D. L.; Elgin, J. D.; Semeniuc, R. F.; Pellechia, P. J.; Smith, M. D. *Chem. Comm.* **2005**, 4068. (d) Reger, D. L.; Semeniuc, R. F.; Elgin, J. D.; Rassolov, V.; Smith, M. D. *Cryst. Growth Des.* **2006**, *6*, 2758. (e) Reger, D. L.; Elgin, J. D.; Smith, M. D; Simpson, B. K. *Polyhedron* **2009**, *28*, 1469.

(3) (a) Castro, S. L.; Sun, Z. M.; Grant, C. M.; Bollinger, J. C.; Hendrickson, D. N.; Christou, G. *J. Am. Chem. Soc.* **1998**, *120*, 2365. (b) Noro, S., Kitagawa, S.; Kondo, M.; Seki, K. *Angew. Chem., Int. Ed.* **2000**, *39*, 2081. (c) Hagrman, P. J.; Hagrman, D.; Zubieta, J. *Angew. Chem., Int. Ed.* **1999**, *38*, 2638. (d) Seo, J. S.; Whang, D.; Lee, H.; Jun, S. I.; Oh, J.; Jeon, Y. J.; Kim, K. *Nature*, **2000**, *404*, 982. (e) Humphrey, S. M.; Chang, J-S.; Jhung, S. H.; Yoon, J. W.; Wood, P. T. *Angew Chem., Int. Ed.* **2007**, *46*, 272. (f) Fabelo, O.; Canadillas-Delgado, L.; Delgado, F. S.; Lorenzo-Luis, P.; M Laz, M.; Julve, M.; Ruiz-Perez, C. *Cryst. Growth Des*. **2005**, *5*, 1163.

(4) (a) Bourne, S. A.; Lu, J.; Mondal, A.; Moulton, B.; Zaworotko, M. J.; Moulton, B. *Angew. Chem., Int. Ed.* **2002**, *40*, 2111. (b) Lu, J.; Hajndl, R.; Hariharan, S.; Zaworotko, M. J. *Angew. Chem., Int. Ed.* **2002**, *41*, 2821. (c) Zhao, D.; Yuan, D.; Yakovenko, A.; Zhou, H.-C. *Chem. Commun.* 2010, *46*, 4196. (d) Burrows, A. D.; Frost, C. G.; Mahon, M. F.; Winsper, M.; Richardson, C.; Attfield, J. P.; Rodgers, J. A. *Dalton Trans.* **2008**, 6788.

(5) (a) Li, H.; Eddaoudi, M.; O'Keeffe, M.; Yaghi, O. M. *Nature* **1999**, *402*, 276. (b) Li, H.; Eddaoudi, M.; Groy, T. L.; Yaghi, O. M. *J. Am. Chem. Soc.* **1998**, *120*, 8571.

(6) (a) Chui, S. S. Y.; Lo, S. M. F.; Charmant, J. P. H.; Orpen, A. G.; Williams, I. D. *Science* **1999**, *283*, 1148. (b) Feréy, G.; Serre, C. *Chem. Soc. Rev.* **2009**, *38*, 1380.

(7) Pan, L.; Woodlock, E. B.; Wang, X.; Lam, K. -C.; Rheingold, A. L. *Chem. Commun.* **2001**, 1762.

(8) Kuznicki, S. M.; Bell, V. A.; Nair, S.; Hillhouse, H. W.; Jacubinas, R. M.; Braunbarth, C. M.; Toby, B. H.; Tsapatsis, M. *Nature* **2001**, *412*, 720.

(9) Yaghi, O. M.; Li, H.; Groy, T. L. *J. Am. Chem. Soc.* **1996**, *118*, 9096.

(10) Pan, L.; Liu, H.; Lei, X.; Huang, X.; Olson, D. H.; Turro, N. J.; Li, J. *Angew. Chem., Int. Ed.* **2003**, *42*, 542.

(11) Kondo, M.; Okubo, T.; Asami, A.; Noro, S. -I.; Yoshitomi, T.; Kitagawa, S.; Ishii, T.; Matsuzaka, H.; Seki, K. *Angew. Chem. Int. Ed.* **1999**, *38*, 140.

(12) Halder, G. H.; Kepert, C. J.; Moubaraki, B.; Murray, K. S.; Cashion, J. D. *Science* **2002**, *298*, 1762.

(13) Lin, W.; Wang, Z.; Ma, L. *J. Am. Chem. Soc.* **1999**, *121*, 11249.

(14) Tao, J.; Yin, X.; Wei, Z. -B.; Huang, R. -B.; Zheng, L. -S.; *Eur. J. Inorg. Chem.* **2004**, 125.

(15) Fletchera, A. J.; Thomasa, K. M.; Rosseinsky, M. J.; *J. Solid State Chem*. **2005**, *178*, 2491.

(16). Anokhina, E. V.; Jacobson, A. J. *J. Am. Chem. Soc*. **2004**, *126*, 3044.

(17). Haurowitz, F. *The chemistry and functions of proteins*, Academic press, New York, **1963**.

(18) (a) Barooah, N.; Sarma, R. J.; Batsanov, A. S.; Baruah, J. B. *Polyhedron* **2006**, *25*, 17. (b) Deka, K.; Barooah, N.; Sarma, R. J.; Baruah, J. B. *J. Mol. Struct.* **2007**, *827*, 44. (c) Barooah, N.; Karmakar, A.; Sarma, R. J.; Baruah, J. B. *Inorg. Chem. Commun.* **2006**, *9*, 1251.

(19) Reger, D. L.; Debreczeni, A.; Reinecke, B.; Rassolov, V.; Smith, M. D. *Inorg Chem.* **2009**, *48*, 8911.

(20) (a) Wieghardt, K. *J. Chem. Soc., Dalton Trans.* **1973**, 2548. (b) Nakamoto, K. *Infrared and Raman Spectra of Inorganic and Coordination Compounds*; John Wiley & Sons: New York, 1986.

(21) Jaber, F.; Charbonnier, F.; Faure, R. *Acta cryst.* **1995**, *C51*, 1765.

(22) Parvej, M.; Anwar, S.; Badshah, A.; Ahmad, B.; Majjeed, A.; Ashfaqb, M. *Acta cryst.* **2000**, *C56*, 159.

(23) Barooah, N.; Sarma, R. J.; Baruah, J. B. *Eur. J. Inorg. Chem.* **2006**, 2942.

(24) (a) Karmakar, A.; Deka, K.; Sarma, J.; Baruah, J. B. *Inorg. Chem. Commun.* **2006**, *9*, 836. (b) Karmakar, A.; Sarma, J.; Baruah, J. B. *Polyhedron* **2007**, *26*, 1347.

(25) Distler, A.; Sevov, S. C. *Chem. Commun.* **1998**, 959.

(26) Lewinski, K.; Eilmes, J. *J. Inclusion Phenomena and Macrocyclic Chem.* **2005**, *52*, 261.

27 (a) Du, M.; Jiang, X-J.; Zhao, X-J. *Inorg. Chem.* **2007**, *46*, 3984. (b) Li, G-B.; Liu, J-M.; Cai, Y-P.; Su, C-Y. *Cryst. Growth Des.* **2011**, *11*, 2763. (c) Aijaz, A.; Sanudo, E. C.; Bharadwaj, P. K. *Cryst. Growth Des.* **2011**, *11*, 1122. (d) Fang, S-M.; Zhang, Q.; Hu, M.; Yang, X-G.; Zhou, L-M.; M.; Du, Liu, C-S. *Cryst. Growth Des.* **2010**, *10*, 4775.

(28) (a) Tzeng, B. C.; Chiu, T. H.; Chen, B. S.; Lee, G. H. *Chem.-Eur. J.* **2008**, *14*, 5237. (b) Ding, B.; Yi, L.; Wang, Y.; Cheng, P.; Liao, D. Z.; Yan, S. P.; Jiang, Z. H.; Song, H. B.; Wang, H. G. *Dalton Trans.* **2006**, 665. (c) Li, J. R.; Tao, Y.; Yu, Q.; Bu, X. H. *Chem. Commun.* **2007**, 1527.

(29) (a) Fang, S-M.; Zhang, Q.; Hu, M.; Yang, X-G.; Zhou, L-M.; Du, M.; Liu, C-S. *Cryst. Growth Des.* **2010**, *10*, 4773. (b) Zheng, S-L.; Yang, J-H.; Yu, X-L.; Chen, X-M.; Wong, W-T. *Inorg. Chem.* **2004**, *43*, 830.

(30) (a) Valeur, B. *Molecular Fluorescence: Principles and Applications*; Wiley-VCH: Weinheim, 2002. (b) Adamson, A. W.; Fleischauer, P. D. *Concepts of Inorganic Photochemistry*; John Wiley & Sons: New York, 1975.

Chapter 6

Cyclic imides containing hydroxy carboxylic acids in the syntheses of manganese(II), zinc(II) and cadmium(II) complexes

In previous chapter, we have shown the assemblies of metal-organic materials (MOMs), of cyclohexane carboxylic acids with conformational flexibility coupled with the imide units, governed by highly directional metal-coordination bonds along with various weak non covalent forces. Of the two primary constituents of a MOM platform, the organic ligand imparts diversity through hydrogen bonding or polarization,[1] one can build virtually any desired architecture by changing the characteristics of the metal ion nodes and the organic ligands.[2] The chemistry of the latter compounds, where single metal ion or small clusters of metal ions are linked by multifunctional organic ligands, has been exploded in the last 20 years. However, the rational design and synthesis of metal-organic frameworks (MOFs) with intriguing architectures and topologies still remain a long-term challenge. Many factors such as the coordination environment of metal centers, the donor sets of ligands, solvent molecules, temperature, templates, counteranions, etc. can affect the final architectures.[3] In particular, the structures of the ligands and the coordination modes of metal ions play key roles in the self-assembly process of MOFs because deliberate modifications on the organic ligand, such as the length, flexibility, symmetry or coordination restraints on metal ions dramatically change the ultimate structural topologies of the coordination frameworks.[4] Moreover, coordination bond between metal and ligand and intermolecular weak interactions are vital in the self-assembly process.[5,6] They are dependent on the functionality and the geometry of the organic ligand used in the assembly.[7] In this respect, hydroxy carboxylic acids are important class of compounds because the position of –OH group with respect to carboxylic acid group plays a decisive role in their binding to a metal ion. There are several ways a hydroxyl/oxy-carboxylate complex can be formed,[8] some of which are shown in Scheme 6.1. A large number of articles are available on metal complexes derived from hydroxy carboxylic acids,[9] but there is less information on complexes derived from ligands in which hydroxy carboxylic acid unit is a part of supramolecular synthon. The structural

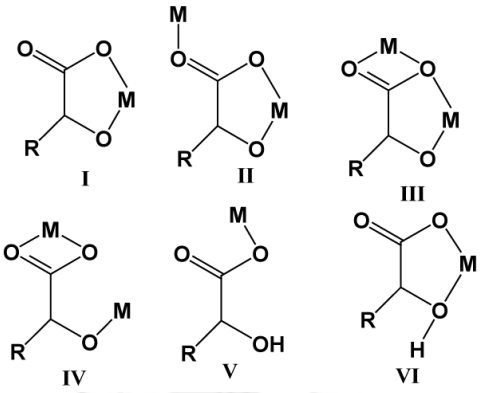

Scheme 6.1: Some of the possible coordination modes derived from hydroxy carboxylic acids.

variations in hydroxyl carboxylate complexes can be brought about by anchoring such ligands to a dipolar unit such as phthalimide unit. Phthalimide has the ability to control weak interactions in host-guest systems by participation of the carbonyl groups in hydrogen bond interactions coupled with dipolar interaction of the ring.[10] The dipolar interactions control π-stacking in 1,8-naphthalimide containing metal complexes.[11] Therefore, understanding of factors influencing the self-assembly is helpful to generate new well-defined products that may have unique structure and function. For these reasons, we have chosen flexible aliphatic and rigid aromatic hydroxy carboxylic acids tethered by phthalimide and naphthalimide units. This chapter deals with the study on the formation of Mn(II), Zn(II) and Cd(II) complexes of **L3H$_2$** and **L4H$_2$** along with the study on their supramolecular structural features. Two ligands, **L3H$_2$** and **L4H$_2$** (**2.2**), employed in this study, are shown in Scheme 6.2.

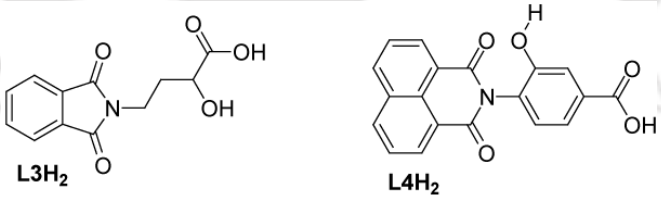

Scheme 6.2: Structures of organic ligands **L3H$_2$** and **L4H$_2$**.

The presence of –OH group next to –COOH group in the flexible aliphatic chain provide an extra site to coordinate with metal ion. Coordinating ability as well as the position of –OH group coupled with the flexibility or rigidity of spacers may provide an avenue to construct the metal complexes of changeable dimensionality. This effect can be visualized clearly in the formation of metal complexes of phthalimide tethered flexible aliphatic hydroxy carboxylic acids (**L3H$_2$**) and naphthalimide tethered rigid aromatic hydroxy carboxylic acid

(**L4H$_2$**). Both –COOH and –OH functional groups are found to coordinate with Mn(II) and Zn(II) metal centers in the 1D coordination polymers of ligand **L3H$_2$** in neutral reaction conditions whereas the –OH group of ligands **L4H$_2$** does not take part in coordination with metal center in the formation of its mononuclear Cd(II) complex even in basic conditions.

The organic ligand 2-hydroxy-4-(1,3-dioxoisoindolin-2-yl)butanoic acid (**L3H$_2$**) is synthesized by solvent free condensation reaction of 4-amino-2-hydroxybutanoic acid with phthalic anhydride under hydrothermal conditions (Scheme 6.3); subsequent crystallization from aqueous ethanol afforded **L3H$_2$** in quantitative yield. The compound is characterized by various spectroscopic techniques and the diffraction quality crystals of its hydrated form are obtained by re-crystallizing it from water.

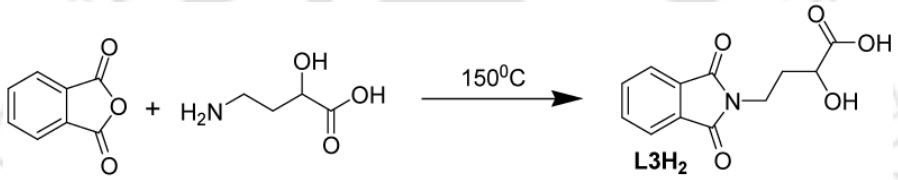

Scheme 6.3. Synthesis of organic ligand **L3H$_2$**.

The trifunctional molecule **L3H$_2$** contain –COOH group, -OH group and a π…π stacking phthalimide unit; hence the formation of homosynthon between the two –COOH groups or two –OH groups and heterosynthon between the –COOH and –OH groups is obvious in the supramolecular architectures of such types of organic solids. However, the structure of hydrate of **L3H$_2$** (**L3H$_2$**.H$_2$O) is devoid of such motifs as well as π…π stacking interactions. Crystal structure shows that the crystallographic asymmetric unit consists of two symmetry nonequivalent molecules of **L3H$_2$** and two water molecules of crystallization (Figure 6.1). The supramolecular structure is stabilized by six component water bridged host-guest assembly in which two water molecules interact with the –COOH and -OH functional groups of two different sets of symmetry non equivalent four host molecules through donor-acceptor hydrogen bonds. One of the water molecules interacts with the –COOH group of a symmetry independent host molecule through donor O12-H12B···O6 ($d_{D\cdots A}$ 2.78Å, <D-H···A 152.06º) interaction and with the –COOH group of another symmetry independent host molecule through acceptor O1-H1···O12 ($d_{D\cdots A}$ 2.50Å, <D-H···A 177.35º) interaction. Similarly, another water molecule also engages in donor-acceptor O11-H11B···O2 ($d_{D\cdots A}$ 2.81Å, <D-H···A 160.70º) and O7-H7A···O11 ($d_{D\cdots A}$ 2.53Å, <D-H···A 176.63º) interactions with two –COOH groups of both the symmetry independent host molecules. The combination of these four O-

H···O interactions makes repeated $R^4_4(12)$ hydrogen bond motifs in the crystal lattice. Further to this, Both the water molecules connect to the –OH groups of two different symmetry non equivalent host molecules through donor O12-H12A···O3 ($d_{D...A}$ 2.65Å, <D-H···A 157.81º) and O11-H11A···O8 ($d_{D...A}$ 2.70Å, <D-H···A 158.19º) interactions. This arrangement leads to the formation of a rare water bridged assembly in which a water molecule is bridged between two –COOH groups and a –OH group via three homomeric O-H···O interactions. Apart from these host-guest interactions, both the carbonyl groups of host molecules participate in the formation of O-H···O (O3-H3···O5; $d_{D...A}$ 2.82Å, <D-H···A 146.81º and O8-H8A···O9; $d_{D...A}$ 2.84Å, <D-H···A 152.36º) and C-H···O (C9-H9···O4; $d_{D...A}$ 3.20Å, <D-H···A 132.94º and C20-H20···O10; $d_{D...A}$ 3.26Å, <D-H···A 128.70º) interactions with –OH group and aromatic phthalimide ring, respectively, making two similar types of $R^2_2(14)$ motifs in the lattice. Formation of one of such motifs is shown in Figure 6.1. It is to be noted that same set of symmetry non equivalent host molecules interact with each other to create such motifs; no interactions between the two different sets of symmetry non equivalent host molecules are observed in the lattice. The phthaloyl glycine results in various polymorphs and pseudo polymorphs and these structures are generally guided by dipolar interaction between the phthaloyl groups.[12] But strong hydrogen bond associated with -OH

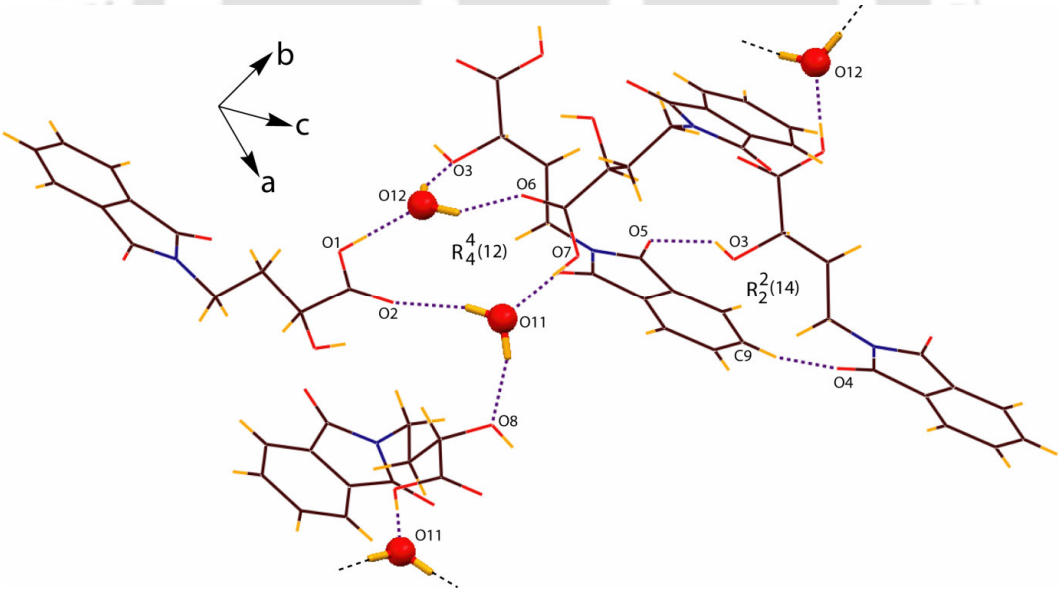

Figure 6.1: Weak interactions in a part of crystal structure of **L3H$_2$**.H$_2$O.

group of the ligand with carbonyl part of the phthaloyl group makes the stacking effect less important. It may be mentioned that $R^2_2(8)$ type of interactions in phthaloylglycine derivatives makes the stacking effect to predominate. The hydrated form of phthaloylglycine donot retain such cyclic dimeric pattern and the dipolar stacking interactions also do not significantly guide the packing pattern.

There is good amount of interest on the use of flexible carboxylate ligands for the synthesis of coordination polymers with various interesting structural features.[13] The flexible ligand **L3H$_2$** is found to be suitable for the construction of coordination polymers by incorporating with both –OH and –COOH metal binding sites. The reaction of organic ligand **L3H$_2$** with Mn(II) acetate, followed by crystallization from water, yields the Mn(II) complex, **6.1**, (Scheme 6.4). Single crystal X-ray structure analysis reveals the formation of one dimensional (1D) coordination polymer, $[\{Mn(L3H)_2(H_2O)\}.8H_2O]_n$ along with mononuclear complex, $[Mn(L3H)_2(H_2O)_2]$, in a single crystal (Figure 6.2). Both these complexes adopt distorted octahedral geometries showing different coordination modes of the carboxylate groups of L3H. The bridging mode of one of the carboxylate group of two L3H ligand in this coordination motif leads to a Mn(II) 1D coordination network along crystallographic b axis with Mn-Mn distance of 5.59 Å. In the octahedral geometry of the mononuclear complex, Mn (II) coordinates with two carboxylate groups in monodentate coordination mode (Mn1-O1 2.115(6) Å, Mn1-O6 2.162(6) Å) and with two hydroxyl groups (Mn1-O3 2.204(7) Å, Mn1-O8 2.269(6) Å) of two L3H ligands as well as two water ligands (Mn1-O11 2.094(7) Å, Mn1-O12 2.165(6) Å) whereas in the case of 1D polymer, octahedral geometry around the Mn(II) center is satisfied by the two oxygen atoms of bridging carboxylate group (Mn2-O13 2.112(8) Å, Mn2-O23 2.155(10) Å), one oxygen atom of monodentate carboxylate group (Mn2-O18 2.145(5) Å), two oxygen atoms of two hydroxyl groups (Mn2-O15 2.249(7) Å, Mn2-O20 2.236(7) Å) and one oxygen atom of water ligand (Mn2-O14 2.076(8) Å) (Figure 6.2). Manganese (IV) oxy-carboxylate complexes have been used as model compounds for water splitting reactions.[14] Manganese (III) glycolate complexes have also been used as mediator for radical cycloaddition of β-dicarbonyl compounds to alkenes.[15]

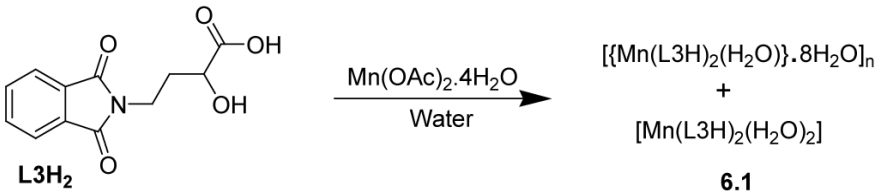

Scheme 6.4: Synthesis of Mn(II) complex (**6.1**) of **L3H$_2$**.

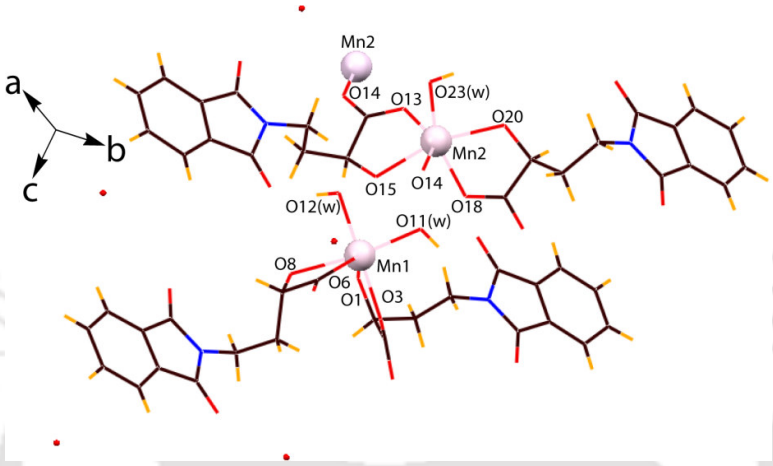

Figure 6.2: Crystallographic asymmetric unit of Mn(II) complex **6.1**.

Crystal structure of complex **6.1** reveals that the self assembled structure is sustained by weak complementary hydrogen bonding interactions. In the structure of **6.1**, the units of 1D coordination polymer interact with each other through intermolecular C-H···O (C33-H33···O19; $d_{D\cdots A}$ 3.18Å, <D-H···A 139.53º and C34-H34···O4; $d_{D\cdots A}$ 3.24Å, <D-H···A 133.41º) hydrogen bonds which are disclosed by aromatic phthalimide ring with the free oxygen atom of carboxylate group and carbonyl oxygen of L3H, respectively (Figure 6.3a). The five membered imide unit and six membered aromatic rings of L3H make strong π…π contacts which is suggested by distance of separation (3.27Å) between the two rings. Hence the 1D polymeric units grow along the c axis to construct a 2D supramolecular channel architecture (Figure 6.3c). Apart from that, the units of mononuclear complex assemble themselves via intermolecular C-H···O (C22-H22···O4; $d_{D\cdots A}$ 3.45Å, <D-H···A 142.06º and C7-H7···O10; $d_{D\cdots A}$ 3.24Å, <D-H···A 133.31º) interactions between phthalimide rings of L3H (Figure 6.3b). In these units, both the coordinated and free oxygen atoms of carboxylate groups also interact with coordinated water and aromatic phthalimide ring via O12-H12A···O6 ($d_{D\cdots A}$ 2.72Å, <D-H···A 162.88º) and C8-H8···O7 ($d_{D\cdots A}$ 3.41Å, <D-H···A 166.33º) interactions, respectively. Formation of a similar kind of 2D supramolecular architecture of

mononuclear complexes occurs in the lattice as observed before in the case of 1D polymeric units. The units of mononuclear complex and 1D polymer also interact with

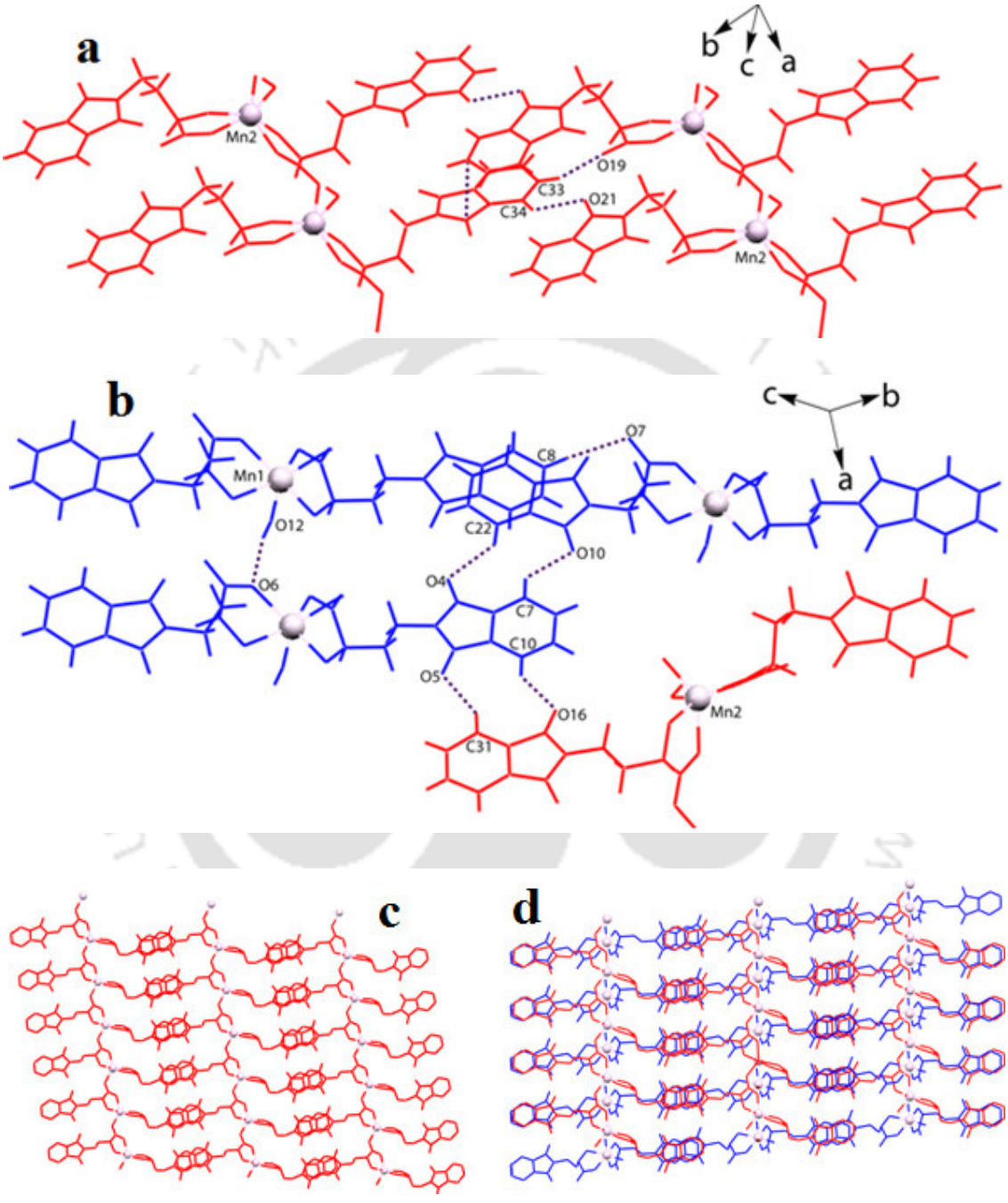

Figure 6.3: (a) Intermolecular interactions among the units of 1D coordination polymer in the structure of **6.1**. (b) Interactions among the units of mononuclear complex and with the 1D coordination polymer. (c) 2D supramolecular channel architecture of 1D coordination polymer after removal of lattice water molecules along c axis. (d) 3D channels in the supramolecular architecture of **6.1** after removal of lattice water molecules along c axis.

each other via two similar C-H···O (C31-H31···O5; $d_{D\cdots A}$ 3.47Å, <D-H···A 150.03º and C10-H10···O16; $d_{D\cdots A}$ 3.35Å, <D-H···A 143.32º) interactions between the phthalimide rings of L3H (Figure 6.1b). All these interactions result in the construction of 3D supramolecular architecture in the crystal lattice of **6.1** in which the units of mononuclear complex and 1D polymer are layered over each other. This layered arrangement further allows the creation of 3D channels which are filled by lattice water molecule as viewed along the c axis (Figure 6.3d). Polymeric Cu(II) complexes of α-hydroxycarboxylate ligands with ancillary bipyridine ligand are reported in which α-hydroxycarboxylate ligands are bidentate chelating monoanions and bipyridine ligand act as bridging ligand creating linear polymeric arrangements.[16] The polymeric chains are interconnected by O-H···O hydrogen bonds creating the cavities of different size in these complexes.

A similar reaction of organic ligand **L3H$_2$** with Zn(II) acetate, followed by crystallization from pyridine, led to the formation of 1D Zn(II) coordination polymer, [{Zn(L3H)$_2$(pyr)}.pyr]$_n$, **6.2**, (Scheme 6.5). The distorted octahedral geometry of this polymer shows similar coordination environment as observed for 1D polymer of **6.1**, only showing difference of a coordinated pyridine ligand than water (Figure 6.4a). The coordination polymer **6.2** comprises of 1D linear chains where the nearby Zn(II) centers are bridged by a carboxylate group (Zn1-O6 2.098(4) Å, Zn1-O7 2.028(4) Å) of one of the L3H ligands with Zn-Zn distance of 5.06 Å. The other four coordination sites of this six coordinated complex are occupied by a monodentate carboxylate group of another L3H ligand (Zn1-O1 2.059(4) Å), two hydroxyl groups of both the L3H (Zn1-O3 2.185(4) Å, Zn1-O8 2.182(5) Å) and an ancillary pyridine ligand (Zn1-N3 2.110(6) Å).

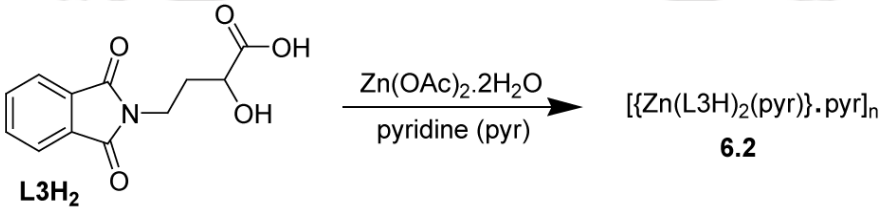

Scheme 6.5: Synthesis of Zn(II) complex (**6.2**) of **L3H$_2$**.

In contrast to the structure of Mn(II) 1D coordination polymer, the 1D polymeric structure of **6.2** is sustained by two different intramolecular C-H···O (C2-H2···O2; $d_{D\cdots A}$ 3.12Å, <D-H···A 120.97º and C15-H15B···O7; $d_{D\cdots A}$ 3.51Å, <D-H···A 142.33º) interactions in which the flexible aliphatic chains of L3H ligands participate as donor and carbonyl oxygen and free

oxygen atom of carboxylate group act as acceptor (Figure 6.4a). The self assembly of complex **6.2** in solid state is governed by weak C-H···O and C-H···π intermolecular hydrogen bonding interaction. The Free oxygen atom of carboxylate group of L3H also interact with coordinated pyridine ring through intermolecular C26-H26···O2 ($d_{D\cdots A}$ 3.20Å, <D-H···A 121.12º) interaction. The carbonyl oxygen atoms and aromatic phthalimide rings of L3H are found to involve in C-H···O (C22-H22···O5; $d_{D\cdots A}$ 3.38Å, <D-H···A 137.85º and C7-H7···O9; $d_{D\cdots A}$ 3.31Å, <D-H···A 137.30º) interactions (Figure 6.4b). These C-H···O interactions grow the 1D polymeric chain into another dimension along the b axis. Further,

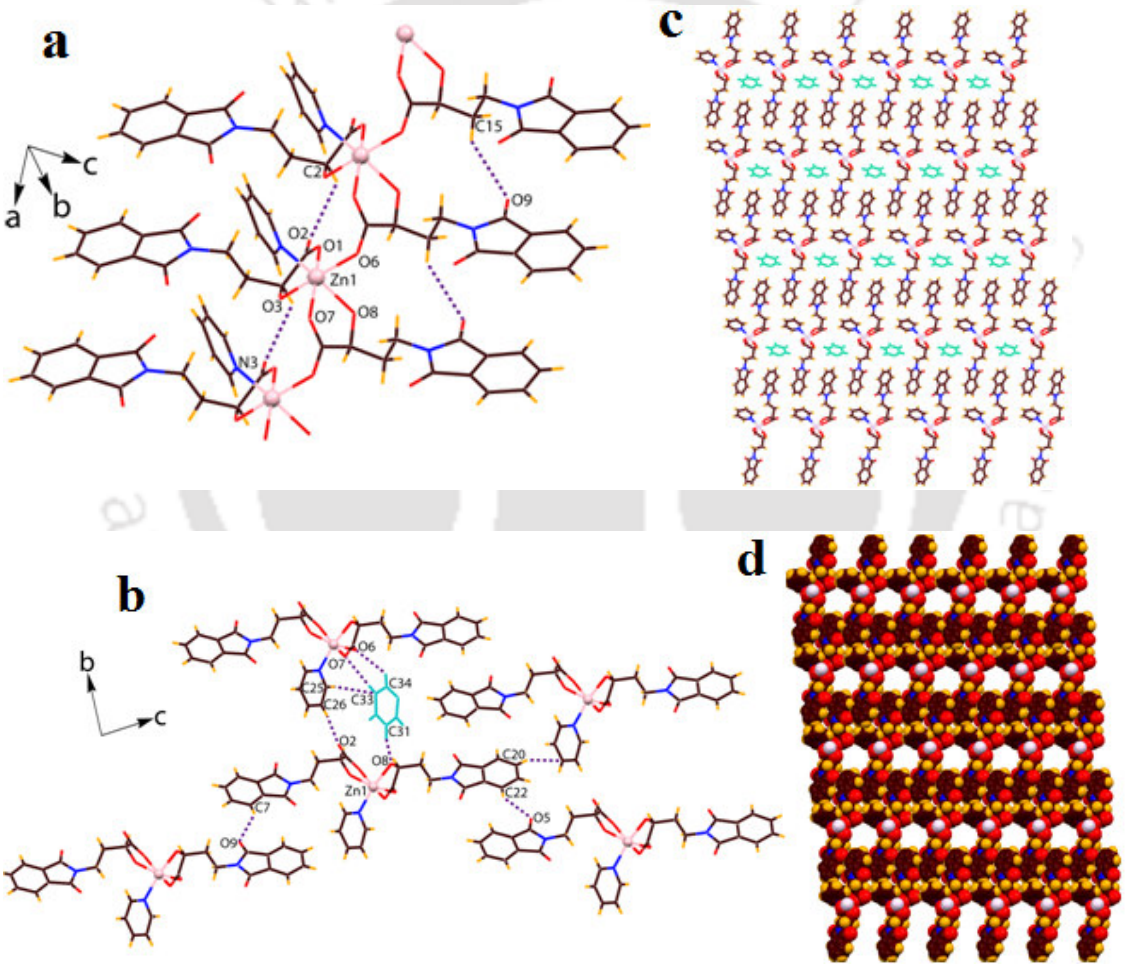

Figure 6.4: (a) A 1D chain of coordination polymer **6.2** showing some intramolecular interactions. (b) Intermolecular interactions in the crystal structure of **6.2**. (c) 3D supramolecular architecture of **6.2** showing voids, filled by lattice pyridine molecules along a axis. (d) Space filling model after removal of pyridine molecules from the hexagonal voids.

the C-H···π (d_{C20}…$_{\pi}$ 3.74Å) interactions between the aromatic rings of L3H and coordinated pyridine rings construct a 3D supramolecular architecture of **6.2** creating hexagonal shape of solvent voids in the lattice. These voids are filled by lattice pyridine molecules as viewed along a axis (Figure 6.4c). The pyridine molecules are tightly held in these voids interacting with L3H via donor C-H···O (C34-H34···O6; $d_{D\cdots A}$ 3.38Å, <D-H···A 133.64º; C33-H33···O7; $d_{D\cdots A}$ 3.44Å, <D-H···A 153.74º and C31-H31···O8; $d_{D\cdots A}$ 2.66Å, <D-H···A 167.38º) interactions and with the coordinated pyridine ring via acceptor C-H···π (d_{C25}…$_{\pi}$ 3.55Å) interaction (Figure 6.4b). The coordination behavior of complex **6.2** is the same as that found in the polymeric Cu(II) complex of lactato and 1,2-bis(4-pyridyl)ethane ligands.[17] The monoanionic lactato ligand acts as bidentate chelate system through one carboxylate oxygen and the hydroxyl oxygen. The bis-pyridyl ligand bridges between neighbouring Cu(II) atoms to form zigzag polymeric chain. Hydrogen bonds and π…π interactions create a 3D open framework with channels which are occupied by crystallization water molecules.

The organic ligand 4-(1,3-dioxo-1*H*,3*H*-benzo[de]isoquinolin-2-yl)-3-hydroxy-benzoic acid (**L4H$_2$**) is synthesized by condensation reaction of 4-amino-3-hydroxybenzoic acid with 1,8-naphthalic anhydride under reflux condition using DMF solvent (Scheme 6.6).

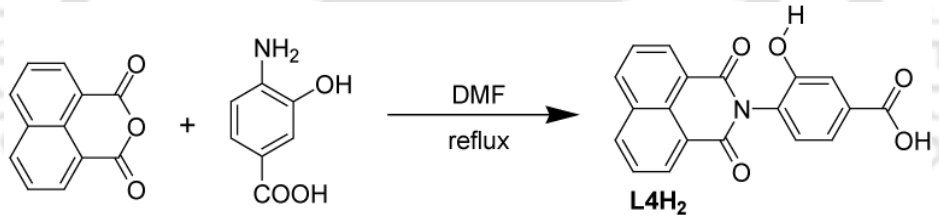

Scheme 6.6. Synthesis of organic ligand **L4H$_2$**.

The coordination chemistry of cadmium is interesting due to its ability to form complexes with different coordination numbers.[18] The multiple possibilities of coordination numbers make cadmium complexes suitable for the construction of diverse supramolecular architectures. Due to the presence of various substituents on ligand and steric factors of ancillary ligands, the structural variations have been achieved in trigonal prismatic and severely distorted octahedral cadmium complexes.[19]

The reaction of organic ligand **L4H$_2$** with Cd(II) acetate in the presence of methanol/DMF (3:1), followed by crystallization from pyridine; afforded brown coloured block crystals of a seven coordinated mononuclear Cd(II) complex, $[Cd_2(L4H)_4(pyr)_6].4pyr.6H_2O$, **6.3** (Scheme 6.7). The Complex **6.3** is crystallized in monoclinic $P2_1/c$ space group and possess two

symmetry non-equivalent Cd(II) complex molecules in its crystallographic asymmetric unit (Figure 6.5). The geometry of these complexes can be best described as distorted pentagonal bipyramid. Two carboxylates groups of L4H are in trans chelating coordination mode; remaining three positions are occupied by pyridine ligand molecules in the distorted pentagonal bipyramidal geometries of each of **6.3**. The bond distances of Cd-O and Cd-N coordinate bonds are ranges from 2.270(3) - 2.642(3) Å and 2.357(4) - 2.394(4) Å, respectively.

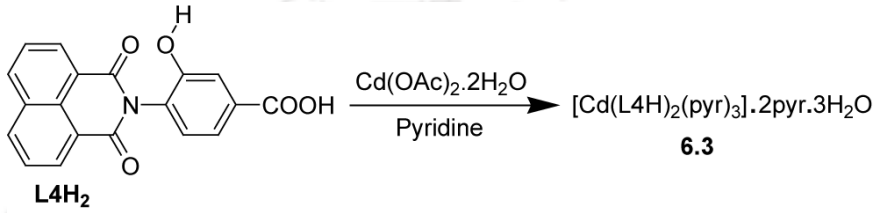

Scheme 6.7: Synthesis of Cd(II) complex (**6.3**) of **$L4H_2$**.

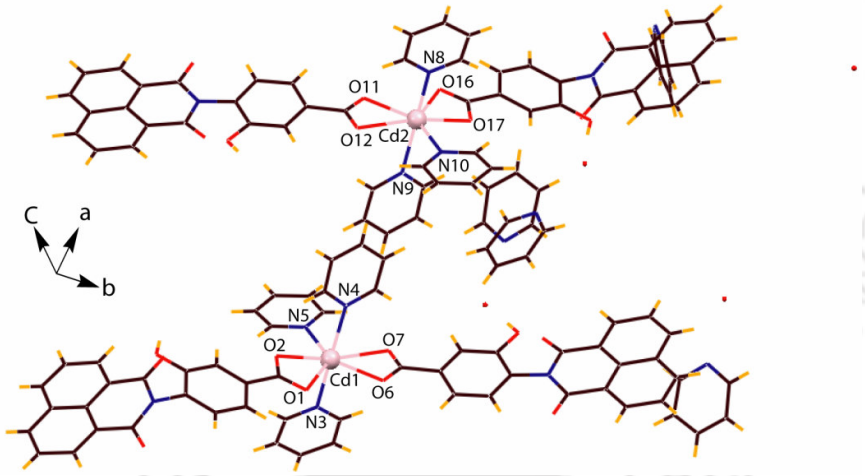

Figure 6.5: Crystallographic asymmetric unit of Cd(II) complex **6.3**.

As there are two sets of symmetry nonequivalent molecules in the crystal lattice of **6.3**; they interact each other through weak intermolecular interactions to construct an interesting supramolecular architecture of **6.3**. First set of symmetry non equivalent molecules self assembles themselves through weak C-H···O, C-H···π and π…π interactions (Figure 6.6a). One of the hydrogen atoms of coordinated pyridine ring participate in bifurcated donor C51-H51···O10 ($d_{D\cdots A}$ 3.16Å, <D-H···A 136.97º) and C-H···π ($d_{C51\ldots\pi}$ 3.53Å) interactions with the carbonyl oxygen and naphthalimide ring of L4H; simultaneously, another hydrogen atom of

same pyridine ring interact with the oxygen atom of –OH group of L4H through donor C52-H52···O3 ($d_{D\cdots A}$ 3.34Å, <D-H···A 143.05º) interaction. The aromatic ring bearing --COOH and –OH group is also found to involve in donor C-H···π ($d_{C25}\ldots_{\pi}$ 3.71Å) interaction with the naphthalimide unit. Strong π…π stacking interactions between the naphthalimide rings of L4H are also observed in the 2D self assembled structure of first set of molecules. Similar types of C-H···O (C104-H104···O15; $d_{D\cdots A}$ 3.18Å, <D-H···A 132.35º; C103-H103···O18; $d_{D\cdots A}$ 3.29Å, <D-H···A 139.94º) and C-H···π ($d_{C104}\ldots_{\pi}$ 3.68Å) interactions among the second set of symmetry non equivalent molecules are recognized which are responsible for the formation of a similar kind of 2D hydrogen bonded assembly of second set of molecules (Figure 6.6b). Notably, the aromatic ring bearing –COOH and –OH group of second set of molecules is involved in bifurcated donor C-H···π ($d_{C78}\ldots_{\pi}$ 3.70Å, 3.73Å) interaction with the naphthalimide unit and no π…π interactions are identified between the naphthalimide rings which are accounted as minor differences in the self assembled structures of both sets. Both sets of symmetry non equivalent molecules also interact with each other through donor-acceptor interactions (Figure 6.6c). The coordinated pyridine rings of first set of molecules take part in the formation of donor C-H···O (C42-H42···O13; $d_{D\cdots A}$ 3.14Å, <D-H···A 129.26º; C46-H46···O18; $d_{D\cdots A}$ 3.44Å, <D-H···A 140.53º) hydrogen bonds with the second set of molecules. Similarly, the coordinated pyridines of second set of molecules also form donor C-H···O (C93-H93···O8; $d_{D\cdots A}$ 3.18Å, <D-H···A 127.81º; C99-H99···O3; $d_{D\cdots A}$ 3.33Å, <D-H···A 140.69º) hydrogen bonds with the first set of molecules. Apart from that, the naphthalimide rings of first set of molecules engages in donor C-H···O (C11-H11···O11; $d_{D\cdots A}$ 3.38Å, <D-H···A 150.09º; C31-H31···O16; $d_{D\cdots A}$ 3.34Å, <D-H···A 137.67º and C14-H14···O14; $d_{D\cdots A}$ 3.44Å, <D-H···A 163.24º) interactions with the coordinated carboxylate groups and carbonyl oxygen of second set of molecules, respectively. The interactions between the two set of molecules construct a 3D supramolecular architecture of **6.3** in the lattice. In this architecture, both set of molecules are layered over each other creating channels of approximately 12×6 Å dimensions which are filled by lattice water and pyridine molecules as viewed along a axis. (Figure 6.6d). The coordination of the complex **6.3** can be compared to the reported cadmium complexes of 2-hydroxy-1-naphthoic acid. In this case, binuclear and polymeric complexes were obtained depending on chelating nitrogen donor ligands.[20]

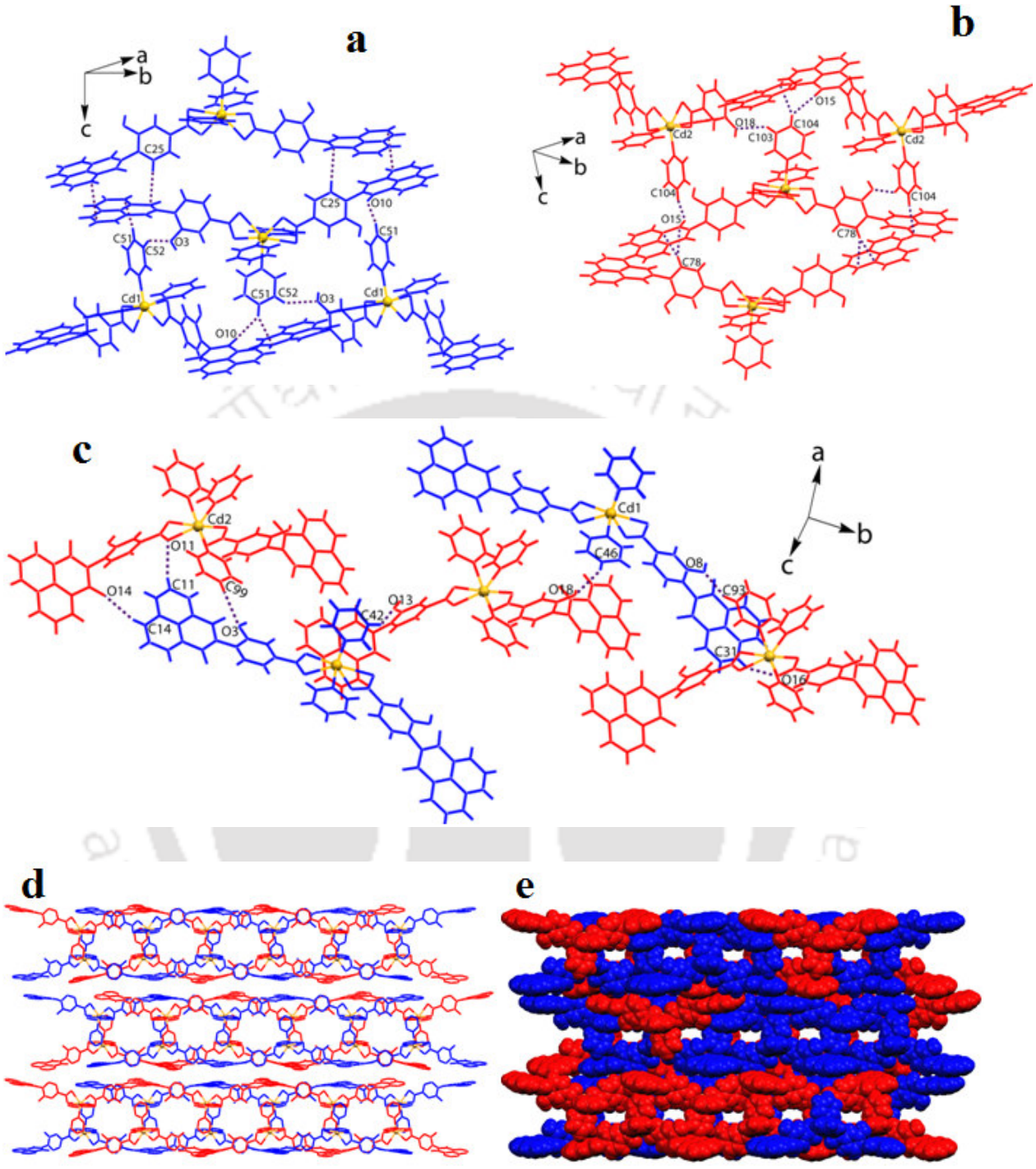

Figure 6.6. (a) Weak intermolecular interactions among the molecules of First set and (b) second set and (c) first and second set in the structure of **6.3**. (d) Crystal packing arrangement showing 3D channels in the separate layers of **6.3** along a axis. (c) Space filling model after removal of lattice pyridine and water molecules inside the channels.

PXRD patterns and Thermogravimetric analyses (TGAs) of the complexes:

The PXRD patterns of complexes **6.1-6.3** are shown in Figure 6.10-6.12 in the Experimental Section. Most of the diffractions peaks of the three complexes can be nearly correlated to their respective peaks of simulated PXRD patterns. Minor differences in some of the peaks are observed which are probably due to the loss of lattice solvent molecules at room temperature, however, these patterns can be consider for the pure phase of complexes.

The thermal stability of M(II) complexes is analyzed by recording TGA curves of complexes **6.1**-**6.3** which are also in agreement with the loss of coordinated and lattice solvent molecules (Figure 6.13-6.15 in Experimental Section). TGA curve of complex **6.1** shows weight loss of lattice and coordinated water molecules in two steps. In first step, 12.08% weight loss occurs, corresponding to eight lattice water molecules between 50 and 100^0C (calcd 11.1%) which is also in agreement with squeeze analysis of the crystal structure of **6.1**. In second step, 5.09% weight loss occurs from the residue of the first step for remaining three coordinated water molecules between 200 and 225^0C (calcd 4.68%). Further weight loss in the temperature range 250-450^0C is accounted for the decomposition of organic ligands. In the case of complex **6.2**, weight loss of lattice and coordinated pyridine molecules also occurs in two steps. The first step within the range 85-135^0C corresponds to a weight loss of 10.5% (calcd 11.01%) due to the loss of one lattice pyridine molecule, and the second step, 140-250^0C, is due to the loss of one coordinated pyridine molecule (weight loss of 10.6% of the residue from the first step; calcd 12.38%). The organic framework of complex **6.2** starts to be decomposed when the temperature is higher than 260^0C. The TGA curve of complex **6.3** shows a continuous weight loss of 34.7% between 65 and 300^0C corresponding to the loss of the six lattice water and four lattice pyridine molecules along with six coordinated pyridine molecules (calcd 36.59%), followed by the degradation of organic ligands in higher temperature range. The squeeze result also confirms the presence of six lattice water molecules in the crystal lattice of **6.3**.

Photoluminescence properties of M(II) complexes:

Photoluminescence of coordination polymers constructed from d^{10} metal centers have often been investigated for their potential applications in chemical sensors, photochemistry, and electroluminescent display.[21] Therefore, the solid state fluorescence properties of organic ligands **L3H$_2$** and **L4H$_2$** along with their M(II) complexes are investigated at room temperature.

The emission spectra of the free organic ligand **L3H$_2$** and its two 1D coordination polymers with Mn(II) and Zn(II), **6.1** and **6.2**, respectively, are shown in Figure 6.7. Upon excitation at 280 nm, a strong emission band appears at 358 nm along with a less intense emission peak at 473 nm in the photoluminescence emission spectra of **L3H$_2$**. These bands may be assigned as ligand to ligand charge transfer transitions (LLCT) or intraligand $\pi \rightarrow \pi^*$ transition.[22] Significant changes are observed in the emission behavior of **L3H$_2$** upon coordination with metal ions. The band appeared at 358 nm in the emission spectrum of **L3H$_2$**, is shifted to longer wavelength by 42 nm and 62 nm in the emission spectra of **6.1** and **6.2**, respectively, and the new emission bands which are less intense than the emission band of **L3H$_2$**, are appeared at 400 and 420 nm in the case of complex **6.1** and **6.2** (λ_{ex} = 280 nm in each case). Another less intense emission band which is appeared at 473 nm in the case of **L3H$_2$**, also shows minor red or blue shifts upon coordination with Mn(II) and Zn(II) ions; further originating new emission bands at 463 and 483 nm in the coordination complexes **6.1** and **6.2**, respectively. Appearance of these new emission bands in the coordination complexes **6.1** and **6.2** may be ascribed to the ligand-to-metal charge transfer (LMCT) transitions.[23] It is to be noted that the emission spectra of Mn(II) and Zn(II) complexes are also distinguished to each other which is probably due to the different composition of organic ligands or different M(II) centers as well as different coordination modes of ligands around the metal centers in these complexes.

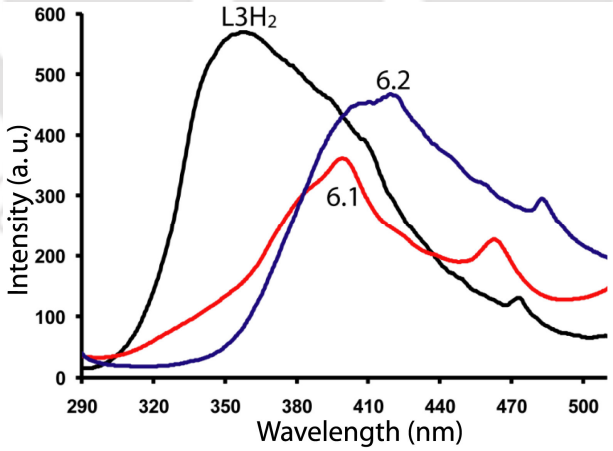

Figure 6.7: The solid state photoluminescence spectra of free organic ligand **L3H$_2$** and its two M(II) complexes **6.1** and **6.2** (λ_{ex} = 280 nm) at room temperature.

The photoluminescence spectra of free organic ligand **L4H$_2$** and its Cd(II) complex **6.3** are recorded upon excitation at 340 nm (Figure 6.8). The photoluminescence spectrum of **L4H$_2$**

shows a broad emission band in the region 430-475 nm; centered at 450 nm and a less intense emission band at 516 nm. The emission spectrum of **6.3** is found to be nearly similar to that of **L4H$_2$** except the intensities of emission of peaks, showing an intense emission band in the region 445-470nm; centered at 460 nm and a less intense emission band at 516 nm. The emission peaks obtained for **L4H$_2$** and its Cd(II) complex are attributed to the intraligand $\pi \rightarrow \pi^*$ transition.[22] However, the appearance of comparatively more intense emission band in the emission spectrum of **6.3** than the **L4H$_2$** is probably due to the strong luminescence characteristics of d^{10} metals.

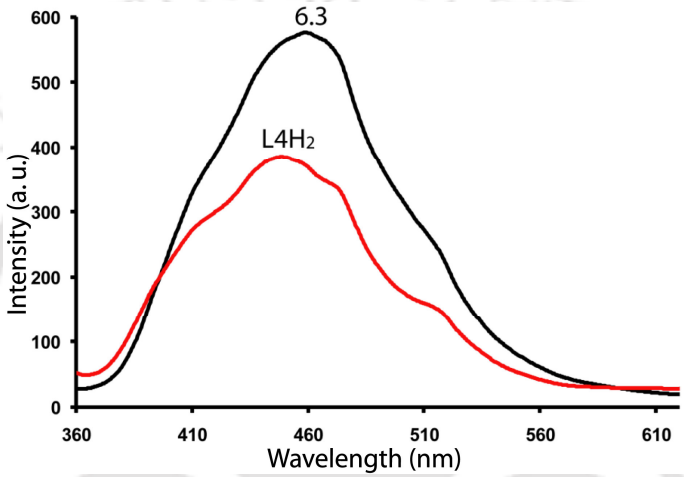

Figure 6.8: The solid state photoluminescence spectra of free organic ligand **L4H$_2$** and its Cd(II) complex **6.3** (λ_{ex} = 340 nm) at room temperature.

In conclusion, we have shown the water bridged solid state assembly of **L3H$_2$** that is formed by a trimeric HCOO···HOH···COOH synthon containing three discrete intermolecular O-H···O interactions. The self assembly of this flexible hydroxy carboxylic acids can be tuned to adopt fascinating supramolecular architectures possessing channels of different dimensionalities and voids of hexagonal nature upon introduction of Mn(II) and Zn(II) metal ions, respectively. The dipolar interactions of phthaloyl group of the **L3H$_2$** overcome the relative competition of O-H···O interactions present in the free ligand, to show predominance of dipolar stacking interactions in the metal complexes. The ancillary ligands (water or pyridine) play a crucial role in the formation of a novel metal organic complex (**6.1**) containing 1D coordination polymer and mononuclear complex in a single crystal. It is also observed that the position of –OH group adjacent to –COOH group and nature of spacers coupled with imide tethers provide an impetus to obtain the polymeric and monomeric M(II) complexes. The supramolecular architecture of seven coordinated Cd(II) complex of ligand

L4H$_2$ is reported to create 3D channels in the separated layers of two symmetry nonequivalent complex molecules. The structure of **6.3** is a representative case of cadmium complex which has special features of coordinated pyridine participating in weak interactions to make self assemblies to accommodate pyridine and water molecules and thereby opens up avenues for search of such ligand systems that would be weakly interacting yet accommodate host molecules. In this study, we have also observed that photoluminescence properties of **L4H$_2$** and its mononuclear Cd(II) complex show resemblance to each other whereas they have different characteristics in the case of **L3H$_2$** and its Mn(II) and Zn (II) coordination polymers.

Experimental Section:

Detailed synthetic methodologies are given below. Analytical data as well as spectroscopic data are listed along with each compound. The instrumental details are given in Appendix.

Synthesis and characterization of compounds and their M(II) complexes:

Compound L3H$_2$: Phthalic anhydride (0.740 gm, 5 mmol) and 4-amino-2-hydroxybutanoic acid (0.595 gm, 5 mmol) were mixed thoroughly in a mortar and pastel. The mixture is then heated under hydrothermal condition to obtain a homogeneous colorless molten mixture. Heating was continued for another 30 minutes and cooled to room temperature. Then content was dissolved in ethanol and left undisturbed for 24 hrs. The white precipitate of product **L3H$_2$** was obtained in 95% yield. IR (KBr, cm^{-1}): 3390 (m), 2528 (w), 1964 (w), 1767 (m), 1695 (s), 1439 (m), 1402 (s), 1372 (s), 1283 (s), 1130 (s), 1107 (s), 1032 (s), 896 (m), 866 (w), 797 (w), 723 (m), 673 (w). ^{1}HNMR (400MHz, $CDCl_3$): 7.49 (s, 2H,), 7.42 (s, 2H,), 3.82 (t, 2H, J = 4.4 Hz), 3.53 (t, 1H, J = 7.2 Hz), 1.84 (s, 1H,) 1.65 (dd, 2H, J = 7.2 Hz). ESI-MS: 250.223 [M + H$^+$]. The crystals of hydrated form of **L3H$_2$** were obtained by re-crystallizing it from water.

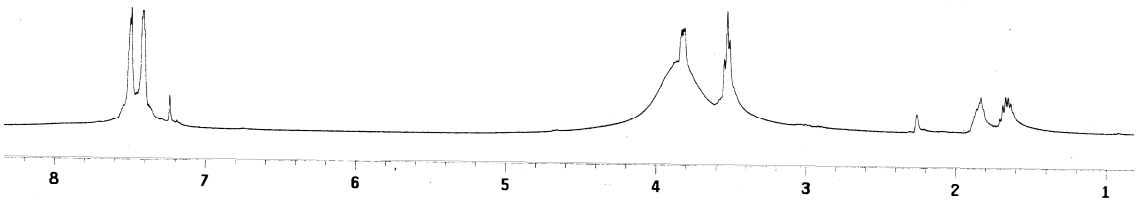

Figure 6.9: ^{1}HNMR spectra of **L3H$_2$**.

Compound L4H$_2$ (2.2): Synthetic details and spectroscopic parameters of **L4H$_2$** are provided in the experimental section of chapter 2.

Complex 6.1: **L3H$_2$** (0.125 gm, 0.5 mmol) was dissolved in methanol at room temperature and a methanolic solution of Mn(OAC)$_2$.4H$_2$O (0.061 gm, 0.25 mmol) was added dropwise with stirring. The solution was stirred for an hour and the resulting white precipitate was collected by filtration, washed with methanol. The wet precipitate was re-dissolved in water (20 ml), concentrated to 10 ml and left undisturbed. Crystals of the complex **6.1** were collected as colourless needles after seven days. Yield: 58%; Elemental anal calcd for $C_{48}H_{59}N_4O_{31}Mn_2$: C, 44.42; H, 4.58; N, 4.32%. Found: C, 44.72; H, 4.32; N, 4.40%. IR (KBr, cm^{-1}): 3429 (m), 1769 (m), 1694 (s), 1614 (s), 1443 (w), 1402 (m), 1325 (m), 1286 (w), 1253 (w), 1138 (m), 1088 (w), 1054 (w), 1008 (w), 965 (w), 864 (w), 723 (m).

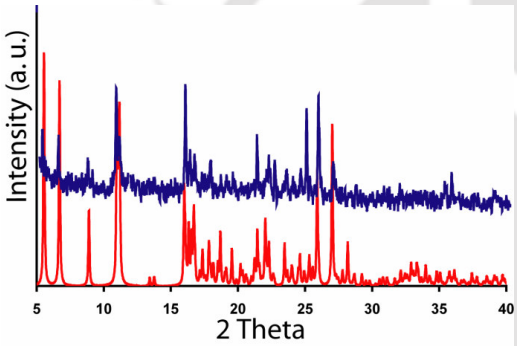

Figure 6.10: Simulated (below) and experimental (above) PXRD patterns of complex **6.1**.

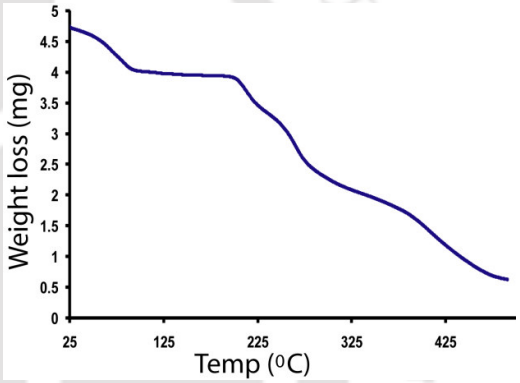

Figure 6.13: TGA curve of complex **6.1**.

Complex 6.2: **L3H$_2$** (0.125 gm, 0.5 mmol) was dissolved in methanol at room temperature and a methanolic solution of Zn(OAC)$_2$.2H$_2$O (0.055 gm, 0.25 mmol) was added dropwise with stirring. The solution was stirred for an hour and the resulting white precipitate was collected by filtration, washed with methanol. The wet precipitate was re-dissolved in pyridine and left undisturbed. Needle shaped colorless crystals of the complex **2** were obtained from pyridine solution. Yield: 65%; Elemental anal calcd for $C_{34}H_{28}N_4O_{10}Zn$: C, 56.88; H, 3.93; N, 7.80%. Found: C, 56.80; H, 3.96; N, 7.90%. IR (KBr, cm^{-1}): 3406 (m), 1769 (m), 1698 (s), 1614 (s), 1432 (m), 1409 (s), 1378 (m), 1334 (w), 1286 (w), 1254 (w), 1167 (w), 1131 (m), 1093 (m), 957 (w), 868 (w), 727 (m), 712 (m).

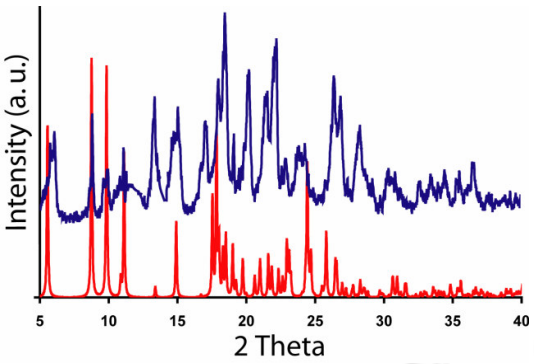

Figure 6.11: Simulated (above) and experimental (below) PXRD patterns of complex **6.2**.

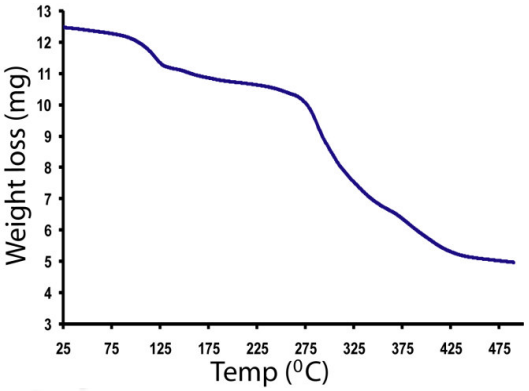

Figure 6.14: TGA curve of complex **6.2**.

Synthesis of complex 6.3: To a solution of **L4H$_2$** (0.144 gm, 0.5 mmol) in methanol and N,N-dimethylformamide, $Cd(OAC)_2.2H_2O$ (0.065 gm, 0.25 mmol) was added and the reaction mixture was stirred for about 30 minutes at room temperature. The precipitate obtained in the reaction mixture, was filtered and dissolved in pyridine. Big block crystals of the complex **6.3** were obtained after five days. Yield: 68%; Elemental anal calcd for $C_{126}H_{102}N_{14}O_{26}Cd_2$: C, 61.69; H, 4.19; N, 7.99%. Found: C, 61.72; H, 4.32; N, 7.96%. IR (KBr, cm^{-1}): 3411 (s), 1700 (s), 1651 (s), 1557 (s), 1412 (m), 1376 (s), 1277 (w), 1240 (m), 1070 (w), 1006 (w), 960 (w), 896 (w), 803 (m), 781 (m), 727 (w).

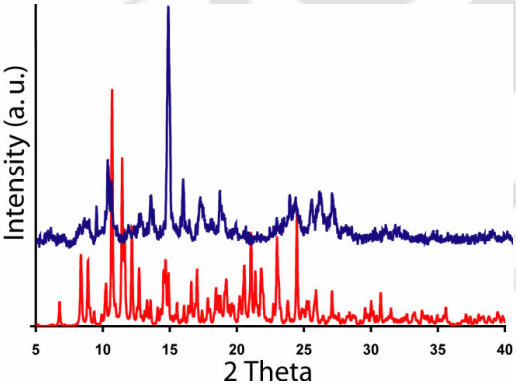

Figure 6.12: Simulated (below) and experimental (above) PXRD patterns of complex **6.3**.

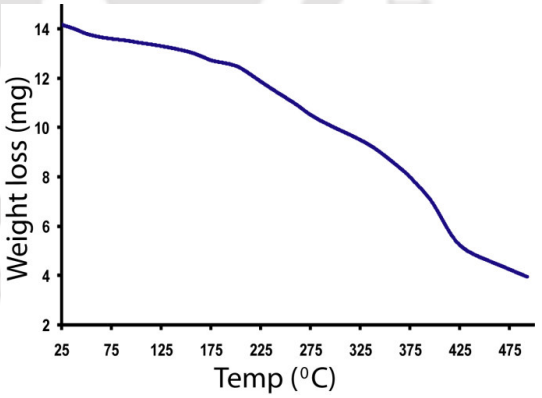

Figure 6.15: TGA curve of complex **6.3**.

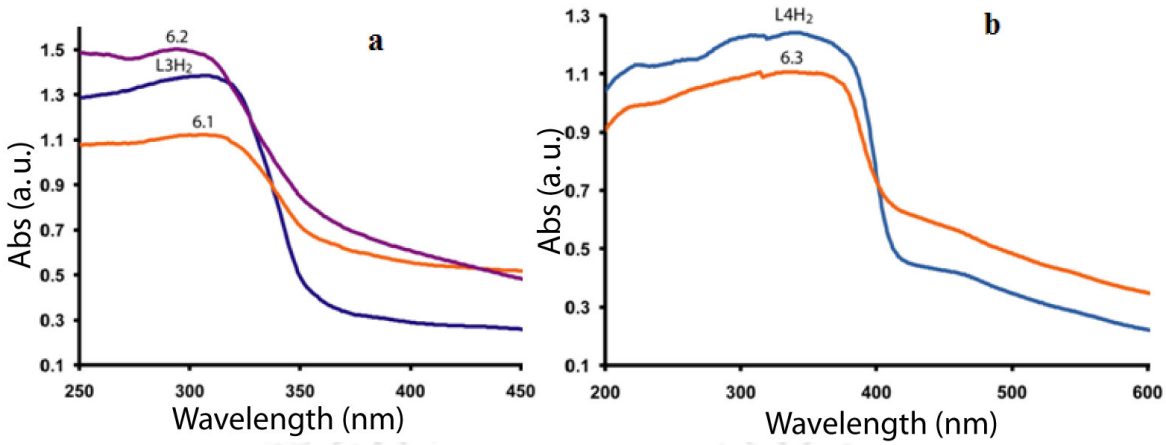

Figure 6.16: Solid state UV-Vis spectra of (a) **L3H2** and its Mn(II) and Zn(II) complexes (**6.1** and **6.2**) showing broad absorbance peaks in the region 280-315 nm and (b) **$L4H_2$** and its Cd(II) complex (**6.3**) showing broad absorbance peaks in the region 320-370 nm.

References:

(1) (a) Barcia, P. S.; Zapata, F.; Silva, J. A. C.; Rodrigues, A. E.; Chen, B. *J. Phys. Chem. B* **2007**, *111*, 6101. (b) Chen, B.;Wang, L.; Zapata, F.; Qian, G.; Lobkovsky, E. B. *J. Am. Chem. Soc.* **2008**, *130*, 6718. (c) Britt, D.; Tranchemontagne, D.;Yaghi, O. M. *Proc. Natl. Acad. Sci. U. S. A.* **2008**, *105*, 11623. (d) Bae, Y.-S.; Mulfort, K. L.; Frost, H.; Ryan, P.; Punnathanam, S.; Broadbelt, L. J.; Hupp, J. T.; Snurr, R. Q. *Langmuir* **2008**, *24*, 8592.

(2) (a) Robson, R. *Dalton Trans.* **2008**, 5113. (b) Tranchemontagne, D. J.; Mendoza-Cortes, J. L.; O'Keeffe, M.; Yaghi, O. M. *Chem. Soc. Rev.* **2009**, *38*, 1257. (c) Rowsell, J. L. C.; Yaghi, O. M. *Microporous Mesoporous Mater.* **2004**, *73*, 3.

(3) (a) Dutta, B.; Adhikary, B.; Bag, P.; Floerke, U.; Nag, K. *J. Chem. Soc., Dalton Trans.* **2002**, 2760. (b) McMorran, D. A. *Inorg. Chem.* **2008**, *47*, 592. (c) Zhang, G.-Q.; Yang, G.-Q; Ma, J.-S. *Cryst. Growth Des.* **2006**, *6*, 1897. (d) Fu, Y.-L.; Xu, Z.-W.; Ren, J.-L.; Yang, J.-Y. *Cryst. Growth Des.* **2007**, *7*, 1198. (e) Wang, R.-H.; Xu, L.-J.; Ji, J.-X.; Shi, Q.; Li, Y.-M.; Zhou, Z.-Y.; Hong, M.-C.; Chan, Albert, S. C. *Eur. J. Inorg. Chem.* **2005**, *4*, 751. (f) Uemura, T.; Kitaura, R.; Ohta, Y.; Nagaoka, M.; Kitagawa, S. *Angew. Chem., Int. Ed.* **2006**, *45*, 4112. (g) Ferey, G.; Mellot-Draznieks, C.; Serre, C.; Millange, F. *Acc. Chem. Res.* **2005**, *38*, 217. (h) Lee, J. Y.; Farha, O. K.; Roberts, J.; Scheidt, K. A.; Nguyen, S. T.; Hupp, J. T. *Chem. Soc. Rev.* **2009**, *38*, 1450.

(4) (a) Liu, Y. Y.; Huang, Y. Q.; Shi, W.; Cheng, P.; Liao, D. Z.; Yan, S. P. *Cryst. Growth Des.* **2007**, *7*, 1483. (b) Chen, X. F.; Cheng, P.; Liu, X.; Hao, B.; Liao, D. Z.; Yan, S. P.;

Jiang, Z. H. *Inorg. Chem.* **2001**, *40,* 2652. (c) Cao, D. K.; Li, Y. Z.; Song, Y.; Zheng, L. M. *Inorg. Chem.* **2005**, *44*, 3599. (d) Mishra, A.; Wernsdorfer, W.; Abboud, K. A.; Christou, G. *J. Am. Chem. Soc.* **2004**, *126*, 15648. (e) Lee, S. Y.; Park, S.; Kim, H. J.; Jung, J. H.; Lee, S. S. *Inorg. Chem.* **2008**, *47*, 1913. (f) Li, Z.; Li, M.; Zhou, X. P.; Wu, T.; Li, D.; Ng, S. W. *Cryst. Growth Des.* **2007**, *7*, 1992. (g) Meng, X.; Song, Y.; Hou, H.; Han, H.; Xiao, B.; Fan, Y.; Zhu, Y. *Inorg. Chem.* **2004**, *43*, 3528. (h) Du, M.; Bu, X.-H.; Guo, Y.-M.; Liu, H.; Batten, S. R.; Ribas, J.; Mak, T. C. W. *Inorg. Chem.* **2002**, *41*, 4904. (i) Lan, A.; Li, K.; Wu, H.; Olson, D. H.; Emge, T. J.; Hong, W.; Ki, M.; Li, J. *Angew. Chem., Int. Ed.* **2009**, *121*, 2370.

(5) (a) Cantrill, S. J.; Chichak, K. S.; Peters, A. J.; Stoddart, J. F. *Acc. Chem. Res.* **2005**, *38*, 1. (b) Seidel, S. R.; Stang, P. J. *Acc. Chem. Res.* **2002**, *35*, 972. (c) Seo, J. S.; Whang, D.; Lee, H.; Jun, S. I.;Oh, J.; Jeon, Y. J.; Kim, K. *Nature* **2000**, *404*, 982. (d) Burchell, T. J.; Eisler, D. J.; Puddephatt, R. J. *Chem. Commun.* **2004**, 944. (e) Lee, W. Z.; Kang, Y. L.;Wang, T. L.; Su, C. C.;Kuo,T. S. *Cryst. Growth Des.* **2008**, *8*, 2614. (f) Su, C. Y.; Yang, X. P.; Kang, B. S.; Mak, T. C. W. *Angew. Chem.,Int. Ed.* **2001**, *40*, 1725. (g) Su, C. Y.; Kang, B. S.; Liu, H. Q.; Wang, Q. G.; Mak, T. C. W. *Chem. Commun.* **1998**, 1551. (h) Zhuang, C.-F.; Zhang, J.; Wang, Q.; Chu, Z.-H.; Fenske, D.; Su, C.-Y. *Chem. Eur. J.* **2009**, *15*, 7578.

(6) (a) Liu, G. F.; Ye, B. H.; Ling, Y. H.; Chen, X. M. *Chem. Commun.* **2002**, 1442. (b) Tynan, E.; Jensen, P.; Kruger, P. E.; Lees, A. C. *Chem. Commun.* **2004**, 776. (c) Li, X. P.; Pan, M.; Zheng, S. R.; Liu, Y. R.; He, Q. T.; Kang, B. S.; Su, C. Y. *Cryst. Growth Des.* **2007**, *7*, 2481. (d) Uemura, K.; Kitagawa, S.; Fukui, K.; Saito, K. *J. Am. Chem. Soc.* **2004**, *126*, 3817. (e) Tiddo, J. M.; Cory, A. B.; Patrick, G.; Jan, R. *Cryst. Growth Des.* **2008**, *8*, 1082. (f) Gotz, R. J.; Robertazzi, A.; Mutikainen, I.; Turpeinen, U.; Gamez, P.; Reedijk, J. *Chem. Commun.* **2008**, 3384. (g) Zhou, X. P.; Zhang, X.; Lin, S. H.; Li, D. C. *Cryst. Growth Des.* **2007**, *7*, 485. (h) Mascal, M.; Armstrong, A.; Bartberger, M. D. *J. Am. Chem. Soc.* **2002**, *124*, 6274.

(7) (a) Liu, Y.-Y.; Huang, Y.-Q.; Shi, W.; Cheng, P.; Liao, D.-Z; Yan, S.-P. *Cryst. Growth Des.* **2007**, *7*, 1483. (b) Chen, X.-F.; Cheng, P.; Liu, X.; Hao, B.; Liao, D. Z.; Yan, S. P.; Jiang, Z. H. *Inorg. Chem.* **2001**, *40*, 2652. (c) Cao, D. K.; Li, Y. Z.; Song, Y.; Zheng, L. M. *Inorg. Chem.* **2005**, *44*, 3599. (d) Mishra, A.; Wernsdorfer, W.; Abboud, K. A.; Christou, G. *J. Am. Chem. Soc.* **2004**, *126*, 15648. (e) Liao, S.; Su, C.-Y.; Yeung, C.-H.; Xu, A.-W.; Zhang, H.-X.; Liu, H.-Q. *Inorg. Chem. Commun.* **2000**, *3*, 405.

(8) (a) Carballo, R; Covelo, B; Balboa, S; Castineiras, A; Niclos, J. Z. *Anorg. Allg. Chem.* **2001**, *627*, 948. (b) Carballo, R.; Covelo, B.; El Fallah, S. M.; Ribas, J.; Vazquez-Lopez, E.

M. *Cryst. Growth Des.* **2007**, *7*, 1069. (c) Carballo, R.; Covelo, B.; Garcia-Martinez, E.; Vazquez-Lopez, E.M. *Appl. Organomet. Chem.* **2005**, *19*, 394-395. (d) Carballo, R.; Castineiras, A.; Balboa, S.; Covelo, B.; Niclos, J. *Polyhedron* **2002**, *21,* 2811. (e) Micera, G.; Sanna, D.; Dessi, A.; Kiss, T.; Bugly, P.; *Gaz. Chim. Ital.* **1993**, *123*, 573-577.

(9) (a) Balboa, S.; Borrás, J.; Brandi, P.; Carballo, R.; Castiñeiras, A.; Lago, A. B.; Niclós-Gutiérrez, J. and Real, J. A. *Cryst. Growth Des.* **2011**, *11*, 4344. (b) Agaskar, P. A.; Cotton, F. A.; Falvello, L. R.; Han, S. *J. Am. Chem. Soc.* **1986**, *108*, 1214. (c) Lanfranchi, M.; Prati, L.; Rossi, M.; Tiripicchio, A. *J. Chem. Soc., Chem. Commun.* **1993**, 1698. (d) Melikyan, G. G.; Amiryan, F.; Visi, M.; Hardcastle, K. I.; Bales, B. L.; Aslanyan, G.; Badanyan, S. H. *Inorg. Chim. Acta* **2000**, 308, 45. (e) Castineiras, A.; Balboa, S.; Bermejo, E.; Carballo, R.; Covelo, B.; Borras, J.; Real, J. A. *Z. Anorg. Allg. Chem.* **2002**, *628,* 1116. (f) Carballo, R.; Castineiras, A.; Covelo, B.; Garcia-Martinez, E.; Niclos, J.; Vazquez-Lopez, E. M. *Polyhedron* **2004**, *23*, 1505. (g) Beghidja, A.; Hallynck, S.; Welter, R.; Rabu, P. *Eur. J. Inorg. Chem.* **2005**, 662. (h) Zhu, L.-N.; Gao, S.; Huo, L.-H.; Zhao, H. *Acta Crystallogr.* **2005**, *E61*, m2646. (i) Beghidja, A.; Rogez, G.; Rabu, P.; Welter, R.; Drillon, M. *J. Mater. Chem.* **2006**, 16, 2715. (j) Cuin, A.; Massabni, A. C.; Leite, C. Q. F.; Sato, D. N.; Neves, A.; Szpoganicz, B.; Silva, M. S.; Bortoluzzi, A. J. *J. Inorg. Biochem.* **2007**, *101*, 291.

(10) (a) Barooah, N.; Karmakar, A.; Sarma, R. J.; Baruah, J. B., *Inorg. Chem. Commun.* **2006**, *9*, 1251-1254. (b) Barooah, N.; Sarma, R. J.; Baruah, J. B., *Eur. J. Inorg. Chem.* **2006**, 2942-2946. (c) Barooah, N.; Sarma, R. J.; Batsanov A. S.; Baruah, J. B. *Polyhedron* **2006**, *25*, 17-24.

(11) (a) Reger, D. L.; Horger, J.J,; Smith, M. D.; Long, G. J.; Grandjean, F. *Inorg. Chem.* **2011**, *50*, 686-704. (b) Reger, D. L.; Debreczni, A.; Smith M. D., *Inorg. Chim. Acta.* **2010**, *364*, 10-15. (c) Reger, D. L.; Sirianni, E.; Horger, J. J.; Smith, M. D.; Semeniuc, R. F., *Cryst. Growth Des.* **2010**, *10*, 386-393.

(12) Barooah, N.; Sarma, R. J.; Batsanov, A. S.; Baruah, J. B., *J. Mole. Struct.* **2006**, *791*, 122-130.

(13) (a) Aakeröy, C.; Champness, N.; Janiak, C. *CrystEngComm* **2010**, *12*, 22. (b) Habib, H. A.; Sanchij, J.; Janiak, C. *Inorg. Chim. Acta* **2009**, *362*, 2452. (c) Henninger, S. K.; Habib, H. A.; Janiak, C. *J. Am. Chem. Soc.* **2009**, *131*, 2776. (d) Habib, H. A.; Hoffmann, A.; Höppe, H. A.; Janiak, C. *J. Chem. Soc. Dalton Trans.* **2009**, 1742. (e) Yang, J.; Ma, J.-F.; Liu, Y.-Y.; Batten, S. R. *CrystEngComm* **2009**, *11*, 151. (f) Du, M.; Zhang, Z.-H.; Wang, X.-G.; Tang,

L.-F.; Zhao, X.-H. *CrystEngComm* **2008**, *10*, 1855. (g) Lan, Y.-Q.; Li, S.-L.; Fu, Y.-M.; Xu, Y.-H.; Li, L.; Su, Z.-M.; Fu, Q. *Dalton Trans.* **2008**, 6796.

(14) Saadeh, S. M.; Lah, M. S.; Pecoraro, V. L. *Inorg. Chem.* **1991**, *30*, 8.

(15) (a) Wu, Q.; Esteghamatian, M.; Hu, N.-X.; Popovic, Z.; Enright, G.; Tao, Y.; D'Iorio, M.; Wang, S. *Chem. Mater.* **2000**, *12*, 79. (b) McGarrah, J. E.; Kim, Y.-J.; Hissler, M.; Eisenberg, R. *Inorg. Chem.* **2001**, *40*, 4510.

(16) Carballo, R.; Castineiras, A.; Covelo, B.; Vazquez-Lopez, E. M. *Polyhedron* **2001**, *20*, 899.

(17) Carballo, R.; Covelo, B.; El Fallah, S. M.; Ribas, J.; Vazquez-Lopez, E. M. *Cryst. Growth Des.* **2007**, *7*, 1069.

(18) (a) Michaelides, A.; Papadimitriou, C. D.; Plakatouras, J. C.; Skoulika, S.; Veltsistas, P. G. *Polyhedron* **2004**, *23*, 2587. (b) Barszcz, B.; Hodorowicz, S.; Jablonska-Wawrzycka, A.; Stadnicka, K. *J. Coord. Chem.* **2005**, *58*, 203. (c) Chen, Z.-F.; Xiong, R.-G.; Abrahams, B. F.; You, X.-Z.; Che, C.-M. *J. Chem. Soc. Dalton Trans.* **2001**, 453. (d) Wang, X.-L.; Qin, C.; Wang, E.-B.; Su, Z.-M. *Chem. Eur. J.* **2006**, *12*, 2680. (e) Sadovel, H. C. L.; Barbabehrens, N.; Bernes, S.; Garcia, N. F.; Hoplf, H. *J. Chem. Soc. Dalton Trans.* **1997**, 3415. (f) Sen, S.; Saha, M. K.; Kundu, P.; Mitra, S.; Kruger, C.; Bruckmann, J. *Inorg. Chim. Acta* **1999**, *288*, 118.

(19) (a) Banerjee, S.; Ghosh, A.; Wu, B.; Lassahn, P.-G.; Janiak, C. *Polyhedron* **2005**, *24*, 593. (b) Banerjee, S.; Lassahn, P.-G.; Janiak, C.; Ghosh, A. *Polyhedron* **2005**, *24*, 593.

(20) Hu, M.; Yang, X-G.; Zhang, Q.; Zhou, L-.M.; Fang, S-M.; Liu, C-S. *Zeits. Anorg. Allg. Chem.* **2011**, *637*, 478.

(21) (a) Wu, Q.; Esteghamatian, M.; Hu, N.-X.; Popovic, Z.; Enright, G.; Tao, Y.; D'Iorio, M.; Wang, S. *Chem. Mater.* **2000**, *12*, 79. (b) McGarrah, J. E.; Kim, Y.-J.; Hissler, M.; Eisenberg, R. *Inorg. Chem.* **2001**, *40*, 4510.

(22) (a) Chen, W.; Wang, J.-Y.; Chen, C.; Yue, Q.; Yuan, H.-M.; Chen, J.-X.; Wang, S.-N. *Inorg. Chem.* **2003**, *42*, 944. (b) Wang, M.-S.; Guo, G.-C.; Fu, M.-L.; Xu, L.; Cai, L.-Z.; Huang, J.-S. *Dalton Trans.* **2005**, 2899.

(23) Yam, V. W. W.; Lo, K. K. W. *Chem. Soc. Rev.*, **1999**, *28*, 323. (b) Wang, L.-Y.; Yang, Y.; Liu, K.; Li, B.-L.; Zhang, Y. *Cryst. Growth Des.* **2008**, *8*, 3902. (c) Hu, T.-L.; Zou, R.-Q.; Li, J.-R.; Bu, X.-H. *Dalton Trans.* **2008**, 1302.

Conclusion

Cyclic imides are important compounds as protecting group for amine functionality. The ease of synthesis and readily accommodated synthetic modification on either the aromatic ring or at the N-imide site make them amenable for various applications. They have been applied for the formation of large macrocycles through their interesting photochemical reaction. The incorporation of varieties of functional groups or structural motifs with cyclic imides have been used for anion and cation sensing, molecular recognition, supramolecular and host-guest chemistry and coordination chemistry. The electron deficient and aromatic nature of cyclic imides is important for face-to-face aromatic interactions and their rigid, planar structure along with the ability to be functionalized with a wide variety of side groups make them attractive with respect to host–guest systems such as intercalation, foldamers, ion channels, catenanes and rotaxanes.

In this study, host-guest complexes of pyridine and quinoline with some of the naphthalimide or naphthalene diimide tethered aromatic hydroxy carboxylic acids are reported to create channels in their 3D supramolecular architectures. Formation of different types of hydrogen bonds motifs in these complexes is established by DFT calculations which suggest that their formation is controlled by the other weak interactions present in the crystal lattices. Minor differences in host-guest interactions are found to be responsible for the formation of polymorphs and pseudopolymorphs of pyridine and quinoline solvates of naphthalene diimide and pyromellitic dimide tethered carboxylic acids. This generates a new kind of host–guest assemblies from amine interactions with a central dicarboxylic acid molecule to encapsulate guest amine/s. The preferential binding of quinoline over pyridine by the host is observed in the formation of polymorphic solvates which is the guiding factor for separation techniques. It is realized that the symmetry non-equivalent solvates with same Z´ value can have different orientations of the parent molecules depending on the solvent attached to it. The crystal packing requirement decides such orientations and leads to new kind of unusual polymorphs. A series of new class of low molecular weight cyclic imide organogelators is prepared and their gel formation properties are studied. The role of solvents in deciding the course of the reaction for the formation of amino derivative cyclic imide or heterocyclic compound bearing isoquinoline backbone is reported. The solvato-emissive properties of heterocyclic compounds derived from planar aromatic ring are described. Different organic

solvents such as dichloromethane, acetonitrile, methanol can be distinguished from the different emission wavelengths of the heterocyclic compounds.

A series of M(II) carboxylates of flexible hydrophobic unit coupled with cyclic imide units are prepared and their supramolecular structural features are described. It is found that coordination environments around the metal centers as well as weak non covalent forces affect the dimensionality and features of supramolecular architectures of such metal complexes. Taking an account on the influence of the nature of spacer and substituent position of the O-donor imide ligands in the formation of coordination frameworks, the supramolecular coordination chemistry of M(II) complexes of flexible aliphatic and rigid aromatic hydroxy carboxylic acids tethered by cyclic imide units is also studied. We observed that the position of –OH group adjacent to –COOH group and flexibility or rigidity of spacer coupled with imide tethers provide an impetus to obtain the polymeric and monomeric M(II) complexes. The self assembly of phthalimide tethered flexible hydroxy carboxylic acids can be tuned to adopt fascinating supramolecular architectures possessing channels of different dimensionalities and voids of hexagonal nature upon introduction of Mn(II) and Zn(II) metal ions, respectively. Thermal studies have shown the differences of coordinated or lattice solvent molecules in these complexes. The solid state photoluminescence properties of as synthesized M(II) complexes as well as their parent ligands are also investigated.

Appendix

Details of the analytical instruments

X-Ray Diffractions

Single crystal X-ray diffraction data were collected on Bruker 3-circle diffractometers with CCD area detectors ProteumM APEX or SMART 6000 or Bruker Nonius Apex 2, using graphite-monochromated Mo-$K\alpha$ radiation (λ = 0.71073 Å) from a 60W microfocus Bede Microsource® with glass polycapillary optics or a sealed tube.

X-ray diffraction data for all crystals were collected using Bruker SMART software. This software was also used for indexing and determination of the unit cell parameters. The structures were solved by direct methods and refined by full-matrix least squares against F^2 of all data, using SHELXTL software. The CIF of all the compounds characterized by single crystal X-ray structure are included in the soft copy.

All non-H atom were refined by full-matrix least squares in anisotropic, all H atoms in isotropic approximation, against F^2 of all reflections. All non-H atoms were refined by full-matrix least squares in the anisotropic approximation and the hydrogen atoms attached to these atoms were treated as 'riding' in calculated positions and in some of the cases the hydrogen atoms have been located on the difference Fourier maps. In all cases the hydrogen atoms attached to polar atoms such as O and N were located on the difference Fourier maps and refined in the final structure in isotropic approximation. The crystallographic tables for all the compounds are given at the end of this section, which includes the crystal parameters and the refinement factors.

Powder X-ray Diffraction data were collected on a Bruker D8 diffractometer in Bragg-Brentano θ-θ geometry with Cu Kα radiation (λ = 1.5418 Å) on a glass surface of an air-dried sample using a secondary curved graphite monochromator. Diffraction patterns were collected over a 2θ range of 5-50^0 at a scan rate of 2^0 min^{-1}.

UV-visible Spectroscopy, Emission and IR Spectroscopy

UV-vis absorption spectra were recorded using Perkin-Elmer Lambda 750 spectrophotometer equipped with double cell compartments. All the chemicals and solvents used were as obtained from the standard suppliers such as E.Merck Germany, Sigma Aldrich USA, Ranbaxy India. The solvents for optical spectroscopy were of HPLC grade (Aldrich or Merck) and used as obtained. The fluorescence spectra were recorded using a Perkin-Elmer LS 55 spectrofluorometer. The FT-IR spectra were recorded on Perkin-Elmer spectrum one spectrometer in the range 4000-400 cm^{-1}.

NMR and Mass Spectroscopy

The ^{1}HNMR and ^{13}CNMR spectra were recorded in a Bruker 400 MHz spectrometer. The chemical shifts in the NMR spectra are all given in ppm and tetramethylsilane as the internal standard. Electrospray ionization mass (ESI-MS) spectra were recorded on a Waters (Micromass MS Technologies) Q-Tof Premier mass spectrometer.

Thermogravimetric Studies and Elemental analysis

The thermogravimetric studies were performed using a Mettler Toledo TGA/ STDA 851^{e} and Mettler Toledo DSC^{e} thermal analyser. Typically about 5-7 mg of the samples were mounted on platinum crucibles and the TG/DSC profiles recorded at the heating rate of 10 °C/min and under nitrogen atmosphere. Elemental analyses were done on a Perkin-Elmer PE 2400 II CHN analyzer 2400.

Scanning Electron Micrographs (SEM)

SEM of the dried sample of gels were recorded on a Scanning Electron Microscope, Leo 1430vp instrument using small glass plates coated by aluminium foils.

Hydrogen bond geometry (Å, °) for compounds

Comp-ounds	D–H···A	d (D–H)	d (H···A)	d (D···A)	<D–H···A
2.1a	O2-H2···O2 [1-x, 1-y, 1-z]	1.24	1.24	2.472 (19)	180
	O3-H3A···N3 [-x, 1-y, 1-z]	0.82	1.96	2.765 (3)	168
	N2-H26···O1	0.99	1.92	2.746 (14)	139
	N2-H26···O2 [1-x, 1-y, 1-z]	0.99	2.59	3.219 (14)	132
	C11-H11···O5 [1+x, y, z]	0.93	2.38	3.129 (2)	137
	C15-H15···O4 [x, y-1, z]	0.93	2.50	3.210 (2)	134
	C20-H20···O4 [1-x, 1-y, 1-z]	0.93	2.55	3.468 (4)	171
2.2a	O2-H2···N2 [-x, -y, 1-z]	0.82	1.78	2.596 (3)	174
	O3-H3···N3 [1-x, 1-y, 1-z]	0.82	1.95	2.701 (3)	153
	C3-H3A···O1	0.93	2.69	3.616 (3)	175
	C16-H16···O4	0.93	2.72	3.360 (3)	127
	C24-H24···O5	0.93	2.62	3.089 (3)	112
	C26-H26···O3	0.93	2.51	3.378 (3)	156
2.5a	O2-H2···N2 [-x, 1-y, z]	0.82	1.87	2.683 (6)	173
	O3-H3A···O6	0.82	1.81	2.621 (6)	170
	O6-H6A···O1 [x, 1+y, z]	0.89	1.89	2.752 (6)	162
	O6-H6B···O2 [1-x, 1-y, 1-z]	0.98	1.80	2.762 (7)	169
	N5-H20A···O7	0.63	2.31	2.930 (4)	172
	C17-H17···O5 [x, 1+y, z]	0.93	2.54	3.085 (6)	118
	C19-H19···O1 [1-x, 1-y, 1-z]	0.93	2.60	3.154 (7)	119
2.3a	N2-H1···O2 [1-x, 1/2+y, 1/2-z]	0.82	1.35	2.541 (3)	172
	O3-H3A···O2 [1-x, 1/2+y, 1/2-z]	0.82	1.80	2.617 (2)	177
	C4-H4···O2 [1-x, 1/2+y, 1/2-z]	0.93	2.57	3.219 (3)	127
	C15-H15···O4 [-1+x, y, z]	0.93	2.58	3.231 (2)	128

2.4a	O2-H2···N3 [1-x, 1-y, 1-z]	0.82	1.79	2.602 (2)	172
	O3-H3A···N2 [x, 1+y, z]	0.82	1.97	2.790 (2)	175
	C16-H16···O5 [-1+x, -1+y, z]	0.93	2.38	3.082 (3)	132
	C40-H40···O3 [-x, 1-y, -z]	0.93	2.53	3.394 (2)	155
	C35-H35···O4	0.93	2.60	3.315	134
	C37-H37···O1	0.93	2.70	3.602	163
2.6a	O1-H1···N4 [1-x, -y, -z]	0.82	1.83	2.647 (5)	171
	O3-H3A···N2 [-1+x, y, z]	0.82	2.00	2.768 (6)	155
	C15-H15···O5	0.93	2.68	3.324 (5)	127
	C17-H17···O2 [x, 1+y, z]	0.93	2.40	3.234 (7)	149
	C30-H30···O4 [-x, -y, 1-z]	0.93	2.43	3.305 (8)	157
	C33-H33···O2	0.93	2.57	3.446 (7)	158
3.1a	O2-H2···N3 [1-x, -y, -z]	0.82	1.80	2.61 (5)	175
	C24-H24···O1 [1/2+x, 1/2-y,-1/2+z]	0.93	2.69	3.29 (4)	122
	C5-H5···O4	0.93	2.43	3.35	170
	C17-H17···O3 [-1/2+x, 1/2-y,-1/2+z]	0.93	2.62	3.27 (5)	126
	C13-H13···O2	0.93	2.70	3.40	132
3.1b	O1-H1···N2 [-1+x, -1+y, z]	0.82	1.81	2.62 (5)	171
	C22-H22···O4 [-x, 1-y, 1-z]	0.93	2.58	3.38 (6)	145
	C21-H21···O2	0.93	2.67	3.55	157
3.1c	O3-H3A···N2 [x, 1+y, z]	0.82	1.88	2.66 (3)	158
	C19-H19···O4 [1-x, 1-y, 1-z]	0.93	2.64	3.52 (4)	159
	C24-H24···O2	0.93	2.43	3.23	124
3.1d	O2-H2···N4 [-x, 1-y, z]	0.82	1.80	2.62 (8)	168
	O8-H8···N5 [1-x, 1/2+y, 1/2-z]	0.93	2.15	2.72 (9)	126
	C38-H38···O1	0.93	2.59	3.26 (11)	130
	C31-H22···O4 [-x, 1/2+y, 1/2-z]	0.93	2.33	3.21 (9)	156
	C39-H39···O3 [-x, -1/2+y, 1/2-z]	0.93	2.32	3.17 (13)	151

	C51-H51···O3	0.93	2.65	3.38 (11)	134
	C48-H48···O6 [1-x, 1-y, 1-z]	0.93	2.46	3.21 (12)	138
3.2a	O3-H3···N2 [1-x, 2-y, -z]	0.82	1.78	2.60 (2)	178
	C12-H12···O4	0.93	2.69	3.28	122
	C10-H10···O1[1+x, y, z]	0.93	2.55	3.34 (4)	142
	C16-H16···O4 [1-x, -y, -z]	0.93	2.55	3.36 (3)	146
	C8-H8···O1	0.93	2.52	3.11 (3)	122
3.2b	O1-H1···N3	0.82	1.80	2.62	176
	C15-H15···O2	0.93	2.62	3.28	128
	C4-H4···O2 [-1+x, y, z]	0.93	2.38	3.30 (4)	168
	C21-H21···O4	0.93	2.52	3.19	129
	C19-H19···O4	0.93	2.49	3.34	153
3.3a	O5-H5A···N3 [1-x, -y, -z]	0.82	1.80	2.61 (5)	172
	O1-H1···N4	0.82	1.86	2.68	173
	C15-H15···O5	0.93	2.40	2.72 (5)	101
	C22-H22···O4 [1-x, 1-y, 1-z]	0.93	2.53	3.29 (4)	138
	C29-H29···O6 [1-x, -y, -z]	0.93	2.56	3.19 (5)	125
	C30-H30···O2 [-1+x, 1+y, z]	0.93	2.61	3.17	118
	C33-H33···O8	0.93	2.49	3.22 (8)	135
3.3b	O5-H1···N5	0.82	1.86	2.68 (5)	175
	O5-H5···N3 [1-x, 1-y, 1-z]	0.82	2.09	2.84 (6)	150
	C10-H10···O7 [1-x, 1-y, 1-z]	0.93	2.47	3.27 (3)	143
	C23-H23···O3 [1-x, 1-y, 1-z]	0.93	2.43	3.22 (4)	144
	C39-H39···O2	0.93	2.63	3.25	123
4.3	O2-H20···O4 [-x, y, -z+1/2]	0.82	1.77	2.59	175
	C10-H10B···O4 [x+1/2, -y+1/2, -z]	0.96	2.58	3.30	132
	C11-H11B···O3 [x+1/2, -y+1/2, -z]	0.96	2.57	3.36	140
4.6	N3-H3A···O7	0.86	2.03	2.86	161

	N3-H3B···O1	0.86	2.19	3.01	161
	C3-H3···O1 [-1+x, y, z]	0.93	2.48	3.36	158
	C14-H14···O4 [1+x, y, z]	0.93	2.42	3.28	155
	C17-H17···O1	0.93	2.66	3.42	139
	C17-H17···O7 [-1+x, y, z]	0.93	2.66	3.30	127
	C24-H24···O2 [-x, 1-y, 1-z]	0.93	2.48	3.36	158
5.1	O5-H5A···O2 [x, 1+y, z]	0.95	1.79	2.70 (4)	160
	O6-H6C···O1 [1-x, 2-y, -z]	0.83	2.00	2.82 (4)	168
	O6-H6D···O2 [-x, 2-y, -z]	0.82	1.97	2.70 (4)	149
	C5-H5···O4 [-1+x, y, z]	0.98	2.51	3.29 (4)	136
	C6-H6A···O4	0.97	2.59	2.93 (5)	100
	C11-H11···O3	0.93	2.52	3.34 (5)	148
5.2	O5-H5A···O2 [-x-, 1+y, 1/2-z]	0.75	1.85	2.60 (18)	170
	C6-H6B···O3	0.97	2.59	2.94 (2)	101
	C11-H11···O2	0.93	2.68	3.47 (3)	142
	C21-H21···O2	0.93	2.71	3.63 (3)	172
5.3	O5-H5A···O2 [-x, 2-y, -z]	0.87	1.74	2.58 (2)	162
	O5-H5B···O1 [1-x, 2-y, -z]	0.81	1.95	2.76 (2)	171
	C2-H2···O2 [1+x, y, z]	0.98	2.59	3.45 (2)	147
	C6-H6A···O3	0.97	2.54	2.90 (3)	102
	C12-H12···O4 [-x, 1-y, 1-z]	0.93	2.59	3.39 (3)	144
	C17-H17···O5	0.93	2.38	3.01 (3)	125
5.4	O5-H5A···O1 [1-x, 2-y, -z]	0.74	1.98	2.72 (3)	170
	O5-H5B···O2 [-x, 2-y, -z]	0.82	1.82	2.63 (4)	171
	C6-H6A···O4	0.97	2.55	2.91 (4)	102
	C17-H17···O5	0.93	2.48	3.15 (5)	129
5.5	O5-H5A···O1	0.82	1.83	2.59 (6)	152
	O5-H5B···O2 [x, -1+y, z]	0.94	1.79	2.72 (6)	175

	C2-H2···O1 [x, 1+y, z]	0.98	2.52	3.40 (8)	149
	C5-H5···O3	0.98	2.59	3.12 (9)	114
	C6-H6B···O4	0.97	2.31	2.73 (10)	105
5.6	O5-H5A···N5 [-x, 1-y, 1-z]	1.05	1.87	2.87 (6)	158
	O5-H5B···O2 [x, 1/2-y, 1/2-z]	0.90	2.28	2.73 (6)	110
	C2-H2···O4 [1-x, -y, 1-z]	0.98	2.52	3.34 (6)	141
	C6-H6B···O4	0.97	2.33	2.72 (4)	103
5.7	O5-H5A···O1 [1-x, 1-y, 1-z]	0.76	1.95	2.70 (3)	172
	O5-H5B···O2 [2-x, 1-y, 1-z]	0.83	1.80	2.62 (3)	168
	C5-H5···O4	0.98	2.58	3.11 (4)	114
	C25-H25···O5	0.93	2.51	3.17 (4)	128
	C6-H6A···O3	0.97	2.31	2.73 (5	105
L3H$_2$	O11-H11···O12 [1/2-x,1/2+y,1-z]	0.82	1.68	2.50 (4)	177
	O3-H3···O2	0.82	2.22	2.66 (3)	113
	O3-H3···O5 [x,y,-1+z]	0.82	2.10	2.82 (2)	147
	O7-H7A···O11 [x,y,-1+z]	0.82	1.71	2.53 (4)	177
	O8-H8A···O6	0.82	2.24	2.67 (3)	113
	O8-H8A···O9 [x,y,-1+z]	0.82	2.09	2.84 (2)	152
	O11-H11A···O8 [1/2-x,-1/2+y,1-z]	0.96	1.79	2.70 (4)	158
	O11-H11B···O2 [1/2-x,-1/2+y,1-z]	0.90	1.95	2.81 (4)	159
	O12-H12A···O3	0.94	1.76	2.65 (4)	158
	O12-H12B···O6 [x,y,1+z]	1.05	1.81	2.78 (4)	152
	C8-H8···O2 [1-x,1-y,1+z]	0.93	2.57	3.35 (4)	142
	C9-H9···O4 [x,y,1+z]	0.93	2.49	3.20 (4)	133
	C16-H16A···O9	0.97	2.55	2.90 (3)	101
	C20-H20···O10 [x,y,1+z]	0.93	2.59	3.26 (3)	129
6.1	O11-H11A···O25 [x, 1+y, z]	0.82	2.08	2.657 (12)	127
	O12-H12A···O6 [1+x, y, z]	0.82	1.93	2.724 (9)	163

	C7-H7···O10 [-1+x, 1+y, z]	0.93	2.54	3.245 (11)	133
	C8-H8···O7 [x, 1+y, z]	0.93	2.50	3.409 (11)	166
	C10-H10···O16 [1+x, 1+y, z]	0.93	2.57	3.356 (13)	143
	C15-H15B···O7	0.97	2.58	2.967 (11)	104
	C19-H19···O22 [x, -1+y, 1+z]	0.93	2.53	3.337 (12)	145
	C27-H27B···O26 [1+x, y, z]	0.97	2.59	3.247 (13)	125
	C28-H28A···O15	0.97	2.50	2.874 (11)	103
	C33-H33···O19 [1+x, -1+y, z]	0.93	2.41	3.177 (11)	140
	C34-H34···O21 [2+x, -1+y, z]	0.93	2.53	3.238 (12)	133
	C39-H39A···O13 [-1+x, y, z]	0.97	2.53	3.462 (12)	161
6.2	C2-H2···O2 [1+x, y, z]	0.98	2.50	3.120 (6)	121
	C4-H4A···O3	0.97	2.55	2.940 (8)	104
	C7-H7···O9 [1+x, y, -1+z]	0.93	2.57	3.312 (12)	137
	C25-H25···O7	0.93	2.45	3.068 (10)	124
	C31-H31···O8	0.93	1.74	2.657 (8)	167
	C33-H33···O7 [x, 1+y, z]	0.93	2.59	3.444 (14)	154
6.3	O3-H3···O24 [-x, 1/2+y, 1/2-z]	0.82	1.86	2.675 (4)	172
	O8-H8···O22	0.82	1.84	2.660 (4)	173
	O18-H18···O21	0.82	1.87	2.688 (4)	172
	O13-H13···O23 [1-x, y-1/2, 1/2-z]	0.82	1.87	2.674 (5)	168
	C11-H11···O11 [-x, 1/2+y, 1/2-z]	0.93	2.54	3.383 (6)	150
	C14-H14···O14 [-x, 1/2+y, 1/2-z]	0.93	2.54	3.445 (6)	163
	C31-H31···O16 [1-x, 1/2+y, 1/2-z]	0.93	2.59	3.338 (7)	138
	C42-H42···O13 [-x, 1/2+y, 1/2-z]	0.93	2.47	3.145 (7)	129
	C46-H46···O18 [1-x, y-1/2, 1/2-z]	0.93	2.57	3.344 (8)	140
	C48-H48···O7	0.93	2.54	3.252 (7)	134
	C49-H49···O1	0.93	2.39	3.040 (6)	127
	C51-H51···O10 [-x, 1/2+y, 1/2-z]	0.93	2.41	3.157 (6)	137

	C52-H52···O3 [-x, 1/2+y, 1/2-z]	0.93	2.55	3.339 (7)	143
	C53-H53···O7	0.93	2.54	3.240 (6)	132
	C93-H93···O8 [1-x, y-1/2, 1/2-z]	0.93	2.53	3.184 (7)	128
	C97-H97···O12	0.93	2.52	3.249 (7)	135
	C99-H99···O3[-x, 1/2+y, 1/2-z]	0.93	2.56	3.328 (8)	141
	C102-H102···O12	0.93	2.58	3.286 (6)	133
	C103-H103···O18 [1-x, y-1/2, 1/2-z]	0.93	2.53	3.298 (7)	140
	C104-H104···O15 [1-x, 1/2+y, 1/2-z]	0.93	2.48	3.178 (7)	132
	C106-H106···O17	0.93	2.42	3.075 (6)	128

Selected inter-nuclear distances (Å) and angles (°) of the metal complexes

Bond distances	Bond angles	Bond angles
Complex 5.1		
Mn1 O1 2.136(2)	O1 Mn1 O1 180.00(12)	O6 Mn1 O5 90.16(12)
Mn1 O1 2.136(2)	O1 Mn1 O6 90.18(10)	O6 Mn1 O5 89.84(12)
Mn1 O6 2.202(3)	O1 Mn1 O6 89.82(10)	O1 Mn1 O5 89.87(12)
Mn1 O6 2.202(3)	O1 Mn1 O6 89.82(10)	O1 Mn1 O5 90.13(12)
Mn1 O5 2.210(3)	O1 Mn1 O6 90.18(10)	O6 Mn1 O5 89.84(12)
Mn1 O5 2.210(3)	O6 Mn1 O6 180.00(14)	O6 Mn1 O5 90.16(12)
	O1 Mn1 O5 90.13(12)	O5 Mn1 O5 180.00(8)
	O1 Mn1 O5 89.87(12)	
Complex 5.2		
Cu1 O1 1.9757(11)	O1 Cu1 O1 175.71(7)	N2 Cu1 N2 172.75(8)
Cu1 O1 1.9757(11)	O1 Cu1 N2 91.70(6)	O1 Cu1 O5 92.15(4)
Cu1 N2 2.0290(16)	O1 Cu1 N2 88.03(6)	O1 Cu1 O5 92.15(4)
Cu1 N2 2.0290(16)	O1 Cu1 N2 88.03(6)	N2 Cu1 O5 93.62(4)
Cu1 O5 2.1514(19)	O1 Cu1 N2 91.70(6)	N2 Cu1 O5 93.62(4)
Complex 5.3		
Zn1 O1 2.1019(11)	O1 Zn1 O1 180.00(6)	O5 Zn1 N2 92.49(5)
Zn1 O1 2.1019(11)	O1 Zn1 O5 91.26(5)	O5 Zn1 N2 87.51(5)
Zn1 O5 2.1036(12)	O1 Zn1 O5 88.74(5)	O1 Zn1 N2 94.60(5)
Zn1 O5 2.1036(12)	O1 Zn1 O5 88.74(5)	O1 Zn1 N2 85.40(5)
Zn1 N2 2.2669(15)	O1 Zn1 O5 91.26(5)	O5 Zn1 N2 87.51(5)
Zn1 N2 2.2669(15)	O5 Zn1 O5 180.0	O5 Zn1 N2 92.49(5)
	O1 Zn1 N2 85.40(5)	N2 Zn1 N2 180.00(8)
	O1 Zn1 N2 94.60(5)	
Complex 5.4		
Cd1 O1 2.2804(19)	O1 Cd1 O1 180.000(1)	O5 Cd1 N2 86.40(8)
Cd1 O1 2.2804(19)	O1 Cd1 O5 90.77(8)	O5 Cd1 N2 93.60(8)
Cd1 O5 2.314(2)	O1 Cd1 O5 89.23(8)	O1 Cd1 N2 95.81(8)
Cd1 O5 2.314(2)	O1 Cd1 O5 89.23(8)	O1 Cd1 N2 84.19(7)
Cd1 N2 2.390(2)	O1 Cd1 O5 90.77(8)	O5 Cd1 N2 93.60(8)
Cd1 N2 2.390(2)	O5 Cd1 O5 180.00(12)	O5 Cd1 N2 86.40(8)
	O1 Cd1 N2 84.19(7)	N2 Cd1 N2 180.000(1)
	O1 Cd1 N2 95.81(8)	

Complex 5.5		
Co1 O5 2.082(4)	O5 Co1 O5 180.000(1)	O2 Co1 N2 91.7(2)
Co1 O5 2.082(4)	O5 Co1 O2 90.98(17)	O2 Co1 N2 88.3(2)
Co1 O2 2.095(4)	O5 Co1 O2 89.02(16)	O5 Co1 N2 91.9(3)?
Co1 O2 2.095(4)	O5 Co1 O2 89.02(16)	O5 Co1 N2 88.1(3)
Co1 N2 2.228(6)	O5 Co1 O2 90.98(17)	O2 Co1 N2 88.3(2)
Co1 N2 2.228(6)	O2 Co1 O2 180.0(2)	O2 Co1 N2 91.7(2)
	O5 Co1 N2 88.1(3)	N2 Co1 N2 180.00(12)
	O5 Co1 N2 91.9(3)	
Complex 5.6		
Cu1 O1 1.951(3)	O1 Cu1 O1 180.00(5)	O1 Cu1 N2 90.18(11)
Cu1 O1 1.951(3)	O1 Cu1 N2 90.18(11)	N2 Cu1 N2 180.00(19)
Cu1 N2 2.002(3)	O1 Cu1 N2 89.82(11)	
Cu1 N2 2.002(3)	O1 Cu1 N2 89.82(11)	
Complex 5.7		
Cd1 O1 2.289(16)	O1 Cd1 O1 180.000(1)	O5 Cd1 N2 86.50(7)
Cd1 O1 2.289(16)	O1 Cd1 O5 89.52(7)	O5 Cd1 N2 93.50(7)
Cd1 O5 2.302(19)	O1 Cd1 O5 90.48(7)	O1 Cd1 N2 83.65(7)
Cd1 O5 2.302(19)	O1 Cd1 O5 90.48(7)	O1 Cd1 N2 96.35(7)
Cd1 N2 2.397(2)	O1 Cd1 O5 89.52(7)	O5 Cd1 N2 93.50(7)
Cd1 N2 2.397	O5 Cd1 O5 180.000(1)	O5 Cd1 N2 86.50(7)
	O1 Cd1 N2 96.35(7)	N2 Cd1 N2 180.000(1)
	O1 Cd1 N2 83.65(7)	
Complex 6.1		
Mn2 O14 2.076(8)	O14 Mn2 O13 139.8(3)	O11 Mn1 O1 95.2(3)
Mn2 O13 2.112(8)	O14 Mn2 O23 86.0(6)	O11 Mn1 O6 95.4(3)
Mn2 O23 2.155(10)	O13 Mn2 O23 84.5(6)	O1 Mn1 O6 86.0(3)
Mn2 O18 2.145(5)	O14 Mn2 O18 93.9(3)	O11 Mn1 O12 86.3(2)
Mn2 O20 2.236(7)	O13 Mn2 O18 108.2(3)	O1 Mn1 O12 165.3(3)
Mn2 O15 2.249(7)	O23 Mn2 O18 159.0(4)	O6 Mn1 O12 108.5(3)
Mn1 O11 2.094(7)	O14 Mn2 O20 114.7(3)	O11 Mn1 O3 102.3(3)
Mn1 O1 2.115(6)	O13 Mn2 O20 103.9(3)	O1 Mn1 O3 74.9(3)
Mn1 O6 2.162(6)	O23 Mn2 O20 87.9(4)	O6 Mn1 O3 154.9(2)
Mn1 O12 2.165(6)	O18 Mn2 O20 73.1(2)	O12 Mn1 O3 90.4(3)
Mn1 O3 2.204(7)	O14 Mn2 O15 78.0(3)	O11 Mn1 O8 166.0(3)
Mn1 O8 2.269(6)	O13 Mn2 O15 72.2(3)	O1 Mn1 O8 92.7(3)
	O23 Mn2 O15 117.5(4)	O6 Mn1 O8 73.6(2)
	O18 Mn2 O15 82.9(2)	O12 Mn1 O8 88.9(2)
	O20 Mn2 O15 153.2(2)	O3 Mn1 O8 90.9(2)

Complex 6.2		
Zn1 O7 2.028(4)	O7 Zn1 O1 162.97(14)	O6 Zn1 O8 86.22(17)
Zn1 O1 2.059(4)	O7 Zn1 O6 98.99(15)	N3 Zn1 O8 170.5(2)
Zn1 O6 2.098(4)	O1 Zn1 O6 94.46(15)	O7 Zn1 O3 89.06(14)
Zn1 N3 2.110(6)	O7 Zn1 N3 94.5(2)	O1 Zn1 O3 76.22(14)
Zn1 O8 2.182(5)	O1 Zn1 N3 95.8(2)	O6 Zn1 O3 168.40(16)
Zn1 O3 2.185(4)	O6 Zn1 N3 90.44(19)	N3 Zn1 O3 97.28(18)
	O7 Zn1 O8 77.29(17)	O8 Zn1 O3 87.44(17)
	O1 Zn1 O8 93.31(17)	
Complex 6.3		
Cd1 O1 2.270(3)	O17 Cd2 O11 137.44(11)	O1 Cd1 O6 138.97(11)
Cd1 O6 2.272(3)	O17 Cd2 N8 93.28(13)	O1 Cd1 N3 93.93(14)
Cd1 N3 2.360(4)	O11 Cd2 N8 93.22(11)	O6 Cd1 N3 92.98(12)
Cd1 N5 2.378(3)	O17 Cd2 N10 84.49(12)	O1 Cd1 N5 83.73(13)
Cd1 N4 2.394(4)	O11 Cd2 N10 138.06(11)	O6 Cd1 N5 137.28(11)
Cd1 O2 2.600(3)	N8 Cd2 N10 82.99(11)	N3 Cd1 N5 83.10(12)
Cd1 O7 2.639(3)	O17 Cd2 N9 91.45(14)	O1 Cd1 N4 90.71(15)
Cd2 O17 2.272(3)	O11 Cd2 N9 89.07(12)	O6 Cd1 N4 88.94(12)
Cd2 O11 2.280(2)	N8 Cd2 N9 170.19(13)	N3 Cd1 N4 170.48(13)
Cd2 N8 2.357(4)	N10 Cd2 N9 88.92(12)	N5 Cd1 N4 89.16(12)
Cd2 N10 2.380(3)	O17 Cd2 O12 169.27(11)	O1 Cd1 O2 51.93(11)
Cd2 N9 2.389(4)	O11 Cd2 O12 52.64(9)	O6 Cd1 O2 87.44(10)
Cd2 O12 2.639(3)	N8 Cd2 O12 89.27(11)	N3 Cd1 O2 92.20(13)
Cd2 O16 2.642(3)	N10 Cd2 O12 85.48(11)	N5 Cd1 O2 135.09(12)
	N9 Cd2 O12 84.55(13)	N4 Cd1 O2 97.20(14)
	O17 Cd2 O16 51.84(11)	O1 Cd1 O7 167.06(10)
	O11 Cd2 O16 85.70(10)	O6 Cd1 O7 53.02(9)
	N8 Cd2 O16 94.91(12)	N3 Cd1 O7 89.59(12)
	N10 Cd2 O16 136.19(11)	N5 Cd1 O7 84.34(11)
	N9 Cd2 O16 94.77(13)	N4 Cd1 O7 84.13(13)
	O12 Cd2 O16 138.32(10)	O2 Cd1 O7 140.45(10)

Crystallographic data and refinement parameters for the compounds

Compound No.	**2.1a**	**2.2a**	**2.5a**
Formula	$C_{53}H_{34}N_5O_{10}$	$C_{29}H_{19}N_3O_5$	$C_{43}H_{34}N_5O_{14}$
Formula wt.	900.85	489.47	844.75
Crystal system	Triclinic	Triclinic	Triclinic
Space group	P-1	P-1	P-1
a /Å	9.3051(3)	9.5761(4)	8.4869(7)
b /Å	9.3350(3)	11.3729(4)	8.8222(8)
c /Å	13.7530(4)	12.5759(5)	14.4413(13)
α/°	98.580(2)	66.664(2)	105.395(6)
β/°	101.655(2)	79.047(2)	102.230(6)
γ/°	96.513(2)	66.456(2)	97.442(6)
V/ Å^3	1144.12(6)	1152.07(8)	998.81(15)
Z	1	2	1
Density/Mgm^{-3}	1.308	1.411	1.404
Abs. Coeff. /mm^{-1}	0.092	0.098	0.107
F(000)	467	508	439
Total no. of reflections	14915	12572	9249
Reflections, $I > 2\sigma(I)$	3233	3157	1503
Max. 2θ/°	50.00	50.00	41.86
Ranges (h, k, l)	$-11 \le h \le 11$ $-15 \le k \le 15$ $-15 \le l \le 16$	$-11 \le h \le 11$ $-13 \le k \le 13$ $-14 \le l \le 14$	$-8 \le h \le 8$ $-8 \le k \le 8$ $-14 \le l \le 14$
Complete to 2θ (%)	99.4	97.2	99.4
Data/ Restraints/Parameters	3995 / 0 / 326	3945 / 0 / 336	2114 / 0 / 310
Goof (F^2)	1.043	1.080	1.027
R indices [$I > 2\sigma(I)$]	0.0475	0.0435	0.0565
R indices (all data)	0.0569	0.0542	0.0813

Compound No.	**2.3a**	**2.4a**	**2.6a**
Formula	$C_{28}H_{18}N_2O_5$	$C_{82}H_{56}N_8O_{10}$	$C_{91}H_{62}N_9O_{10}$
Formula wt.	462.44	1313.35	1441.50
Crystal system	Monoclinic	Triclinic	Triclinic
Space group	$P2_1/c$	P-1	P-1
a /Å	9.2947(7)	9.5272(6)	7.9780(7)
b /Å	15.4314(12)	13.2380(9)	10.9945(9)
c /Å	15.7079(11)	13.3281(9)	22.1724(18)
α/°	90.00	95.328(3)	76.991(5)
β/°	95.373(4)	97.809(4)	84.185(6)
γ/°	90.00	93.357(3)	86.845(6)
V/ $Å^3$	2243.1(3)	1653.85(19)	1884.1(3)
Z	4	1	1
Density/Mgm^{-3}	1.369	1.319	1.270
Abs. Coeff. /mm^{-1}	0.095	0.088	0.084
F(000)	960	684	751
Total no. of reflections	29702	21948	30847
Reflections, $I > 2\sigma(I)$	2802	4353	3076
Max. 2θ/°	50.00	50.00	50.00
Ranges (h, k, l)	$-11 \le h \le 11$ $-17 \le k \le 18$ $-18 \le l \le 18$	$-11 \le h \le 11$ $-15 \le k \le 15$ $-15 \le l \le 15$	$-9 \le h \le 9$ $-13 \le k \le 13$ $-25 \le l \le 26$
Complete to 2θ (%)	100.0	99.4	98.8
Data/ Restraints/Parameters	3944 / 0 / 321	5810 / 0 / 453	6565 / 0 / 511
Goof (F^2)	1.017	1.031	1.164
R indices [$I > 2\sigma(I)$]	0.0470	0.0421	0.0783
R indices (all data)	0.0698	0.0584	0.1690

Compound No.	**3.1a**	**3.1b**	**3.1c**
Formula	$C_{48}H_{34}N_6O_8$	$C_{48}H_{34}N_6O_8$	$C_{73}H_{49}N_7O_8$
Formula wt.	822.81	822.81	1152.19
Crystal system	Monoclinic	Triclinic	Triclinic
Space group	$P2_1/n$	P-1	P-1
a /Å	8.5529(2)	8.7635(6)	9.3000(3)
b /Å	20.5796(5)	11.8723(9)	12.2201(4)
c /Å	11.9813(2)	12.1962(14)	12.9800(5)
α/°	90.00	116.061(6)	97.639(2)
β/°	96.5940(10)	95.775(6)	90.821(3)
γ/°	90.00	107.994(4)	99.932(2)
V/ $Å^3$	2094.94(8)	1041.85(16)	1439.08(9)
Z	2	1	1
Density/Mgm^{-3}	1.304	1.318	1.329
Abs. Coeff. /mm^{-1}	0.091	0.093	0.088
F(000)	856	430	600
Total no. of reflections	22511	11332	13410
Reflections, $I > 2\sigma(I)$	2821	2183	2514
Max. θ/°	56.42	49.00	49.00
Ranges (h, k, l)	$-11 \le h \le 11$ $-27 \le k \le 27$ $-15 \le l \le 15$	$-10 \le h \le 9$ $-13 \le k \le 13$ $-14 \le l \le 14$	$-10 \le h \le 10$ $-14 \le k \le 12$ $-13 \le l \le 15$
Completeness to 2θ (%)	98.3	94.8	95.4
Data/ Restraints/Parameters	5076/0/281	3292/0/281	4574/0/408
Goof (F^2)	1.044	1.062	1.030
R indices [$I > 2\sigma(I)$]	0.0500	0.0588	0.0532
R indices (all data)	0.0984	0.0855	0.1123

Compound No.	**3.1d**	**3.2a**	**3.2b**
Formula	$C_{55}H_{35}N_5O_8$	$C_{43}H_{29}N_5O_8$	$C_{55}H_{35}NO_8$
Formula wt.	893.88	743.71	893.88
Crystal system	Monoclinic	Triclinic	Triclinic
Space group	$P2_1/C$	P-1	P-1
a /Å	16.228(3)	7.2585(4)	7.5934(5)
b /Å	15.687(3)	8.3289(5)	9.3850(7)
c /Å	18.544(3)	15.4654(9)	15.9125(11)
α/°	90.00	96.907(3)	101.006(4)
β/°	108.182(9)	102.363(3)	98.361(4)
γ/°	90.00	97.388(3)	95.640(4)
V/ $Å^3$	4485.0(14)	895.10(9)	1091.99(13)
Z	4	1	1
Density/Mgm^{-3}	1.324	1.380	1.359
Abs. Coeff. /mm^{-1}	0.090	0.097	0.093
F(000)	1856	386	464
Total no. of reflections	28724	13117	15800
Reflections, $I > 2\sigma(I)$	2714	2563	2493
Max. θ/°	49.00	56.62	51.00
Ranges (h, k, l)	$-18 \le h \le 18$ $-17 \le k \le 8$ $-21 \le l \le 21$	$-9 \le h \le 9$ $-11 \le k \le 10$ $-20 \le l \le 20$	$-9 \le h \le 9$ $-11 \le k \le 11$ $-18 \le l \le 19$
Completeness to 2θ (%)	95.0	94.3	96.1
Data/ Restraints/Parameters	7096/0/601	4212/0/264	3918/0/318
Goof (F^2)	1.004	1.066	1.018
R indices [$I > 2\sigma(I)$]	0.0911	0.0871	0.0875
R indices (all data)	0.2006	0.0517	0.0490

Compound No.	**3.3a**	**3.3b**	**4.3**
Formula	$C_{39}H_{27}N_5O_8$	$C_{34}H_{22}N_4O_8$	$C_{20}H_{23}NO_8S_2$
Formula wt.	693.66	614.56	469.51
Crystal system	Triclinic	Triclinic	Orthorhombic
Space group	P-1	P-1	Pbcn
a /Å	10.1284(5)	10.9902(8)	7.8097(13)
b /Å	13.6116(7)	12.4771(9)	12.895(2)
c /Å	14.2771(7)	13.2683(10)	22.050(3)
α/°	92.706(3)	116.622(4)	90.00
β/°	110.091(3)	90.239(5)	90.00
γ/°	108.302(3)	107.989(5)	90.00
V/ $Å^3$	1728.26(15)	1525.12(19)	2220.6(6)
Z	2	2	4
Density/Mgm^{-3}	1.333	1.338	1.404
Abs. Coeff. /mm^{-1}	0.095	0.097	0.286
F(000)	720	636	984
Total no. of reflections	21127	15651	9183
Reflections, $I > 2\sigma(I)$	3680	2957	1412
Max. θ/°	28.23	25.00	51.00
Ranges (h, k, l)	-13 ≤ h ≤ 13 - 17≤ k ≤ 17 -18≤ l ≤ 18	-12 ≤ h ≤ 12 - 14≤ k ≤ 14 -15≤ l ≤ 15	-24 ≤ h ≤ 23 -11 ≤ k ≤ 15 -12 ≤ l ≤ 10
Completeness to 2θ (%)	97.3	95.8	85.3
Data/ Restraints/Parameters	8294/0/472	5142/0/417	1770/ 0 / 145
Goof (F^2)	1.068	1.016	1.129
R indices [$I > 2\sigma(I)$]	0.0790	0.0556	0.0448
R indices (all data)	0.1635	0.1043	0. 0559

Compound No.	**4.6**	**5.1**	**5.2**
Formula	$C_{21}H_{18}N_4O_5$	$C_{32}H_{40}N_2O_{12}Mn$	$C_{42}H_{44}N_4O_9Cu$
Formula wt.	406.39	699.60	812.36
Crystal system	Orthorhombic	Monoclinic	Monoclinic
Space group	$Pna2_1$	$P2_1/c$	C2/c
a /Å	18.5494(9)	5.4520(4)	30.798(2)
b /Å	11.2661(6)	6.3891(4)	5.6340(4)
c /Å	9.3670(4)	45.711(3)	24.491(2)
α/°	90.00	90.00	90.00
β/°	90.00	91.796(3)	114.536(6)
γ/°	90.00	90.00	90.00
V/ $Å^3$	1957.51(16)	1591.48(19)	3865.8(5)
Z	4	2	4
Density/Mgm^{-3}	1.379	1.460	1.396
Abs. Coeff. /mm^{-1}	0.101	0.483	0.627
F(000)	848	734	1700
Total no. of reflections	19450	21936	20843
Reflections, $I > 2\sigma(I)$	3071	2709	3591
Max. θ/°	56.72	50.00	54.12
Ranges (h, k, l)	$-24 \le h \le 23$ $-11 \le k \le 15$ $-12 \le l \le 10$	$-6 \le h \le 6$ $-7 \le k \le 7$ $-53 \le l \le 54$	$-38 \le h \le 39$ $-7 \le k \le 7$ $-31 \le l \le 31$
Completeness to 2θ (%)	99.2	99.9	99.4
Data/ Restraints/Parameters	4498/ 1 / 273	2796 / 0 / 224	4229 / 0 / 254
Goof (F^2)	1.044	1.382	1.054
R indices [$I > 2\sigma(I)$]	0.0387	0.0543	0.0331
R indices (all data)	0. 0637	0.0566	0.0388

Compound No.	**5.3**	**5.4**	**5.5**
Formula	$C_{42}H_{46}N_4O_{10}Zn$	$C_{42}H_{46}N_4O_{10}Cd$	$C_{55}H_{40}N_5O_{10}Co$
Formula wt.	832.20	879.24	989.85
Crystal system	Triclinic	Triclinic	Monoclinic
Space group	P-1	P-1	$P2_1/c$
a /Å	5.4784(10)	5.5386(2)	19.0706(19)
b /Å	13.0745(4)	13.1183(4)	5.3626(5)
c /Å	15.1085(6)	15.2664(4)	25.392(3)
α/°	112.077(2)	112.863(2)	90.00
β/°	94.582(2)	94.311(2)	104.218(7)
γ/°	100.6590(10)	100.602(2)	90.00
V/ Å^3	972.18(5)	991.36(6)	2517.30(4)
Z	1	1	2
Density/Mgm^{-3}	1.421	1.473	1.306
Abs. Coeff. /mm^{-1}	0.697	0.615	0.404
F(000)	436	454	1024
Total no. of reflections	14419	7557	13034
Reflections, $I > 2\sigma(I)$	3094	2368	1262
Max. θ/°	50.00	44.22	34.32
Ranges (h, k, l)	$-6 \le h \le 6$ $-15 \le k \le 15$ $-17 \le l \le 17$	$-5 \le h \le 5$ $-13 \le k \le 13$ $-16 \le l \le 16$	$-15 \le h \le 15$ $-4 \le k \le 4$ $-21 \le l \le 21$
Completeness to 2θ (%)	98.9	97.5	99.9
Data/ Restraints/Parameters	3398 / 0 / 263	2399 / 0 / 267	1515 / 0 / 372
Goof (F^2)	1.078	1.111	1.075
R indices [$I > 2\sigma(I)$]	0.0304	0.0293	0.0402
R indices (all data)	0.0335	0.0296	0.0514

Compound No.	**5.6**	**5.7**	**L3H$_2$**
Formula	$C_{60}H_{60}N_6O_{10}Cu$	$C_{55}H_{54}N_5O_{10}Cd$	$C_{12}H_{13}NO_6$
Formula wt.	1088.69	1057.44	267.23
Crystal system	Monoclinic	Triclinic	Orthorhombic
Space group	$P2_1/c$	P-1	$P2_12_12$
a /Å	15.0683(7)	5.5409(2)	21.196(2)
b /Å	19.5440(10)	13.2051(4)	15.0676(17)
c /Å	9.2955(5)	17.7936(6)	8.0827(9)
α/°	90.00	75.104(2)	90.00
β/°	103.023(3)	81.318(2)	90.00
γ/°	90.00	78.586(2)	90.00
V/ Å^3	2667.10(2)	122639(7)	2581.4(5)
Z	2	1	8
Density/Mgm^{-3}	1.356	1.432	1.375
Abs. Coeff. /mm^{-1}	0.476	0.511	0.112
F(000)	1142	547	1120
Total no. of reflections	38853	13435	31967
Reflections, $I > 2\sigma(I)$	2884	4083	3146
Max. θ/°	50.00	50.00	50.00
Ranges (h, k, l)	-17 ≤ h ≤17 -22 ≤ k ≤23 -11 ≤1 ≤ 11	-6 ≤ h ≤ 6 -15 ≤ k ≤ 15 -20 ≤ 1 ≤ 21	-24 ≤ h ≤ 25 -16 ≤ k ≤ 17 -9 ≤1 ≤ 9
Completeness to 2θ (%)	100.0	97.5	99.9
Data/ Restraints/Parameters	4679 / 0 /357	4224 / 0 / 339	4548 / 0 / 363
Goof (F^2)	1.019	1.027	0.916
R indices [$I > 2\sigma(I)$]	0.0584	0.0390	0.0451
R indices (all data)	0.1098	0.403	0.0681

Compound No.	**6.1**	**6.2**	**6.3**
Formula	$C_{48}H_{39}N_4O_{28}Mn_2$	$C_{34}H_{28}N_4O_{10}Zn$	$C_{63}H_{45}N_7O_{12}Cd$
Formula wt.	1229.71	717.99	1204.47
Crystal system	Triclinic	Triclinic	Monoclinic
Space group	P1	P1	$P2_1/c$
a /Å	5.5897(4)	5.0612(3)	18.9798(5)
b /Å	16.5961(10)	10.1638(6)	21.1468(5)
c /Å	16.6125(11)	16.0051(9)	29.1998(8)
α/°	73.622(4)	83.651(3)	90.00
β/°	85.665(4)	88.514(3)	95.448(2)
γ/°	82.482(4)	87.149(3)	90.00
V/ Å^3	1464.64(17)	817.08(8)	11666.7(5)
Z	1	1	8
Density/Mgm^{-3}	1.394	1.459	1.372
Abs. Coeff. /mm^{-1}	0.519	0.817	0.443
F(000)	629	370	4928
Total no. of reflections	14606	6286	128124
Reflections, $I > 2\sigma(I)$	6568	3586	10731
Max. θ/°	50.00	50.00	46.12
Ranges (h, k, l)	$-6 \le h \le 6$ $-19 \le k \le 19$ $-19 \le l \le 19$	$-6 \le h \le 6$ $-12 \le k \le 12$ $-19 \le l \le 19$	$-20 \le h \le 20$ $-23 \le k \le 23$ $-32 \le l \le 32$
Completeness to 2θ (%)	94.9	82.2	99.6
Data/ Restraints/Parameters	8084 / 3 / 742	3738 / 3 / 442	16300 / 0 / 1499
Goof (F^2)	1.099	1.110	1.008
R indices [$I > 2\sigma(I)$]	0.0724	0.0348	0.0416
R indices (all data)	0.0832	0.0377	0. 0706

List of Publication

1. **D. Singh**, J. B. Baruah. Solvation controlling reaction paths and gel-formation in imide derivatives.
   Tetrahedron Letters, **2008***, 49,* 4374-4377.

2. **D. Singh**, J. B. Baruah. Different solvates of two isomeric dicarboxylic acids with pyridine and quinoline.
   CrystEngComm., **2009***, 11,* 2688-2694.

3. **D. Singh**, J. B. Baruah. Varieties in symmetry non-equivalent structural arrangements in solvates of 2-(3-methylene-1,3,7-trioxo-6-(2-carboxy-phenyl)-3,5,6,7-tetrahydro-1H-pyrrolo[3,4-f]isoindol-2-yl)benzoic acid.
   Journal of Molecular Structure, **2009**, *937*, 75-80.

4. **D. Singh**, S. K. Ghosh, J. B. Baruah. Solvent-dependent fluorescence emission in heterocyclic compounds having isoquinoline backbone.
   Journal of Heterocyclic Chemistry, **2010**, *47*, 199-206.

5. **D. Singh**, P. Bhattacharyya, J. B. Baruah. Structural studies on solvates of cyclic imide tethered carboxylic acids with pyridine and quinoline.
   Crystal Growth & Design, **2010***, 10,* 348-356.

6. **D. Singh**, J. B. Baruah. Structural study on solvates of dopamine-based cyclic imide derivatives.
   Crystal Growth & Design, **2011***, 11,* 768-777.

7. **D. Singh**, J. B. Baruah. Metal (II) complexes derived from conformation flexible cyclic imides tethered carboxylic acids: syntheses, supramolecular structures and molecular properties
   Crystal Growth & Design, **DOI**: 10.1021/cg300113f.

8. **D. Singh**, J. B. Baruah. Two different binuclear copper complexes in a single crystal.
   Communicated

9. **D. Singh**, J. B. Baruah. Influence of guest molecules in crystal packing of solvates of cyclic imide tethered carboxylic acids.
   Communicated

10. **D. Singh**, J. B. Baruah. Solid state assemblies of solvates of cyclic imides tethered hydroxy benzoic acids with pyridine and quinoline.
    Communicated